DISTORTION INDUCED ENGINE INSTABILITY

Advisory Group for Aerospace Research and Development
Paris, France

October 1974

AGARD

ADVISORY GROUP FOR AEROSPACE RESEARCH & DEVELOPMENT

7 RUE ANCELLE 92200 NEUILLY SUR SEINE FRANCE

AGARD LECTURE SERIES No. 72

on

Distortion Induced Engine Instability

NORTH ATLANTIC TREATY ORGANIZATION

NORTH ATLANTIC TREATY ORGANIZATION

ADVISORY GROUP FOR AEROSPACE RESEARCH AND DEVELOPMENT

(ORGANISATION DU TRAITE DE L'ATLANTIQUE NORD)

AGARD Lecture Series No.72

DISTORTION INDUCED ENGINE INSTABILITY

The material in this book has been assembled to support a Lecture Series under the sponsorship of the Propulsion and Energetics Panel and the Consultant and Exchange Programme of AGARD, presented on 7–8 November 1974 in London; 11–12 November 1974 at the Wright-Patterson Air Force Base (USA); 14–15 November at the Naval Air Propulsion Test Center (USA).

THE MISSION OF AGARD

The mission of AGARD is to bring together the leading personalities of the NATO nations in the fields of science and technology relating to aerospace for the following purposes:

- Exchanging of scientific and technical information;
- Continuously stimulating advances in the aerospace sciences relevant to strengthening the common defence posture;
- Improving the co-operation among member nations in aerospace research and development;
- Providing scientific and technical advice and assistance to the North Atlantic Military Committee in the field of aerospace research and development;
- Rendering scientific and technical assistance, as requested, to other NATO bodies and to member nations in connection with research and development problems in the aerospace field;
- Providing assistance to member nations for the purpose of increasing their scientific and technical potential;
- Recommending effective ways for the member nations to use their research and development capabilities for the common benefit of the NATO community.

The highest authority within AGARD is the National Delegates Board consisting of officially appointed senior representatives from each member nation. The mission of AGARD is carried out through the Panels which are composed of experts appointed by the National Delegates, the Consultant and Exchange Program and the Aerospace Applications Studies Program. The results of AGARD work are reported to the member nations and the NATO Authorities through the AGARD series of publications of which this is one.

Participation in AGARD activities is by invitation only and is normally limited to citizens of the NATO nations.

Published October 1974

533.697.2:629.73.036.3:533.6.048

Printed by Technical Editing and Reproduction Ltd
Harford House, 7–9 Charlotte St, London, W1P 1HD

PREFACE

A propulsion system which is completely stable throughout the M-h and V-n flight envelopes is a necessary but elusive condition. Immunity to distorted inlet flow must be present in the basic design and cannot be added as an accessory following flight test failures. Among the major problems of achieving a stable propulsion system (i.e., no stalls, surges, or rumbles) are matching inlet and engine designs, knowing when a critical problem exists, and introducing corrective design changes in a timely manner.

This Lecture Series, sponsored by the Propulsion and Energetics Panel and the Consultant and Exchange Programme, discusses sources of distortion and both the aerodynamic and mechanical response of engines. Valid techniques for predicting and measuring stability are necessary for establishing confidence during development and to avoid surprises late in the program during flight test. Specialized instrumentation and test procedures, both in engine test cells and flight test, have evolved. Of considerable interest is the final lecture on methods to increase tolerance to distorted flow thereby enhancing stability. Although the Lecture Series is of primary interest to inlet engineers from airframe manufacturers and compressor technologists from engine companies, the seven lectures include information of value to external aerodynamicists, preliminary designers, test engineers, and persons responsible for engine life and integrity.

Allen E.FUHS
Lecture Series Director

LIST OF SPEAKERS

Lecture Series Director — Professor Allen E.Fuhs
Department of Aeronautics (Code 57 FU)
Naval Postgraduate School
Monterey, California 93940
USA

Mr R.Bouillet
Chef de Département Turbomachines (71.F)
SNECMA
Centre d'Essais de Villaroche
77550 Moissy-Cramayel
France

Dr A.A.Mikolajczak
Assistant Chief Engineer
Engineering Building EB2H-2
Pratt and Whitney Aircraft
400 Main Street
East Hartford, Conn. 06108
USA

Dr Hans Mokelke
Motoren- und Turbinen-Union München GmbH
8 München 50
Postfach 50 06 40
Germany

Dr William G.Schweikhard
Deputy Director
Propulsion and Performance Research
NASA Flight Research Center
P.O.Box 273
Edwards Air Force Base
California 93523
USA

Professor Fernando Sisto
Head, Department of Mechanical Engineering
Stevens Institute of Technology
Castle Point Station
Hoboken, New Jersey 07030
USA

Mr D.D.Williams
Head of Installation Aerodynamics Department
Rolls-Royce (1971) Limited
Bristol Engine Division
P.O. Box 3, Filton
Bristol BS12 7QE
England

CONTENTS

INTRODUCTION TO DISTORTION INDUCED ENGINE INSTABILITY

by
Dr. Allen E. Fuhs
Professor of Aeronautics
Naval Postgraduate School
Monterey, California 93940
United States of America

SUMMARY

Propulsion system instability, which may be caused by distorted inlet flow, is a recurring problem which must be solved in each new aircraft development program. Trends in engine and airframe design that keep distortion sensitivity as a continuing problem are discussed. Sources of inlet flow distortion are catalogued; this information is used to assess the potential difficulties in development of a variety of aircraft types, e.g., fighter, attack, and transport aircraft. Methods for describing distortion both experimentally and conceptually are introduced. Sufficient background is stated to provide a perspective of the lecture series.

IMPORTANCE OF DISTORTION

Influence on Aircraft Engine Development[1-5]

Distorted flow into an aircraft gas turbine can trigger engine instability. The axial flow compressor is particularly sensitive to flow nonuniformities. Compressor stall can lead to engine surge. Surge may or may not be serious depending on the particular propulsion installation and engine. In any event, compressor stall and engine surge must be avoided.

The source of air for the engine and the source of much of the flow irregularities is the inlet. Establishing compatibility between the inlet and engine involves a substantial portion of development effort[1], both on the part of the airframe manufacturer and the engine contractor. Compatibility must be assured before flight and cannot be added as an accessory when stability problems develop during flight test.

The effects of distortion on compressor performance and stability are extensively studied during engine development. Studies take the form of experimental investigations in the test cell[2-4] as well as computer analyses using a variety of computer models[5].

From the airframe manufacturer's point of view, the development of a new propulsion system requires extensive wind tunnel tests with subscale aircraft and inlet models. As development progresses, the scale of the inlets increases from 1/20 to 1/6 and finally to 1/1 scale. Accuracy of the complete airframe model also increases.

A continuing aspect of development is identification of incompatibility between the inlet and the engine. The managers may proceed unaware of a compatibility problem or may be overconfident that a solution in full scale hardware will be achieved.

Influence on Aircraft Operation

Performance of an aircraft is decreased by a series of margins. Each margin requires a heavier and larger vehicle to perform a fixed mission. Among the propulsion system margins are buzz or inlet unstart, compressor stall, turbine inlet temperature, and mixture ratio limits to maintain combustor flame stability. The airframe has its margins also, e.g., transonic buffet, maximum C_L, and structural limits. The operator of the aircraft adds a few margins. For example, with increasing pilot proficiency, the aircraft can be flown to the verge of spin.

A balanced aircraft design has all boundaries to performance close together. Figure 1 illustrates the concept of design balance; actually Figure 1 shows an unbalanced design. Curves of specific excess power, P_S, as used in the sense of energy maneuverability, are plotted as a function of G-loading with power setting as a parameter. With increasing G-loading, either positive or negative, P_S decays as a result of increased drag. At a particular power setting and loading, P_S is zero; for example, in Figure 1 P_S is zero for military power at 4.6G. For higher loading the specific excess power becomes negative and the aircraft cannot sustain the maneuver in steady state.

Structural limits are shown at both the positive and negative boundaries. A boundary is given for useful aerodynamic limit. The limit may be, for example, transonic buffet. Also shown in Figure 1 are the propulsion stability limits. To achieve high G loading, large angles of attack are necessary. The aircraft may be in a tight turn with large yaw angles. Large angles of attack and yaw cause severe flow distortion, which in turn induces compressor stall. Propulsion stability limits are established by engine surge and compressor stall.

The aircraft of Figure 1 does not have a balanced design. Due to propulsion instability, neither the positive nor the negative structural limits can be attained. Even if the propulsion stability limit is moved to 7.2G, transonic buffet at 6.4G limits performance.

Extra weight is necessary for a structural limit of 7.2G. If the operating limits were as depicted in Figure 1, the aircraft customer would exert tremendous pressure on the engine contractor to move the propulsion stability limit toward higher G.

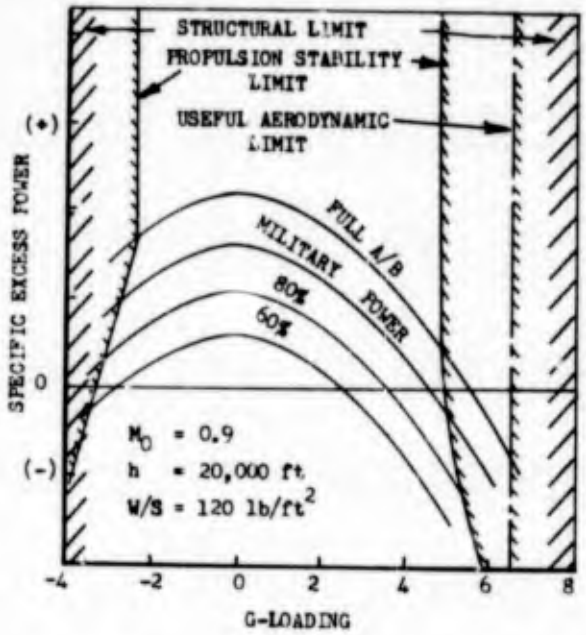

Figure 1. Operating Limits Imposed by Propulsion System and Airframe.

The limits of Figure 1 are for a highly trained, proficient pilot. A less proficient pilot will add his own margin and will fly the aircraft in order to avoid engine instability or severe buffet. Consequently, margins are added in twice—once in basic aircraft design and once by the pilot who flies the aircraft.

Noise Caused by Distorted Flow

Commercial aircraft must meet noise specifications. Even most military aircraft are required to satisfy noise limitations. One advantage of commercial V/STOL aircraft is the ability to operate from the center of the city; this fact imposes additional noise restrictions.

A certain noise level is generated with uniform flow into the aircraft engine. Distorted flow tends to increase noise level. In one set of experiments, personnel at NASA Lewis Research Center[6] measured a 10 dB increase in sound due to flow distortion.

TRENDS THAT HAVE CAUSED DISTORTION SENSITIVITY

Aircraft, including the propulsion system, have historically been designed for steady conditions with minimum attention to the effect of distorted flow. Operation of the aircraft is in an environment which is unsteady, and the propulsion system experiences distorted flow. In the not too distant past there have been aircraft that have missed the design goals by a wide margin. After roll-out of the aircraft, extensive modifications were required to meet specifications. Certain trends in aircraft design deviated enough from past experience so that problems were not recognized in the developmental phase. This section identifies some of these trends.

Expanded Flight Envelopes

Modern, multimission, aircraft will experience a wide range of Mach numbers, Reynolds numbers, angles of attack, and angles of yaw. Figure 2 shows the usual Mach number-altitude performance envelope. At high altitude and with slow speed flight, the Reynolds number is low. At low Reynolds number, the flow on compressor blades may be transitional or even laminar, whereas the normal condition of boundary layer is turbulent. Thinking of a compressor map, the stall line moves downward at low Reynolds number. High-and-slow causes propulsion stability problems.

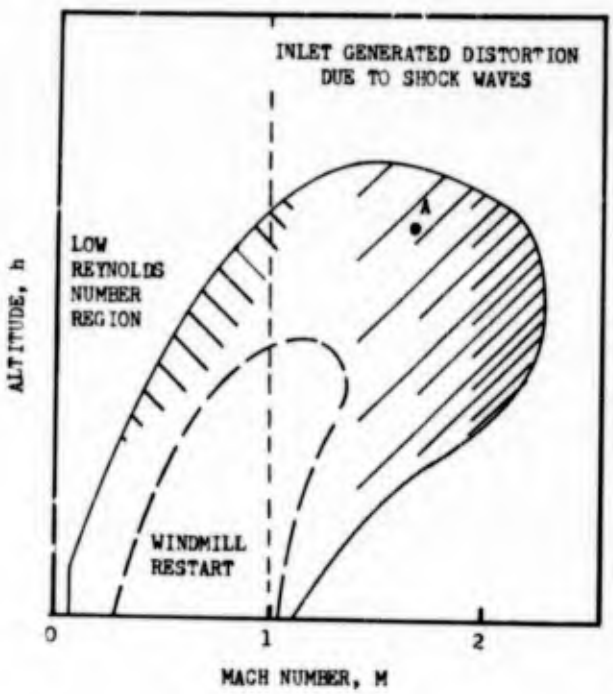

Figure 2. Performance Envelope of Supersonic Aircraft.

At high Mach number, there are a variety of shock waves in the inlet. These shock waves move in response to boundary layer interaction, unsteadiness in ambient atmosphere (e.g., clear air turbulence), and other causes. Distortion levels may be higher in supersonic flow.

Also shown in Figure 2 is the boundary of windmill restart. Compressor stall undoubtedly will cause flame out. If stall occurs at point A in the flight envelope of Figure 2, the pilot must descend to lower altitudes and lower Mach number to achieve relight.

Violent flight maneuvers can cause high levels of distortion. Figure 3 illustrates regions of propulsion instability in the velocity-load factor (V-n) plane. At low velocities, very large angles of attack are necessary to generate lift. Large angle of attack adversely influences propulsion stability. At higher velocities, the angle of attack is less for a particular load factor as a result of increased dynamic pressure. Unfortunately the increased dynamic pressure also means increased distortion levels.

Reference to Figures 1-3 shows that propulsion stability depends on Mach number, Reynolds number, angle of attack, angle of yaw, and power setting.

Introduction of Turbofan

Although a turbojet compressor is not isolated completely from conditions downstream of the turbine, there is a much greater degree of isolation than in the case of a turbofan. Disturbances downstream of

the fan are communicated directly to the fan. An example is ignition in an afterburner which has both fan and engine core flows. Ignition may cause a pressure pulse which appears at the fan discharge and results in fan stall.

A fan typically has a very small hub-to-tip ratio. In the root region the fan blade must be highly loaded to achieve uniform work spanwise.

Turbofans have a nominal bypass ratio. Depending on operating conditions, the division of air between engine core and fan changes. Flow patterns change when bypass ratio changes resulting in alteration of blade loading.

The flow passage geometry out of the fan root region into the engine core may involve large turning in the radial plane. This is especially true in high bypass turbofans. Distorted inlet flow may lead to increased secondary flow losses within the passage itself.

Figure 4 summarizes those features of a turbofan which increase sensitivity to distorted flow.

Highly Loaded Fans and Compressors[7-8]

Pressure ratio per stage in compressors has had a steady growth since the early 1950's. The growth is due mainly to increased tip speed although blade loading has increased also. The pressure ratio per stage, P_2/P_1, can be calculated from

$$\frac{P_2}{P_1} = 1 + \frac{\gamma}{\gamma - 1} n \frac{U^2}{C_p T_1} \Delta\Gamma \qquad (1)$$

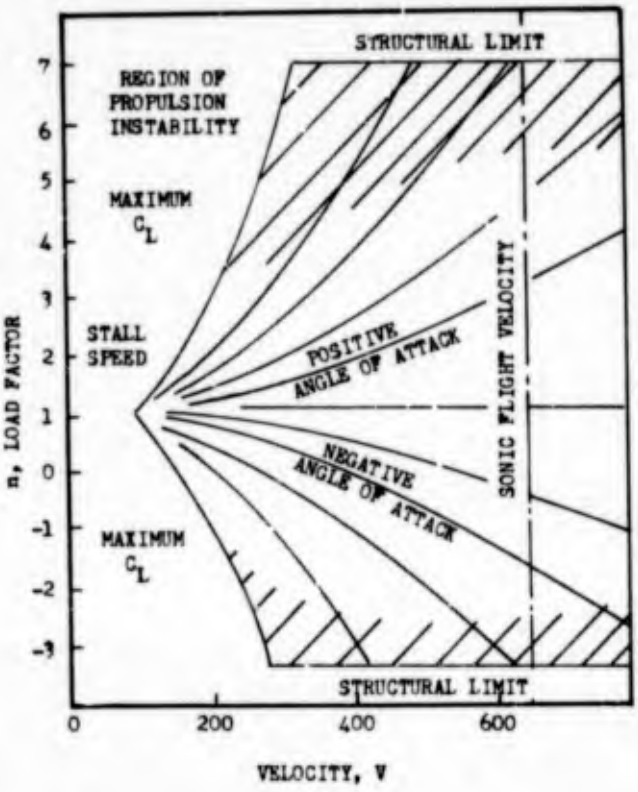

Figure 3. Regions of Propulsion Instability in the V-n Diagram.

where γ is the ratio of heat capacities, n is stage efficiency, U is wheel speed, C_p is specific heat capacity at constant pressure, T_1 is stagnation temperature at the compressor inlet, and $\Delta\Gamma$ is the blade* loading[7]. Equation (1) shows the strong advantage of increased wheel speed or tip speed. Equation (1) also demonstrates that pressure ratio can be increased by either larger U or $\Delta\Gamma$. Figure 5(a) shows the blade loading of compressors in operational engines as of 1966. Also shown are performance points for 1970 vintage NASA research compressors[8]. Present day compressors fall in a tip speed range $1000 < U < 1600$ ft/sec. Blade loading is about 0.35 with research compressors leading to 0.45 and 0.50.

Figure 5(a) indicates blade loading decreasing as tip speed increases. The rate of decay, or negative slope, of the curves is less for the NASA research compressors. Figure 5(b) emphasizes the fact that improved pressure ratio can be attained by improvement in blade loading or tip speed.

To summarize, the growth in pressure ratio per stage to date has been obtained by large increases in tip speed with only modest gains in blade loading. Current research and development is directed toward increased blade loading while maintaining efficiency levels.

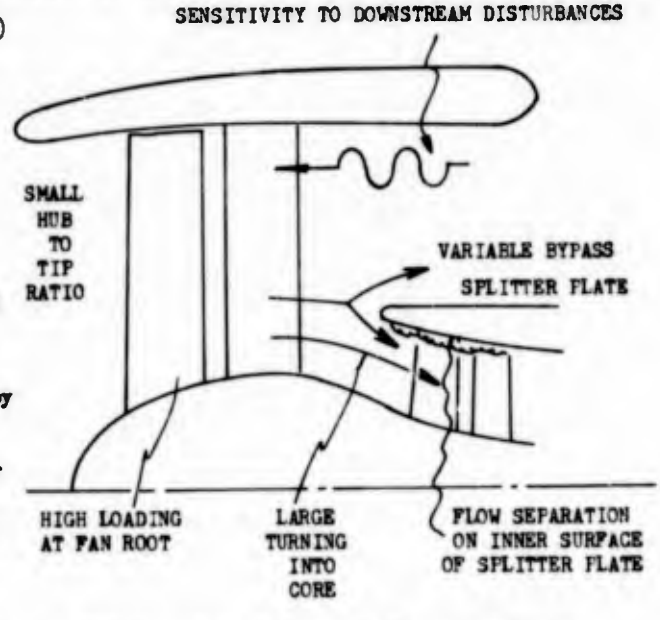

Figure 4. Turbofan Features Which Complicate Distortion Effects.

Relative tip Mach numbers on advanced fans and compressors are well into the supersonic region. Blades are carefully shaped to generate shock wave geometries giving low losses. Distorted flow perturbs the shock waves leading to greater losses or, in severe cases, compressor stall.

Increased blade loading, which is the route to higher pressure ratio per stage that currently is being investigated, implies larger diffusion factors, turning angles, or lift coefficients. Past experience indicates greater adverse effects due to distorted flow when blade loading is high.

*Blade loading can be related to lift coefficient or turning angle.

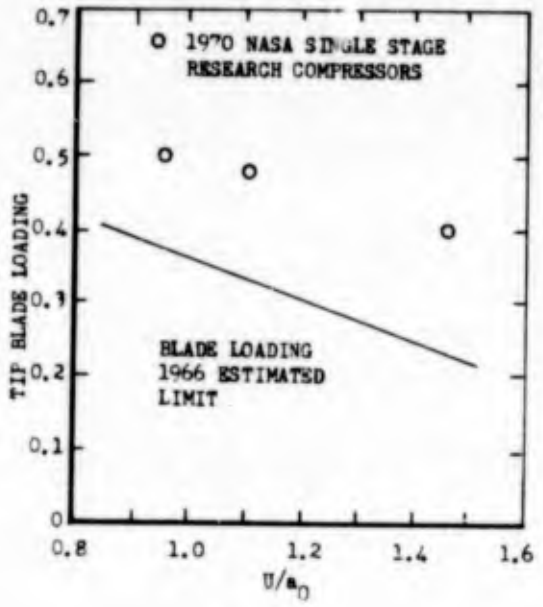

(a) Blade Loading of Operational Compressors. (Adapted from Reference 7.)

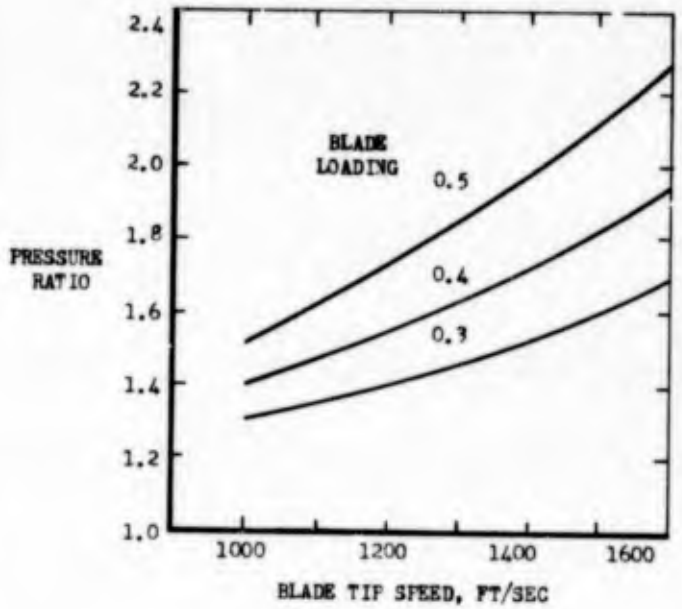

(b) Pressure Ratio of a Single Stage as a Function of Tip Speed. (Reproduced from Reference 8.)

Figure 5. Relationship of Pressure Ratio Per Stage to Blade Loading and Tip Speed.

New Aircraft Configurations

One could assess trends in each of the various categories of aircraft, i.e., military aircraft such as fighter, attack, transport, etc., and commercial aircraft in flight regimes of high-subsonic, transonic, and supersonic. The aim is to substantiate the statement that there are many new aircraft configurations being examined and that each configuration may generate propulsion stability problems unlike those in the past. V/STOL aircraft have the most pronounced changes in configuration and hence represent the greatest departures from known technology. Hence examples from V/STOL aircraft will be discussed.

Aircraft are being developed, e.g., the XFV-12A, using ejectors in the wings to achieve thrust augmentation. Primary gases for the ejectors come from the engine exhaust. In hover and transition, the normal exhaust nozzle is plugged, and the gases are ducted to the ejectors. The plug can cause backpressure on the engine leading to stall.

Consider the fan-in-wing VTOL configuration[9]. During transition from hover to forward flight, cross flow velocities across the fan face develop. Pressure ratio for various parts of the fan vary as the wing develops circulation. The local pressure ratio depends on local C_p differences between the top and the bottom of the wing.

DISTORTION SENSITIVITY BY ENGINE TYPE AND APPLICATION

Selection of the engine cycle depends on aircraft mission. Cycle parameters, e.g., pressure ratio, bypass ratio, turbine inlet temperature, and fan pressure ratio, are chosen to minimize aircraft takeoff gross weight or other criteria of excellence. A particular engine fits a specified mission. The mission is defined in part by the flight envelopes of Figures 1 to 3. Based on this reasoning, some general statements can be made about the categories of aircraft likely to encounter propulsion instability.

Figure 6 locates the various types of aircraft in the specific thrust and specific fuel consumption plane. Almost all aircraft fall along a band with a positive slope. Naturally the propulsion engineers would like to offer an engine at point B in Figure 6. Unfortunately an engine with very large F/ṁ and small SFC does not exist.

For a mission requiring large F/ṁ, for example, a short-range, high-Mach intercepter, a turbojet is the best engine choice. Within the turbojet range of engines, as aircraft range increases, the cycle pressure ratio increases. Increased cycle pressure ratio improves SFC.

Once a turbofan becomes the optimum choice, bypass ratio is a variable to be determined. Two factors strongly influence the choice of bypass ratio; these are aircraft range and whether or not the mission specifies supersonic, subsonic, or alternative of either supersonic or subsonic cruise.

Fan pressure ratio must be correlated with bypass ratio. Fan horsepower is determined by these two quantities, and the gas generator of the turbofan can provide only so much power.

Compressor performance and stability are key elements in achieving propulsion stability. Different aircraft place different demands on the compressor. A long range, subsonic transport aircraft places a large premium on low SFC. Low SFC can be obtained from two general approaches; one is proper selection of cycle parameters, e.g., high cycle pressure ratio, and the other is high efficiency of every component including the compressor.

A separate lift engine, which provides VTOL and hover capability, is used only a few minutes each flight. Low SFC is not important; high thrust-to-weight is vital. High specific thrust is consistent with large thrust-to-weight. High specific thrust is obtained from a large temperature rise across the combustor. There is a span of temperature from ambient air to turbine inlet conditions. A fraction of that span is used by ram and compressor work. The remaining fraction is the combustor increment. A lift engine has insignificant ram, obviously. For a lift engine, low cycle pressure ratio is desirable.

Table I provides a summary of the preceding discussion. These facts can be combined with the section on trends that have caused distortion sensitivity to yield perspective on propulsion stability by aircraft category. Table II is a summary of propulsion stability problems by aircraft type.

Every aircraft requires developmental effort related to propulsion stability. Fighter aircraft and intercepters have many propulsion design features that must be validated. V/STOL aircraft have several stability problems unique to that type of aircraft.

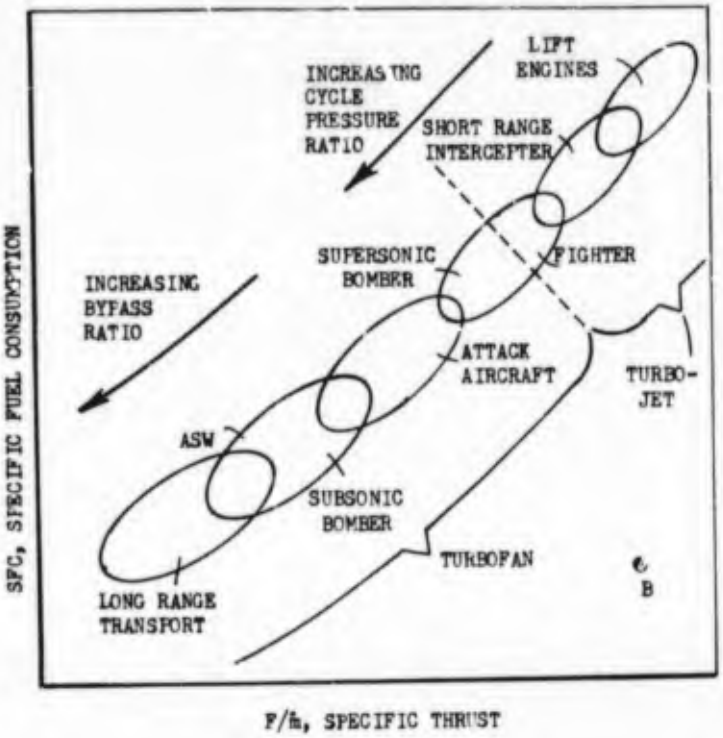

Figure 6. Position of Various Categories of Aircraft in the Specific Thrust and Specific Fuel Consumption Plane.

SOURCES OF DISTORTION

There are many causes for engine instability, not all of which are related to distorted flow. In this section, the sources of distortion are catalogued. There is mention of several causes of propulsion instability distinct from distorted flow.

Table I. Summary of Engine Selection for Various Types of Aircraft.

	Cycle Pressure Ratio	Combustor Temperature Increment	Bypass Ratio	Turbine Inlet Temperature	Compressor Efficiency	Fan Pressure Ratio
LIFT ENGINES	small	large	zero	maximum possible	not too important	-
INTERCEPTER, short range, high Mach	small	large	zero	maximum possible	not too important	-
FIGHTER, short range	medium	large	zero	maximum possible	not dominant	-
FIGHTER, long range	large	medium	less than one	maximum possible	not dominant	large
SUPERSONIC BOMBER	large	large	near unity	maximum possible	not dominant	large
SUBSONIC BOMBER	large	medium	medium	less than maximum	important	medium
ATTACK AIRCRAFT	large	medium	medium	less than maximum	important	medium
ASW	large	small	large	less than maximum	important	small
TRANSPORT, long range	large	small	large	less than maximum possible	extremely important	small

Engine Transients and Control Response

Changes in throttle setting, e.g., throttle chop or throttle burst, require the propulsion system to seek a new operating point. The control system must move the engine along a succession of points

Table II. Matrix of Propulsion Stability Problems by Aircraft Type.

Factors Tending to Cause Propulsion Stability Problems	V/STOL	V/STOL				INTERCEPTOR	FIGHTER, short range	FIGHTER, long range	SUPERSONIC BOMBER	SUBSONIC BOMBER	ATTACK	ASW	ELECTRONIC WARFARE	LONG RANGE TRANSPORT
	V/STOL	Lift Engine	Fan in Wing	Thrust Augmentation	Blow Flaps									
Large bypass ratio					X							X	X	X
High blade loading						X	X	X	X					
High tip speed		X				X	X	X	X					
Low speed at high altitude							X	X			X	X	X	
High Mach number flight				X		X	X	X	X					
Large angle of attack	X					X	X	X			X			
Large angle of yaw	X					X	X	X			X			
Possibility of exhaust recirculation	X											X*	X*	X*
Cross flow at inlet		X	X									X**	X**	X**
Valves at engine exhaust				X	X									
Pressure variations on engine due to external aerodynamics		X	X		X							X	X	X
Armament firing	X					X	X	X	X	X	X	X		

*Where thrust reversers are installed.

**Cross winds at takeoff and taxi.

without excursion into forbidden regions. There are lags in any control system, and these lags can cause the inlet, engine, and nozzle to be off schedule.

A propulsion system control for a supersonic aircraft is complicated. There are many functions to be controlled. For example, the inlet may require control of ramp angle, bypass door position, boundary layer bleed flow, terminal shock position, duct pressure level to avoid overpressure, throat area, and position of auxiliary duct valves. The engine may require control of fuel flow, inlet guide vane angle, stator angle, and interstage bleeds. For the engine, there are several monitoring functions for the control to avoid overspeed and overtemperature. The nozzle system may require control of throat area, ratio of nozzle throat to exit area, and secondary mass flow. Engines with afterburners have more complicated control systems.

As a result of the fact that all variables are not on schedule during transients, distorted flow may be generated. Consider retarding the throttle in an aircraft flying supersonically. Engine mass flow rate decreases. The bypass door should open. Pressure in the duct increases, and the terminal shock system moves toward the inlet throat. The streamlines that separate the bypass flow from the engine flow shift as the bypass door opens. When the bypass door attains the correct opening, the duct pressure decreases, and the shock waves move downstream. Shock wave motion and shifting of dividing streamlines cause nonuniform flow at compressor face. Before the throttle was retarded, the variable stators were set to accept a large mass flow through the engine. Retarding the mass flow finds the stators at small stagger angle with control moving toward large stagger angle. This lag makes the stators vulnerable to stall.

There are aircraft that can fly straight up supersonically. Even at takeoff, some aircraft can climb so fast that by the time the aircraft is over the end of the runway, the altitude exceeds the runway length. The rate of change of the total temperature at the compressor face, i.e., $\partial T_{T2}/\partial t$, may be $\pm$ 30°R/sec. The plus sign applies to a dive, and the minus, to a climb. To prevent overtemperature of the turbine, the fuel control must decrease fuel-air ratio in a dive. To maintain engine RPM and thrust, the fuel control must increase fuel-air ratio in a climb. Changes in engine mass flow due to changes in fuel-air ratio can cause the inlet to operate off schedule; a consequence is distorted flow.

Inlet Aerodynamic Problems

An inlet designed for supersonic flight has sharp lips. In low speed flight at high power, the flow has a tendency to separate at the lips. Flow separation causes nonuniform flow at the compressor.

Pressure recovery of an inlet depends on ramp angles and contraction ratio. If the ramp angle or throat area are not correct, the shock waves are not in correct position relative to boundary layer bleed ports, and the mass flow ratio may be in error compared to design. Shock wave unsteadiness leads to distorted flow.

Boundary layer bleed uses a pattern of small holes in the inlet walls. Plugging the holes, e.g., by ice or dirt, can cause a very large increase in distortion level.

Some inlets are designed with a center body or spike. At angle of attack, lift is generated by the center body causing shed vortices. The compressor is exposed to the vortices. Furthermore, to hold the spike in position, struts must be used. Strut wakes are another source of distortion.

External Aerodynamics

Mention has been made of the adverse effects of angle of attack and yaw. There are other aspects related to aircraft external aerodynamics. For example, variation of wing sweep can influence the flow into the inlet. Control deflection, e.g., rudder angle, can influence inlet flow. Such events as flap deployment, wheel extension, deployment of ram air turbines, etc., alter the external aerodynamics and the flow presented to the inlet.

Foreign Gas Ingestion

A foreign gas is any gas with specific gas constant or ratio of heat capacities different than the values for air. Even if the temperature of air and the temperature of foreign gas are equal, the different speed of sound of foreign gas can cause compressor stall.

Sources of foreign gas include exhaust of other aircraft when flying in formation, steam from a catapult, firing of armament including rockets and guns, and exhaust gas recirculation. This problem is usually associated with V/STOL; it can be a source of difficulty for nacelle mounted engines with thrust reversers. When rocket exhaust gases are ingested, there may be an additional problem beyond compressor stall. The exhaust gases are fuel rich and can cause explosions internal to the engine compartment.

Back Pressure Distortion

The back pressure caused by plugging the nozzle for thrust augmented V/STOL aircraft has been discussed. Pylon mounted turbofans are subjected to a circumferentially varying back pressure. When the wing is operating at high lift, the pressure at the fan exit near the wing is greater than at the bottom of the nacelle. This constitutes circumferential distortion.

Other sources of downstream disturbance in a fan duct are the pylon and struts which form the load path to transfer the thrust to the airframe. The struts alter the exit angle from the fan. Rubbert, Boctor, Cowan, and LaPrete designed a set of stator blades which shield the fan from the influence of the struts; see Reference 184.

Afterburner (Reheater) Transients

Afterburner transients, caused by ignition, shut down, or blow off, usually do not adversely affect turbojets. There are several arrangements for afterburners or duct burners as shown in Figure 7. The mixed flow turbofan afterburner of Figure 7(c) is particularly sensitive to transients. During afterburner ignition, a pressure pulse may be generated. The pressure pulse propagates upstream along the fan duct to the fan outlet. Momentarily the fan sees a much larger pressure ratio; fan stall may result.

Combustion in afterburners tends to be unstable[10]. Screech liners are added to suppress combustion instability. In the arrangements of either Figure 7(b) or 7(c), pressure waves associated with combustion instability can interact with the fan. The reflection coefficient for a fan is a complex quantity, i.e., a phase shift as well as gain or attenuation may occur.

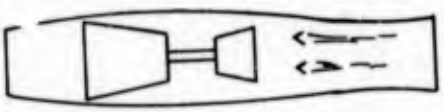

(a) Turbojet Afterburner

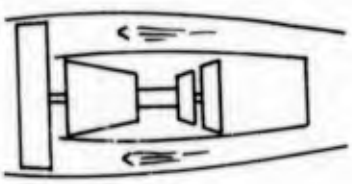

(b) Turbofan Duct Burner

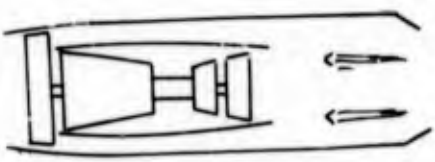

(c) Mixed Flow Turbofan Afterburner

Figure 7. Thrust Augmenters

Splitter Plate Stalls

A splitter plate in a turbofan engine is illustrated in Figure 4. At those operating points where the core mass flow is relatively large, or stated another way, where the bypass ratio is decreased, there is a large radial component of velocity. Flow separation can occur on the inner surface of the splitter plate as sketched in Figure 4. The separated flow region can generate unsteady, nonuniform flow into the core compressor.

Vortex Ingestion on Ground

When the wind blows over the ground, a boundary layer develops[11]. This boundary layer may extend 30 meters or more above the ground. As with all boundary layers, the flow is rotational. A turbofan or turbojet pumping air from the boundary layer concentrates the vorticity. This is analogous to the vortex in a draining bath tub; the vorticity present in the bath water is concentrated as the tub drains. The vorticity entering the compressor or fan can affect the stall margin in an adverse manner.

Similar vortex ingestion occurs during takeoff of aircraft with aft mounted engines such as Caravelle, DC-9, or 727. After brake release while the aircraft is moving slowly, the Reynolds number of the flow over the fuselage is small. A very thick boundary layer develops. At the same time, the engine inlet appears like a mass sink; the streamtube entering the engine diverges widely upstream of the inlet lips. The fuselage boundary layer is ingested. The vorticity could have a deleterious effect on compressor stall margin.

Clear Air Turbulence

Clear air turbulence (CAT) is generated by a variety of mechanisms including convective currents, high-level mountain waves, low-level terrain disturbances, and wind shear. Ultimately the source of energy for the turbulence is solar created temperature gradients in the atmosphere.

So far as the engine is concerned, the clear air turbulence results in a fluctuating velocity vector at the engine inlet. Local Mach numbers are varying. Experience has shown that engines which successfully qualify under other sources of distortion are not influenced greatly by CAT. Propulsion stability problems due to CAT are rare.

Stall Hammershock[12]

Stall hammershock is not a cause of engine instability but a consequence. When the compressor stalls, it no longer pumps air; the results are almost as if a valve had been closed. A shock wave propagates out the duct and inlet bringing the flow to rest behind it.

Auxiliary Power

The engine may supply power in a variety of forms for an array of uses. Power can be extracted in the form of bleed air, in the form of hydraulic pressure, or in the form of electrical power from the alternators. When power is switched on and off, the engine undergoes transients. If a bleed air valve is opened to drive pneumatic actuators somewhere in the aircraft, the mass flow into the compressor increases. Pressure ratio drops for a moment. Stages downstream of the bleed port have decreased mass flow which alters stage loading.

Transients due to varying auxiliary power extraction can initiate engine instability.

TYPES OF DISTORTION

Flow distortion is usually identified as pressure, temperature, or a foreign gas type of distortion. The types of distortion that are reported in engineering literature and employed to establish propulsion system compatibility are a reflection of instrumentation capability[13]. A long history of experience in dynamic pressure measurement is available; hence stagnation pressure is one measurement. Although most total temperature probes are very limited in frequency response (a few Hertz), it was recognized early that temperature distortion could cause stall. Consequently temperature distortion is another type. Measurements are rarely made of species concentration for foreign gas distortion. Impact of foreign gases on compressor behavior is not well known.

As yet measurements of velocity components have not been accomplished except in isolated tests. Furthermore, the vorticity components in a distorted flow must play a role.

In unsteady flow, spectral analysis and suitable moments of a distribution function are determined. The quantity most frequently measured is stagnation pressure.

Stagnation Pressure Distortion

Think of stagnation pressure as a function of three spatial coordinates, r, θ, and z, and time, t; cylindrical coordinates are convenient. Measurements are made at a plane, z = constant, upstream of the compressor. See Figure 8. The stagnation pressure is unsteady. A small fraction of the fluctuation is spatially in-phase; this can be expressed as

$$P(r,\theta,z,t) = P'(r,\theta,z,t) + P''(z,t) \qquad (2)$$

The pressure variation observed by a probe at (r,θ,z) consists of a spatially, uncorrelated portion, P', plus a spatially correlated pressure, P".

Stagnation pressure data are commonly processed in one of two ways[14]. One method, termed the deterministic method, is to plot instantaneous maps showing constant pressure contours. From the maps distortion indices may be evaluated. The other data reduction procedure, which is termed the statistical method, is to calculate mean values, correlations, power spectral density, amplitude probability density, and similar parameters. In either case, an attempt is made to correlate loss of stall margin with distortion parameters.

Stagnation Temperature Distortion[15-18]

Variations in stagnation temperature can cause compressor stall. Temperature variations may involve only air, but frequently a change in temperature is accompanied by foreign gases.

In one case a turbojet engine surged due to hot air which was cooling air. The propulsion system installation had a secondary air flow around the turbojet; the air was circulated by an ejector nozzle. The aircraft was taxiing with the wind up its tailpipe. Reversal of secondary air flow occurred; the hot air was ingested by the turbojet causing stall.

Many airports have grassy areas near the runway. Temperature differences between air adjacent to runway surface and nearby grass may be 30°F. Depending on local winds, or vortices from prior aircraft departures, the air temperature may vary markedly during takeoff.

As discussed previously, ingestion of steam, rocket exhaust, aircraft exhaust, gun propellant exhaust, etc., can cause temperature variations. One method to analyse the impact of temperature distortion is to use the parallel compressor model. Temperature variations cause a shift in corrected speed.

Temperature data are processed in a manner similar to pressure distortion. One distinction between pressure and temperature data is the frequency response of the respective transducers. Consequently, temperature data have limited frequency content.

Foreign Gas Ingestion[19-26]

Compressor maps give performance in terms of corrected variables; pressure ratio is plotted as a function of corrected weight flow rate with corrected angular speed $N/\sqrt{\theta}$ as a parameter. In the derivation of corrected variables, nondimensional similarity parameters are first derived. The appropriate nondimensional angular speed is NL/a, where L is a characteristic compressor length (e.g., tip radius) and a is a reference sound speed. The fact that sound speed is the appropriate quantity determining similarity is frequently overlooked. Since sound speed squared is given by

$$a^2 = \gamma RT/M \qquad (3)$$

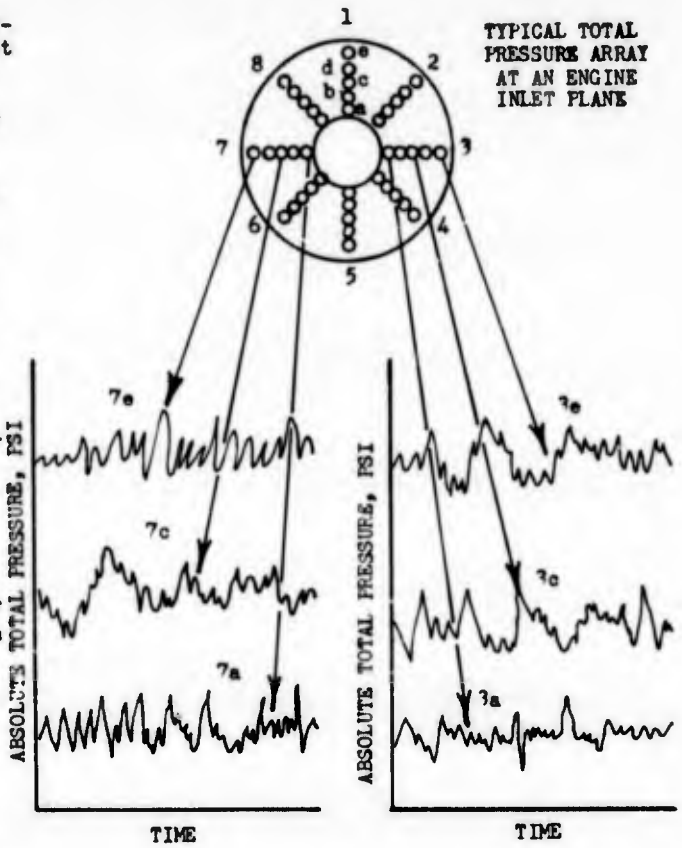

Figure 8. Typical Variation of Absolute Total Pressure at the Inlet of a Turbofan Engine. (Reproduced from Reference 14.)

it is apparent that foreign gases can be an important factor. In Equation (3) γ is heat capacity ratio, R is universal gas constant, M is molecular weight, and T is static temperature.

At room temperature, air has a sound speed of 1120 ft/sec. At the same temperature, steam has a sound speed of 1420 ft/sec. If corrected angular velocity is properly evaluated (i.e., using sound speed instead of θ only), pure steam causes a 27% shift.

Compressor stalls[20] were observed in the A-7A aircraft due to ingestion of steam from the catapult. One test that military engines must pass is that due to ingestion of rocket gases. Rocket gases are another case where both γ and M differ from air.

MANAGEMENT ASPECTS

Management Philosophy

Development of a complex aircraft has many facets; stability is only one of these. However, stability is important and merits careful attention by managers. Failure to achieve stability during flight test is a major deficiency.

One key to successful development is to know when the propulsion system is in trouble. To establish confidence and to insure compatibility between engine and inlet, it is necessary to conduct an adequate test program. The test program, which includes experiments conducted by both the airframe and engine companies, should have precise test goals written.

Traditionally aircraft manufacture is split into two distinct types of companies--the airframe and the engine companies. Having stated this well known fact, what are the implications for managers? Since two separate companies are involved, there must be an easy flow of information. Establish and maintain communication.

As an example of the need for communication, consider a decision by the engine company to change engine mass flow rate. This immediately has an impact on inlet duct and throat areas as well as spillage or additive drags. The airframe company must be aware of such changes.

Avoid split responsibility. Whoever is responsible must focus attention on the complete aircraft and not on the airframe and engine separately. There are three parties involved in the development of a new military aircraft; these are the customer, the airframe company, and the engine companies. One of these three groups must have or assume complete responsibility.

If an engine fails Military Qualification Test (MQT), there are serious repercussions for the engine company and the customer. There is tremendous emphasis on passing MQT, perhaps to the detriment of a complete engine stability developmental effort. Thought and discussion[27] have been given to revamping the FFRT/MQT method of qualifying military engines.

The inlet/engine, engine/nozzle, and airframe/inlet/nozzle interfaces must be defined precisely. Attempts have been made to model engine performance under all operating conditions including steady and unsteady flow. A successful model provides an extremely effective communication tool. The airframe company can run the engine model on its computer using its inlet and nozzle models.

Specifications

There are a vast array of specifications for procurement of military equipment. Known as MILSPEC, the specifications cover everything from application of paint, instruction manuals, packaging, electromagnetic interference, to blueprint drafting techniques. Some specifications[28] have sections devoted to distorted flow. For example, NAVAIR Specification AS 2684, "Engines, Aircraft, Turbojet, and Turbofan, General Specification for," covers "Adverse Inlet Conditions." Adverse conditions include steady and unsteady distortion, rocket exhaust ingestion, steam ingestion, anti-icing, atmospheric rain, sand ingestion, and engine wind milling.

A complete mastery of distortion induced engine instability has not been attained. Evidence for that statement is the fact that every major engine company and government propulsion research laboratory has one or more distortion indices. Without a complete understanding of distortion induced engine instability, it is impossible to write a definitive engine specification. However, present day engine specifications should, and do, reflect the latest thinking that has been experimentally verified.

SAE Aerospace Recommended Practice

The Chairman of SAE S-16 Committee, Mr. H. I. Bush[29], prepared a short resume of the purpose and progress as of mid-1974; his comments are quoted:

> "The Society of Automotive Engineers (SAE) Aerospace Council Divisional Technical Committee S-16 was formed in 1972. The purpose of S-16 is to formulate and propose a set of 'Aerospace Recommended Practices' (ARP) to provide a procedure by which the stability and performance of the propulsion system, as affected by inlet flow distortion, can be elevated to a key factor in trade studies, interface agreements, engine qualification, and aircraft flight. An ARP is employed for 'dimensional, design, or performance recommendations based on sound engineering principles and which is intended as a guide toward standard engineering practice.' The Committee recognizes that technical disciplines that directly affect this important aspect of engine design, development, and use are presently undergoing rapid technological advances. It also recognizes that a start must be made toward reducing to industry-wide accepted practice the advances that have been made over the last five years. Therefore the ARP, while intended as a guide toward standard practice, may be subject to frequent change to keep pace with experience and technical advances.
>
> "Active, participating membership of the Committee consists of representatives of the Air Force, Navy, NASA, FAA, four major engine companies, and seven major aircraft companies. The format of the ARP has been defined as a working outline. Definitions of various terms critical to engine stability have been agreed upon. A working outline has been established which describes the uses of a distortion descriptor system during various phases of a development program. Technical guidelines for a distortion descriptor system have been established which will be used by the Committee as criteria upon which the descriptor system to be adopted will be based. The Committee expects to formulate this descriptor system during the next year, and submit the resulting proposed ARP to the Aerospace Council shortly thereafter. At that time the proposed ARP will probably be made available for review."

STATISTICAL NATURE OF DISTORTION AND ENGINE INSTABILITY[14, 30-33]

Pressure measured by a single transducer as a function of time shows a random distribution with a few discrete frequencies.[31] The pressure probability density distributions typically have a near-Gaussian shape; slight skewing may be present[30]. Distortion indices, which are derived from pressure measurements by algebraic manipulations, likewise have near-Gaussian shape.

Since the pressure fluctuations are random in nature, the contours of pressure maps at the compressor face do not repeat geometric shape. The function of the distortion index is to reduce the geometry of a map to a single number. For any value of the index, there are many different map geometries. Hopefully the index captures those features of the map geometry causing adverse flow conditions for the compressor. For a critical value of the distortion index, the compressor should have zero stall margin remaining. Values of index larger than critical cause stall.

Since the values of the index occur in a random manner, measurement of pressure over a finite time span may not yield the peak instantaneous distortion. Jacocks[30] has investigated the statistics of extremum values of distortion, D. Using experimental data, he found that D could be represented by

$$D(y) = a + by \tag{4}$$

where a is expected or most probable maximum instantaneous distortion, b is the expected rate of increase of D with time, and y is a probability variate related to observation time. Jacocks[30] proposes that quantities a and b be used to characterize an engine/inlet system in lieu of distortion, D.

As pointed out by Kimzen and McIlveen[14], two approaches generally are taken for interpretation of distortion data. One approach, which is termed deterministic, is to generate an instantaneous pressure map or distortion index at a frequency near compressor rotational speed. Compressor behavior is determined as a function of the time-sequence of maps or indices. The other approach is called statistical and involves calculation of rms values, autocorrelations, cross correlations, power

spectral density, amplitude probability density functions, etc. These statistical parameters are used to assess engine stability.

Briefly stated, the random character of distortion means that engine stability can be stated only in a probabilistic sense; e.g., at Mach 0.8, 23,000 feet altitude, and 18° angle of attack, the probability of engine surge with military power is 5% for a time span of 6 minutes.

PERSPECTIVE ON LECTURE SERIES

Sources of Distortion and Engine/Inlet Compatibility[34-50]

As mentioned earlier, the inlet is the primary source of distortion. Inlets can be designed to minimize distortion; e.g., usually increased boundary layer bleed decreases distortion levels. Inlet parameters influencing distortion include inlet location relative to airframe, compression surface design, choice of degree of internal compression, bleed, bypass, and location of auxiliary intakes for low-speed, high-power, flight.

What constitutes a complete inlet specification and test? This question will be addressed.

Correlations can be obtained between pressure recovery, turbulence intensity, and $\Delta P_T/\bar{P}_T$. Poor pressure recovery frequently results in high distortion.

There is a trade possible to achieve propulsion compatibility. By adding weight and drag, the inlet can provide almost any level of flow uniformity. Perhaps the added weight would be better invested in the compressor by decreasing stage loading. A trade exists between inlet distortion level and engine distortion tolerance.

Lecture 2 discusses many of the aspects mentioned above.

Aerodynamic Response[51-142]

Distorted flow may cause engine surge. The surge is a consequence of compressor stall. Stall results from flow separation on stator or rotor blades. The separation phenomena may be steady, i.e., confined to a fixed location, or unsteady. Unsteadiness may be the consequence of unsteady distorted flow, rotor motion, or rotating stall. Understanding of unsteady stall requires a mastery of unsteady boundary layer flows.

Compressor maps are altered by distorted flow. Stall lines are depressed. Efficiency contours are shifted. Mass flow rates usually decrease.

One model that is used to describe aerodynamic response is the parallel compressor. Surge sensitivity can be understood by use of this model. Another approach is the critical sector concept.

Separately, or in combination, pressure, foreign gas, and temperature distortion can be understood, at least partially, by the parallel compressor model.

Lecture 3 addresses aerodynamic response.

Aeromechanical Response[143-147]

The unsteady forces generated by compressor stall can cause large dynamic stresses in the blades. In the absence of stall, blade flutter also creates abnormal stresses. Fatigue life of blades is consumed rapidly by the dynamic response.

Distorted flow can cause stall in one of the late stages of a multistage compressor. A hammershock forms and passes over the upstream blades creating large transient loads.

Transient loads generated by or as a consequence of distorted inlet flow are discussed in Lecture 4.

Prediction Techniques[148-165]

One goal of analysis and experiments is to develop an ability to predict compressor instability as a function of distorted flow parameters. Models are developed for three classes of problem depending on influence of spatial or temporal features. The models are first, space-dependent, time-independent; second, space-independent, time-dependent; and third, both space and time dependent.

Lecture 5 incorporates the analytical models necessary for predicting compressor stability.

Test Techniques, Instrumentation, and Data Processing[149, 166-180]

When 40 pressure transducers are providing measurements at a rate of 2000 Hz, every 12.5 seconds 10^6 data points are generated. Data processing must be efficient to avoid large costs and long time delay.

Tests may be conducted in a propulsion wind tunnel, altitude test facility, test cell, or in flight. In any of these tests, the environment for transducers is severe. High temperature, large noise and vibration levels, etc., place rigid demands on instrumentation.

Lecture 6 discusses how to make the measurements necessary for understanding distortion induced engine instability.

Methods to Increase Stability and Distortion Tolerance[7, 8, 181-189]

One way to solve the problem of distorted flow is to make the compressor and engine completely tolerant of any flow. Obviously, this is not possible; however, substantial improvement can be made by suitable design. The designer has at his disposal such variables as tip clearance, casing treatment, blade aspect ratio, external cavities, operating point, and solidity.

The interaction of various compressor design variables with radial and circumferential distorted flow is discussed in Lecture 7.

CONCLUSIONS

Propulsion systems must operate stably throughout the flight envelope. Assurance of stable operation requires a significant fraction of funds and time required to develop a new airframe and propulsion system.

Distorted flow is random in nature so that engine stability can only be stated as a probability. Measurement techniques are complex, and numerous transducers are needed to quantify distortion and its influence.

Engine instability continues as a problem with each new development. Trends in engine design, e.g., higher tip speeds, highly loaded blades, etc., and in aircraft requirements, e.g., broad Mach and Reynolds number operation, keep propulsion stability as an active item.

Engine response, either aerodynamic or mechanical, is not completely understood, although there have been large gains in the past decade. Due to the complexity of the problem, it probably will be a long time before attainment of engine stability is reduced to a cook book procedure.

REFERENCES

1. J. L. Campbell and S. Ellis, "Inlet-Engine Compatibility Analysis," AIAA Paper 70-941, June 1970.

2. J. S. Holchusen, "Analysis and Demonstration Techniques for Installation Aerodynamic Effects on High Bypass Turbofans," 32nd Meeting, PEP, AGARD, NATO, Sept. 1968.

3. J. Matechak and L. A. Thomas, "Final Report J52-P-8A Engine Stall Margin Investigation," Naval Air Test Center, Patuxent River, MD, NATC-ST-64R-69, August 1969, AD 857 849L.

4. J. H. Povolny, "Stall and Distortion Investigation of a YTF30-P-1 Turbofan Engine," Airframe-Propulsion Compatibility Symposium, AFAPL/AFFDL, WPAFB, June 1969.

5. R. A. Mays, "Inlet Dynamics and Compressor Surge," AIAA Paper 69-484, 1969.

6. F. P. Povinelli, J. H. Dittmar, and R. P. Woodward, "Effects of Installation Caused Flow Distortion on Noise from a Fan Designed for Turbofan Engines," NASA TN D-7076, November 1972.

7. J. W. McBride, "Compressor Development - Art or Science?" AIAA Paper 66-614, 1966.

8. M. J. Hartmann, W. A. Benser, C. H. Hauser, and R. S. Ruggeri, "Fan and Compressor Technology," Chapter I, Aircraft Propulsion, NASA SP 259, 1971.

9. U. W. Schaub and R. W. Bassett, "Flow Distortion and Performance Measurements on a 12" Fan-in Wing Model for a Range of Forward Speeds and Angle of Attack Settings," Paper 17, AGARD-CP-91-71, 1971.

10. A. E. Fuhs, "Combustion Research Problems Associated with Advanced Air Breathing Engines," AIAA Paper 71-1, 1971.

11. J. L. Colehour and B. W. Farquhar, "Inlet Vortex," J. Aircraft, 8, pp. 39-43, January 1971.

12. F. L. Marshall, "Prediction of Inlet Duct Overpressures Resulting from Engine Surge," AIAA Paper 72-1142, 1972.

13. A. E. Fuhs and M. Kingery, Editors, Instrumentation for Air Breathing Propulsion, Volume 34, AIAA Progress Series in Aeronautics and Astronautics, MIT Press, Cambridge, Mass., 1974.

14. W. F. Kimzey and M. W. McIlveen, "Analysis and Synthesis of Distorted and Unsteady Turbo Engine Inlet Flow Fields," paper presented at AIAA Seventh Propulsion Joint Specialist Conference, Salt Lake City, Utah, June 1971.

15. D. S. Gabriel and others, "Some Effects of Transients in Inlet Pressure and Temperature on Turbojet Engine," Preprint 709, IAS, New York, New York, January 1957.

16. L. E. Wallner, J. W. Useller, and M. J. Saari, "A Study of Temperature Transients at the Inlet of a Turbojet Engine," NACA RM E57022, 1957.

17. R. A. Rudey and R. J. Antl, "The Effect of Inlet Temperature Distortion on the Performance of a Turbofan Engine Compressor System," AIAA Paper 70-625, 1970.

18. W. M. Braithwaite, E. J. Graber, Jr., and C. M. Mehalic, "The Effect of Inlet Temperature and Pressure Distortion on Turbojet Performance," AIAA Paper 73-1316, 1973.

19. T. J. McCarey and J. A. Stephens, "TF34-GE-2 Engine Qualification, Rocket Gas Ingestion Test," General Electric Report R71AEG432, 31 December 1971.

20. W. E. Mallett and E. M. Parcells, "Catapult Steam Ingestion Test of Three Turbofan Engines in the A-7 Aircraft," paper presented at the Tenth National Conference on Environmental Effects on Aircraft and Propulsion Systems Trenton, New Jersey, 18-20 May 1971.

21. J. H. Childs and others, "Stall and Flame-Out Resulting from Firing of Armament," NACA RM E55E25, 1955.

22. N. R. Tomassetti, "Steam Ingestion by Aircraft Gas Turbine Engines," paper presented at the Seventh National Conference on Environmental Effects on Aircraft and Propulsion Systems, Princeton, New Jersey, 25-27 September 1967.

23. N. R. Tomassetti and G. R. Mink, "Steam Ingestion by Aircraft Gas Turbine Engines-II," paper presented at the Eighth National Conference on Environmental Effects on Aircraft and Propulsion Systems, Bordentown, New Jersey, 8-10 October 1968.

24. P. Worobel, "Steam Ingestion Tests of a Pratt and Whitney Aircraft TF30-P-8 Turbofan Engine," NAPTC-ATD-183, November 1971.

25. W. A. Rich and R. A. Real, "J52-P-6A Engine, Sea Level Missile Exhaust Gas Ingestion Tests," May 1969.

26. W. A. Rich, "The Simulation of the Ingestion of Missile Exhaust by Turbojets," paper presented at the Tenth National Conference on Environmental Effects on Aircraft and Propulsion Systems, Trenton, New Jersey, 18-20 May 1971.

27. "Announcement for Symposium on Propulsion System Structural Integration and Engine Integrity," Naval Postgraduate School, Monterey, CA, September 3-6, 1974.

28. "General Specification for Aircraft Turbojet and Turbofan Engines," Naval Air Systems Command, AS 2684, 3 December 1970.

29. H. I. Bush, Chairman, SAE Committee S-16, Personal Communication, 26 April 1974.

30. J. L. Jacocks, "Statistical Analysis of Distortion Factors," AIAA Paper 72-1100, 1972.

31. D. A. Sherman, D. L. Motycka, and G. C. Oates, "Experimental Evaluation of a Hypothesis for Scaling Inlet Turbulence Data," AIAA Paper 71-669, 1969.

32. R. C. Crites and M. V. Heckart, "Application of Random Data Techniques to Aircraft Inlet Diagnostics," AIAA Paper 70-597, 1970.

33. J. E. Calogeras, P. L. Burstadt, and R. E. Coltrin, "Instantaneous and Dynamic Analysis of Supersonic Inlet Engine Compatibility," AIAA Paper 71-667, June 1971.

34. A. W. Martin, L. C. Kostin, and S. D. Millstone, "Dynamic Distortion at the Exit of a Subsonic Diffuser of a Mixed Compression Inlet," NASA CR-1644, December 1970.

35. H. Eibl and R. Friedrichs, "Wind Tunnel Investigations of a Supersonic Air Intake with Various Auxiliary Intakes at Low Speeds," Paper 35, AGARD-CP-91-71, 1971.

36. R. J. Baumbick, R. E. Wallhagen, and R. C. Seidel, "Terminal Shock and Restart Control of a Mach 2.5, Axisymmetric, Mixed-Compression Inlet with 40-Percent Internal Contraction," NASA TMX-2992, February 1974.

37. A. C. Brown, H. F. Nawrocki, and P. N. Paley, "Subsonic Diffusers Designed Integrally with Vortex Generators," J. Aircraft, 5, pp. 221-229, 1968.

38. J. L. Livesey and A. O. Odukwe, "Some Effects of Normal Shock Boundary Layer Interaction on the Performance of Straight Walled Conical Diffusers," AIAA Paper 72-1140, 1972.

39. J. M. Saylor and R. E. Smith, Jr., "Internal and External Aerodynamics of the C-141A Nacelle," AIAA Paper 65-604, 1965.

40. R. G. Schweikhardt and R. P. Grippe, "Investigations in the Design and Development of a Bypass Door Control System for an SST Axisymmetric Intake Operating in the External Compression Mode," AIAA 70-695, 1970.

41. T. A. Reyhner and T. E. Hickcox, "A Procedure for Combined Viscous-Inviscid Analysis of Supersonic Inlet Flow Fields," AIAA Paper 72-44, 1972.

42. D. N. Bowditch, "Some Design Considerations for Supersonic Cruise Mixed Compression Inlets," AIAA Paper 73-1269, 1973.

43. W. W. Rhoades, "A Semi-Empirical Method for Predicting Subsonic Diffuser Performance," AIAA Paper 73-1272, 1973.

44. J. F. Wasserbauer, R. J. Shaw, and H. E. Neumann, "Minimizing Boundary-Layer Bleed for a Mixed Compression Inlet," AIAA Paper 73-1270, 1973.

45. J. P. Hancock and B. L. Hinson, "Inlet Development for the L-500," AIAA Paper 69-448, 1969.

46. N. E. Sorensen and D. B. Smeltzer, "Performance Estimates for a Supersonic Axisymmetric Inlet System," AIAA Paper 72-45, 1972.

47. J. Syberg and J. L. Koncsek, "Bleed System Design Technology for Supersonic Inlets," AIAA Paper 72-1138, 1972.

48. N. E. Sorensen and D. P. Bencze, "Possibilities for Improved Supersonic Inlet Performance," AIAA Paper 73-1271, 1973.

49. C. J. MacMiller, "Investigation of Subsonic Duct Distortion," AIAA Paper 69-449, 1969.

50. W. E. Anderson and N. D. Wong, "A Two-Dimensional Mixed Compression, Inlet System Designed to Self-Restart at a Mach Number of 3.5," AIAA Paper 69-447, 1969.

51. E. J. Graber, Jr., and W. S. Braithwaite, "Summary of Recent Investigation of Inlet Flow Distortion Effects on Engine Stability," AIAA Paper 74-236, 1974.

52. L. M. Wenzel, "Experimental Investigation of the Effects of Pulse Pressure Distortions Imposed on the Inlet of a Turbofan Engine," NASA TMX-1928, November 1969.

53. E. A. VanDeusen and V. R. Mardoc, "Distortion and Turbulence Interaction, A Method for Evaluating Engine/Inlet Compatibility," AIAA Paper 70-632, June 1970.

54. G. A. Flourde and B. Brimelow, "Pressure Fluctuations Cause Compressor Instability," paper presented at the Airframe/Propulsion Compatibility Symposium sponsored by AFAFL/AFFDL, WPAFB, Ohio, 25 June 1969.

55. F. F. Ehrich, "Circumferential Inlet Distortions in Axial Flow Turbomachinery," J. Aero. Sci, 24, pp. 413-417, June 1957.

56. J. E. Calogeras, C. M. Mehalic, and P. L. Bursvadt, "Experimental Investigation of the Effect of Screen-Induced Total Pressure Distortion on Turbojet Stall Margin," NASA TMX-2239, March 1971.

57. J. E. McAulay, "Effect of Dynamic Variations in Engine-Inlet Pressure on the Compressor System of a Twin-Spool Turbofan Engine," NASA TMX-2081, September 1970.

58. C. J. Farmer, "Inlet Distortion, Vorticity, and Stall in an Axial-Flow Compressor," MSAE Thesis, Naval Postgraduate School, Monterey, CA, March 1972.

59. M. M. Iverson, "Conversion of Inlet Temperature Distortions to Vorticity for an Axial-Flow Compressor," MSAE Thesis, Naval Postgraduate School, Monterey, CA, June 1972.

60. J. H. Povolny and others, "Effects of Engine Inlet Disturbances on Engine Stall Performance," NASA SP-259, 1971.

61. H. Mokelke, "The Unsteady Response of an Axial Flow Compressor with a Distorted Inlet Flow," paper submitted to the Turbomachinery Subcommittee of the ARC Meeting, 2 October 1970, CP 1203, 1972.

62. D. Zonars, "Dynamic Characteristics of Engine Inlets," AGARD NATO Lecture Series No. 53, 1972.

63. D. D. Williams and J. J. Yost, "Some Aspects of Inlet/Engine Compatibility," ICAS Paper 72-19, 1972.

64. H. Mokelke, "The Development of Inlet Flow Distortions in Multi-Stage Axial Compressors of High Hub-Tip Ratio," AIAA Paper.

65. B. Brimelow, "Performance Matching of the Propulsion System," SAE Preprint 680712, Aeronautics and Space Engineering and Manufacturing Meeting, Los Angeles, CA, Oct. 7-11, 1968.

66. J. J. Adamczyk and F. O. Carta, "Unsteady Fluid Dynamic Response of an Isolated Rotor with Distorted Flow," AIAA Paper 74-49, 1974.

67. J. A. Korn, "The Effect of Inlet Distortion on the Performance and Stability of the Low Speed Spool of a Turbofan Engine," AIAA Paper 74-233, 1974.

68. C. Reid, "The Response of Axial Flow Compressors to Intake Flow Distortion," ASME Paper 69-GT-29, 1969.

69. G. A. Plourde and A. H. Stenning, "Attenuation of Circumferential Inlet Distortion in Multistage Axial Compressors," J. Aircraft, 5, pp. 236-242, 1968.

70. I. A. Johnsen and R. O. Bullock, Editors, Aerodynamics Design of Axial Flow Compressor, NASA SP-36, 1965.

71. P. Crimi and B. L. Reeves, "A Method for Analyzing Dynamic Stall of Helicopter Rotor Blades," NASA CR-2009, May 1972.

72. P. Crimi, "Analysis of Stall Flutter of a Helicopter Rotor Blade," NASA CR-2322, November 1973.

73. P. Crimi and B. L. Reeves, "A Method for Analyzing Dynamic Stall," AIAA Paper 72-37, January 1972.

74. W. R. Hawthorne, "Secondary Circulation in Fluid Flow," Proc. Roy. Soc., Series A, Math and Phys. Sciences, No. 1086, 206, pp. 374-387, 7 May 1951.

75. J. H. Horlock, "Annulus Wall Boundary Layers in Axial Compressor Stages," Trans. ASME, J. Basic Eng., pp. 55-65, March 1963.

76. J. M. Stephson, "Secondary Flow in Cascades," J. Aero Sci., 18, pp. 699-700, 1951.

77. A. G. Smith, "On the Generation of the Streamwise Component of Vorticity for Flows in Rotating Passages," Aero Quarterly, VIII, Part 4, pp. 369-383, 1957.

78. H. E. Herzig and A. G. Hanson, "Visualization Studies of Secondary Flows with Applications to Turbomachines," ASME Transactions, 77, pp. 249-266, 1955.

79. R. A. Hartunian, "Research on Rotating Stall in Axial Flow Compressors," Wright Air Development Center Tech. Rep. 59-75, Parts I and II, Cornell Aero. Lab., Inc., Buffalo, N. Y., January 1959.

80. H. Yeh, "An Actuator Disc Analysis of Inlet Distortion and Rotating Stall in Axial Flow Turbomachines," J. Aero Sci., 26, pp. 739-753, November 1959.

81. H. Schlichting and A. Das, "On the Influence of Turbulence Level on the Aerodynamic Losses of Axial Turbomachines," Flow Research on Blading, edited by L. S. Dzung, Elsevier, pp. 243-274, 1970.

82. W. R. Hawthorne and others, Aerodynamics of Turbines and Compressors, Princeton University Press, pp. 277-296 and pp. 342-367, 1964.

83. J. Valensi, "Experimental Investigation of the Rotating Stall in a Single-Stage Axial Compressor," J. Aero. Sci., 25, pp. 1-10, January 1958.

84. J. H. Horlock, Axial Flow Compressors, Butterworths, 1958.

85. M. C. Huppert and W. A. Benser, "Some Stall and Surge Phenomena in Axial Flow Compressors," J. Aero. Sci., 20, pp. 835-845, December 1953.

86. L. S. Dzung and C. Seippel, "Aerodynamic Aspects of Blading Research," Flow Research on Blading, edited by L. S. Dzung, Elsevier, pp. 1-50, 1970.

87. W. R. Hawthorne and R. A. Novak, "The Aerodynamics of Turbomachinery," Annual Review of Fluid Mechanics, edited by W. R. Sears, Annual Reviews, pp. 341-366, 1969.

88. F. E. Marble, "Three-Dimensional Flow in Turbo-Machines," Aerodynamics of Turbines and Compressors, edited by W. R. Hawthorne, Princeton University Press, pp. 83-165, 1964.

89. W. D. Rannie, "The Axial Compressor Stage," Aerodynamics of Turbines and Compressors, edited by W. R. Hawthorne, Princeton University Press, pp. 313-367, 1964.

90. L. E. Ericsson and J. P. Reding, "Unsteady Airfoil Stall, Review and Extension," J. of Aircraft, 8, pp. 609-616, 1971.

91. F. O. Carta, "Effect of Unsteady Pressure Gradient Reduction on Dynamic Stall Delay," J. of Aircraft, 8, pp. 839-841, 1971.

92. F. O. Carta, "Unsteady Normal Force on an Airfoil in a Periodically Stalled Inlet Flow," J. of Aircraft, 4, pp. 416-421, 1967.

93. G. S. Samoylovich, "Unsteady Flow Around and Aeroelastic Vibration in Turbomachine Cascades," Air Force Systems Command, Foreign Technology Division Report AD 721 959, 23 February 1971.

94. B. Schorr and K. C. Reddy, "Inviscid Flow Through Cascades in Oscillatory and Distorted Flow," AIAA Paper 70-131, January 1970.

95. S. Lieblein, F. C. Schwenk, and R. L. Broderick, "Diffusion Factor for Estimating Losses and Limiting Blade Loadings in Axial-Flow-Compressor Blade Elements," NACA RM E53D01, 1953.

96. S. Lieblein, "Loss and Stall Analysis of Compressor Cascades," Trans. ASME, J. Basic Eng., pp. 387-400, September 1959.

97. B. Lakshminarayana and J. H. Horlock, "Review: Secondary Flows and Losses in Cascades and Axial-Flow Turbomachines," Int'l. J. Mech. Sci., 5, pp. 287-307, 1963.

98. J. H. Horlock, J. F. Louis, P. M. E. Percival, and B. Lakshminarayana, "Wall Stall in Compressor Cascades," Trans. ASME, J. Basic Eng., pp. 637-648, September 1966.

99. R. H. Tindell, "F-14 Inlet Maneuvering Capability," AIAA Paper 73-1273, 1973.

100. J. F. Louis, "Secondary Flow and Losses in a Compressor Cascade," ARC Reports and Memoranda No. 3136, March 1958.

101. J. Fabri, "Rotating Stall in Axial Flow Compressors," Conference on Internal Aerodynamics, Internal Aerodynamics, Institution of Mech. Eng., Cambridge, July 1967.

102. W. G. Brady, G. R. Ludwig, R. S. Rice, Jr., and E. F. Schroeder, "Analytical and Experimental Investigation of Rotating Stall Phenomena in Turbine Engine Compressors," AFAPL-TR-67-19, Cornell Aero. Lab., Inc., Buffalo, N. Y., March 1967.

103. G. R. Ludwig, J. P. Nenni, and R. S. Rice, Jr., "An Investigation of Rotating Stall Phenomena in Turbine Engine Compressors," AFAPL-TR-70-26, Cornell Aero. Lab., Inc., Buffalo, N. Y., May 1970.

104. W. G. Brady and G. R. Ludwig, "Basic Studies of Rotating Stall and an Investigation of Flow-Instability Sensing Devices," AFAPL-TR-65-115, Part I, Cornell Aero. Lab., Inc., Buffalo, N. Y., October 1965.

105. F. F. Ehrich and R. W. Detra, "Transport of the Boundary Layer in Secondary Flow," J. Aero. Sci., 21, pp. 136-138, February 1954.

106. D. G. Gregory-Smith, "An Investigation of Annulus Wall Boundary Layers in Axial-Flow Turbomachines," J. Eng. Power, 92, pp. 369-376, October 1970.

107. A. D. S. Carter, "Three-Dimensional-Flow Theories for Axial Compressors and Turbines," Proc. Instn. Mech. Engrs., 159, pp. 255-268, 1948.

108. H. Griepentrog, "Secondary Flow Losses in Axial Compressors," AGARD Lecture Series No. 39 on Advanced Compressors, May 1970.

109. T. Iura and W. D. Rannie, "Experimental Investigation of Propagating Stall in Axial-Flow Compressors," Trans. ASME, 76, pp. 463-471, April 1954.

110. F. E. Marble, "Propagation of Stall in a Compressor Blade Row," J. Aero. Sci., 22, pp. 541-554, August 1955.

111. W. R. Hawthorne, "Some Formulae for the Calculation of Secondary Flow in Cascades," ARC Report 17519, March 1955.

112. B. Lakshminarayana and J. H. Horlock, "Leakage and Secondary Flows in Compressor Cascades," ARC Reports and Memoranda No. 3483, March 1955.

113. H. B. Squire and K. G. Winter, "The Secondary Flow in a Cascade of Airfoils in a Nonuniform Stream," J. Aero. Sci., 18, pp. 271-277, April 1951.

114. J. H. Preston, "A Simple Approach to the Theory of Secondary Flows," Aero. Quarterly, V, pp. 218-234, September 1954.

115. W. R. Hawthorne, "Rotational Flow Through Cascades, Part I. The Components of Vorticity," Quart. J. Mech. Applied Math., VIII, pp. 266-279, 1955.

116. W. R. Hawthorne and W. D. Armstrong, "Rotational Flow Through Cascades, Part II. The Circulation about the Cascade," Quart. J. Mech. Applied Math., VIII, pp. 280-292, 1955.

117. G. F. Hausmann, "The Theoretical Induced Deflection Angle in Cascades Having Wall Boundary Layers," J. Aero. Sci., 15, pp. 686-690, November 1948.

118. E. J. Milner, L. M. Wenzel, and F. J. Paulovich, "Frequency Response of an Axial-Flow Compressor Exposed to Inlet Pressure Perturbations," NASA TMX-3012, April 1974.

119. L. H. Smith, "Secondary Flow in Axial-Flow Turbomachinery," Trans. ASME, 77, pp. 1065-1076, October 1955.

120. F. F. Ehrich, "Secondary Flows in Cascades of Twisted Blades," J. Aero. Sci., 22, pp. 51-60, January 1955.

121. M. Honda, "Theory of Shear Flow Through a Cascade," Proc. R. Soc., 265, pp. 46-70, 1961.

122. F. O. Carta, "Analysis of Unsteady Aerodynamics Effects on an Axial Flow Compressor Stage with Distorted Inflow," Project SQUID Tech. Rep. UARL-1-FU, July 1972.

123. A. A. Mikolajczak, J. L. Kerrebrock, and F. Roberts, "Intra Stator Transport of Rotor Wakes and Its Effect on Compressor Performance," Pratt and Whitney Aircraft, Technical Report MR-1068.

124. J. Dunham, Non-Axisymmetric Flows in Axial Compressors, Mechanical Engineering Science Monograph No. 3, Inst. of M. E., London, 1965.

125. J. F. Louis, "A Different Type of Propagating Stall. Propagation of a Reverse Flow Cell in a Rotor," Univ. of Cambridge, D. D. G. (Eng), Ref: Eng R/280/0/21 TIL (BR)280, September 1957, Ministry of Supply, U. K.

126. H. Kuhl, H. Weyer, and M. Lecht. "Experimentelle Ergebnisse an einer Transsonischen Axialverdichterstufe bei Stationärer Gesamtdruckstörung im Einlauf," DFVLR, December 1972.

127. R. A. Werner, M. Abdelwahab, and W. M. Braithwaite, "Performance and Stall Limits of an Afterburner-Equipped Turbofan Engine With and Without Inlet Flow Distortion," NASA TMX-1947, April 1970.

128. G. C. Oates, D. A. Sherman, and D. L. Motycka, "Experimental Study of Inlet-Generated Pressure Fluctuations," Pratt and Whitney Aircraft, Technical Report PWA-3682.

129. T. Bratanow, A. Ecer, and M. Kobiske, "Numerical Calculations of Velocity and Pressure Distribution Around Oscillating Airfoils," NASA CR-2368, February 1974.

130. E. E. Bailey and R. S. Ruggeri, "Experimental Data for Two 1400 Feet-per-Second Tip Speed Compressor Rotors Operated with Inlet Flow Distortions," NASA TMX-1798, May 1969.

131. J. J. Adamczyk and F. O. Carta, "Unsteady Fluid Dynamic Response of an Axial-Flow Compressor Stage with Distorted Inflow," Project SQUID Technical Report UARL-2-PU, July 1973.

132. F. Roberts, G. Flourde, and F. Smakula, "Insights into Axial Compressor Response to Distortion," AIAA Fourth Propulsion Joint Specialist Conference, 1968.

133. W. Jansen, M. C. Sworden, and A. W. Carlson, "Compressor Sensitivity to Transient and Distorted Transient Flows," AIAA Paper 71-670, 1971.

134. R. E. Henderson and J. H. Horlock, "An Approximate Analysis of the Unsteady Lift on Airfoils in Cascades," ASME Paper 72-GT-5, 1972.

135. H. J. Schroder and P. Schuster, "Actuator Disc Flow Calculated by Relaxation - An Approach to the Analysis Problem of Turbomachinery," ASME 72-GT-26, 1972.

136. H. Naumann and H. Yeh, "Lift and Pressure Fluctuations of a Cambered Airfoil under Periodic Gusts and Applications in Turbomachinery," ASME Paper 72-GT-30, 1972.

137. K. Bammert and R. Milsch, "Boundary Layers on Rough Compressor Blades," ASME 72-GT-48, 1972.

138. H. Takata and S. Nagano, "Nonlinear Analysis of Rotating Stall," ASME 72-GT-3, 1972.

139. S. Nagano, H. Takata, and Y. Machida, "Dynamic Performance of Stalled Blade Rows," JSME/ASME Paper JSME-11, 1971.

140. G. Mellor, "A Combined Theoretical and Empirical Method of Axial Compressor Cascade Prediction," ASME Paper 72-WA/GT-5, 1972.

141. R. M. Scruggs, J. F. Nash, and R. E. Singleton, "Analysis of Flow Reversal Delay for a Pitching Foil," AIAA Paper 74-183, 1974.

142. T. Katsanis, "Quasi-Three-Dimensional Calculation of Velocities in Turbomachine Blade Rows," ASME Paper 72-WA/GT-7, 1972.

143. W. E. Trumpler, Jr., and H. M. Owens, "Turbine-Blade Vibration and Strength," Trans. ASME, 77, pp. 337-342, 1955.

144. S. Fleeter, "Aeroelasticity in Turbomachines - A Field All Aflutter," Astro. and Aero., 10, pp. 56-59, 1972.

145. C. Danforth, "Distortion Induced Vibration in Fan and Compressor Blades," AIAA Paper 74-232, 1974.

146. Y. Cavaillé, "Aerodynamic Damping in Turbomachinery," ASME 72-GT-8, 1972.

147. J. F. Ward, "Helicopter Rotor Differential Pressures and Structural Response Measured in Transient and Steady-State Maneuvers," J. Am. Helicopter Soc., 16, pp. 16-25, January 1971.

148. R. J. Martin and H. C. Melick, Jr., "A Feasibility Study for Definition of Inlet Flow Quality and Development Criteria," AIAA Paper 72-1098, 1972.

149. R. E. Coltrin and J. E. Calogeras, "Supersonic Wind Tunnel Investigation of Inlet-Engine Compatibility," AIAA Paper 69-487, 1969.

150. J. A. Korn, "Estimated Effect of Circumferential Distortion on Axial Compressors Using Parallel Compressor Theory and Dynamic Stall Delay," AIAA Paper 74-233, 1974.

151. D. A. Oliver and P. Sparis, "A Computational Study of Three-Dimensional Transonic Shear Flow in Turbomachine Cascades," AIAA Paper 71-83, 1971.

152. R. B. Gray and G. A. Pierce, "Exploratory Investigation of Sound Pressure Level in the Wake of an Oscillating Airfoil in the Vicinity of Stall," NASA CR-1948, February 1972.

153. J. F. Kuhlberg, D. E. Sheppard, E. O. King, and J. R. Baker, "Dynamic Simulation of Turbine Engine Compressors," AIAA Paper 69-486, 1969.

154. D. F. Brunda and J. F. Boytos, "A Steady-State Circumferential Inlet Pressure Distortion Index for Axial-Flow Compressors," paper presented at the ASME Gas Turbine Conference Products Show, Houston, Texas, March 28 - April 1, 1971.

155. D. F. Brunda and J. F. Boytos, "A Steady-State Radial Inlet Pressure Distortion Index for Axial-Flow Compressors," ASME 92-GT-109, March 1972.

156. D. F. Brunda and J. F. Boytos, "Evaluation of a Circumferential Inlet Pressure Distortion Index on a TF30-P-12 Turbofan Engine," NAPTC-ATD-193, July 1970. AD 873 229.

157. D. F. Brunda and J. F. Boytos, "Derivation and Evaluation of a Radial Inlet Pressure Distortion Index," NAPTC-ATD-216, April 1972.

158. J. E. Shoemaker, "An Analytical Analysis of the Effects of Instantaneous Vorticity on Compressor Performance," Naval Postgraduate School, MSAE Thesis, June 1973.

159. J. H. Dicus, "Fortran Program to Generate Engine Inlet Flow Contour Maps and Distortion Parameters," NASA TMX-2967, February 1974.

160. S. H. Ellis and B. J. Brownstein, "A Procedure for Estimating Maximum Time-Variant Distortion Levels with Limited Instrumentation," AIAA Paper 72-1099, 1972.

161. H. C. Melick, Jr., and W. E. Simpkin, "A Unified Theory of Inlet/Engine Compatibility," AIAA Paper 72-1115, 1972.

162. G. M. Callahan and A. H. Stenning, "Attenuation of Inlet Flow Distortion Upstream of Axial Flow Compressors," AIAA Paper 69-485, 1969.

163. M. T. Moore and J. E. Lueke, "A Similarity Parameter for Scaling Dynamic Inlet Distortion," ASME Paper 73-WA/Aero-3, 1973.

164. C. M. Mehalic and R. A. Lottig, "Steady-State Inlet Temperature Distortion Effects on the Stall Limits of a J85-GE-13 Turbojet Engine," NASA TMX-2990, February 1974.

165. C. Farmer, M. Iverson, and A. Fuhs, "A New Approach to Distortion Induced Compressor Stall - Vorticity Maps," AIAA Paper 72-1116, 1972.

166. F. W. Burcham, Jr., and D. L. Hughes, "Analysis of In-Flight Pressure Fluctuations Leading to Engine Compressor Surge in an F-111A Airplane for Mach Numbers to 2.17," AIAA Paper 70-624, June 1970.

167. D. R. Bellman and D. L. Hughes, "The Flight Investigation of Pressure Phenomena in the Air Intake of an F-111A Airplane," AIAA Paper 69-488, 1969.

168. F. W. Burcham and D. R. Bellman, "A Flight Investigation of Steady-State and Dynamic Pressure Phenomena in the Air-Inlets of Supersonic Aircraft," paper presented at 38th Meeting of PEP, AGARD, Sandefjord, Norway, September 1971.

169. C. R. Dawson, "Simulation and Measurement of Pressure Transients in a Mixed-Compression Supersonic Intake During Engine Surge," AIAA Paper 71-671, 1971.

170. J. H. Gutman, M. A. Stibich, and J. N. Untz, "Compressor Research Facility," AIAA Paper 73-1282, 1973.

171. F. R. Lynch and C. J. Slade, "Data Acquisition and Automated Editing Techniques for Engine-Inlet Tests," AIAA Paper 70-596, 1970.

172. F. W. Burcham, Jr., J. K. Holzman, and F. J. Reukauf, "Preliminary Results of Flight Tests of the Propulsion System of a YF-12 Airplane at Mach Numbers to 3.0," AIAA Paper 73-1314, 1973.

173. R. C. Crites, "The Philosophy of Analog Techniques Applied to the Analysis and High Speed Screening of Dynamic Data," AIAA Paper 70-595, 1970.

174. P. Czysz, "A Data System Concept for the Acquisition, Identification, and Analysis of Critical Time Variant Pressure Parameters for Engine/Airframe Compatibility Programs," AIAA Paper 70-594, 1970.

175. M. Christianson and J. Yustinich, "Circumferential Traversing Technique for Intra-Stage Analysis of Axial Flow Compressors," ASME Paper 71-FE-33, 1971.

176. W. H. Ball and P. A. Ross, "Experimental Correlation of Installation Effects for Inlet/Airplane Integration," AIAA Paper 71-759, 1971.

177. S. Fujii and M. Matsuki, "Several Topics of Axial-Flow Compressor Research at the National Aerospace Laboratory (Japan)," ASME/JSME Paper JSME-6, 1971.

178. P. H. Kutschenreuter, Jr., T. P. Collins, and W. F. Vier, III, "The P3G--A New Dynamic Distortion Generator," AIAA Paper 73-1317, 1973.

179. J. L. Livesey and E. M. Laws, "The Simulation of Internal Flow Velocity Profiles by Means of Shaped Wire Gauze Screens," AIAA Paper 72-165, 1972.

180. R. W. Synder and R. J. Blade, "Analytical Study of Effect of Casing Treatment on Performance of a Multistage Compressor," NASA TN D-6917, August 1972.

181. M. B. Sussman, "A Remark Concerning Engine Inlet Distortion," J. Aircraft. 5, pp. 95-96, 1968.

182. W. M. Osborn, G. W. Lewis, Jr., and L. J. Heidelberg, "Effect of Several Porous Casing Treatments on Stall Limit and on Overall Performance of an Axial-Flow Compressor Rotor," NASA TN D-6537, November 1971.

183. J. E. Bayati and R. M. Tyson, "Propulsion Flow Transient Accommodation Control," AIAA Paper 70-694, 1970.

184. F. E. Rubbert, M. L. Boctor, S. J. Cowan, and R. D. LaPrete, "Concept and Design of Stators Tailored to Shield a Fan from Pressure Disturbances Arising in the Downstream Fan Duct," AIAA Paper 72-84, 1972.

185. P. C. Tramm and G. D. Huffman, "Airfoil Design for High Tip Speed Compressors," AIAA Paper 73-1248, 1973.

186. J. B. Day and M. S. Coalson, "Qualitative Effects of Cycle Variables on Turbine Engine Performance and Stability," AIAA Paper 73-1315, 1973.

187. M. K. Kurosaka, "On the Unsteady Supersonic Cascade with a Subsonic Leading Edge," Part I, ASME J. of Eng. Power, 96, Series A, pp. 13-22, 1974.

188. M. K. Kurosaka, "On the Unsteady Supersonic Cascade with a Subsonic Leading Edge," Part II, ASME J. of Eng. Power, 96, Series A, pp. 23-31, 1974.

189. M. F. Platzer and H. G. Chalkley, "Theoretical Investigation of Supersonic Cascade Flutter and Related Interference Problems," AIAA Paper 72-377, 1972.

SOURCES OF DISTORTION AND COMPATIBILITY

R. BOUILLET - J.M. BRASSEUR
SNECMA - FRANCE

1. INTRODUCTION

When developing a new aircraft, one of the most time consuming and difficult problems facing the Design Engineer is the air intake. The air intake must, in fact, provide for the best possible operating conditions for the engine, i-e must be able to operate at maximum or economical rating, with both minimized internal (maximum efficiency) and external (minimized external drag) losses.

Such a performance over the complete flight envelope would require a high degree of variable geometry involving unacceptable weight penalties.

Therefore, the final design will be the result of a number of trade-offs which may be reflected as engine operation troubles caused by flow distortions at compressor face in some flight conditions. Predicting all conditions which may arise is not possible, and this is why the first flight of a prototype aircraft is always a thrilling experience to those who have managed the project.

Risks must be minimized to the best possible extent and, to meet this purpose, considerable design work is made providing a few criteria which, even if not generating solutions for the air intake or compressor design, can be used as guide lines by the experimental development engineers.

We think further progress is still possible through a more detailed analysis of distortion in the sense of air intake/engine compatibility. This paper proposes to provide some indications rather than to describe methods, since such methods are not sufficiently developed yet.

The following aspects will be successively reviewed :

- The various operating cases of air intakes
- Air intake/engine compatibility
- Test facilities required to compensate the lack of theoretical data, and to confirm predictions.

To conclude, typical examples of air intake modifications aiming at a significant improvement of the internal flow will be presented.

2. EXAMPLES OF INTAKE DISTORTION PATTERNS

This chapter has been divided in two sections. The first section covers the normal operation, i-e the velocity field around the aircraft in an assumed infinite atmosphere is the only factor considered ; in the second section, disturbances due to ground effect are assumed to combine with this field : typical examples are a VTOL aircraft taking off and an aircraft slowed down at landing by means of a thrust reverser.

2.1. Normal operation

In this paragraph, the air intakes for supersonic and subsonic aircraft will be considered separately :

2.11. Air intake for supersonic aircraft

As already stated in the Introduction, a satisfactory air intake is a predominent factor in making the aircraft successful. This is particularly true for a supersonic commercial aircraft, where any efficiency loss in subsonic or supersonic flight and any external drag increase (mainly in supersonic flight) corresponding to 1 % of the installed thrust entail a loss of several percent points in payload.

In all cases, the main concern of the Design Engineer is to select the optimum type of air intake for the mission envisaged.

Three types of air intake outlined in figure 1 can be envisaged :

- The supersonic external compression air intake
- The supersonic internal compression air intake
- The mixed compression air intake.

Let it be recalled here that, up to an infinite Mach number of 2.5, the best choice is the supersonic external compression air intake, because of its acceptable performance and simplicity compared to the other two ; however, beyond Mach 2.5, external losses considerably increased and, to maintain a satisfactory efficiency, the other two types must be used.

For instance, when calculating a supersonic external compression air intake, an approach in several steps should be used :

- Calculation of external recompression : The methods are now well proven for the main flow and the wall boundary layer
- Calculation of normal shock and its interaction with the boundary layer : available methods are far from being adequate today
- Calculation of diffuser : semi-empirical formulae have been proposed by Seddon and others. To day, calculation methods provide a satisfactory prediction of the flow at the diffuser outlet, even in the viscous region (three-dimensional boundary layer Ref. 19).

For the calculation of diffuser, the inlet conditions, i-e the conditions behind the normal shock, must be fully known.

../..

This is described in Figure 2. Associated with this interaction, the increased boundary layer thickness causing flow separation in the diffuser, a boundary layer diverter had to be introduced to stabilize the shock, thereby reducing its effects. A description of the flow at the boundary layer diverter as it applies to Concorde is given by figure 3. This provides some idea about the significantly disturbed conditions observed at the diffuser inlet. Such disturbances are reflected at the diffuser outlet, mainly as total pressure distortions.

In addition, the following effects should be considered :

a) transient effects : excursion in sub-critical range - pitching up or down, sideslip.

Consider the Concorde air intake. In zero or negative incidence as well as sub-critical conditions, the shear line originating from the focalization point of recompression waves produced by the external ramp penetrates into the air intake (fig.4). This results in a quite significant increase of flow distortion in terms of total pressure and also in terms of velocity angle, chiefly at the cowl end (fig. 5).

In sideslip, distortion is caused by a cornet vortex produced on one lateral side and entering the air intake (fig. 6).

Although currently explained, these airflow distortions, with their associated efficiency losses, are not prone to a theoretical description. However, when satisfactorily understood, guidelines are available to the Engineers to select efficient designs.

In aircraft installations where the engine is supplied through two separate air intakes, another type of highly distorted airflow in sideslip conditions is observed. The investigation of wakes produced at the splitter wall trailing edge is essential. Figure 7 shows the structure of a flow separation downstream of this trailing edge.

Here again, such flow separations could be avoided as early as the initial design stage, if a better knowledge of boundary layer in diffusers were available.

b) Unsteady effects :

Pressure fluctuations with time about the mean values described above, generally larger than with internal compression intakes, are essentially due to unsteadiness of shock waves in the air intake in particular, but which may also come from the external flow.

This assumption was confirmed by a considerable amount of experimental work, such as work made on the F 111 air intakes, and also by Lewis Research Center on a bench capable of simulating a Mach number of 2.5 feeding a J85 engine housed in a nacelle fitted with an internal compression supersonic air intake.

Fluctuation amplitude can be quite high, as demonstrated by D.N. Bowditch (ref. 3), and as illustrated by figures 8 and 9. These fluctuations can have a significant effect on the boundary layer behaviour. Work is being done on this matter.

Knowledge of shock wave/boundary layer interaction is still very limited, in particular in the unsteady flow regime. Considerable work remains to be done, both to know the fluctuation frequencies and intensity.

It should not be forgotten in fact that, if the presence of the engine can affect the amplitude of average and fluctuating distortions as compared to what is measured on a air intake tested alone, the presence of a standing wave pattern may create in the pattern nodes pronounced interactions with the viscous layer which may lead to separation.

This damping phenomenon has already been approached, but using a very simplified theory, by Callaghan and Stenning (ref. 5).

To conclude this review of air intakes for supersonic aircraft, it can be stated that three types of distortion may occur :

- Time averaged variations of moderate total pressure and low velocity angle towards the flowpath centerline, and a little higher on the walls in normal operating cases
- High amplitude variations of total pressure and velocity angle always towards the periphery, caused by flow separation in particular operating regimes of the air intake (incidence, sideslip...).
- Pressure and velocity angle variations about these mean values.

Chapter 3 describes how these findings should be taken into account.

.../...

2.12. Air intakes for subsonic aircraft

The air intake of a subsonic aircraft engine nacelle is also based on a trade-off between a design optimized for take-off and a design optimized for cruise, with the additional objective of keeping the weight as low as possible.

In general, the compromise made by the air intake manufacturer favors the cruise case, which leads to design a system having an inlet area two small for the take-off case, requiring the introduction of auxiliary air inlet doors to compensate this deficiency (Fig. 10.a).

Calculation methods are available to-day, providing a very close approach to the final configuration of the air intake, in clean and viscous flow condition. However, as in the previous case, a few phenomena are not mastered yet always resulting in flow distortions :

- Separations : In general, flow separation occurs in crosswind conditions. In fact, overspeed occurs on the lip, and the diffuser boundary layer cannot stand the slowing down required (Fig. 10.b).

- Vortex swallowing : This is due to ground effect, or to wing effect if the engine is installed above the wing, during static running or taxiing : before arriving to the engine, the air skims along the ground or wing surface, and this boundary layer creates a vortex which enters the air intake, then producing a distortion highly detrimental to the flow, since the component normal to the theoretical direction of the velocity (stream line of an irrotational flow) is quite strong.

A fully predictable type of air intake distortion, which can be observed in a clean flow, should also be considered. This type of flow distortion is dependent only on the air intake lip contour and length : a velocity distortion without total pressure distortion.

Turbulence raises a less critical problem than in supersonic intakes, provided the intake operation can be kept free from choking.

2.2. Particular cases

To complete our review of intake distortion types, a few particular cases, arising when the variations of the incoming flow total temperature are high, should be mentioned :

- Aircraft using a thrust reverser at landing
- Missile firing from a military aircraft
- VTOL aircraft taking off.

In the above three configurations, the aircraft air intake is fed with an uneven temperature air.

If we consider the Concorde air intake (fig. 11) it can be seen that the air entering the intake is the thrust reverser efflux mixed with ambient air.

With a military aircraft, the missile exhaust wake may affect the complete intake which will swallow a highly turbulent flow but, during a transient phase, a part only of the air intake swallows hot gas.

With a VTOL aircraft, the situation is practically identical to what happens on Concorde, hot gases being deviated by the ground to the air intakes.

This concludes our review of causes of air intake distortion, which we have been trying to make as complete as possible. We will now discuss how the engine will stand such distortion.

3. COMPATIBILITY BETWEEN AIR INTAKE AERODYNAMIC CHARACTERISTICS AND THE COMPRESSOR OPERATING RANGE.

When analyzing the response of a compressor to the types on incoming flow, we will see that few calculation methods are available to predict such response, and that any effort in this field should essentially be based on experience.

In this chapter, we will consider first the steady aspect of problems, and then we will briefly discuss the unsteady aspect.

3.1. Steady aspect

3.11. Steady running

Assume a well defined flight case, with known external conditions (incidence angle, Mach number etc..), and installed thrust required or engine conditions fixed.

In a first step, the air intake configuration matched to these engine conditions must be defined, viz :

- in supersonic flight, either the design geometry if the flight case is the supersonic cruise for a commercial aircraft, or a geometry derived from the above by moving center bodies or by changing the angular position of the recompression ramp.

- in subsonic flight, cowl lip variable geometry, or auxiliary doors should be considered. Then, as explained in the previous chapter, the diffuser outlet flow conditions - velocity vector, total temperature and pressure - can be known from calculation and test.

../..

In steady running, the variations of these parameters relative to an average value are small, and therefore, satisfactory compressor operation can be verified by means of theoretical calculations. These calculations will successively provide :

- from strict methods, the average flow in the flowpath in non viscous conditions, and the complete flow around airfoils
- from semi-empirical methods which may be based on Mellor's work, the "secondary" flows (viscous flows on walls).

In these conditions, we do think we have the adequate means to discuss the engine behaviourin steady running as early as the project design stage. However, this represents a small portion only of the range to be explored. In addition, we have assumed that the air intake was a variable geometry design in order to match several flight cases. This is known to cause a significant increase of air intake weight, and the engineer will be faced with a compromise between performance and weight.

3.12. Transient running

In the case of a slow rate variation of flight conditions, this variation can be considered as a succession of different steady running regimes. This is in as much true as, in general, the matched running range of an air intake, in terms of flow and Mach number, around a given geometrical configuration is not negligible, ensuring smooth transition from one level to the other.

However, these conditions are not always met. We will mentioned the following few examples :

- Sharp manoeuvers of a military aircraft, the air intake of which can be submitted to large variations of the angle of attack or yaw.
- Cross-wind induced distortions, not compensated by air intake adjustment.
- Missile firing or thrust reversal.

Coefficients of influence of these variations on average efficiency were derived from detailed experimental work. V.H. BALL and P.A. ROSS have reported such results from their work on an air intake designed for a nominal Mach number of 2.2. These results are summarized in the following table.

Influence Coefficient	Configuration : - M_∞ = 2.2 (Design point) - Sharp cowl lip - 50 % Sideplates - Ramp angles 7 - 14 - 25°			
Effect of upwash $\frac{\partial \eta}{\partial \alpha}$	$-5° < \alpha < 0°$		$0° < \alpha < +5°$	
	+ 0,0175		- 0,0252	
Effect of Sidewash $\frac{\partial \eta}{\partial \beta}$	$0° < \beta < 1°$	$1° < \beta < 2°$	$2° < \beta < 3°$	$3° < \beta < 4°$
	- 0,007	- 0,009	- 0,0105	- 0,0115
Effect of local Mach number $\frac{\partial \eta}{\partial M_L}$	$2,1 < M_L < 2.2$		$2.2 < M_L < 2.3$	
	- 0,0015		- 0,0082	
Effect of Mach Number Gradient $\frac{\partial \eta}{\partial \Delta M}$	$0 < M < 0,10$			
	- 0,228			

This information enables the aircraft manufacturer to know the theoretical evolutions of the powerplant performance, and, in this manner, the order of magnitude of reactions to such manoeuvers. However, it will not provide a prediction of the actual behaviour of the engine, and will not be able to tell if the engine response will not be quite different, e-g when surge conditions are reached.

In an attempt to predict the engine surge line in highly distorted airflow conditions, a few simplified approaches can be used. Two of these will be described, these problems being covered in detail by other authors in this Lecture Series

../..

- Method of the equivalent compressor

On an "iso-rpm", at the design point corresponding to the uniform mean flow representative of the actual flow, it is possible to compare the extreme operating points correlating to the extreme total pressure levels upstream of the compressor, assuming the downstream pressures are the same in both cases. From fig. 12 (mean point A) it can be seen that surge can be reached rapidly if the pressure margin is not adequate.

When operating with a high temperature gradient at the compressor face, the extreme operating point lies on a reduced "iso rpm" lower than the "iso rpm" corresponding to a normal atmosphere and, by assuming that the pressure ratio is maintained, it is also obvious that surge may be reached if the pressure margin is not adequate (Fig. 12).

The above two examples show that in a first approximation, some idea, although not fully satisfactory, of the compressor behaviour can be obtained. Full information can be obtained from tests only, and this will be covered in the next chapter.

3.2. Unsteady aspect

It has been explained earlier that we are unable, for the air intake, to predict the frequencies and amplitudes of fluctuations affecting the characteristic parameters. Also, we are unable to introduce these unsteady effects into our project calculation methods.

For the time being, we are in an experimental stage and, in the next chapter, we will see how difficult a task these tests are.

4. EXPERIMENTAL CHARACTERIZATION OF AIR INTAKES

For a number of reasons stated in the preceding chapters, combined air intake/engine testing is desirable.

Obviously, developing these two powerplant components on a single test bed is out of question : this kind of test will not be made before the end of the complete development process to validate the complete assembly before the first flight.

However, it remains that the engine must be tested in as representative aircraft conditions as possible. Therefore the air intake and engine designers must get together to establish rules according to which both agree either not to exceed on the air intake a given value of a criterion to be defined, or to guarantee satisfactory compressor operation up to this value.

In general, these criteria consider steady distortions only.

Attempts are currently being made to introduce unsteady effects in these criteria. For instance, the work made by P.J. MARTIN and H. CLYDE MELICK (ref.18), who have tried to defined air intake flow quality criteria, should be mentioned.

As it will be seen from the following table, obtaining a target value for these criteria is quite difficult. The actual flow field around the aircraft and the air intake/engine coupling must, in fact, be considered. In some cases it is not before prototype flight that an accurate value can be obtained, and this raises a problem in the aircraft development, since there is nothing which can prove that the quality of the prototype air intake will be maintained during the development process.

For engine tests, introducing the effect of static distortion is relatively easy ; on the other hand, simulation of dynamic effects leads to very costly and cumbersome facilities.

The following table shows a typical procedure applied to develop an air intake. The data obtained from the various tests are also given.

TEST	VARIABLE	MEASURE	OBSERVATION
Inlet alone	M_∞ , α , β	ε , η Bleed system Buzz limit Steady-state Distortion	uniform flow in front of inlet
Integrated intake (partial wind and fore-body)	M_∞ , α , β	ε , η Buzz limit Steady-state Distortion	Realistic flow in front of inlet
Inlet/engine testing in nacelle	Some M_∞	ε , η Bleed system Buzz limit Steady-state and dynamic distortion	Realistic test for inlet/engine interaction

.../...

5. REDUCING THE FLOW DISTORTIONS IN AIR INTAKES

A number of deficiencies of the available means of dealing with these problems have been highlighted. Therefore, investigation work must go on, both from the fundamental point of view mainly in the field or shock wave/boundary layer interaction, and to develop calculation methods, which, however approximate, take account of our experience.

Now, the art of the design engineer is to interprete ; he must also make the best use of his analysis capacity in order to find solutions.

This applies to the aircraft manufacturer as well as to the engine manufacturer who must pool their efforts to achieve the best possible operation of the powerplant.

We will give here some examples which yielded significant reductions of distortion levels in air intakes.

For Concorde, we have mentioned the problems associated with sideslip. It has been found that a simple, small-size cut-back on the external wall is sufficient to achieve practically complete elimination of distortion by eliminating its cause, i-e the swallowing of the vortex (fig 13). The generation of vortex is prevented by the reduction of the angle of attack of the leading edge of this wall due to the front shock being moved rearward.

In the case of subsonic air intakes, we have mentioned supply problems at take-off, giving rise to an increase of the Mach number at the diffusor throat, followed by excessive deceleration followed by flow separation; in this connection, the introduction of auxiliary doors as a fix to this problem was also mentioned. Such doors are not recommended and no longer in use due to the associated noise level. Then, it becomes necessary to find either a new fixed air intake design by reconsidering the compromise between take-off and cruise requirements, or to introduce new variable geometry features as illustrated by fig. 14.

Many other examples could be presented, but we do not think it is the purpose of this paper to describe such examples and to propose solutions. Instead, our wish was to present the problems and to try to analyze them.

REFERENCES

1. P.F. ASHWOOD — Free-jet tests of a full scale supersonic intake/engine combination
38th Meeting of the Agard Propulsion - Sept.71.

2. W.H. BALL - P.A. ROSS — Experimental correlation of installation effects for Inlet/Airplane integration.
AIAA Paper n° 71 - 759.

3. D.N. BOWDITCH — Inlet-engine-nozzle wind tunnel test techniques.
38th Meeting of the Agard Propulsion - Sept.71.

4. P. BRADSHAW — The understanding and prediction of turbulent flow
1972 - Reynolds-Prandtl-Lecture.

5. G.M. CALLAHAN - A.H. STENNING — Attenuation of inlet distorsion upstream of axial flow compressor
Journal of Aircraft vol. 8 n° 4 (Avril 71).

6. J.L. CAMPBELL & S. ELLIS — Inlet/engine compatibility Analysis
AIAA Paper n° 70 - 941.

7. P. CARRIERE — Aperçu de quelques problèmes aérodynamiques actuels posés par les prises d'air supersoniques.
1er Symposium international sur les progrès des réacteurs d'aviation.
Marseille 72.

8. P. CARRIERE — Aérodynamique interne des réacteurs.
Cours de l'Ecole Nationale Supérieure de l'Aéronautique et de l'Espace - Toulouse 72.

9. COUSTEIX-QUEMARD-MICHEL — Application d'un schéma amélioré de longueur de mélange à l'étude des couches limites turbulentes tridimensionnelles.
AGARD - Turbulent shear flows - Londres 71 - TP ONERA 985.

10. H. EIBL - R. FRIEDRICHS — Wind tunnel investigations of a supersonic air intake with various auxiliary intakes at low speeds.
38th Meeting of the Agard Propulsion - Sept.71.

11. S.H. ELLIS — Inlet Engine compatibility Development.
38th Meeting of the Agard Propulsion - Sept.71.

12. I. Mc GREGOR — Some applications of boundary layer control by blowing to air inlets for V/STOL Aircraft.
38th Meeting of the Agard Propulsion - Sept.71.

13. J.R. JONES - W.M. DOUGLAS — Dynamic flow in engine air inlets for subsonic Aircraft.
Prop. SQUID - Prudue Univ. Oct.71.

14. C.S. LEYMAN - D.P. MORRISS — Concorde powerplant Development.
38th Meeting of the Agard Propulsion - Sept.71.

15. J. LEYNAERT — Etude par analogie rhéoélectrique de prises d'air auxiliaires pour le décollage des avions supersoniques.
La Recherche Aérospatiale n° 119 (Juillet-Août 67).

16. J. LEYNAERT — Pompage dans les entrées d'air supersoniques.
Aéronautique et Astronautique n° 22 (6-1970).

17. J. LEYNAERT — Prediction Methods of Aircraft Aerodynamic Characteristics.
Agard - Lecture series n° 67-1974.

18. R.J. MARTIN - H. CLYDE MELICK — A feasibility study for definition of inlet flow quality and development criteria.
A.IAA/SAE 8th joint propulsion specialist conference - 1972

19. MICHEL-QUEMARD-COUSTEIX — Méthode pratique de précision des couches limites turbulentes bi et tridimensionnelles.
La Recherche Aérospatiale n° 1-1972

20. D.P. MORISS - D.D. WILLIAMS — Free jet testing of a supersonic Engine/Intake combination
Journal of the Royal Aeronautical Society - Vol 74 p. 213-218.

21. G. de RICHEMONT — L'intégration du propulseur et de la cellule sur un avion de combat supersonique.
La Haye - Sept. 69.

22. J.C. RIPOLL - J.B. COCHETEUX — Moyens et exemples d'essais au CEPr
38th Meeting of the Agard Propulsion - Sept. 71.

23. SEDDON — Boundary layer interaction effects in intakes with particular reference to these designed for dual subsonic and supersonic performance.
Agardograph 103. Aerodynamics of power plant installation.

24. R.E. STANLEY — The analysis of a subsonic axisymmetric inlet for compressor matching.
38th Meeting of the Agard Propulsion - Sept. 71.

25. E.A. VANDEUSEN - V.R. MARDOC — Distortion and turbulence interaction, a method for evaluating engine/inlet compatibility.
AIAA 6th Propulsion joint specialist conference - 1970.

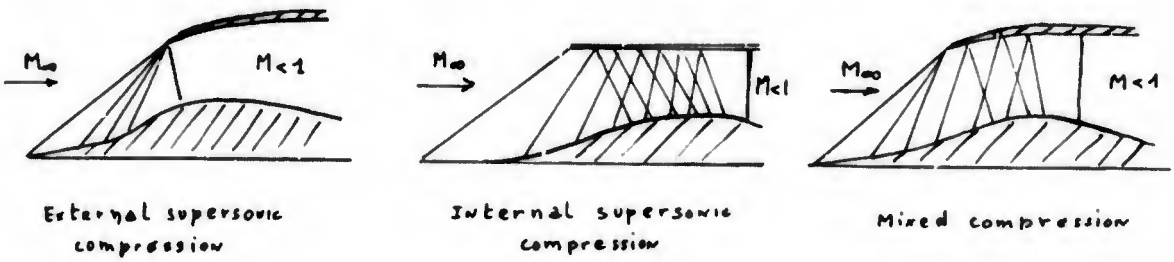

Fig.1 Intake configuration

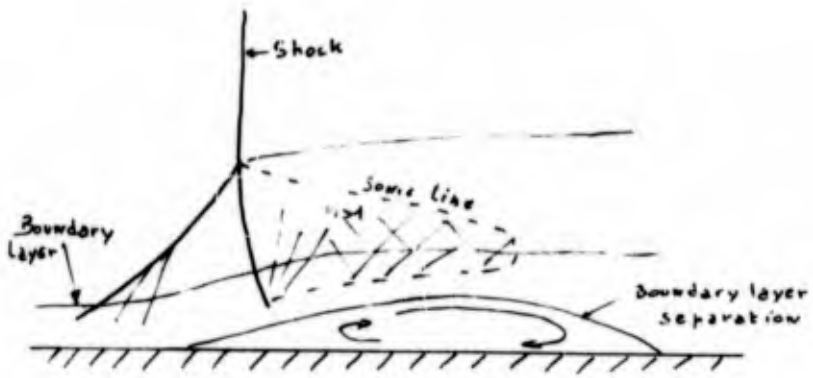

Fig.2 Shock-boundary-layer interaction

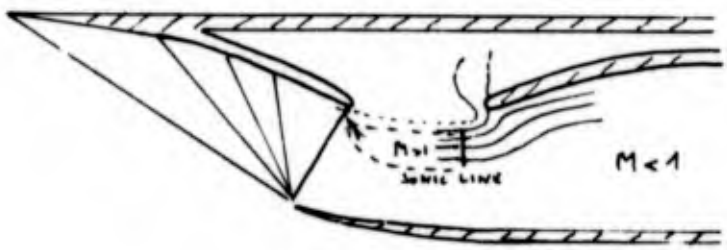

Fig.3 Concorde air-intake

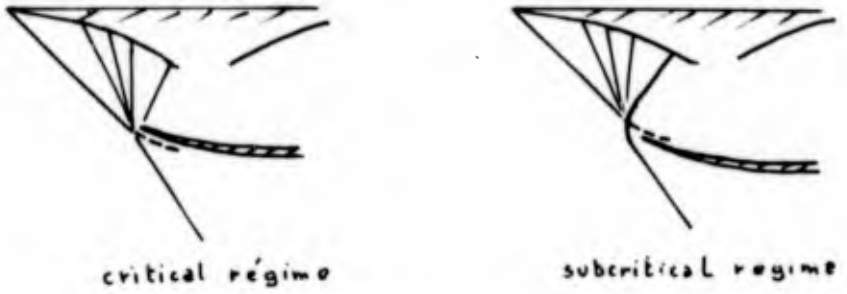

Fig.4 Concorde air-intake

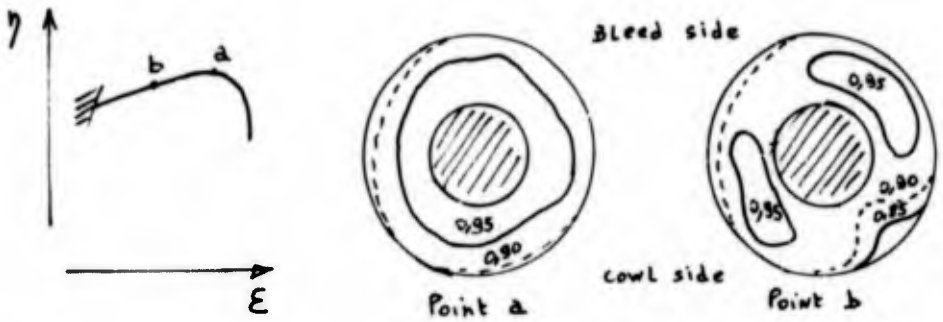

Fig.5 Concorde. Distortion example (P.Carriere)

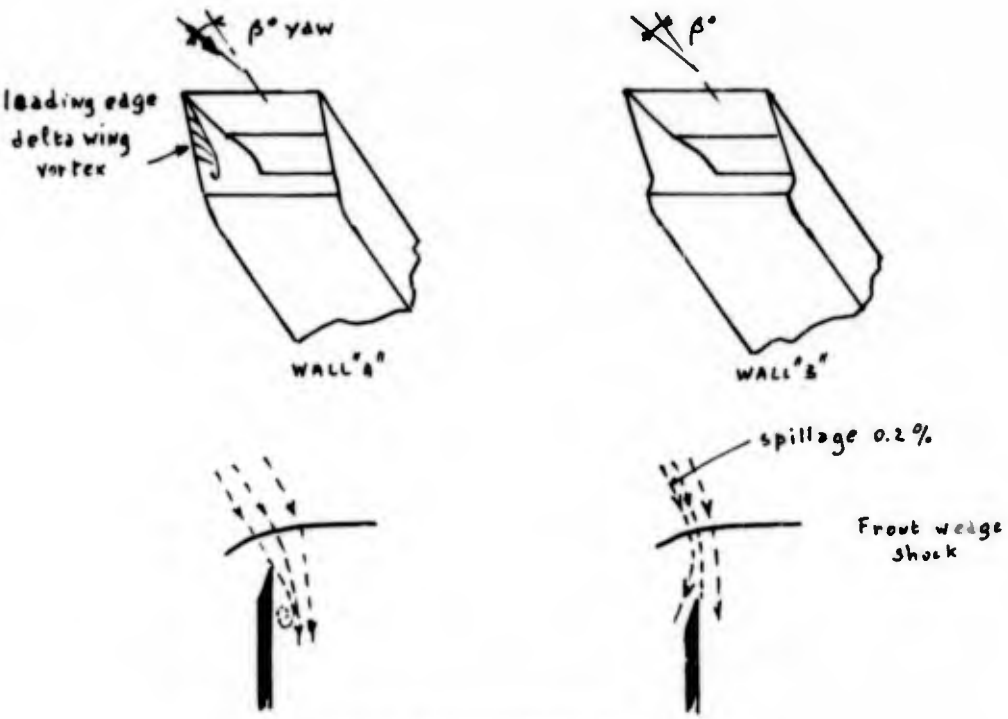

Fig.6 Yaw effect on two-dimensional intake (J.Leynaert)

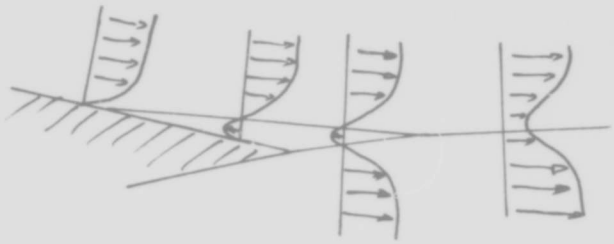

Fig.7 Boundary-layer separation

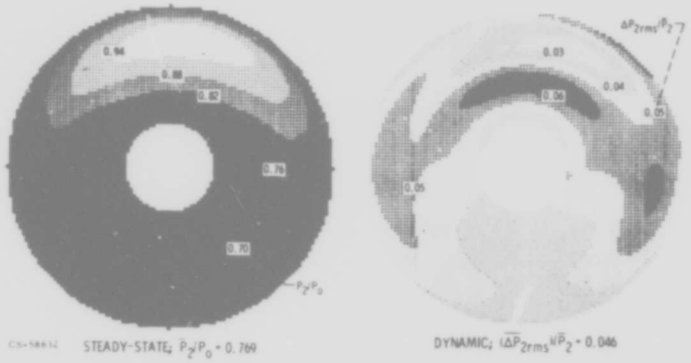

Fig.8 Dynamic and steady state distortion. $M_0 = 2.6$; 5° angle of attack (D.N.Bowditch)

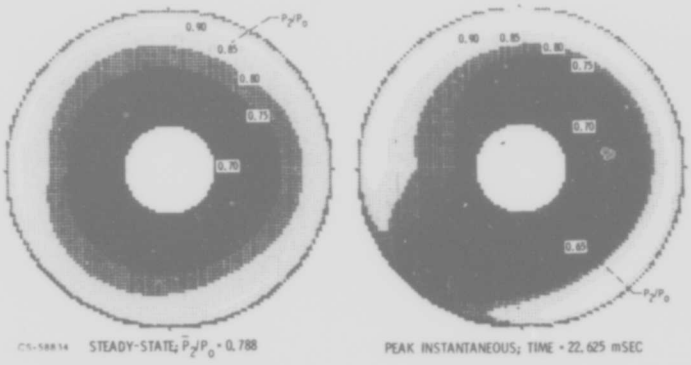

Fig.9 Comparison of steady state and peak instantaneous distortion. $M_0 = 2.5$; 0° angle of attack (D.N.Bowditch)

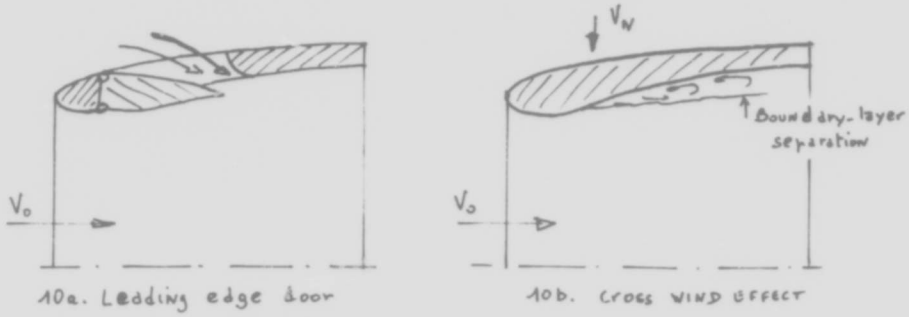

Fig.10 Air-intake for subsonic aircraft

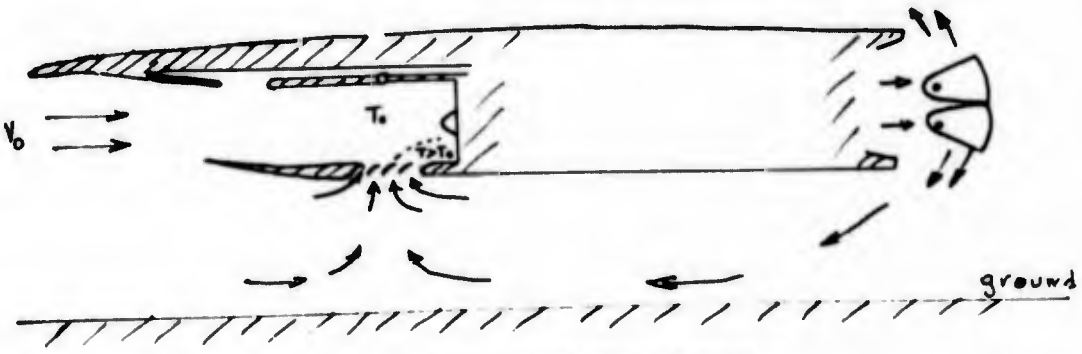

Fig.11 Ground effect in inversion

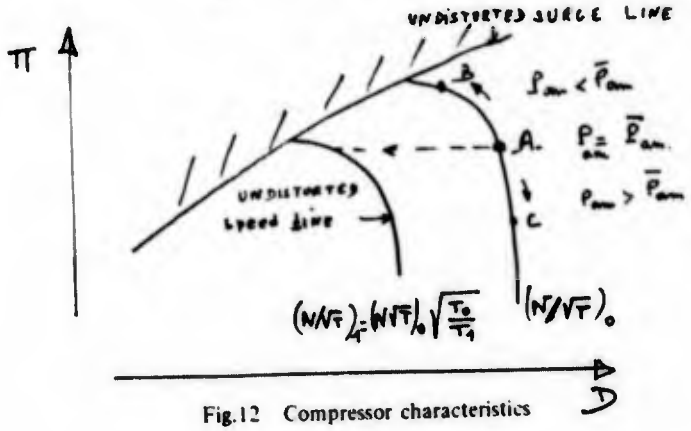

Fig.12 Compressor characteristics

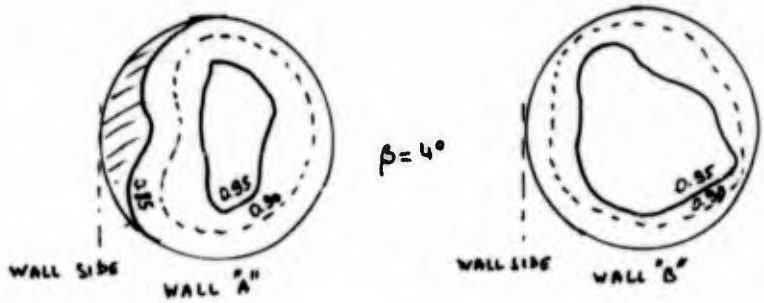

Fig.13 Yaw effect suppression (see Figure 6) (P.Carriere)

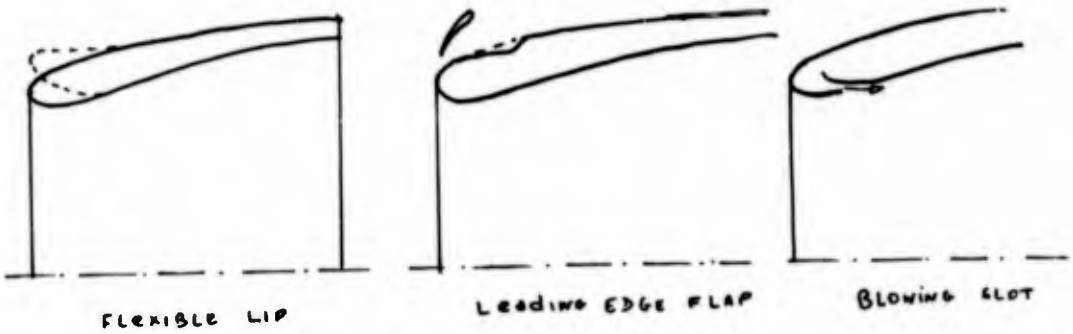

Fig.14 Auxiliary take-off devices (J.Lemaert)

AERODYNAMIC RESPONSE

by

R G Hercock and D D Williams
Installation Aerodynamics Department
Rolls-Royce (1971) Limited
Bristol Engine Division
Filton PO Box 3
Bristol BS 12 7QE
England

SUMMARY

This paper contributes a discussion of the aerodynamic response of turbomachinery to steady and time-variant total pressure and temperature distortion. Examples of changes in compressor characteristics are presented. Experimental correlations of surge margin loss, the concept of a critical or effective spoiled sector angle and compressor sensitivity are then discussed in relation to simple theoretical ideas for circumferential distortion. The development of the distortion index approach to account for the effect of radial and mixed radial - circumferential total pressure distortion and the impact of turbulence or unsteady flow is outlined. Comments on foreign gas ingestion are made. Some current auditing procedures are described. Limitations of isolated spool rig tests are discussed, and surge hammershock data are presented.

SYMBOLS

b	Superposition Factor
c	Chord
C_L	Lift Coefficient
DC, ID	Total Pressure Distortion Indices
f	Frequency
f( )	Function
Hz	Hertz
K	Distortion Index, Reduced Frequency Parameter ($\omega C/2Vr$)
M	Mach Number
N	Engine Speed (rpm)
P	Total Pressure
p	Static Pressure
R	Compressor Pressure Ratio
RMS	Root Mean Square
S	Sensitivity (ΔPRS per unit distortion index)
SM	Surge Margin
T	Total Temperature
TC	Total Temperature Distortion Index
t	Time
V_a	Axial Velocity
V_r	Rotor Relative Velocity
W	Mass Flow
x	Axial Distance
Δ, δ	Change
ΔPRS	Loss of Surge Pressure Ratio ($\Delta R/R_{su}$)
θ	Circumferential Position

SYMBOLS

θ^- Circumferential extent of total pressure regions below the mean value

ω Circular frequency

Subscripts

c Critical, circumferential, corrected

e Effective

i Instantaneous

N Constant corrected speed

NO Normal operating

r Radial

su Surge

t Total

w Constant corrected flow

Superscripts

$(\dot{})$ Rate of Change

$(\bar{})$ Mean or Average Value

Note: Other symbols are defined in the text and appendix.

1. INTRODUCTION

The main aim of this paper is to discuss the effects of inlet flow distortion on overall compressor and engine stability characteristics. Details of blade or stage response, eg blade row, wall or corner stall, and the important question of stage matching will not be addressed in depth. As the aerodynamic response of compressors and engines to prescribed distortion patterns is extremely complex and particular experiences are as yet difficult to generalise, specific cases are chosen by way of example to illustrate some of the more important considerations that arise.

The synthesis of engine response from rig compressor test results can pose considerable problems, particularly for by-pass engines, due to difficulties of accounting completely for component rematching, spool/spool interactions etc, within the engine, which can modify significantly rig compressor response data and distortion indices. For such reasons engine tests with distortion during early phases of engine development are important. The effects of Reynolds number, ageing, manufacturing and control tolerances, bleed and power off-take affect clean surge margin and hence contribute to engine distortion tolerance. Accuracy questions and the non-deterministic nature of time-varient distortion, which has helped explain engine 'drift' surges, add statistical elements to engine distortion response.

In order to properly describe flow distortion at the inlet/engine interface the variations of the major flow variables eg total pressure, temperature, velocity components, static pressure and flow angularity, from their spatially-uniform steady mean values need to be evaluated, References 1, 2, 3, 4, 5. The mean values themselves require to be defined consistently, Reference 6. A consequence of the need to interface between inlet and engine components, which implies inlet-engine flow interference effects may not be represented correctly during component testing, coupled with the practical need to contain the measurement task to manageable proportions, is that it has become usual in all but cases of closely coupled inlet/engine installations operating in highly curved flow fields to consider only the question of total pressure and temperature distortion. Clearly, situations where this simplified description may be considered adequate must be distinguished from those where it may not. The distinction is fundamental for example to the selection of distortion indices and appropriate component test facility and programme requirements.

A considerable body of total pressure distortion response data now exists on various compressor and engine designs. Rather less is known about total temperature distortion. An increasing need for a unified practical approach to the subject has been felt. Efforts towards this goal have been considerably assisted by appealing to theoretical models in order to provide the necessary physical insight, and some theoretical concepts, eg the parallel compressor theory, References 7, 8; rotor blade and row dynamic response theories, References 9, 10, 11, 12, 13, 14 15, and various actuator disc methods, References 3, 16, 17, 18, 19, have proved to be valuable in this respect. By and large however due to the evident complexity of the aerodynamic problems involved available theoretical methods are limited in scope and inlet/engine compatibility is still largely

an experimental subject

2. TOTAL PRESSURE DISTORTION

2.1 DISTORTION GENERATION

The traditional method of testing compressors with spatial distortion uses gauze screens of varying blockage to generate 'steady' distortion. Alternative methods of producing the distortion utilise air jets to discharge high velocity air against the incoming flow so producing local momentum defects, References 20, 21, 22. As virtually all aerodynamic processes are unsteady and the importance of turbulence-generated time-variant distortion on compressor stability is now firmly established, References 20, 23, 24, 25, 26, 27, 28 29, the term 'steady' requires considerable qualification. Distortion can be regarded so only if turbulence intensity and its scale in relation to a characteristic compressor dimension, eg annulus width, is small; time-variant and time-averaged spatial distortion patterns are then sensible identical and low response instrumentation may be used to describe the distortion. It is currently held that screen-generated distortion falls into this category.

To simplify experimental testing and help identify numerical distortion indices initial compressor work is performed generally with pure circumferential and radial profiles using 'classical' or square-wave screens. Later testing may include mixed radial/circumferential profiles and representative inlet patterns to develop general distortion indices and refine compressor sensitivities, ie rates of loss of surge pressure ratio (ΔPRS) with distortion index. Further testing with turbulence generators, inlet simulators, and with the actual inlets follow, References 4, 26, 30, 31.

Figure 1 shows a typical distortion screen assembly.

2.2 GENERAL RESPONSE CHARACTERISTICS

Examples of the effects of various screen-generated patterns on compressor performance maps are illustrated in Figures 2, 3 and 4. In Figure 2 the clean and distorted characteristics of a five-stage, 2.5 pressure ratio axial flow research compressor are shown. The compressor was tested with three square-wave screens of 45°, 90°, and 135° angular extents. Distortion level, defined as $(P_{max}-P_{min})/\bar{P}$ was 4%, approximately, at design flow. Results are shown in terms of mean inlet and exit total pressures derived from 48 circumferential rake positions (a rotatable screen was used to achieve accuracy). Changes in non-dimensional flow and efficiency were small and the shapes of the constant speed lines remained invariant. Significant losses of surge pressure ratio occurred despite the comparatively modest distortion level. Similar results were achieved at increased levels. Compressor exit static pressure was found to be sensible constant during the tests.

Figure 3, Reference 4, presents response data for a seven-stage high specific flow 0.315 hub/tip ratio transonic compressor. Moderate intensity distortions having spoiled sector angles less than 90° had little effect on stall pressure ratio. An increased intensity 90° screen and a 180° screen produced dramatic changes in the shapes of the constant speed lines, flow and efficiency. The compressor was tested with square-wave tip-low and linearly-distributed tip-low radial distortions, a square-wave hub-low radial, and a mixed tip-low radial/90° circumferential distortion, (Figure 4). Tip-low distortion increased corrected flow and surge pressure ratio. Hub distortion reduced flow and surge pressure ratio. The favourable effect of tip distortion more than offset losses due to circumferential distortion in this case.

Numerous ad hoc results are available in the literature. Circumferential distortion is found generally to be destabilising; radial distortion can, depending on its location and intensity, stabilise or destabilise a compressor.

Table I shows examples of losses of surge pressure ratio due to screen-generated square-wave circumferential distortion for single and multi-lobed patterns circa design speed.

TABLE I - ΔPRS DUE TO CIRCUMFERENTIAL DISTORTION

Spoiled Sector Angle (0°)°	Single-lobe							Multi-lobe					Reference
	315	270	180	90	60	45	30	2 x 90	2 x 60	2 x 45	4 x 45	4 x 22½	
Surge Pressure Ratio Loss ΔPRS%	-	-	8.6	6.5	4.5	-	0.5	1.8	-	-	0.7	-	5
	0.7	2.2	5.0	6.5	-	4.8	-	-	-	4.2	-	0.9	7
(constant flow)	-	-	9.0	9.6	9.2	-	7.3	-	7.2	-	-	-	38

It is well established, both experimentally and analytically, that multi-lobed pattern response is less than or equal to that of single-lobed patterns having the same screen blockage. Due to relatively high resistance to circumferential flow between blade rows, depending on blade gaps, circumferential distortion persists, generally in attenuated form, to the rear stages of the compressor so causing higher losses in surge pressure ratio in the intermediate to high speed regime when rear stages are more highly loaded. Radial distortions tend to wash out in early stages as spanwise resistance to flow is comparatively low. Radial distortion thus exerts a bigger destabilising influence at lower speeds when front stages are highly loaded.

The effect of distortion on corrected flow, pressure ratio and efficiency may produce significant rematching of the installed compressor so producing operating line shifts which may act to reduce surge margin and so destabilise the engine. In general, compressor performance changes and spool rematching cannot be quantified by means of distortion indices invented to correlate losses in surge pressure ratio.

The distortion response of LP compressors of turbofan engines, particularly those having close-coupled splitters separating by-pass and core flows, is complicated by spanwise flow coupling resulting from by-pass ratio changes. Fan core and by-pass flows have separate characteristics, representing average or 'split' efficiency and flow/pressure ratio characteristics, defined on either side of the dividing stream line, and have separate stall and operating lines, References 32, 33. Single and multi-stage fan tests have shown that steady circumferential distortion located within the by-pass stream may cause significant losses in the LPC-IPC or core compressor surge pressure ratio due to hub/tip radial outflow within the fan and downstream of the conventional inlet/engine interface instrumentation plane (Figure 5). Independent throttling of core and by-pass flows is an essential facility requirement for distortion tests on these fan units.

Overall stability response characteristics are complex and highly configuration dependent. Results are presented in Reference 34.

Distortion transfer characteristics can differ markedly along the blade span, References 4, 34, 35. Reference 35 presents an extreme result for a single stage transonic design where distortion attenuation occurred at the tip together with amplification at the hub. Because of the intrinsic design difficulties of by-pass fan designs it is important that hub-low distortions are minimised.

In order to contain compressor test programmes to manageable proportions it is evidently important to identify specific distortion patterns associated with particular installations early in the propulsion system design-development programme. Careful work-sharing between rig and engine testing is necessary.

Engine tests with representative inlet distortions are reported in References 36, 37, 38, 39, 40, among many others. Engines which employ variable elements, eg, compressor blading, resized turbine stator throats, final nozzle area, bleed off-take or in-bleeding; to vary installed compressor surge margin are extremely useful tools for distortion work as they allow compressor distortion response to be established in situ so that problems associated with synthesising engine response from the results of rig component tests are circumvented. Tests on fixed geometry engines involve identifying the surge-inducing event in terms of the engine primary control variables. An increasing awareness of the difficulty of accounting accurately for engine stability response in terms of numerical distortion indices has led to a greater emphasis on the use of 'pattern descriptors' - for example, for engine qualification.

2.3 SURGE LINE LOSS CORRELATIONS - CIRCUMFERENTIAL DISTORTION

Rotor Blade Response

Experimental results have shown that surge pressure ratio reduces with increasing distortion width, θ^-, and intensity, $(\bar{P} - Pmin)/\bar{P}$. Regions of total pressure below the average promote pre-whirl, reductions in axial velocity, local static pressure changes, and hence transient increases in rotor blade loading. For some combinations of blade stagger angle and pitch/chord ratio the behaviour of an individual blade in the rotor row may be similar to that of an isolated aerofoil so that it is instructive to consider aerofoil lift response to distortion. Departures from isolated blade response occur in high solidity, low stagger cascades due to interference between blade flow fields.

In passing through the circumferential distortion the rotor blade experiences simultaneous transverse and chordwise velocity perturbations. Linearised vortex line theories for 'thin' rigid blades indicate that transient lift response is given by the sum of a pair of terms relating lift and perturbation velocities via the complex Sears and Horlock transfer functions, which depend on reduced frequency parameter, $K = \omega C/2Vr$. The lift response differs from that experienced by a vibrating blade in uniform flow and may not, in general, be calculated on a quasi-steady basis.

Lift response trajectories computed for a square-wave 90^o pattern and varying axial velocity perturbations for a blade having a mean lift coefficient of 0.86 are shown in Figure 6. As spoiled sector angle, θ^-, increases for a given perturbation the lift increment becomes progressively less so that, for any assigned stalling C_L and perturbation, stall becomes sensibly independent of θ^-. The distortion intensity required to promote stall reduces as θ^- increases and tends to a constant value which depends on

reduced frequency parameter, K. Increasing K leads to improved stability. Figure 7 illustrates these results, which are in qualitative agreement with test experience. A tendency is seen for a 'critical' sector width, $\theta\bar{c}$, (ie a width beyond which very little or no change in intensity is required to promote stall) to exist at a given K.

In deriving Figure 7 a stall lift coefficient equal to the steady stall value has been assumed in the absence of an adequate theory for predicting unsteady stall. This is clearly inadequate and much further work is required here. Reference 41 presents normal force results derived from high response rotor blade static pressure recordings aimed at yielding experimental data in this area.

It should be recalled that the above applies to rotor stall induced surges. Compressor instability may, of course, be promoted by stator stall, wall, or corner stall, etc.

Effective Minimum Total Pressure

In an attempt to overcome the dynamic stall problem an effective incidence or effective minimum total pressure, which lags the 'instantaneous' value may be hypothesised, Reference 42, 43. Blade stalls and rotor-induced surges are then supposed to occur when the effective incidence or distortion intensity is such that steady stall or fixed-throttle surge pressure ratio limits are reached. This approach obviates the need to calculate dynamic lift overshoot but substitutes an equivalent need to evaluate appropriate time constants.

For a simple first order system it may be shown that an effective distortion intensity may be defined for single-lobe square-wave circumferential distortions such that:

$$\frac{(\bar{P} - P_{min\ e})/\bar{P}}{(\bar{P} - P_{min\ i})/\bar{P}} = (1 - \theta^-/_{2\pi})^{-1} \left[\frac{1 - e^{-\theta^-/_{2K}}}{1 - e^{-\pi/K}} - \frac{\theta^-}{2\pi} \right]$$

Here, Pmin i represents the actual total pressure in the θ^- sector and K is the reduced frequency parameter.

Results from this equation and a comparable second order analysis are presented in Figures 8 and 9. The 'effective' sector angle (Figure 8) is of the same order as the 'critical' sector angle predicted by the Sears/Horlock analysis. Intensity 'shape factors' are also similar (Figure 9) and are of the same order as single stage fan test results, Reference 44.

Sensitivity

A simple application of the parallel compressor theory indicates for a strictly vertical compressor constant speed line that the loss of surge pressure ratio

$\Delta PRS \propto (\bar{P} - Pmin\ e)/\bar{P}$

The ordinate of Figure 9 then becomes the sensitivity, Si, where

$$Si = \frac{\Delta PRS}{(\bar{P} - Pmin\ i)/\bar{P}}$$

Sensitivity expressed in these terms represents the rate of loss of surge pressure ratio with distortion intensity.

$Si = 1$ for $\theta^- \geq \theta^-$ crit

$Si < 1$ for $\theta^- < \theta^-$ crit

The approaches of References 42, 43, 44 are conceptually similar.

As square-wave distortions seldom occur in practical installations and blade response evidently depends on the wave form of the distortion, 'form factor' considerations arise, and it is interesting to speculate on the validity of traditional square-wave screen tests.

Cascade Effects

Current theoretical analyses of cascade lift response to oscillatory or spatial distortions suggest that flow interference between individual blades tends to result in a more nearly quasi-steady response. This suggests that critical or effective sector angles for cascades may be lower than those of isolated blades, particularly at the low values of reduced frequency parameter representative of current blade designs, say 0.04 to 0.20. If this is so it suggests cascades may have higher effective stall intensities than isolated blades.

Multi-stage Compressors

Rotor blade lift response may be expected to have a direct bearing on single stage compressor stability response to distortion when stall is initiated in the rotor row. Theoretical analyses point to the idea of a critical or effective distorted sector width,

$\bar{\theta}_c$, which is related to reduced frequency parameter and hence to blade dynamic response. They introduce 'sensitivity' and effective distortion intensity concepts.

Results from such analyses cannot sensibly be carried across to multi-stage compressors in an a-priori quantitative sense due to the large number of considerations which influence their stability response - stage design and matching, stator stall, distortion propogation or transfer characteristics, inter-row volume dynamics, etc. Nevertheless the ideas developed for isolated blades appear to have close counterparts in multi-stage machines. Figure 10 shows an arbitrary estimate of compressor response based on the above approach. Trends agree tolerably well with experimental observations (cf Table 1). The concept of a critical sector angle has been established experimentally for some time, Reference 7.

The parallel compressor theory provides a means for estimating multi-stage compressor stability response to circumferential distortion. The theory assumes compressor exit static pressure is constant, no circumferential flow mixing occurs within the compressor, low and high total pressure sectors of the compressor operate on an undistorted corrected speed characteristic. In order to achieve quantitative agreement with this theoretical model - which uses the fixed throttle datum surge line, the foregoing suggests that experimental correlations should be based on seeking an effective distortion intensity such that

$$(\bar{P} - P_{min\ e})/\bar{P} = (\bar{P} - P_{min\ i})/\bar{P} \quad \text{for} \quad \bar{\theta} \geq \bar{\theta}_c$$

$$(\bar{P} - P_{min\ e})/\bar{P} < (\bar{P} - P_{min\ i})/\bar{P} \quad \text{for} \quad \bar{\theta} < \bar{\theta}_c$$

In the latter case, for square-wave distortions, simple area weighting allows effective distortion intensity to be evaluated once actual intensity, $\bar{\theta}$, and $\bar{\theta}_c$ are known.

If the above considerations are correct then all Δ PRS dependency on $\bar{\theta}$ should be removed, ie,

$$\Delta PRS = f\left(\bar{\theta}, (\bar{P} - P_{min\ i})/\bar{P}\right)$$

should reduce to

$$\Delta PRS = f\left((\bar{P} - P_{min\ e})/\bar{P}\right)$$

A compressor sensitivity, Se, may then be defined such that

$$Se = \frac{\Delta PRS}{(\bar{P} - P_{min\ e})/\bar{P}}$$

In general, Se, may be expected to depend on distortion intensity level. As stage matching varies with speed there appears to be no fundamental reason why $\bar{\theta}_c$, which represents effectively a multi-stage dynamic response factor, should not vary with compressor speed or flow.

Theoretical and experimental results for a range of single-lobe square wave patterns and flows for a five-stage research compressor (Figure 2) are compared on this basis in Figure 11. Agreement is good. Figure 12 presents similar results for a four-stage research compressor.

Previous comparisons with the parallel compressor theory have tended to be cruder as the selected value of critical sector angle was less finely tuned. Similar agreement has been found for the data of Reference 38. Where evident departures from the parallel compressor assumptions occur, eg, the bending of the corrected speed line of Figure 3, agreement with theory is less good, References 4, 7. Nevertheless reasonable experimental correlations have been achieved. An important aspect to be borne in mind in attempting such correlations is that of measurement accuracy.

The variation of $\bar{\theta}_c$ with flow, established experimentally for five compressors is shown in Figure 13. Critical values are lower at reduced flow. It has been found that general levels are higher for LP compressors than for HP compressors. No satisfactory method of predicting $\bar{\theta}_c$ for multi-stage compressors has yet been established.

Figure 14, (based on the data of Figure 11) illustrates how sensitivity, Se, varies with distortion intensity. Se is generally greater but tends to unity at higher flows where the compressor speed characteristics are more nearly vertical, and as intensity increases, ie, as more of the (steepening) speed characteristic is used up.

2.4 SURGE LINE LOSS CORRELATIONS - RADIAL DISTORTION

It is usual for both tip and hub-low radial distortions to attenuate to the normal interstage radial flow gradients through the front stages of a well designed multi-stage compressor. Stability response is strongly dependent on stage design rules and radial matching of these stages, Reference 20. As they tend to be highly developed (eg to in-

crease flow capacity) continuous updating of distortion response data is required. It may be expected that highly loaded single stage fans tend to be more sensitive to such distortions than multi-stage units. Fixed-geometry multi-stage compressors are generally more sensitive at intermediate to low speeds when front stages are more highly loaded. This result is illustrated in Figure 16a which presents turbojet engine surge pressure ratio loss correlations for various square-wave radial distortions, Reference 38. The radial distortion index reflects hub-tip radial pressure differences defined in the annulus areas indicated. In this case some hub spoiling was found to be beneficial. Tip spoiling destabilised the compressor.

The hub performance of low hub/tip ratio turbofans is particularly sensitive to hub-low distortion: the relatively flat characteristics of the blade root sections means that work available to make up a flow defect is limited so that distortion attenuation tends to be poorer - which impacts core engine stability. Hub blade speeds are relatively low so that root sections tend to be highly loaded.

Theoretical treatments of radial distortion using axisymmetric computer solutions, possibly with zero wall velocity, de Haller number, or diffusion factor as indicators of incipient stall may provide insight into radial distortion response. Stage stacking problems and the need for surge criteria arise.

Data on the effects of representative inlet profiles are comparatively sparse. Results obtained from compressor rig tests using square-wave screens may be misleading in this respect, particularly on low hub/tip ratio designs, as flow defect regions are exaggerated and radial rematching may consequently be unrepresentative.

It is believed that generalised correlations of ΔPRS with distortion for different compressor designs in pure radial distortion is not possible within the current state of the art for the above reasons. To illustrate this point Figure 16b presents correlations of ΔPRS with a radial distortion index identical to that used in Figure 16a for the seven-stage compressor result given in Figure 4. While sensitivity trends with flow are the same the stability response is in the opposite sense, for example tip low distortions stabilise the compressor.

2.5 SURGE LINE LOSS CORRELATIONS - MIXED DISTORTION

The distortion response of advanced technology engines is complex and its description is essentially one of developing experimentally more sophisticated numerical distortion indices to achieve adequate stability correlations. As stated earlier different indices may be required to account for losses of surge pressure ratio and rematching. A consequence of the attenuation of radial distortion is that HP spool sensitivity is predominately a question of its response to residual inlet circumferential distortion. As HP spools can exert strong stabilising influences on LP spools, designing for engine tolerance requires balancing surge margin requirements and sensitivities on both. Optimum distortion indices will differ for both. It follows that the inlet/engine interface descriptor represents a compromise expression and engine response data scatter arises.

The accuracy to which distortion indices and compressor surge pressure ratio losses - which represent differences between comparatively large quantities, can be defined in mixed distortion adds to the difficulties of correlating mixed distortion data. An ostensible failure of one index to correlate one set of compressor response data as well as another does a different set may, in fact, merely represent sampling inaccuracy, for example. The problem is particularly acute for time-variant distortion. A 10% loss of surge pressure ratio is very significant. Sampling errors may account for up to $\pm$ 2% correlation scatter.

Figure 15 indicates the order of magnitude of surge pressure ratio loss for various levels of the DC (θ crit) index, (Appendix), for eight compressor designs. The data covers a range of circumferential and mixed distortion, and engine speeds.

2.6 DISTORTION INDICES

Correlations of losses of surge pressure ratio due to circumferential distortion using comparatively simple indices of the DC (θ crit) type have, in general, worked well, and, at least in some cases, agreed with parallel compressor theory extremely closely. The treatment of radial distortion is less amenable and adequate theoretical guide lines have not as yet been developed. For mixed distortions comprising circumferential and moderate radial distortion components comparable correlations of turbojet engine response have been achieved using radially-averaged pressures, Reference 7. Bypass engine response has been correlated using DC (θ crit) parameters defined separately for core and bypass flows, utilising appropriate datum mean total pressures.

A major compatibility goal, Reference 45, is the evolution of numerical descriptors or indices which are sufficiently general that all major aspects of distortion shape, intensity etc, which affect surge pressure ratio are correlated with minimum scatter. Efforts over the past few years have led to the development of complex algebraic indices which contain terms that are assigned values once compressor response has been established experimentally. These are based on the idea that compressor response to complex patterns may be built up by superposition of pure circumferential and radial response data.

In simplified terms:

$$(\Delta PRS)_{mixed} = (\Delta PRS)_C + b\,(\Delta PRS)_R$$

Where b represents a superposition factor

Denoting any distortion index by K and assuming sensitivity, S, is independent of intensity level:

$$(\Delta PRS)_C = S_C.K_C$$

$$(\Delta PRS)_R = S_R.K_R$$

$$(\Delta PRS)_{C+R} = S_{C+R}.K_{C+R}$$

so that

$$K_{C+R} = \left(\frac{S_C}{S_{C+R}}\right) K_C + b\left(\frac{S_R}{S_{C+R}}\right) K_R$$

$$= A.K_C + B.K_R$$

In its simplest form therefore the definition represents a linear combination of circumferential and radial distortion indices. This type of index is capable of considerable elaboration, eg K_C may contain radial weighting terms; K_R circumferential extent factors and each may be chosen to be a maximum value with respect to radius, etc. An important feature is that turbomachinery response data is implicit in the definition which is consequently more soundly based than purely descriptive complex indices that have been suggested in the past.

It is currently held that a general distortion index should comprise the following elements.

- Magnitude or Intensity
- Shape factor
- Spatial extent factor
- Multiples per revolution
- Sensitivity
- Superposition factors
- Weighting factors

An additional term to account for compressor frequency response needs to be specified for time-variant distortion.

Such indices are flexible, more difficult to comprehend physically, and may demand a large amount of compressor test data in order to be evaluated. In view of accuracy questions and the lack of coordinated data available in the literature it is not clear at present to what extent current complex descriptors have bettered simpler ones either in correlating particular compressor/engine experience or in improving practical prospects of universality. It appears reasonably certain however that indices sufficiently general to describe turbomachinery stability response to arbitrary distortions accurately will necessarily be complex and expensive to evaluate. Clearly, it is important to identify dominant patterns at the inlet/engine interface to minimise descriptor complexity.

Two indices of the above type are KA_2, Reference 46, and 'Method D', Reference 47, (see Appendix).

$$KA_2 = K\theta + b.Kra_2$$

$$ID = b.S_C.IDC + S_r.IDR$$

The former index reflects developments from earlier radially-weighted circumferential indices such as KD2, $K\theta$, KC2, (see Appendix). Direct comparison of these indices is not in general possible as numerical exponents differ in specific applications. Efforts to standardise the descriptor system are underway.

Indications of the relationships between some of these and the θcrit based indices are illustrated in Figure 17 (KD2 - ΔP120), Figure 18 ($K\theta$ - DC120), and Figure 19 (KA_2 - DC120), using subsonic inlet steady state data. The various descriptors agree reasonably well within the data scatter shown, indicating that surge-inducing distortions may be expressed in terms of alternative indices in this particular case. Similar agreement was found when comparing KC2 and DC90.

A comparison of calculated and experimental losses of surge pressure ratio, based on method D, is shown for a wide range of radial, circumferential and mixed distortions in Figure 20, Reference 48.

2.7 TIME-VARIANT DISTORTION

Dynamic or time-variant distortions arise from a number of sources external to and within the inlet and are generally of the in-phase spatially uniform (buzz) type, or, more generally, contain significant out of phase spatial components arising, for example, from turbulence. The question has now been studied for over a decade and is a fundamental stability issue where intake flow is significantly unsteady, References 49, 50, 51, 52.

In-Phase (Oscillatory) Flows

The major feature of flows occurring at frequencies higher than those which invoke engine control system response is dynamic stage mismatch promoted by interstage and interspool volume lags and dynamic blade row response. The problem is amenable to theoretical treatment using analytical methods based on steady stage characteristics and, for the greater part, on lumped unsteady continuity, momentum, and energy conservation equations utilised to account for interstage volume lags. References 53, 54, 55, 56, 57. Where stage characteristics are well defined results have proved quite successful in predicting undistorted surge lines and oscillatory distortion response. Typical results are shown in Figure 21. Further experimental work remains to be done to clarify the range over which analytical assumptions may be regarded as valid.

Models with combined dynamic blade row response have been discussed in References 58 and 59.

Some of the main turbomachinery response considerations are:

- Fixed throttle surge lines do not indicate stability limits in oscillatory flow.
- The main mechanism of stage mismatch is amplitude attenuation and phase shift at constant frequency.
- Large interstage and spool exit volumes are destabilising. Thus LP compressors of bypass engines tend to be more sensitive to unsteady flow due to large bypass duct volumes.
- Compressors tend to be more tolerant to oscillatory inlet flows at low frequency and at very high frequency.
- Stages matched away from stall and having steep characteristics tend to be more stable.

Spatial Distortion

Early work aimed at improving stability correlations was based on using spatially-averaged RMS total pressure turbulence levels. While correlations improved, these were far from satisfactory - principally because RMS levels, themselves stationary quantities, could not properly account for spatial phase differences of the unsteady flow and hence dynamic distortion. Developments have subsequently shown that the major stability features of turbulence- induced distortion can be described as an extension of steady-state distortion concepts to a time scale of the order of a rotor revolution- typically 5 milliseconds (200 Hz). This has meant that sophisticated data acquisition and processing techniques utilising high response instrumentation and analogue/digital computation have been developed to handle the enormous quantities of data involved: For an inlet test point of 16 seconds a total of 16×10^3 distortion patterns and indices could be involved in a full digital analysis, implying, for a 40 pitot probe array no less than 64×10^4 so-called instantaneous readouts would need processing. A programme involving 150 test points would imply ?.4 million indices and 98 million pitot readings. To contain the computational task to sensible limits analogue data processing is required, Reference 46, digital processing being restricted to providing detailed information circa the peak distortion. Engine tests during which time-variant distortion data are obtained require that the peak "surge inducing distortion event" be identified.

A typical result, derived from a full-scale inlet-engine assembly tested under simulated supersonic flight conditions is shown in Figure 22. The lower curve shows total pressure recovery, representing in-phase oscillations, for a time period of approximately 350 milliseconds prior to the appearance of a surge hammershock at the inlet instrumentation plane. The upper curve represents spatial distortion expressed in terms of the DC90 distortion index. Peak distortion occurred within 20 ms of the appearance of the hammershock indicating this was the surge inducing event. The time lag (usually between 10 to 25 ms, Reference 39) represents the time for the distorted flow to stall the compressor stages and for the resulting hammershock wave to propogate forwards to the instrumentation plane. The majority of engine testing involves identifying this peak distortion in terms of aircraft, inlet, and engine primary variables.

It is currently believed that stability response to peak time-variant distortion

may be simulated by means of screens. Support for this view is shown in Figure 23, Reference 23, 63.

A number of recent developments have indicated that further work is required:

(1) To evaluate time-variant distortion transfer characteristics across LP compressors. This is required to establish HPC dyramic response correctly.

(2) To establish the variation of filter cut-off frequency or digital averaging time with engine speed - Dynamic response considerations, analogous to those for in-phase oscillations (involving stage matching), indicate that stability is significantly affected. Data, Reference 51, confirms this and suggests that averaging times might vary from 0.5 to 4 LP rotor revolutions.

(3) To improve data acquisition monitoring and accuracy.

(4) To determine the length of time required on test condition to establish that representative peak distortions have been experienced, Reference 64.

An important result which emerges from the above considerations together with those of the previous section is that the nature of engine stability response to peak time-variant distortion remains probabilistic or statistical. Reference 39 has indicated, for example, that the surge-inducing peak distortion level, expressed as K_θ, exceeded previous peaks only in 73% of all surge cases investigated. Time-averaged distortion was a poor indication of engine stability response.

Efforts have had to be made to understand the mechanisms of random processes - studies which rely heavily on applying statistical methods, References 60, 61, 62. Some progress has been made in estimating time-variant distortion from local RMS total pressure recordings, Reference 49.

3. TEMPERATURE DISTORTION

Inlet temperature distortion, arising from such sources as hot-gas ingestion during thrust reversal, V/STOL operations, armament firing, and from steam ingestion, can cause serious performance losses, engine control and stability problems, References 8, 42, 43, 65, 66, 67, 68, 69. Designing for ingestion avoidance rather than for tolerance is thus a major aircraft and powerplant activity - it is common practice on a wide range of civil transport aircraft for example to vector reverser jets to achieve the best ingestion-free reverser cancellation boundaries. Contributory reasons for avoiding time-variant ingestion from such sources are, firstly, that, once it has started, it is difficult to limit to values dictated by available engine stability margins; and, secondly, temperature distortion, unlike pressure distortion attenuates only to a small extent through the engine and therefore affects downstream engine components to a greater degree.

Figure 24 shows, by way of example, the time-variant growth of temperature distortion due to near field ingestion of exhaust gases of the Pegasus/Harrier V/STOL installation, illustrated in Figure 25. The aircraft was held down for these tests in order to investigate maximum temperature distortion characteristics. Maximum (peak to peak) temperature distortion is represented by the difference between the upper and lower lines of the figure. Temperature rise is expressed as a percentage of excess front nozzle temperature above ambient and was approximately 100°C for this engine. Peak local temperature distortion did not exceed 16°C due to shielding of the inlet by the relatively cold front nozzles. Temperature rise rates are slow. Surge was not experienced.

Temperature distortion generated at compressor exit as a consequence of inlet total pressure distortion attenuation across the compressor may also be a significant factor in destabilising a downstream compressor and needs to be taken into account in compatibility audits.

Steady Spatial Distortion

Figure 26, produced from Reference 66, illustrates, for a turbofan engine, typical losses of surge pressure ratio that can be experienced due to steady spatial distortion by an HP compressor having a representative surge margin. The right hand diagram presents a correlation of the compressor data and compares predictions from the parallel compressor hypothesis. A correlation parameter, $\left(\frac{T_{max\,\theta crit} - \bar{T}}{\bar{T}}\right)$, having $\theta crit = 120^\circ$ approximately, was found to be best in this case. For complete loss of surge margin, $\Delta PRS = 20\%$, the permissible distortion level is approximately 10%. Thus, referring to Figure 24, an installation having, say, a front nozzle excess temperature of 1000°C and a 6% mean temperature ingestion characteristic would experience surge, if the high temperature region were sufficiently great and located near the hub, about two-tenths of a second after nozzle rotation to the vertical position - approximately half way up the maximum temperature rise characteristic. Ingestion, once allowed to start, would have proved difficult to stabilise.

A more general attempt to correlate steady spatial distortion data available is presented in Figure 27. This incorporates the data of References 8 and 66 and uses the generalised TCθ crit parameter. Reference 8 presents comparable pressure and temperature sensitivity data for a turbojet engine operating in the high speed regime, pressure and temperature 180° extent distortion data being expressed as (maximum - minimum)/average. Loss of pressure ratio was defined either at constant speed or constant corrected flow, (Table II).

TABLE II - TEMPERATURE DISTORTION SENSITIVITIES

Distortion, $(\frac{\text{Max - Min}}{\text{average}})$	Sensitivity, S = ΔPRS/Distortion	
	Constant N_C	Constant W_C
Total Pressure	0.6	0.5 to 1.0
Total Temperature	0.62	0.75

In these terms sensitivities are of comparable order and correlations were found to be better when ΔPRS was formulated at constant corrected speed. To use such correlations, however, changes in corrected flow with distortion need also to be defined.

The results of turbofan tests, Reference 66, show that a total pressure distortion having a magnitude and extent directly related to that of the imposed total temperature distortion can be produced as the flow passes through the turbomachinery. The same effect was not observed during the turbojet engine tests reported in Reference 8. In the turbofan case surge was promoted by the effect of the temperature distortion on the HP compressor, local shifts in the operating points occurring at virtually constant pressure ratio due to changes in corrected speed - as assumed by the parallel compressor theory.

Rapid Inlet Temperature Transients

The treatment of transient temperature distortion requires the use of high response measurement techniques similar to those needed for treating time-variant pressure distortion (Section 2.7). Such techniques have not generally been used largely due to the intractability of the ingestion problem, the practice of designing to avoid ingestion, and the difficulty of simulating it properly in rig compressor and engine test facilities. Controlled experimental work has been carried out to establish the effect of rapid temperature transients, typical of those experienced during gun and rocket wake ingestion, eg, 2000°C to 8000°C/sec, in fixed portions of the inlet duct, References 66, 68.

Data from steam ingestion tests, which include representative pattern growth, are also available, Reference 69.

Early NASA tests on a turbojet engine, Reference 68, showed that dynamic stage mismatch and stall, followed either by recovery, surge, or flameout could occur during rapid temperature ramps, depending on ramp rate. Three important observations were made:-

- Engine response to uniform temperature ramps was stable provided ramp rates did not exceed 1000°C/sec, approximately.
- For rates above this threshold value stage stall and surge occurred rapidly, within 20 milliseconds approximately, due to a transient shift in corrected speed at sensibly constant pressure ratio - transient pressures throughout the compressor had not had time to change.
- The additional compression work during the transient was approximately offset by heat transfer effects.

It may be shown from the flow conservation equations and the latter observations that the transient temperature rise at entry to any stage for a ramp input is given to a first order by a simple gas transport equation:-

$$(\delta T_t)_{\text{stage}} = (\delta T_t)_{\substack{\text{comp} \\ \text{inlet}}} - \left(\frac{x}{Va}\right).\dot{T}_t = \dot{T}_t.\left(t - \frac{x}{Va}\right)$$

At high corrected speed, circa design, if stage stall may be assumed to be a sufficient condition to promote surge (rear stages are well matched) then, as mechanical speed is constant, equating $(\delta T_t)_{\text{stage}}$ to the value required for stage stall at constant stage pressure ratio, given by:-

$$(\delta T_t)_{\substack{\text{stage} \\ \text{stall}}} = (T_t)_{\substack{NO \\ \text{entry}}} \left[\frac{(N/\sqrt{T})^2_{N.O.}}{(N/\sqrt{T})^2_{\text{stall}}} - 1\right]$$

a first estimate of the inlet temperature rise necessary to cause surge may be made.

The time to surge from the commencement of the temperature rise is then given by:-

$$t = (\delta T_t)_{inlet} / \dot{T}_t$$

The above considerations apply for an unlimited temperature ramp. For an inlet temperature spike stage stall would occur when:

$$(\delta T_t)_{inlet} = (\delta T_t)_{\substack{stage \\ stall}}$$

Figure 28 shows the result of applying this method to available experimental results for unlimited ramps. The data includes that for ramps in hot sectors of less than 360° circumferential extent. The experimental scatter of the data may in part reflect difficulties in the measurement of fast transients.

At sufficiently low ramp rates surge does not occur as the time to stall is sufficiently long to allow stage pressure ratio to drop. Little is known about the magnitude of this threshold value. Correlations suggest about 1200°C/sec. Some data indicate quasi-steady response at about 100 milliseconds, the corresponding threshold rate being in the region of 500 to 1000°C/sec. Figure 28 illustrates the need for information at lower temperature distortion rates, of the order of those expected during thrust reversal or V/STOL operations. The correlation suggests a critical combination of distortion extent and rate exists.

At off design conditions it is unlikely that a single stage stall criterion would provide a sufficient condition for surge prediction due to stage mismatching. A stage-by-stage dynamic compressor model similar to that developed for in-phase pressure oscillations would be required.

4. COMBINED TEMPERATURE AND PRESSURE DISTORTION

Inlet temperature distortion, when encountered in practice, is usually accompanied by total pressure distortion or superimposed on base-line inlet pressure distortion. Attenuation of pressure distortion through the compressor creates temperature distortion. In general both are time-variant problems. It is evident that the spatial orientation of locally high temperature zones in the inlet may not coincide with zones of minimum pressure. As pressure distortion propogates through the compressor the created temperature distortion may be spatially out of phase - the maximum temperature zone may be rotated 45° to 90° or so in the direction of rotation relative to the pressure distortion zone, References 8, 66.

The effect of superimposed temperature and pressure distortions of 90° circumferential extent on the HP compressor of the Spey engine, is shown in Figure 29. These tests were conducted with maximum temperature and minimum pressure zones superimposed. ΔPRS is defined at constant corrected flow.

Reference 8 presents an excellent treatment of this question: It is shown that superpositioning 180° extent pressure and temperature distortion exerts the largest destabilising influence; diametrically opposed distortions having considerably less effect - to the point where pressure distortion induced instability may be cancelled by imposing the appropriate temperature distortion. The major effects may be predicted using a simplified parallel compressor theory. Figure 30, reproduced from Reference 8, compares predicted and measured results on the basis of ΔPRS defined at constant speed.

The question of overlapping is important to that of stability auditing. The worst destabilising configuration is that given by superimposed distortions which may readily be predicted by the parallel compressor theory.

$$\Delta PRS_{total} = \Delta PRS_P + b.\Delta PRS_T$$

Very little or no controlled experimental work appears to have been done on combined time-variant total pressure and temperature distortion.

5. STABILITY AUDITING PROCEDURES

On all but the simplest powerplants or those with an established and relevant historical background the development of a compatible propulsion system requires that inlet distortion and engine stability response characteristics be evaluated sufficiently early in the system development cycle for distortion considerations to impact component design. The foregoing has shown the subject to be extremely complex, requiring a high degree of cooperation between the aircraft and engine manufacture, procurement agency and customer. Adequate distortion indices, means of assessing performance and stability, and test techniques need to be evolved if the risk of encountering flight stability problems is to be minimised, Reference 31.

Six interrelated phases of the propulsion system evolutionary process may be identified. These are summarised in Table III, Reference 63.

TABLE III - STABILITY EVALUATION PHASES

PHASE	ACTIVITY DURING PHASE	PROPULSION SYSTEM STATUS AT END OF PHASE
Conceptual Studies	Analytical Evaluation of many aircraft and propulsion system configurations.	Candidates that can potentially meet requirements.
Preliminary Design	Design, analysis and test of inlet and engine components.	Mission defined. Propulsion system defined.
Development	Development of required quality by continuing analysis, component and engine tests.	Propulsion system ready for qualification. Data Bank established.
Engine Qualification	Definition and certification of the flight engine.	Engine with acceptable performance and stability quality at specified conditions.
Flight Test	Inlet and engine improvements are flight tested to produce best combination of performance and stability.	Aircraft with acceptable performance and stability quality over flight and manoeuvre envelopes.
Operational	Production configuration used by customer.	Operational capability defined.

The engine stability audit may need to include all or some of the following major elements:-

- Identification of Datum Surge and operating lines
- Performance changes due to distortion
- Surge line losses due to distortion (component sensitivities)
- Distortion transfer characteristics
- Engine component rematching
- Spool flow interference
- Reynolds number effects on surge, operating lines, and sensitivities
- Horse-power and bleed off takes
- Engine throttle and reheat transients
- Inlet/engine dynamic coupling
- Engine manufacturing tolerances
- Control system (operating line) tolerances
- Distortion effects on control system sensors
- Deterioration
- Accommodation fixes (eg, fuel dipping, blow-off)

Denoting pressure and temperature distortion coefficients, sensitivities, and fractional surge pressure ratio losses by K_P, K_T; S_P, S_T; ΔPRS_P, ΔPRS_T, respectively, a simple illustration of the manner in which the stability response of downstream compressors to steady engine inlet total pressure distortion at a given corrected flow or speed is given below:-

$$\Delta PRS_{total} = \Delta PRS_P + b.\Delta PRS_T = (S_P A + bS_T C_T) K_{P1}$$

where,

$A = K_{P2}/K_{P1}$ = Pressure Distortion Attenuation Factor

$C_T = K_{T2}/K_{P1}$ = Temperature Distortion Generation Factor

Subscripts 1 and 2 refer to LP compressor inlet and exit, respectively.

Hence, if available surge margin, taking account of operating line shifts due to distortion, is such that:-

$$SM_{HPC} = \Delta PRS_{total}$$

$$\text{then, } K_{P1} = \frac{SM_{HPC}}{\left[S_p A + b S_T C_T\right]}$$

ie Engine Inlet Distortion Tolerance of HP Spool

$$= \frac{\text{Available Surge Margin}}{\text{Overall Sensitivity}}$$

The denominator in this expression represents a "lumped" sensitivity incorporating LP compressor distortion transfer terms. In practice the auditing process is more involved because of the need to account properly for the various factors listed above, eg Reynolds number, rematching, interference, bleeds, etc. Computer solutions are usually used.

Compressor Rig Test Limitations

It is becoming increasingly evident that great care is required when reading across to the engine distortion response characteristics established from compressor rig tests. Some of the factors involved are:-

- Reynolds number differences (eg for installed HP compressors).
- The effects of rig duct volumes which are generally unrepresentatively large so that dynamic response to in-phase and time-variant spatial distortion and transfer characteristics may be affected.
- Spool interactions in the presence of distortion may be atypical, eg, due to exit static pressure distortions imposed by the downstream spool.
- Close-coupled compressor exit diffusers may be destabilising, particularly for lower pressure ratio fans, Reference 70.
- Engine component rematching is not represented during testing, eg, dynamic core/bypass flow coupling.
- Representative temperature distortion tests are difficult to implement.

It should be borne in mind therefore that synthesising stability response from rig data is not an exact science. It follows that a degree of flexibility in interpreting pre-engine test estimates is necessary

6. FOREIGN GAS

In this paper attention is restricted to consideration of gases that may enter the inlet as a consequence of armament wake ingestion, specifically from rockets. Engine response depends not only on temperature and pressure distortion but also on the quantity and nature of the gas ingested - which is virtually impossible to define adequately at the inlet/engine interface. The complexity of the total problem has led to the advocation of simulated rocket wake tests, Reference 68.

A large rocket may have the following relevant characteristics:-

Mass Flow	40 to 50 lb/sec for 2 to 3 seconds
Exhaust Velocity	7000 to 8000 ft/sec
Exhaust Pressure	1000 psia
Exhaust Temperature	2000°K
Flame Length	50 ft
Plume Diameter	2 to 3 ft

Wake ingestion promotes time-variant pressure and temperature distortion whose (varying) spatial extent at engine entry depends on altitude, inlet and rocket location, launch trajectory; aircraft forward speed, attitude and engine power setting. Engine stability may be affected by gas chemical composition and its concentration relative to the inlet air supply and the duration of the ingestion. Burning within the ingested wake may continue to occur.

Approximate examples of gas product weight concentrations are shown tabulated for illustration:-

TABLE IV - PRODUCT WEIGHT CONCENTRATION

Product		Concentration (10^{-3} Gram Mol per Gram)	Gram Molecular Weight	Weight Product ($W_{product}/W_{gas}$) %
Aluminium Oxide	Al_2O_3	3.03	101.96	30.8
Carbon Dioxide	CO_2	0.84	44.01	3.7
Carbon Monoxide	CO	8.85	28.01	24.8
Hydrogen	H_2	11.90	2.016	2.4
Water	H_2O	5.36	18.02	9.7
Nitrogen	N_2	2.90	28.02	8.1
Hydrochloric Acid Gas	HCL	5.56	36.46	20.3
Free Hydroxyl Radicle	(OH)	0.001	17.008	-
Chlorine	CL	0.01	35.45	-

The effect on the engine depends upon the weight of product ingested in relation to the engine airflow demand;-

$$\left(\frac{W_{product}}{W_{air}}\right)\% = \left(\frac{W_{product}}{W_{gas}}\right)\% \times \frac{W_{gas}}{W_{air}}$$

and, for bypass engines, on how much enters the core engine.

Carbon monoxide and hydrogen are fuels. Considering, by way of example, a low altitude condition for a bypass engine having an airflow demand of 400 lb/sec and a total fan:core flow ratio of 2.7, (BPR = 1.7) then for full ingestion of 40 lb/sec of gas, the by-weight concentration of these products to air is approximately:

Fan Flow: CO% ⎍ 3 ; H_2% ⎍ 0.3

Core Flow: CO% ⎍ 9 ; H_2% ⎍ 0.8

On the basis of a seven-stage single-spool turbojet engine test the core flow quantities may be sufficient to cause surge by creating a fuel rich situation, Figure 31.

The main results from these tests, in which products and gun gases were injected cold, were:

Nitrogen - No effect for quantities up to 12% by weight of airflow.

Carbon Dioxide - Slight drop in engine speed and jet pipe temperature for quantities up to 13.6%.

Hydrogen - Small Quantities - acceleration due to overfuelling.

Increased Quantities - Overfuelling surge followed by recovery and flame flashback.

(Engine response was dictated by instantaneous flow rate and not the total quantity of gas ingested).

Carbon Monoxide - Small Quantities - Overfuelling Acceleration.

Larger Quantities - Overfuelling Surge.

Simulated Gun Gas - Overfuelling Acceleration and Surge at 22% weight flow.

It is extremely difficult to decide to what extent gas chemical composition influences engine stability response to rocket wake ingestion. The cold gas tests referred to above indicate foreign gases may be destabilising-depending on their composition, the quantity ingested and its spatial location. Reference 67 indicates however that compressor mismatch and operating point trajectories during simulated rocket wake ingestion tests were not changed though the products of combustion were.

7. SURGE HAMMERSHOCKS

One of the problems involved in stressing fixed and moving inlet structures is that of dynamic loads experienced during engine surge. Compression and expansion wave over- and under-pressures relative to pre-surge steady levels occur as a consequence of flow breakdown within the compressor. Pressure amplitudes depend on engine operating conditions, inlet design and operational environment. Stressing for such loads involves determining pressure ratios and wave forms or signatures at various locations within the inlet and, in particular, at the inlet/engine interface. The initial 'shock wave' following surge initiation is a characteristic of the engine stalling process, the rarefaction waves depend upon inlet configuration. Cyclic surge may occur, typical frequencies being of the order of 10 Hz. The surge cycle comprises a flow stoppage/reversal period represented by the 'four wave transit time' and a recovery period of approximately the same duration, Reference 7.

Discussions of surge hammershocks may be found in References 27, 34 and 72.

Figure 32 presents interface overpressure data correlated against overall compressor steady state pressure ratio immediately prior to surge. The data obtains from equilibrium surge experience on various turbojet and turbofan engines. The data is scattered due to the statistical nature of the surging process, asymmetry of the shockwave front and measurement inaccuracies, etc. The Olympus data obtained is from a wide range of sources representative of ground, subsonic and supersonic flight conditions. The overpressures at the interface may be thought of as representing a compressor delivery back pressure level attenuated via the complex wave reflections that occur within the compressor. Each engine may be expected to have its own characteristics.

Reasonable first order estimates of the overpressure may be accomplished using shock theory provided a mass flow assumption after the shock is made. Thus for a uniform shock propogating upstream against the flow in a constant area duct:

$$\frac{p_2}{p_1} = \frac{7M_s^2 - 1}{6}$$

$$M_1 = \frac{5M_s\,(M_s^2 - 1)}{6M_s^2 - (5 + M_s^2)\,(1 - K)}$$

where, $K = (W_1 - W_2)/W_1$ = Relative mass flow change across the shock

M_1 = Flow Mach number upstream of the shock

M_s = Shock Mach number relative to upstream flow conditions

p = static pressure

A useful approximation is presented in Reference 72 in the unique form:

$$\text{Overpressure Parameter} = \frac{\Delta p}{p_1 M_1^{1.26}} = f(K)$$

For complete flow stoppage behind the shock, ($K = 1$), a reasonable approximation to the interface surge overpressure has been found at moderate to intermediate levels of overall pressure ratio. Thus for a duct steady state Mach number of 0.5 immediately prior to surge an overpressure of approximately 1.9 is predicted. The corresponding shock propogation Mach number relative to the upstream flow is approximately 1.35. At higher overall pressure ratios the assumption of flow stoppage is inadequate and flow reversal behind the shock has to be invoked to explain the experimental shock strengths.

Turbofan overpressures are generally less than those of turbojets due to the expansion of the shock as it leaves the core engine and expands to the full compressor face area. Reference 72 presents a theoretical model utilising the flow conservation equations which accounts for the effect. It may be shown that these predictions may be approximated closely by a simpler application of the shock expansion theory of Reference 73 provided that the hammershock is regarded as propogating through the fan prior to its expansion.

Wave rise times at the interface - an important ingredient in panel and moving vane dynamic response calculations can be surprisingly low, approximately 5 to 15 milliseconds.

REFERENCES

(1) Schaub U. W. and Bassett R. W. 'Flow Distortion and Performance Measurements on a 12 in. Fan-in-Wing Model for a range of Forward Speeds and Angle of Attack Settings'. Paper 17, AGARD Conference Proceedings No 91 'Inlets and Nozzles for Aerospace Engines'. Sandefjord, Norway. September, 1971.

(2) Tyson B. I. 'Tests to Establish Flow Distortion Criteria for Lift Engines'. AIAA Paper 64-608, Seattle, Washington. August, 1964.

(3) Plourde G. A. and Stenning A. H. 'The Attenuation of Circumferential Inlet Distortion in Multi-stage Axial Compressors'. Journal of Aircraft Volume 5 No 3 May - June,1968

(4) Williams D. D. and Yost J. O. 'Some Aspects of Inlet/Engine Flow Compatibility! The Aeronautical Journal of the Royal Aeronautical Society. Volume LXXVII. January - December, 1973.

(5) Langston C. E. 'Distortion Tolerance - By Design Instead of By Accident'. ASME Paper 69-GE-115. Gas Turbine Conference and Products Show. Cleveland Ohio. March 1969.

(6) Livesey J. L and Hugh T. 'Suitable Mean Values in One-Dimensional Gas Dynamics'. Journal Mechanical Engineering Science, Volume 8 No 4. 1966.

(7) Reid C. 'The Response of Axial Flow Compressors to Intake Flow Distortion'. ASME Paper 69-GT-29. Gas Turbine Conference and Products Show, Cleveland, Ohio. March 1969.

(8) Braithwaite W. M., Graber E. J. and Mehalic C. M. 'The Effect of Inlet Temperature and Pressure Distortion on Turbojet Performance'. AIAA 73-1316. November, 1973.

(9) Horlock J. H. 'Fluctuating Lift Forces on Aerofoils Moving Through Transverse and Chordwise Gusts'. Journal of Basic Engineering. December, 1968.

(10) Schorr B. and Reddy K. C. 'Inviscid Flow Through Cascades in Oscillatory and Distorted Flow'. AIAA Paper 70-131. Eighth Aerospace Sciences Meeting, New York. January, 1970.

(11) Henderson R. E. 'The Unsteady Response of a Blade Row From Measurements of the Time-Mean Total Pressure'. ASME 73-GT-94. April, 1973.

(12) Ericsson L. E. and Reding J. P. 'Stall-Flutter Analysis'. Journal of Aircraft. Volume 10 No 1. January, 1973.

(13) Fleeter S. 'Fluctuating Lift and Moment Coefficients for Cascaded Airfoils in a Non-Uniform Compressible Flow'. Journal of Aircraft Volume 10 No 2. February, 1973.

(14) Ericsson L. E. and Reding J. P. 'Unsteady Airfoil Stall, Review and Extension'. Journal of Aircraft Volume 8 No 8. August, 1971.

(15) Henderson R. E. and Horlock J. H. 'An Approximate Analysis of the Unsteady Lift on Airfoils in Cascade'. ASME Paper 72-GT-5. March 1972.

(16) Dunham J. 'Non-Axisymmetric Flow in Axial Compressors'. Mechanical Engineering Science Monograph No 3. October, 1965.

(17) Mokelke H. 'The Development of Inlet Flow Distortions in Multi-Stage Axial Compressors of High Hub-Tip Ratio'. ICAS Paper 72-20 September, 1972.

(18) Yeh H. 'An Actuator Disc Analysis of Inlet Distortion and Rotating Stall in Axial Flow Turbomachines'. Journal of Aero-Space Sciences. November, 1959.

(19) Callahan G. M. and Stenning A. H. 'Attenuation of Inlet Flow Distortion Upstream of Axial Flow Compressors'. AIAA 69-485. USAF Academy, Colorado. June,1969.

(20) Povolny J. H., Burcham F. W. Jr., Calogeras J. E., Mayer C. L. and Rudey R. A. 'Effects of Engine Inlet Disturbance on Engine Stall Performance'. Paper X, NASA Conference Proceedings SP-259. Lewis Research Centre, Cleveland, Ohio. November, 1970.

(21) Baumbick R. J. 'Device for Producing Dynamic Distortion Patterns at Inlets of Air Breathing Engines'. NASA TMX-2026. June, 1970.

(22) Braithwaite W. M., Dicus J. H. and Moss J. E. 'Evaluation with a Turbofan Engine of Air Jets as a Steady State Inflow Distortion Device'. NASA TMX-1955. 1970.

(23) Zonars D. 'Dynamic Characteristics of Engine Inlets'. Paper 6 of AGARD LS 53. May, 1972.

(24) Plourde G. A. and Brimelow B. 'Pressure Fluctuations Cause Compressor Instability'. Proceedings of the Air Force Airframe - Propulsion Compatibility Symposium AFAPL-TR-69-103. Wright-Patterson AFB, Ohio. June, 1970.

(25) Bowditch D. N., Coltrin R. E. Sanders N. E., Sorensen N. E. and Wasserbauer J. F. 'Supersonic Cruise Inlets'. Paper IX, NASA Conference Proceedings SP-259. Lewis Research Centre, Cleveland, Ohio. November, 1970.

(26) Ellis S. H. 'Inlet-Engine Compatibility Analysis'. Paper 26 AGARD Conference Proceedings No 91. 'Inlets and Nozzles for Aerospace Engines'. Sandefjord, Norway. September 1971.

(27) Bellman D. R. and Hughes D. L. 'The Flight Investigation of Pressure Phenomena in the Air Intake of an FIIIA Airplane'. AIAA Paper 69-488. USAF Academy, Colorado. June, 1969.

(28) Burcham F. W. Jr. and Hughes D. L. 'Analysis of In-Flight Pressure Fluctuations Leading to Engine Compressor Surge in an FIIIA Airplane for Mach Numbers to 2.17'. AIAA Paper 70-624. San Diego, California. June, 1970.

(29) Van Deusen E. A. and Mardoc V. R. 'Distortion and Turbulence Interaction, A Method for Evaluating Engine Inlet Compatibility'. AIAA 70-632. June, 1970.

(30) Campbell J. L. and Ellis S. H. 'Engine/Inlet Compatibility Analysis Procedure'. AIAA Paper 70-941. June, 1970.

(31) Richey G. K., Stava D. J., Brimelow B., and Bush H. I. 'Airframe-Propulsion Integration for Future Aircraft Systems' SAE Paper 680288. May, 1968.

(32) Braithwaite W. M. and Vollmar W. R. 'Performance and Stall Limits of a YTF30-P-1 Turbofan Engine with Uniform Inlet Flow'. Lewis Research Center. NASA TMX-1803.

(33) Povolny J. H. 'Stall and Distortion Investigation of a YTF30-P-1 Turbofan Engine'. NASA TMX-52622. June, 1969.

(34) Korn J. A. 'The Effect of Inlet Distortion on the Performance and Stability of the Low-Speed Spool of a Turbofan Engine'. AIAA 74-234. January - February, 1974.

(35) Lecht M. and Weyer H. 'Experimental Investigations of a Transonic Axial Flow Compressor Stage with Steady State Distorted Inlet Flow'. Paper presented at the second International Symposium on Air Breathing Engines. Sheffield, England. March, 1974.

(36) Morriss D. P. and Williams D.D. 'Free Jet Testing of a Supersonic Engine/Intake Combination'. The Aeronautical Journal of The Royal Aeronautical Society. Volume 74 Nos 711/712. March - April, 1970.

(37) Brunda D. F. and Boytos J. F. 'A Steady-State Circumferential Inlet Pressure Distortion Index for Axial-Flow Compressors'. Proceedings of the Tenth National Conference on the Environmental Effects on Aircraft and Propulsion Systems.' NAPTC Paper 71-ENV-12. May, 1971.

(38) Calogeras J. E., Mehalic C. M. and Burstadt P. L. 'Experimental Investigation of the Effect of Screen-Induced Total-Pressure Distortion on Turbojet Stall Margin'. NASA TMX-2239, Cleveland, Ohio. 1971.

(39) Burcham F. W., Hughes D. L. and Holzman J. K. 'Steady State and Dynamic Pressure Phenomena in the Propulsion System of an FIIIA Airplane'. NASA TND-7328. July, 1973.

(40) Werner R. A., Abdelwahats M. and Braithwaite W. M. 'Performance and Stall Limits of an Afterburning-Equipped Turbofan Engine with and without Inlet Flow Distortion'. Lewis Research Center. NASA TMX-1947. April, 1970

(41) Peacock R. E. 'Observations of Compressor Rotor Blade Performance in an Inlet Flow with Circumferential Pressure Distortion'. Paper presented at the Fourth Canadian Congress of Applied Mechanics, Ecole Polytechnique, Montreal, Canada. 28th May - 1st June, 1973.

(42) Melick H. C. Jr. and Simpkin W. E. 'A Unified Theory of Inlet/Engine Compatibility'. AIAA 72-1115. November 29th - December 1st, 1972.

(43) Melick H. C. 'Analysis of Inlet Flow Distortion and Turbulence Effects on Compressor Stability'. NASA CR 114577. 31st March 1973.

(44) Korn J. A. 'Estimated Effect of Circumferential Distortion on Axial Compressors Using Parallel Compressor Theory and Dynamic Stall Delay'. AIAA No 74-233. January - February, 1974.

(45) Martin R. J. and Melick H. C. 'A Feasibility Study for Definition of Inlet Flow Quality and Development Criteria'. AIAA 72-1098. December, 1972.

(46) Farr A. P. 'Evaluation of F-15 Inlet Dynamic Distortion'. AIAA 73-784. August 1973.

(47) Moore M. T. and Lueke J. E. 'A Similarity Parameter for Scaling Dynamic Inlet Distortion'. ASME 73-WA/Aero-3. November, 1973.

(48) Steenken W. G. 'F101 Engine Approach to Stability Assessment'. Paper prepared for SAE S-16 Committee. Turbine Engine Inlet Flow Distortion. December, 1973.

(49) Ellis S. H. and Brownstein B. J. 'A Procedure for Estimating maximum Time Variant Distortion Levels with Limited Instrumentation'. AIAA 72-1099. December, 1972.

(50) Calogeras J. E., Burstadt P. L. and Coltrin R. E. 'Instantaneous and Dynamic Analysis of Supersonic Inlet-Engine Compatibility'. AIAA 71-667. June, 1971.

(51) Calogeras J. E. 'Instantaneous Distortion Analysis'. NASA TMX-68189.

(52) Kutschenreuter P. H., Moore M. T. and Collin T. P. — 'Inlet Data for Engine Analysis'. AIAA 70-1214. June, 1970.

(53) Lubick R. J. and Wallner L. E. — 'Stall Prediction In Gas Turbine Engines'. Journal of Basic Engineering. September, 1959.

(54) Kuhlberg J. F., Sheppard D. E., King E. O. and Baker J. R. — 'The Dynamic Simulation of Turbine Engine Compressors'. Fifth Propulsion Joint Specialist Conference, Colorado. AIAA Paper 69-486. June, 1969.

(55) Willoh R. G. and Seldner K. — 'Multi-Stage Compressor Simulation Applied to the Prediction of Axial Flow Instabilities'. NASA TMX-1880. Cleveland, Ohio. 1969.

(56) Corbett A. G. and Elder R. L. — 'The Stability of some Mathematical Models of an Axial Flow Compressor'. University of Leicester - Rolls-Royce Research Study, 1970 - 1972.

(57) Goethert B. H. and Kimzey W. F. — 'Effect of High Frequency Fluctuations of Inlet Flow on Compressor Stall'. Paper presented at the 32nd Meeting of the Propulsion and Energetics Panel of AGARD. Toulouse, September, 1968.

(58) Adamczyk J. J. — 'Unsteady Fluid Dynamic Response of an Isolated Rotor with Distorted Inflow'. AIAA 74-49. February, 1974.

(59) Goethert B. H. and Reddy R. C. — 'Unsteady Aerodynamics of Rotor Blades of a Compressor Under Distorted Flow Conditions'. The University of Tennessee Space Institute. Tullahoma, Tennessee.

(60) Crites R. C. and Heckart M. V. — 'Application of Random Data Techniques to Aircraft Inlet Diagnostics'. AIAA 70-597. May, 1970.

(61) Crites R. C. — 'The Philosophy of Analog Techniques Applied to the Analysis and High Speed Screening of Dynamic Data'. AIAA 70-595. May, 1970.

(62) Sherman D. A., Motycka D. L. and Oates G. C. — 'Experimental Evaluation of a Hypothesis for Scaling Inlet Turbulence Data'. AIAA 71-669. June, 1971.

(63) Schumacker H. E. and Lampard G. W. N. — 'Turbine Engine Inlet Flow Distortion - SAE S-16 Committee Status Report'. Paper presented at AIAA/SAE Ninth Propulsion Conference. November, 1973.

(64) Jacocks J. L. — 'Statistical Analysis of Distortion Factors'. AIAA 72-1100. December, 1972.

(65) Mallett W. E. and Parcells R. F. — 'Catapult Steam Ingestion Tests of Three Turbofan Engines in The A-7 Aircraft'. Paper presented at National Conference on Environmental Effects on Aircraft and Propulsion Systems. Trenton, N. J. May, 1971.

(66) Rudey R. A. and Antl J. — 'The Effect of Inlet Temperature Distortion on the Performance of a Turbofan Engine Compressor System'. AIAA 70-625. June, 1970.

(67) Rich W. A. and Reale R. A. — 'Specification Rocket Test for Turbojet/ Turbofan Missile Gas Ingestion'. NAPTC-ATD-197. February, 1971.

(68) Wallner L. E., Useller J. W. and Saari M. J. — 'A Study of Temperature Transients at the Inlet of a Turbojet Engine'. NACA RM E57C22. June, 1957.

(69) Rich W. A. 'The Simulation of the Ingestion of Missile Exhaust by Turbojets'. Paper presented at National Conference on Environmental Effects on Aircraft and Propulsion Systems. Trenton, N.J. Paper 71-Env-8. May, 1971.

(70) Greitzer E. M. 'Presentation on Fan/Diffuser Flow Coupling' given at University of Cambridge, 20th March,1974.

(71) Denning R. M. and Williams D.D. 'A Discussion of Pressure Variations and the Basic Surge Process in Two Spool Turbojet Engines'. Rolls-Royce Report PPE 49. May, 1966.

(72) Marshall F. L. 'Prediction of Inlet Duct Overpressures Resulting from Engine Surge'. Journal of Aircraft, Volume 10 No 5 pp 274-8. May, 1973.

(73) Davies P. O. A. L and Dwyer M. J. 'A Simple Theory for Pressure Pulses in Exhaust Systems'. Proceedings of the Institution of Mechanical Engineers. Volume 179. PartI. Number 10. 1964 - 1965.

ACKNOWLEDGEMENTS

The authors wish to acknowledge their indebtedness to their colleagues at Rolls-Royce for their help in the preparation of this paper. The views expressed are their own and not necessarily those of their Company. Their thanks are due to the Directors of Rolls-Royce (1971) Limited, (Bristol Engine Division) for permission to publish the lecture.

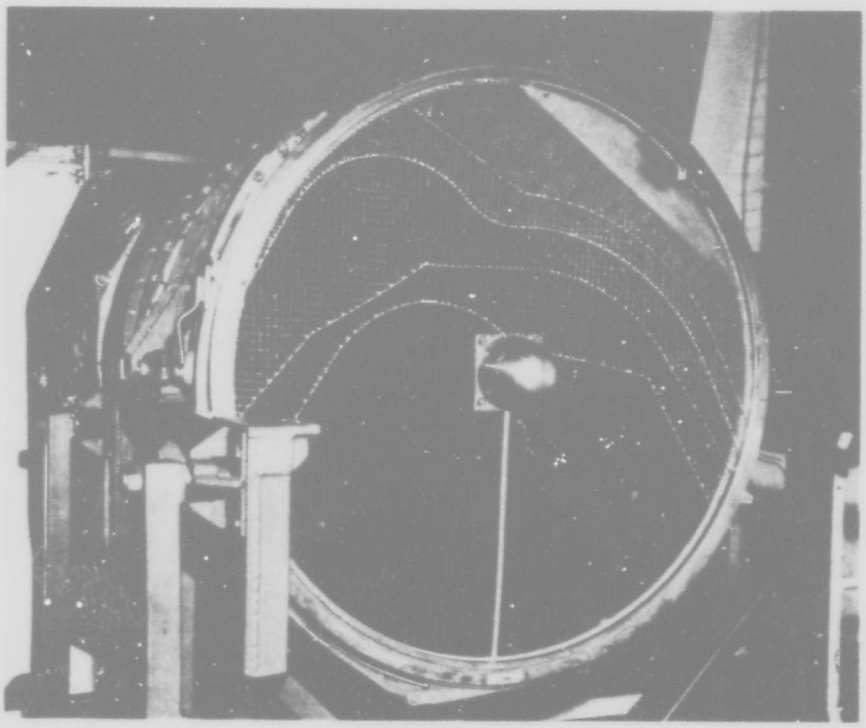

Figure 1

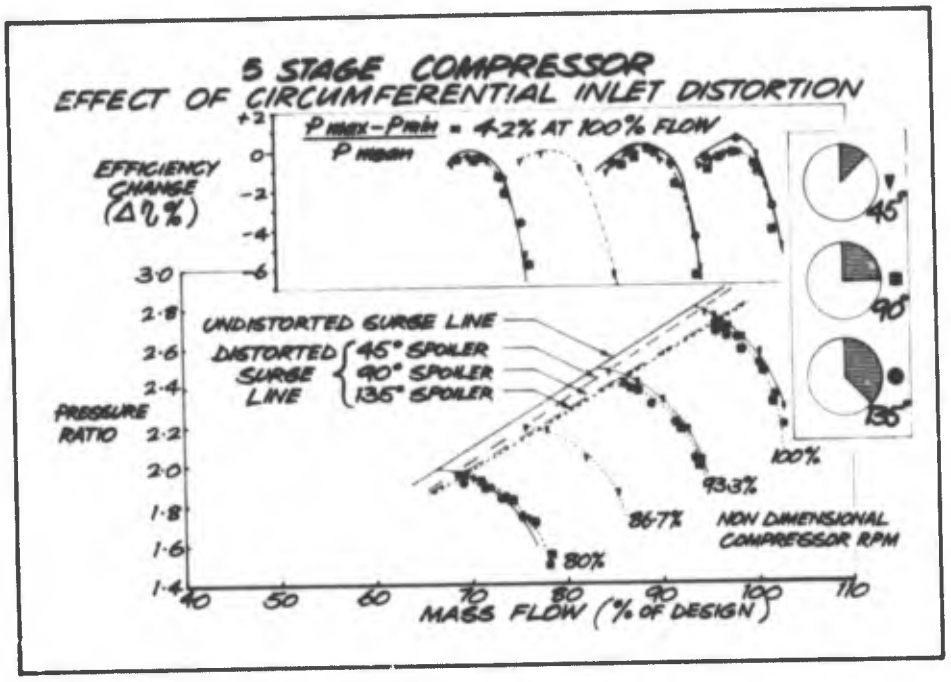

Figure 2

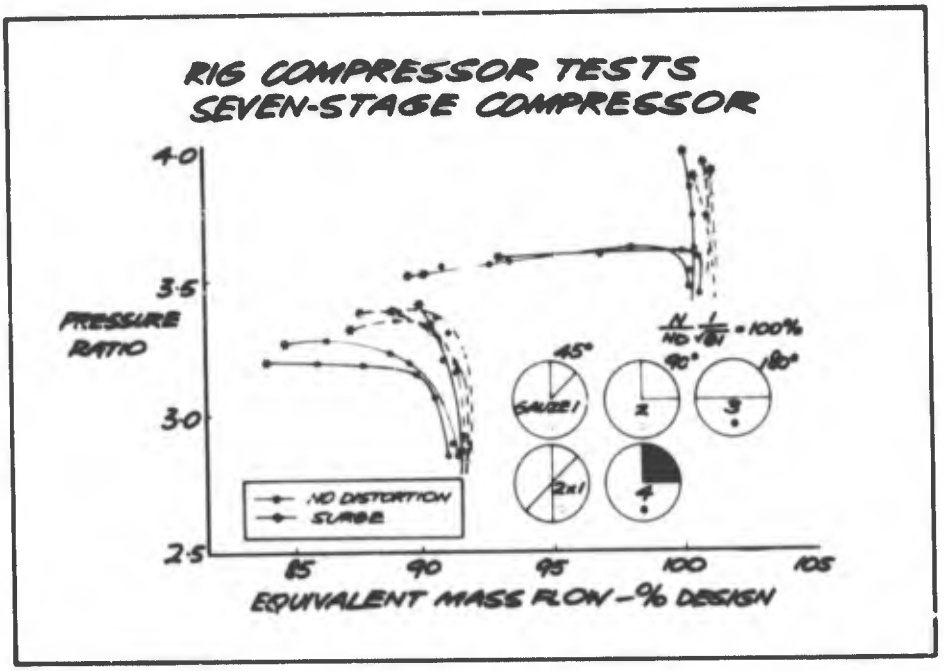

Figure 3

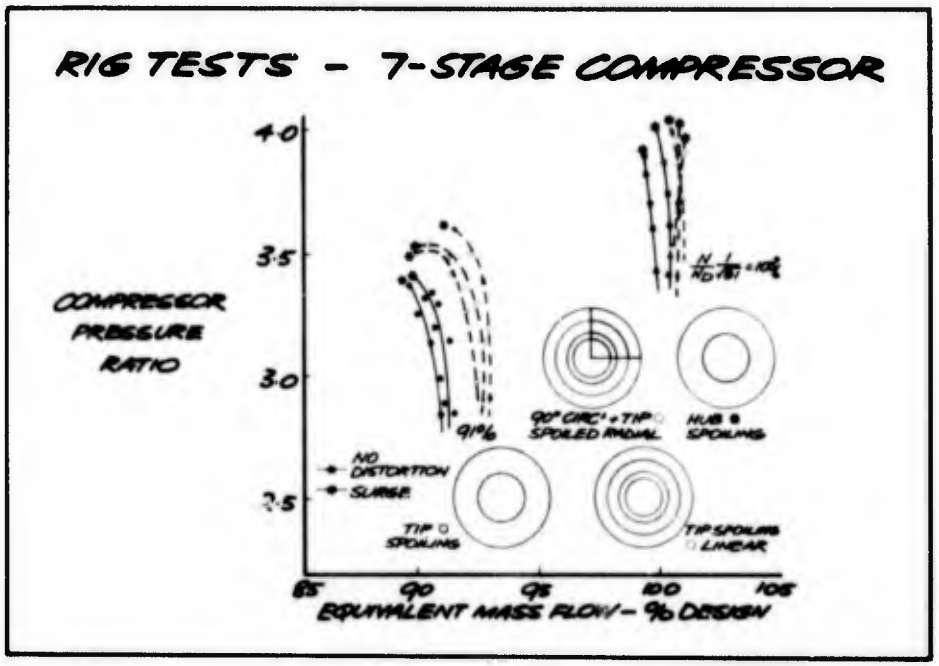

Figure 4

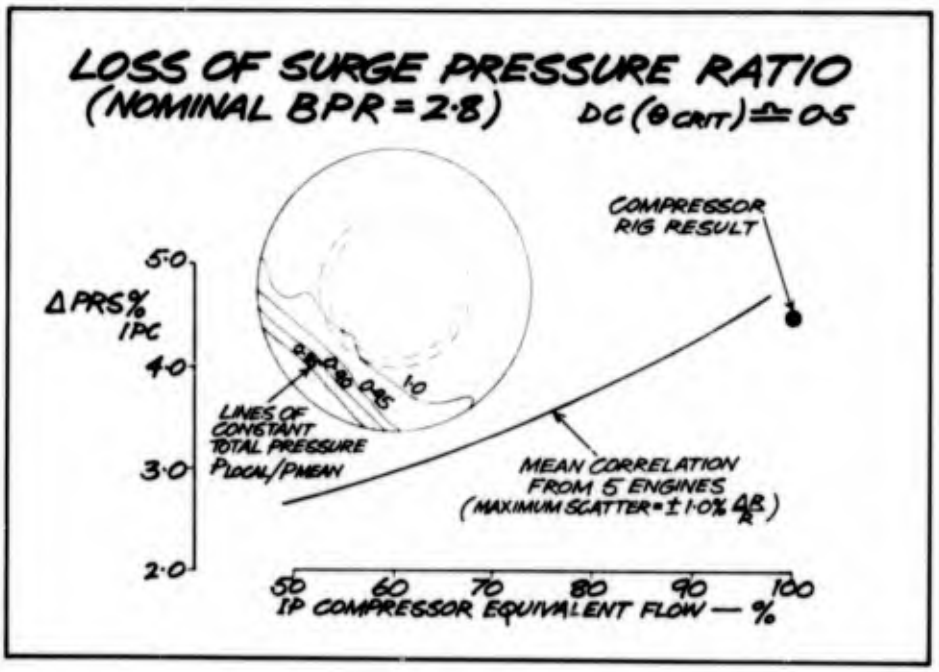

Figure 5

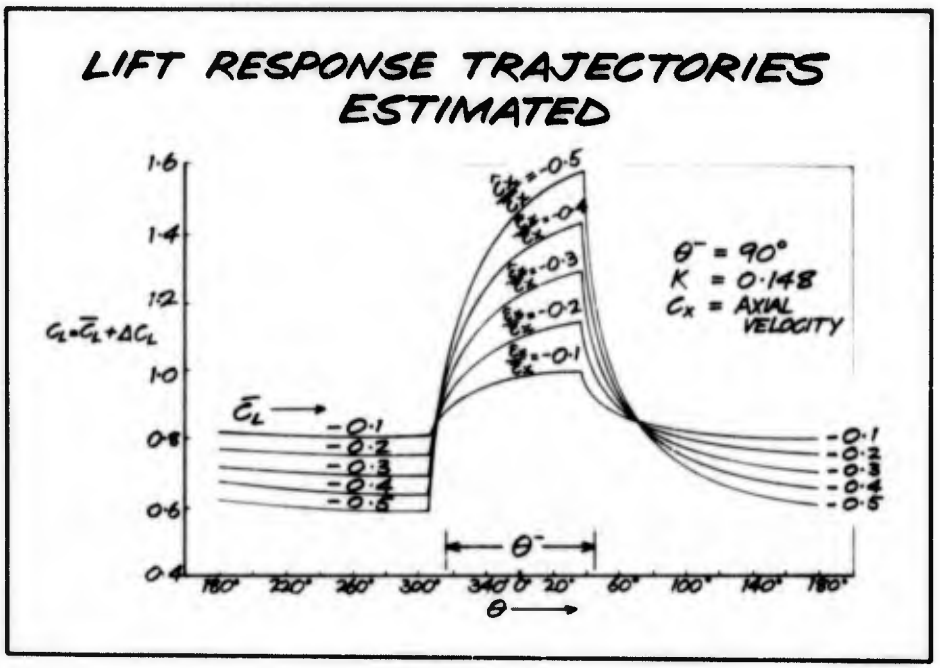

Figure 6

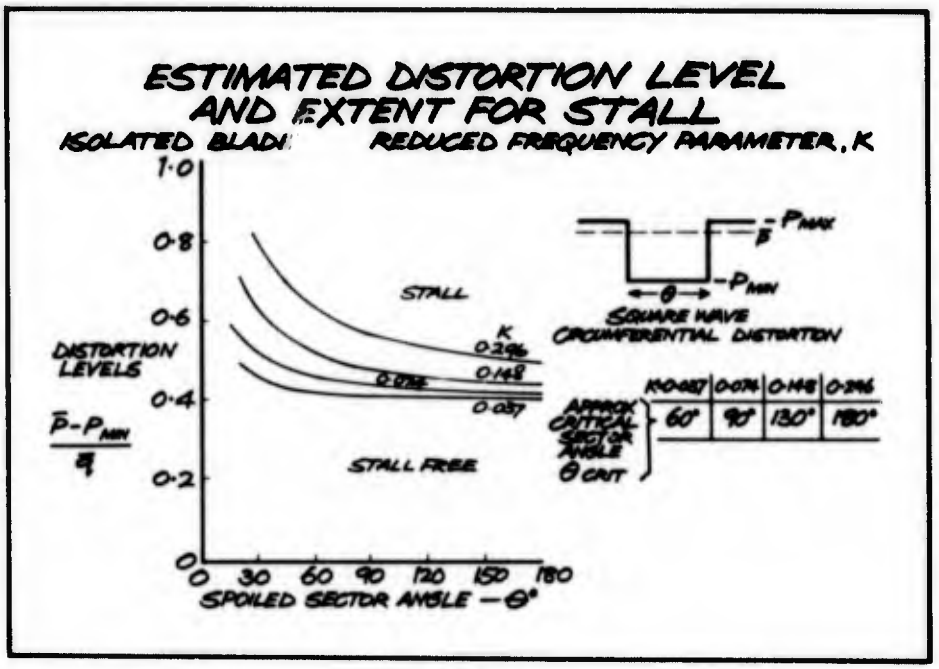

Figure 7

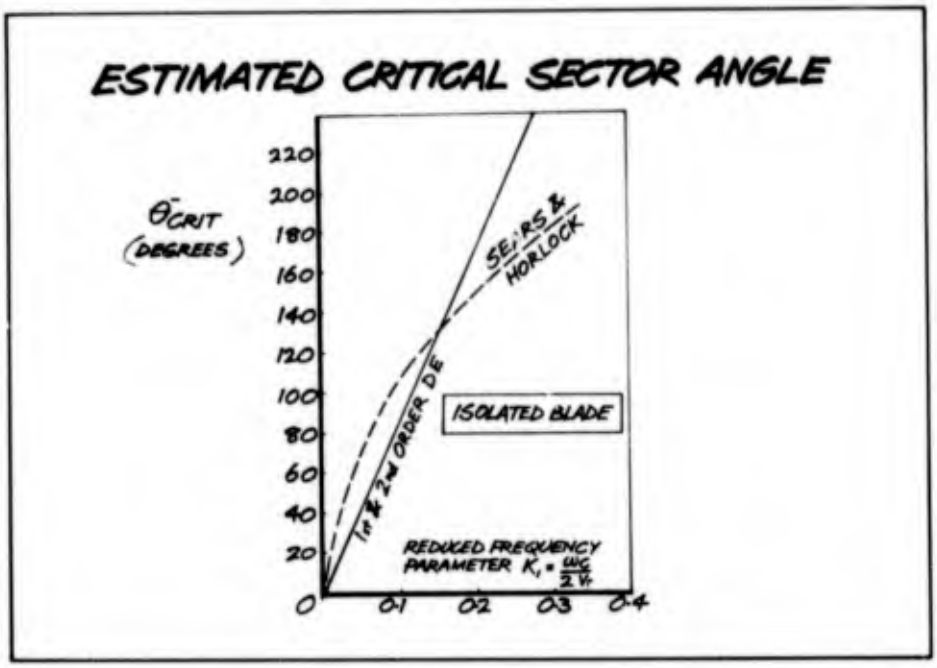

Figure 8

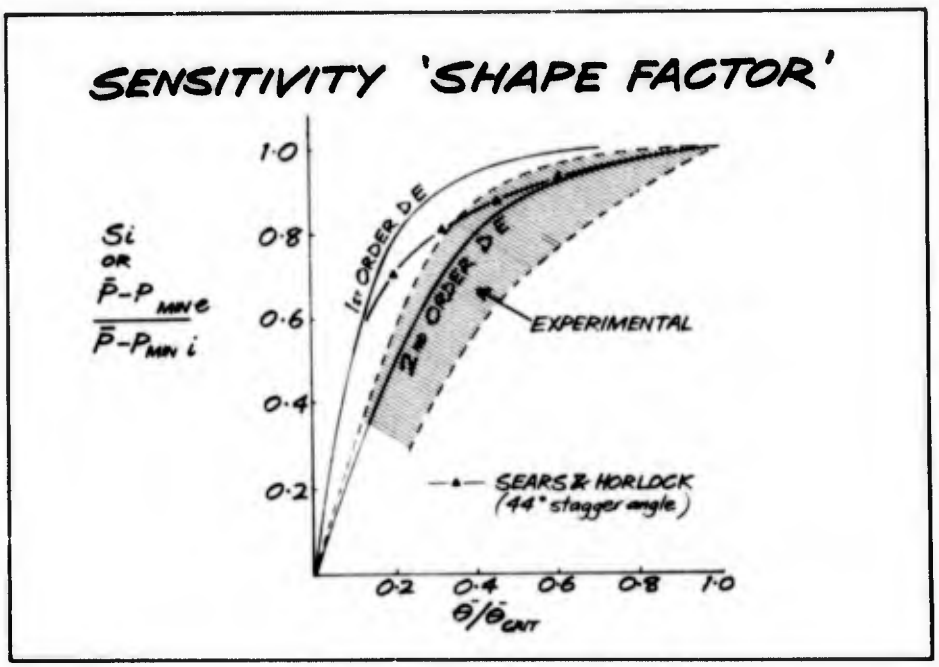

Figure 9

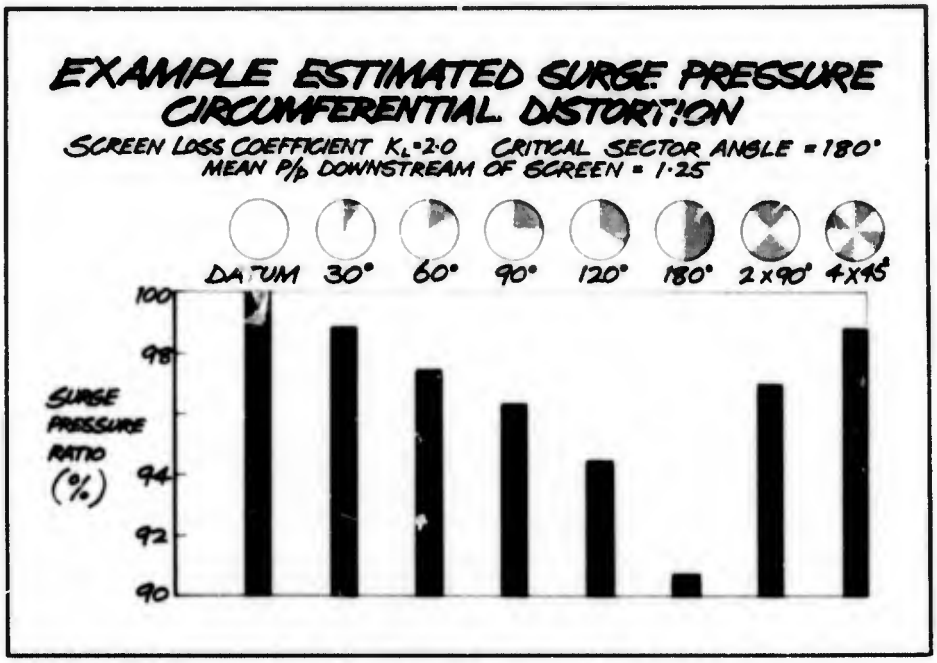

Figure 10

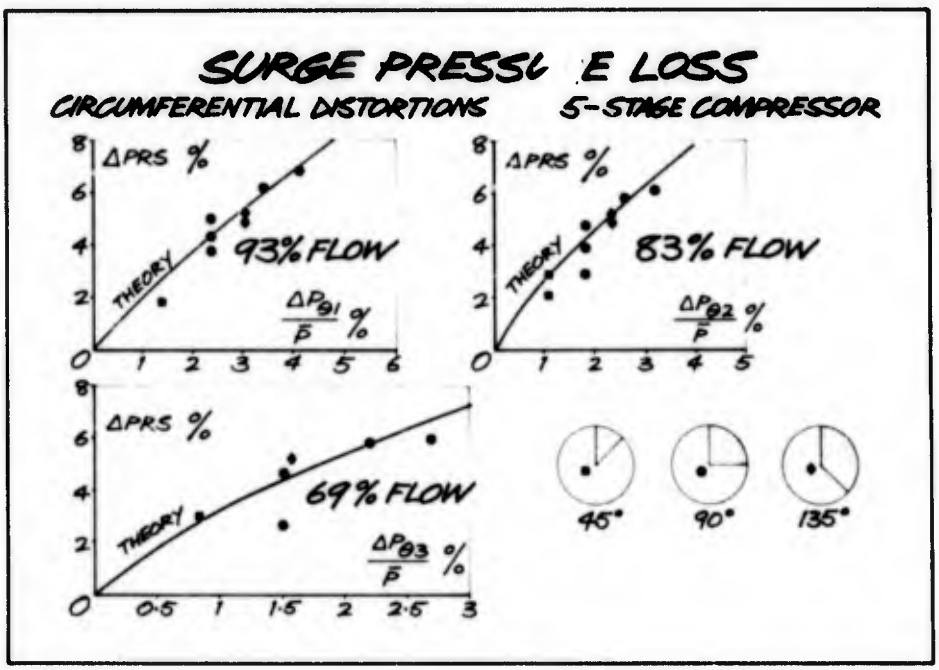

Figure 11

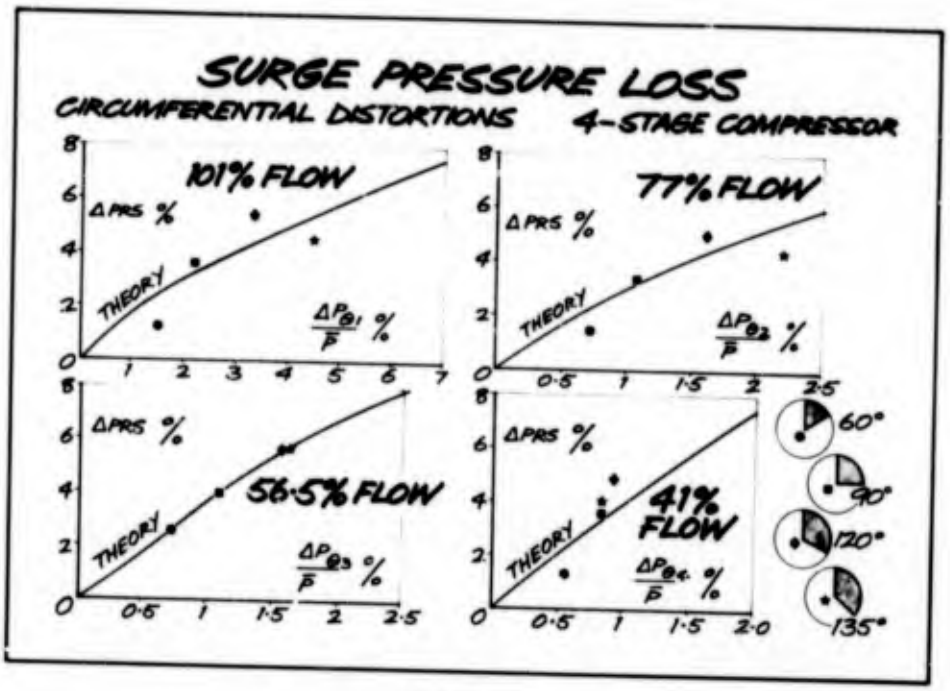

Figure 12

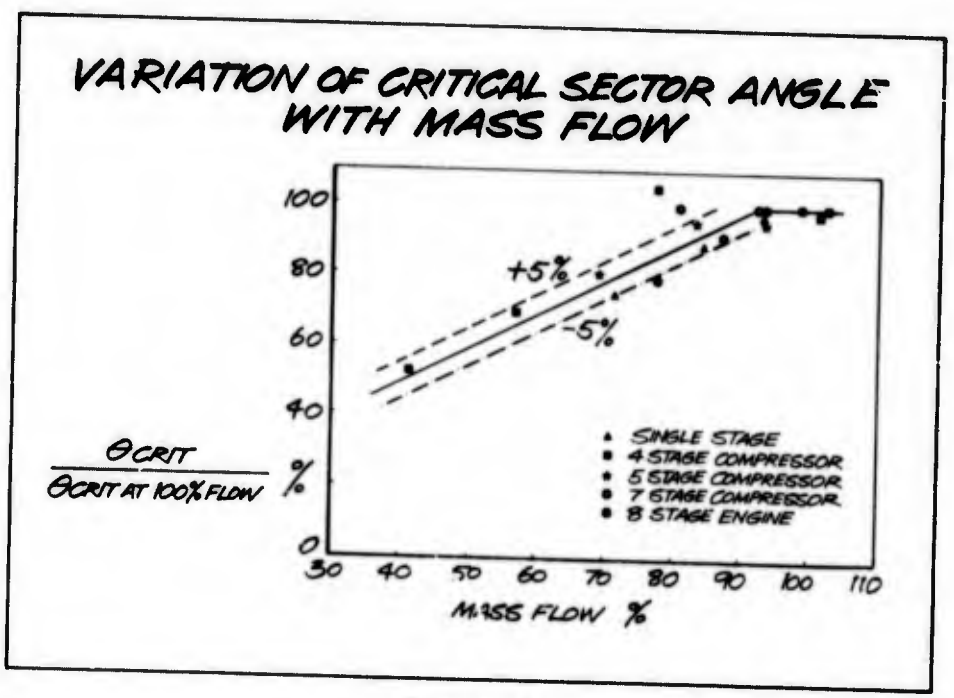

Figure 13

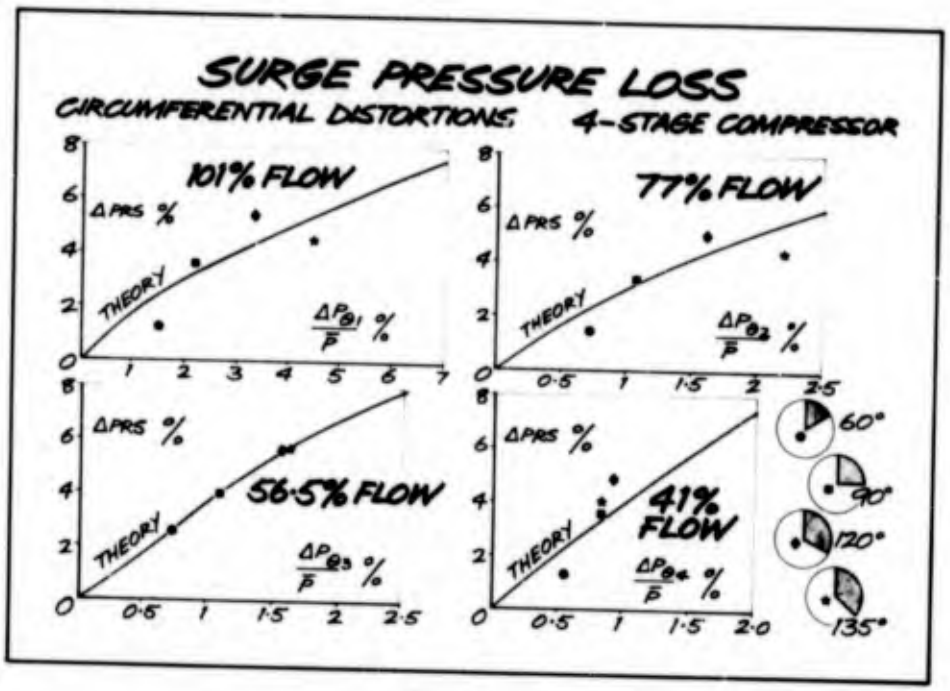

Figure 12

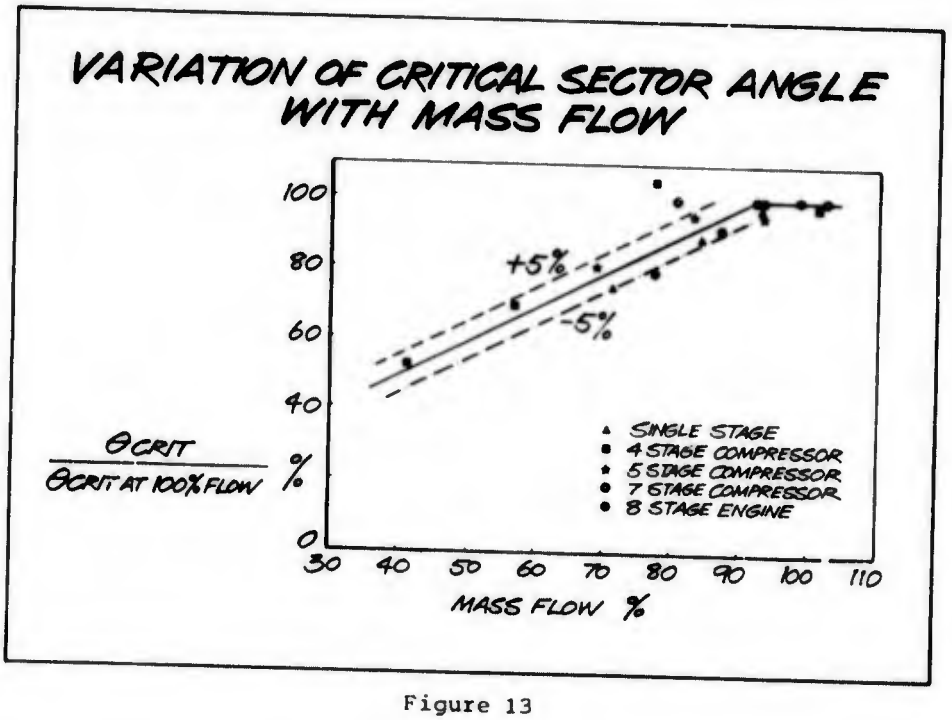

Figure 13

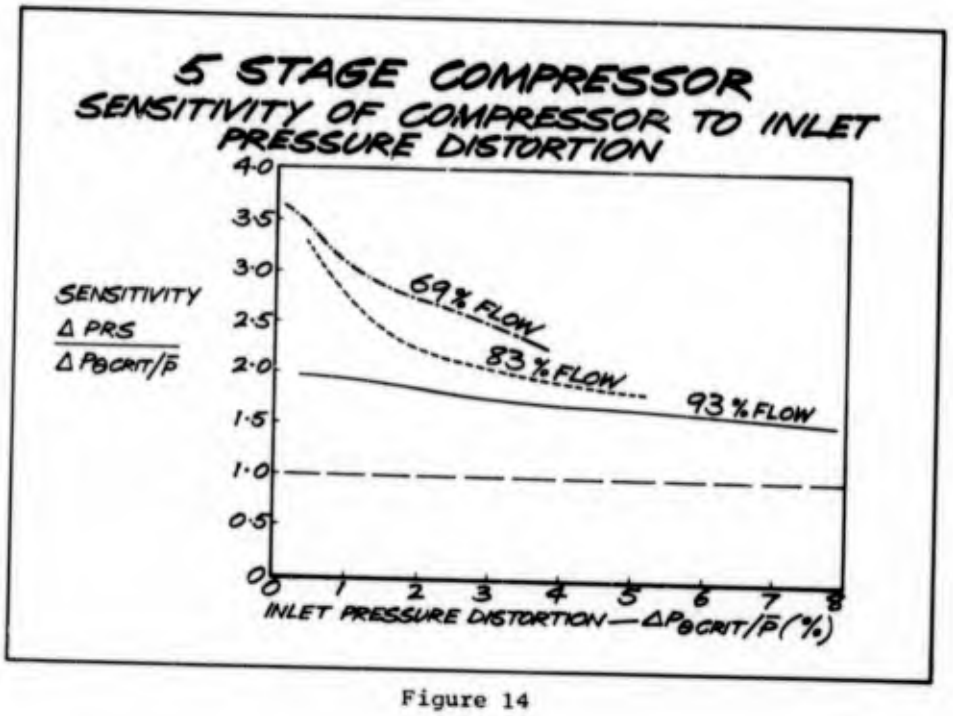

Figure 14

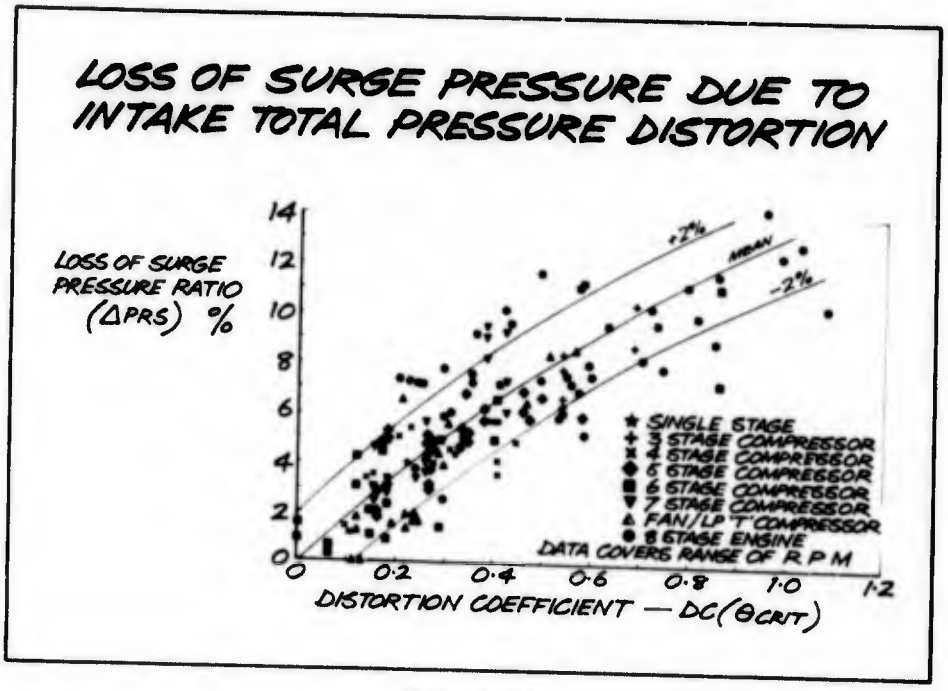

Figure 15

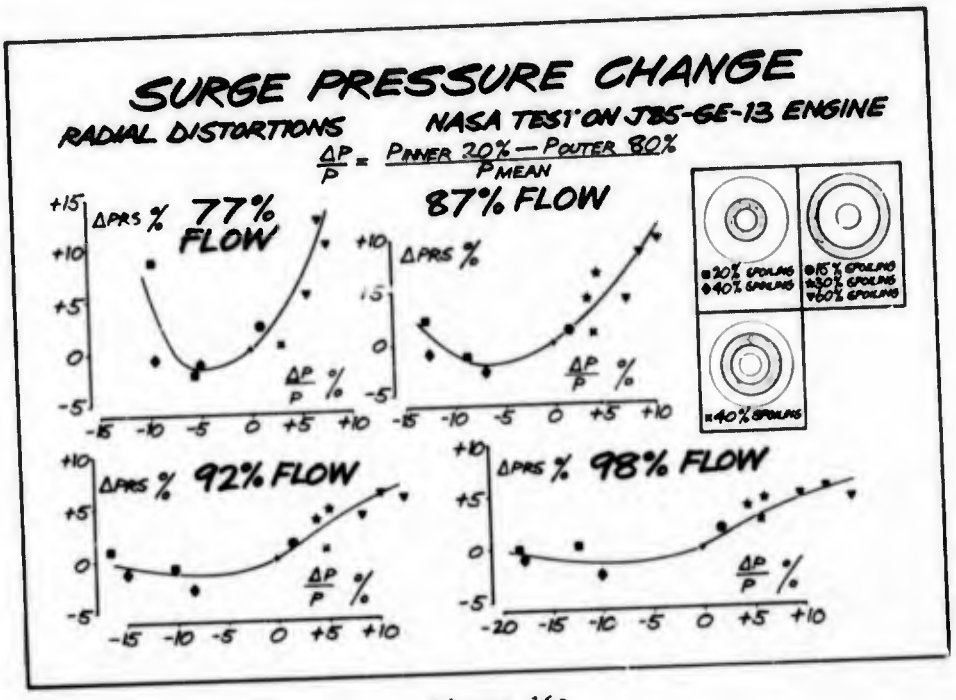

Figure 16a

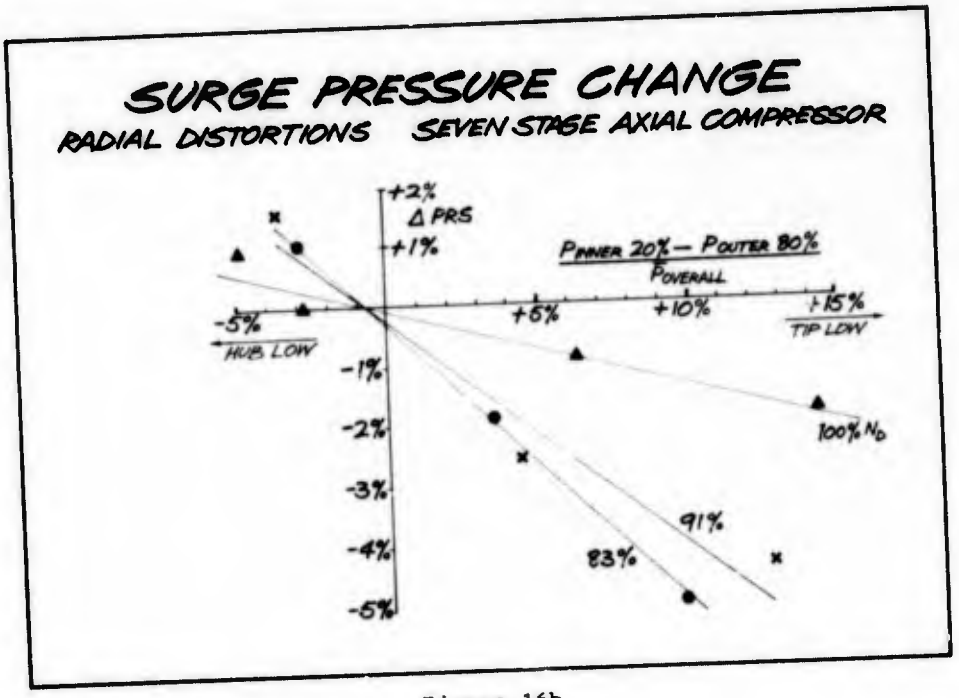

Figure 16b

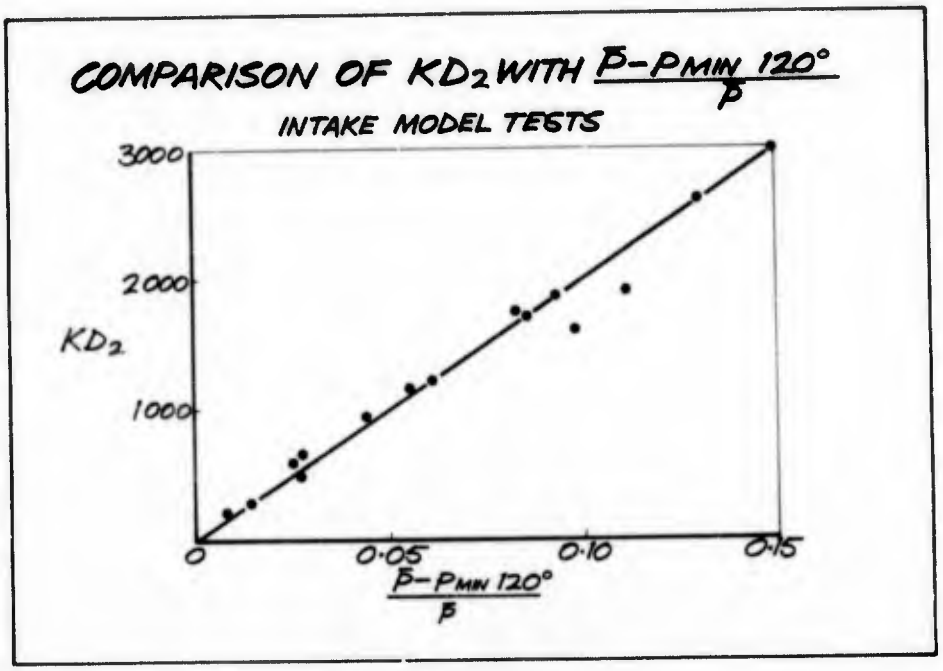

Figure 17

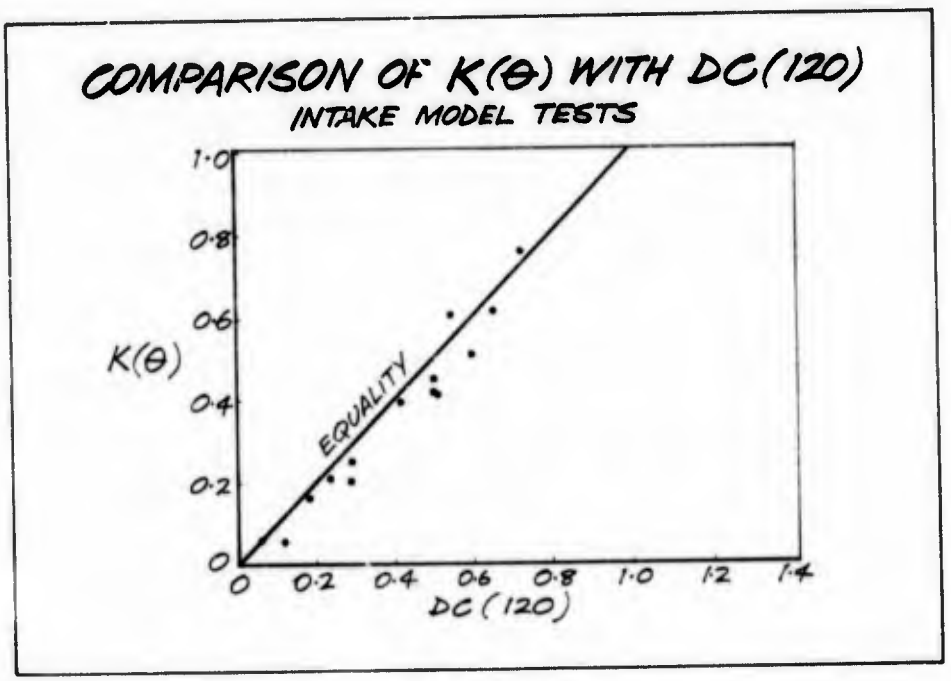

Figure 18

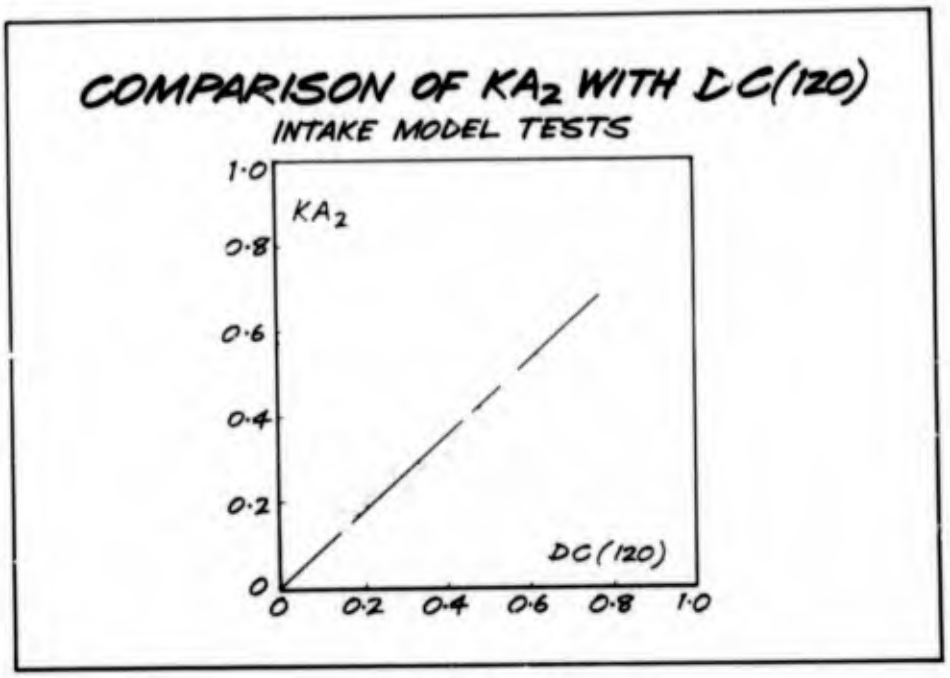

Figure 19

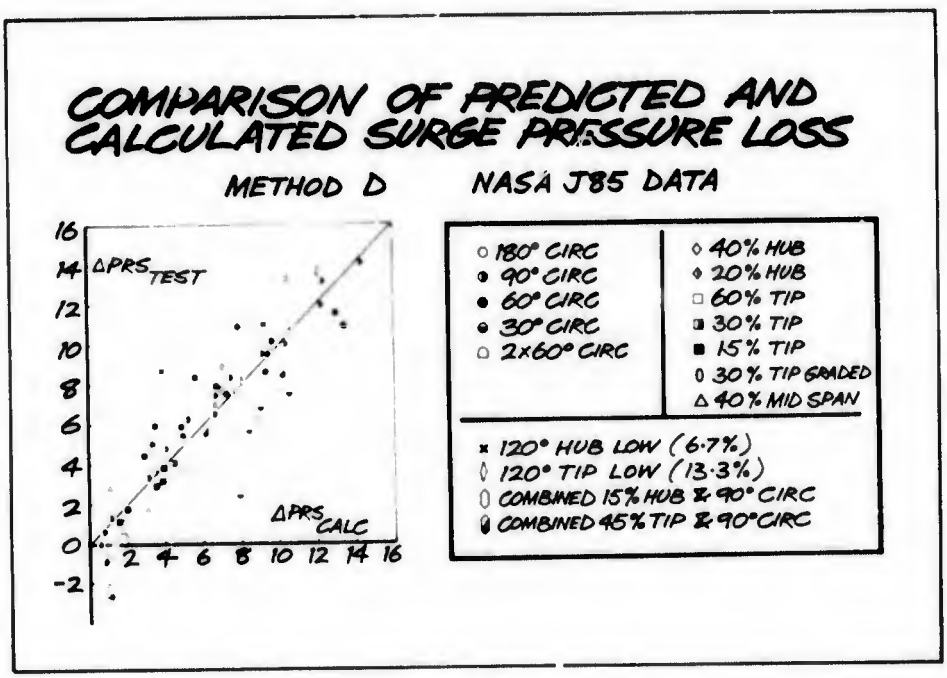

Figure 20

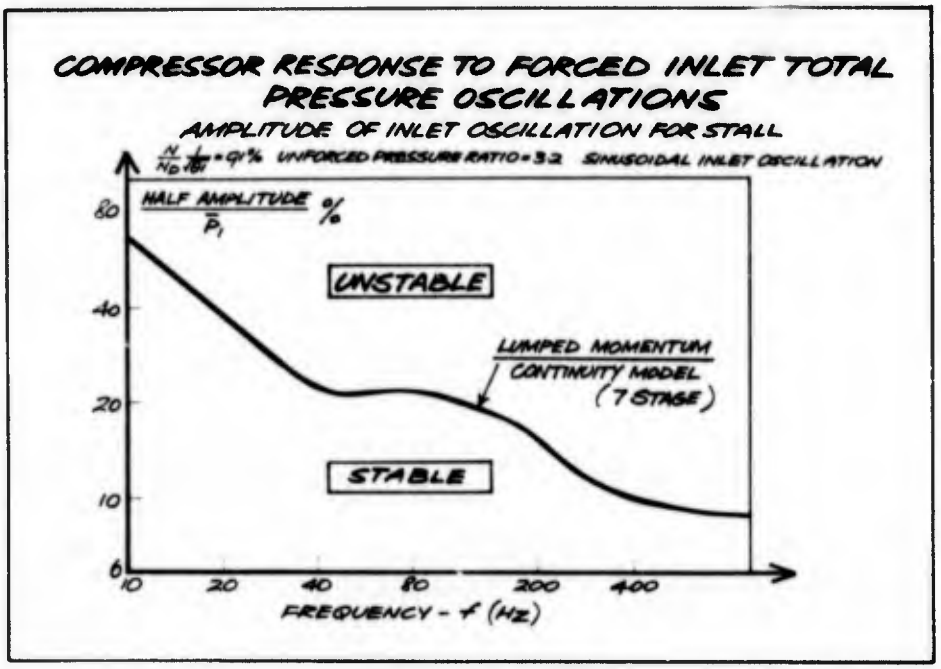

Figure 21

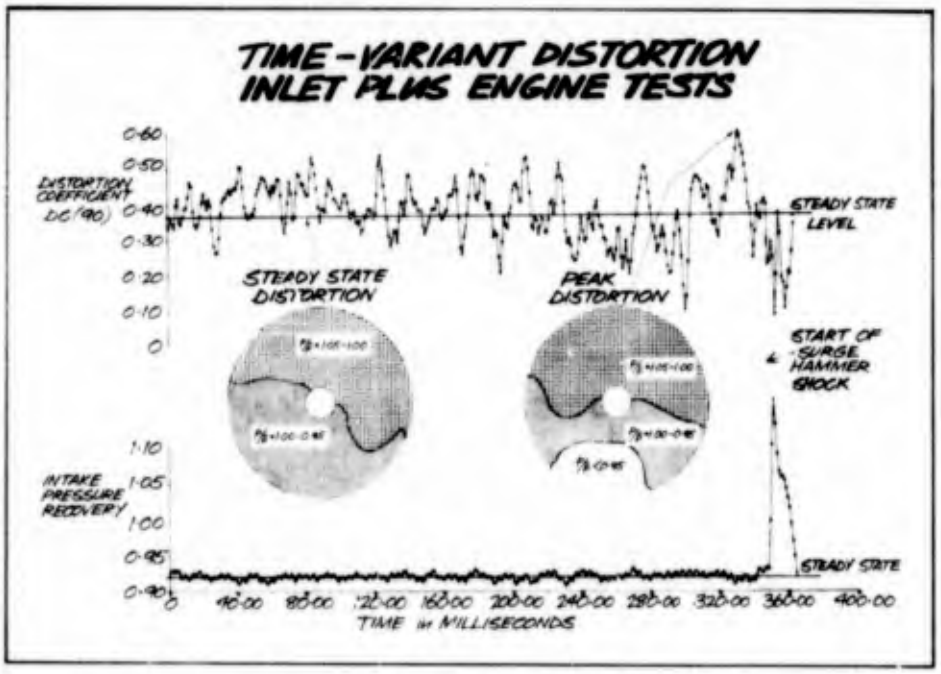

Figure 22

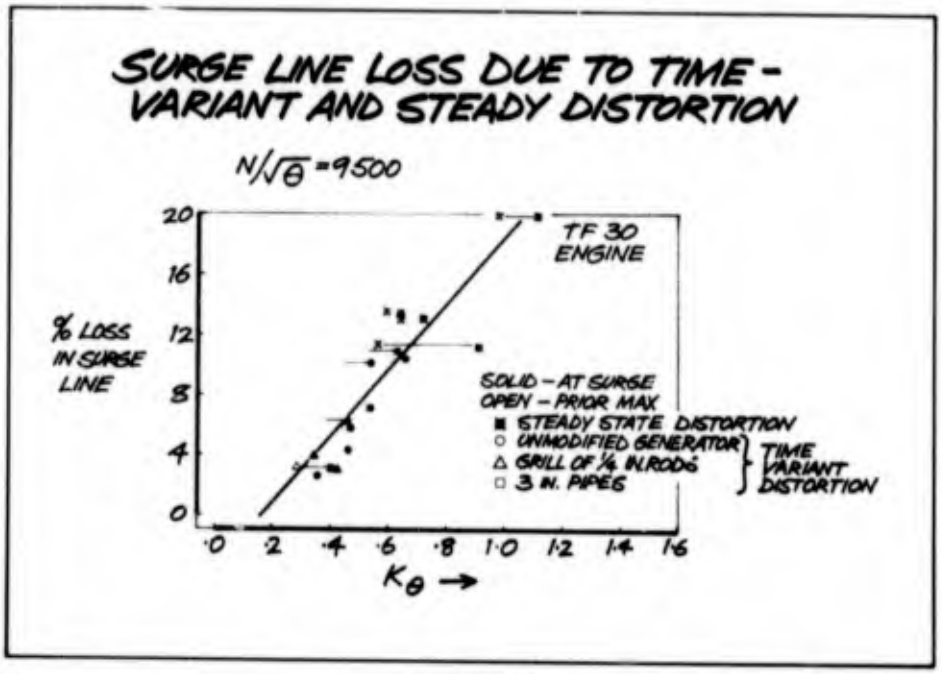

Figure 23

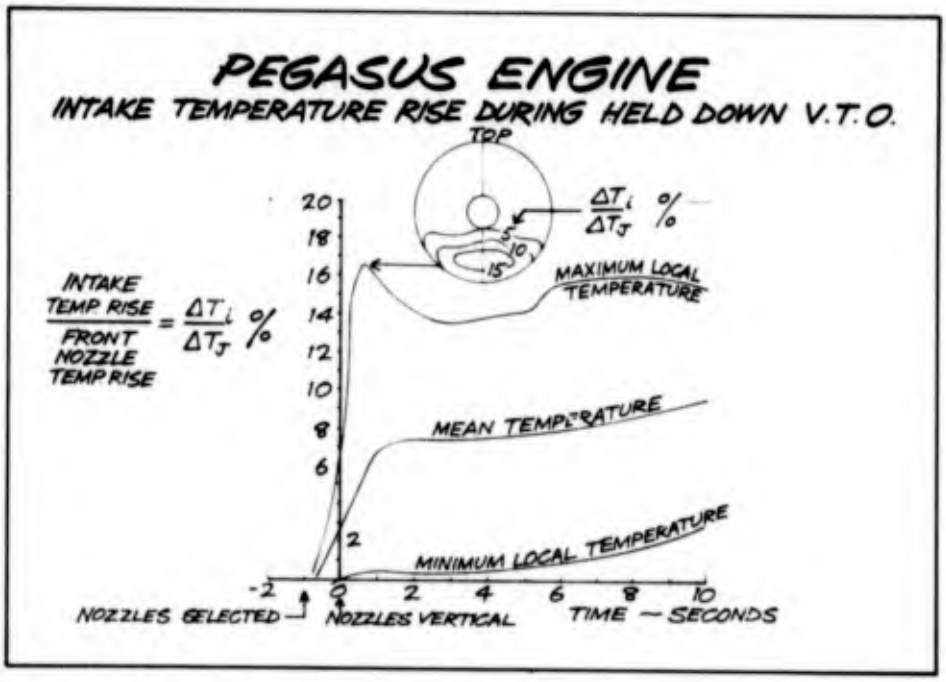

Figure 24

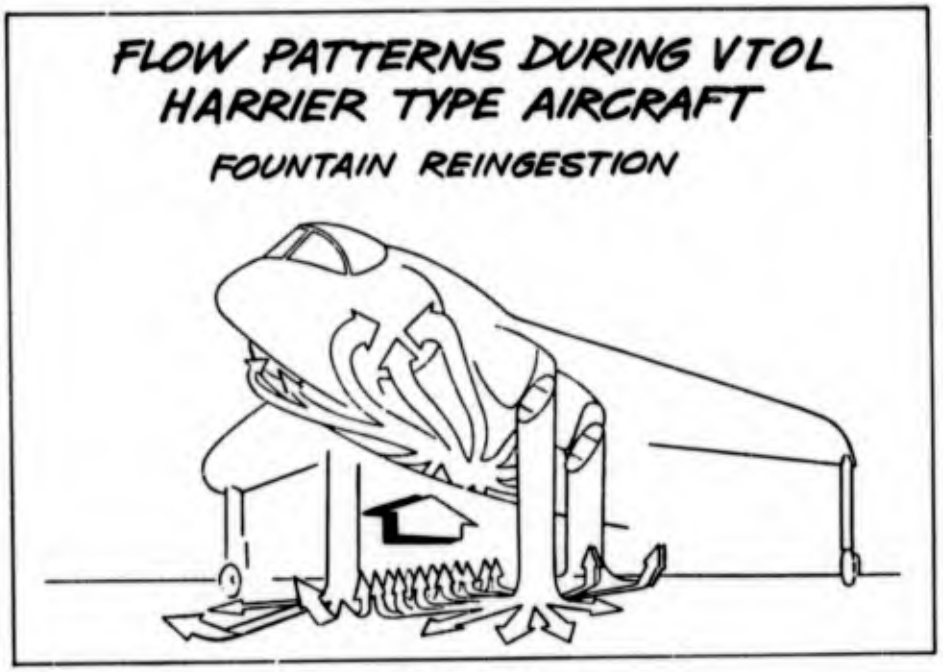

Figure 25

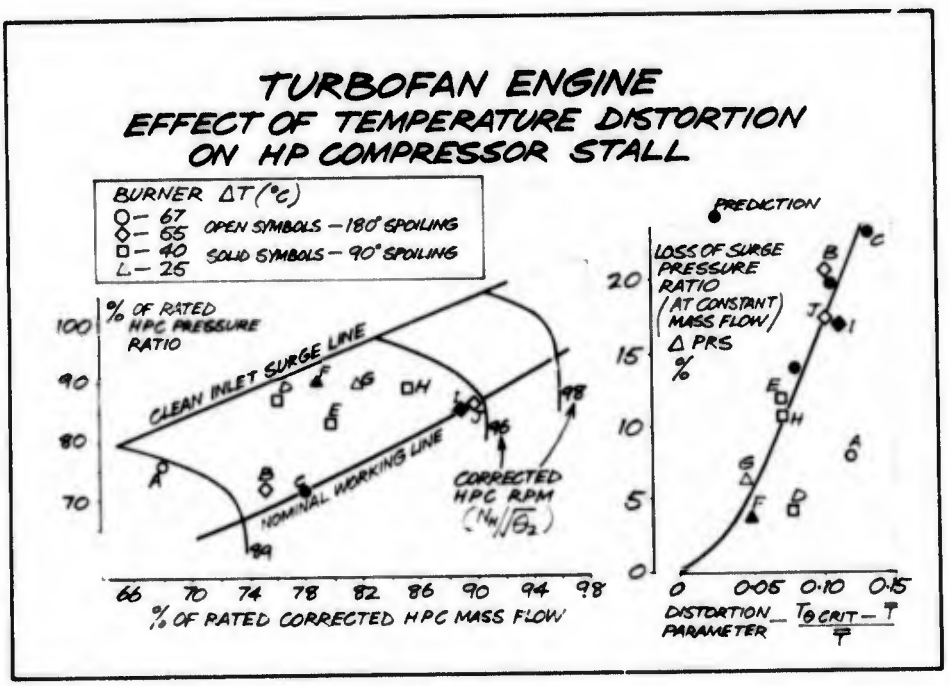

Figure 26

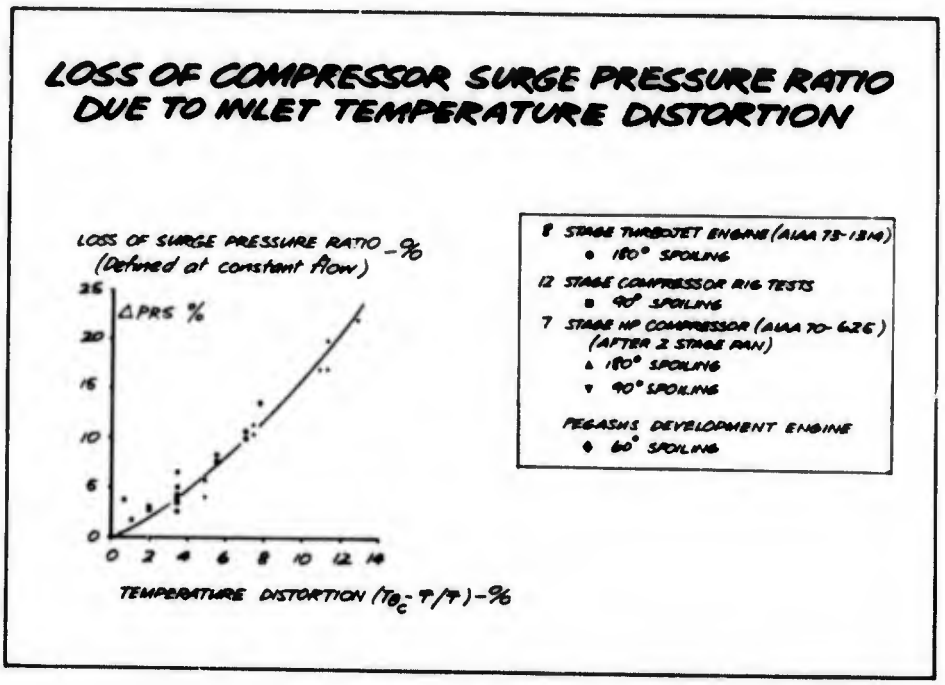

Figure 27

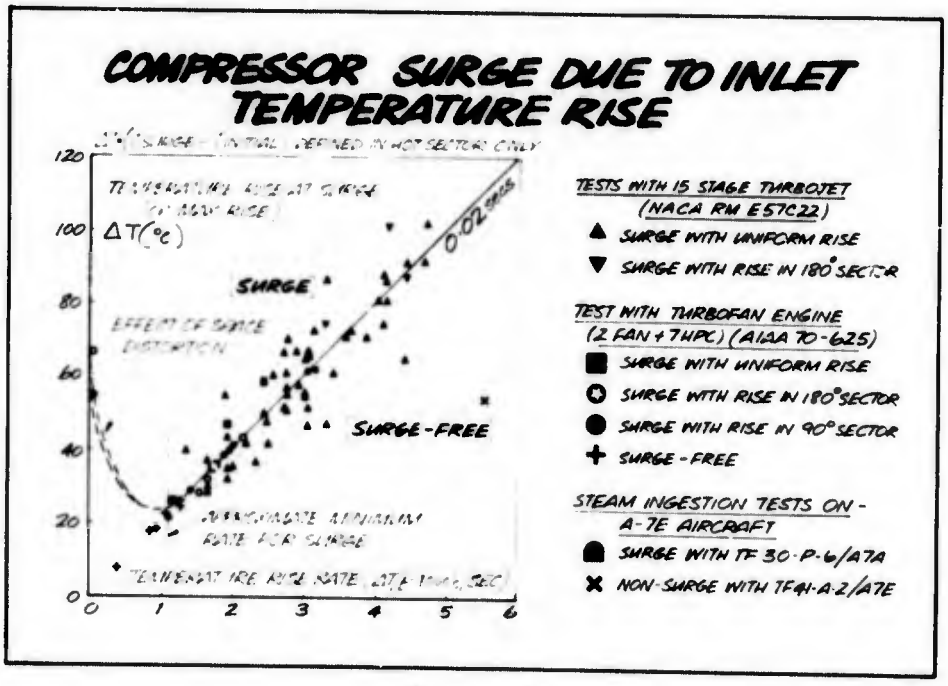

Figure 28

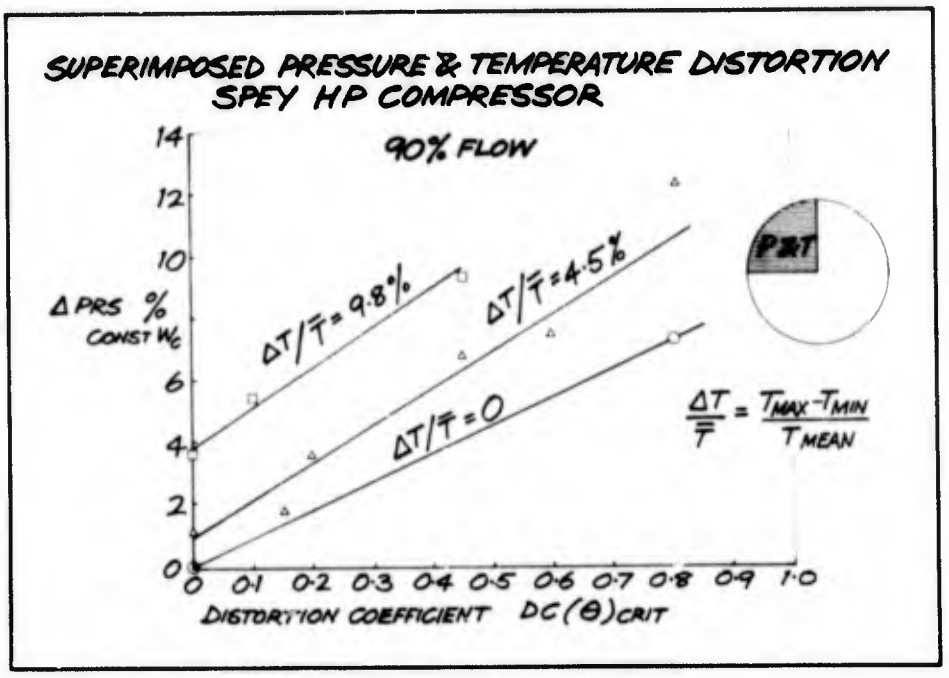

Figure 29

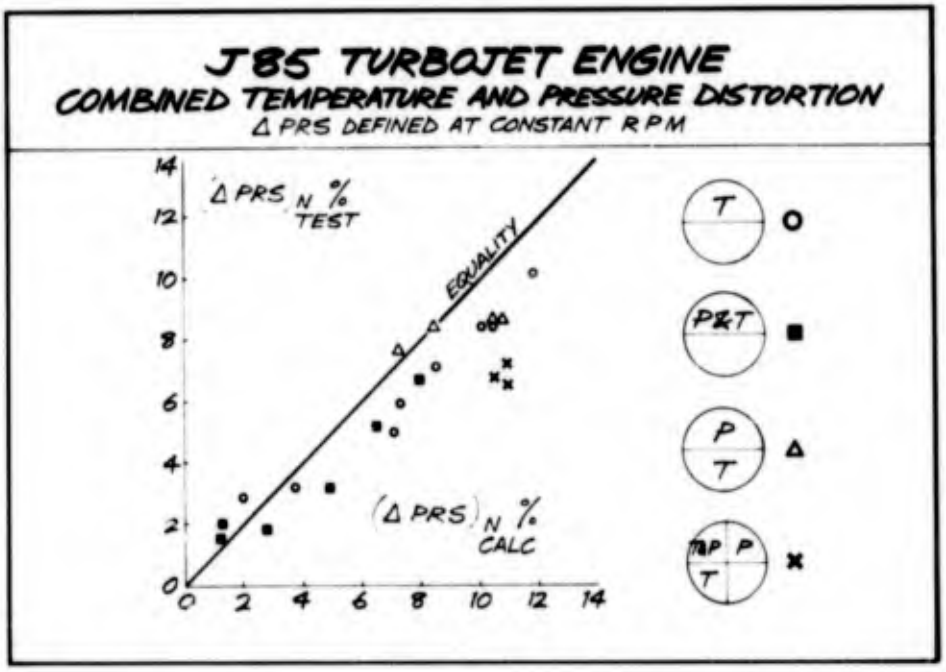

Figure 30

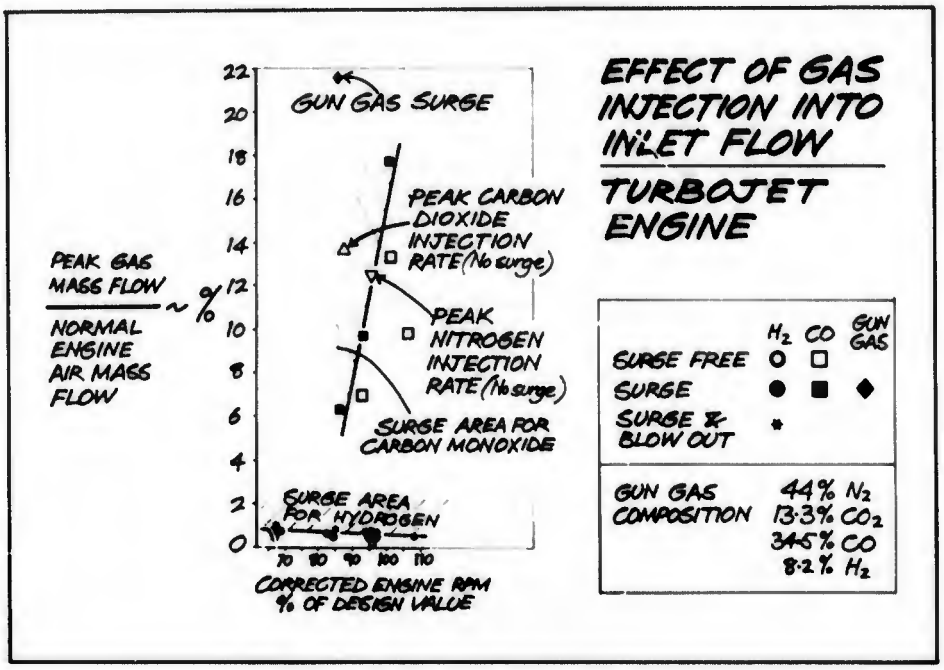

Figure 31

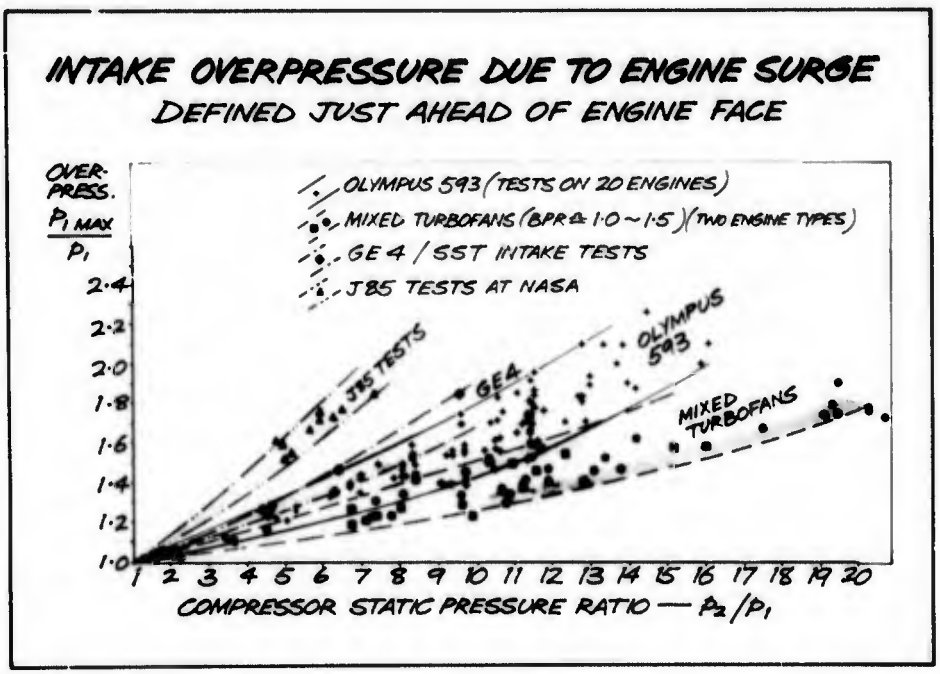

Figure 32

APPENDIX

EXAMPLE DISTORTION DESCRIPTORS

INTERFACE PLANE

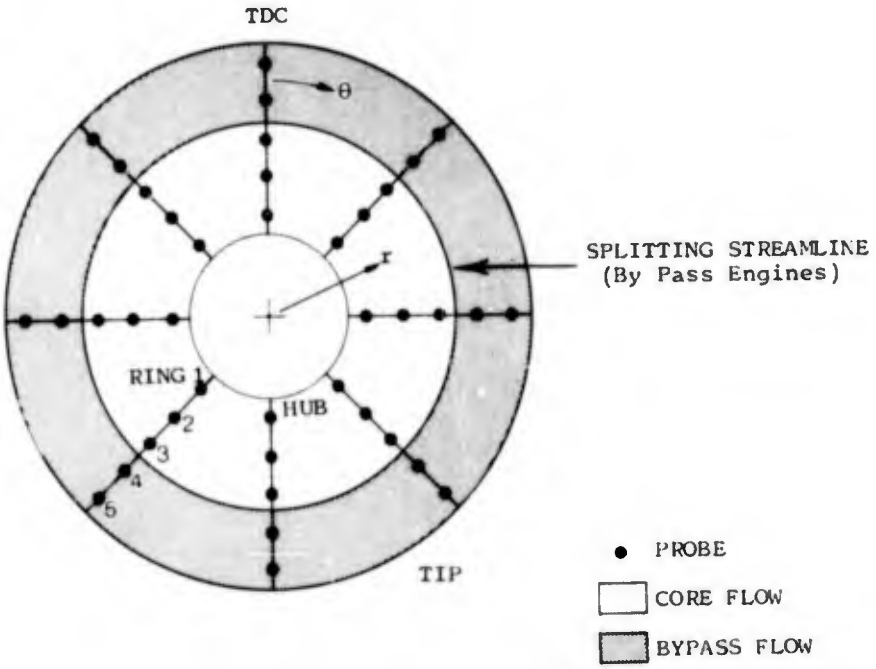

SYMBOLS

A_N = Nth Fourier Coefficient of $(P/\bar{P}ov)_{Ring}$ expressed as a function of θ

A_j = Area represented by each Ring/Interface Area

b = Superposition Factor

C = Radial Weighting Factor

D = Ring Diameter

E = Circumferential Extent Factor

F = Pattern Shape Factor

j = Number of Rings of Pitot Probes

K, DC, ID, IDC, IDR = Distortion Indices

M = Multiple Low Pressure Areas Factor

N = Fourier Harmonic Number

P = Total Pressure

q = Dynamic Head

r = Radius

S = Sensitivity (Stability Usage) Factor

x, y = empirical exponents

α = Radial Extent Factor

θ = Circumferential Position

θ^- = Circumferential extent of total pressure less than the ring or interface mean value

Superscripts

($\bar{}$) = Mean Quantity

Subscripts

ov = Overall interface plane

r, R = Radial, Ring

C = Circumferential

H = Hub

T = Tip

D = Diameter

THE $\frac{\Delta P_\theta}{\bar{P}}$ crit AND $DC(\theta)_{crit}$ INDICES

$$\frac{\Delta P_\theta}{\bar{P}}_{crit} = \frac{\bar{P}ov - P_{min\,\theta\,crit}}{\bar{P}_{ov}}$$

$$DC(\theta)_{crit} = \frac{\bar{P}_{ov} - P_{min\,\theta\,crit}}{\bar{q}_{ov}}$$

$P_{min\,\theta\,crit}$ = the spatial mean value of total pressure defined in a 'critical' or 'effective' sector angle about the lowest total pressure region at the interface.

The index may be defined across the entire interface plane, or in core (hub), or bypass (tip) regions separately.

THE KD_2 INDEX

$$KD_2 = \frac{\sum_{Ring=1}^{j} \left[\frac{\Delta P}{P} \cdot \theta^-\right]_{Ring} C_{Ring}}{\sum_{Ring=1}^{j} \left[C_{Ring}\right]}$$

$$\frac{\Delta P}{P} = \frac{\bar{P}_{Ring} - P_{min\ probe}}{\bar{P}_{Ring}}$$

$$C_{Ring} = \frac{\text{Tip Radius}}{\text{Ring Radius}}$$

THE KA_2 INDEX

$$KA_2 = K\theta + b.Kra_2$$

THE $K\theta$ INDEX

$$K\theta = \frac{\sum_{Ring=1}^{j} \left[\left(\frac{A_N}{N^2}\right)_{max}\right]_{Ring} \cdot \frac{\bar{P}_{ov}}{\bar{q}_{ov}} \cdot \frac{1}{D^y_{Ring}} \cdot A_j}{\sum_{Ring=1}^{j} \frac{A_j}{D^y_{Ring}}}$$

$\bar{P}$, $\bar{q}$ defined over the interface plane

THE K_{ra2} INDEX

$$K_{ra_2} = \frac{\sum_{Ring=1}^{j} \left[\frac{\Delta P}{\bar{P}}\right]_{Ring} \cdot \frac{\bar{P}_{ov}}{\bar{q}_{ov}} \cdot \frac{1}{D^x_{Ring}}}{\sum_{Ring=1}^{j} \frac{1}{D^x_{Ring}}}$$

$$\frac{\Delta P}{\bar{P}} = \frac{\bar{P}_{ov} - \bar{P}_{Ring}}{\bar{P}_{ov}}$$

THE K_{C2} INDEX

$$K_{C2} = \frac{\sum_{Ring=1}^{j} \left[\left(\frac{A_N}{N^2}\right)_{max}\right]_{Ring} \cdot \frac{\bar{P}_{ov}}{\bar{q}_{ov}} \cdot \frac{1}{D^y_{Ring}} \cdot A_j \left(\frac{180}{\bar{\theta}_{max}}\right)_{Ring}}{\sum_{Ring=1}^{j} \frac{A_j}{D^y_{Ring}}}$$

If defined in the core flow, for example, j = number of rings having diameters less than or equal to the diameter of the splitting streamline.

$$\bar{\theta}_{crit} \leq \bar{\theta}_{max} \leq 180^o$$

THE 'METHOD D' INDEX SYSTEM

The index is based on five rings located in centres of equal area and is determined as follows:

$$ID = b.S_c.IDC + S_R.IDR$$

IDC = Circumferential Index = larger of (IDC_H, IDC_T)

$$IDC_H = (IDC_1 + IDC_2)/2$$

$$IDC_T = (IDC_5 + IDC_4)/2$$

$$IDC_r = E_r.F_r.M_r.\left(\frac{\Delta P}{P}\right)_r.$$

$$\left(\frac{\Delta P}{P}\right)_r = \frac{\bar{P}_{Ring} - P_{min.Ring}}{\bar{P}_{ov}} \quad , r = 1, 2, 3, 4, 5.$$

$P_{Min.Ring}$ = Minimum Total Pressure within largest low pressure area.

IDR = Radial Index = larger of $\left(\frac{S_H.IDR_H}{S_R}, \frac{S_T.IDR_T}{S_R}\right)$

$$IDR_H = \left(\frac{\Delta P}{P}\right)_{D1} + \alpha_H.\left(\frac{\Delta P}{P}\right)_{D2}$$

$$IDR_T = \left(\frac{\Delta P}{P}\right)_{D5} + \alpha_T.\left(\frac{\Delta P}{P}\right)_{D4}$$

$$\left(\frac{\Delta P}{P}\right)_{Dr} = \frac{\bar{P}_{ov} - \bar{P}_{Ring}}{\bar{P}_{ov}} \quad , r = 1, 2, 3, 4, 5.$$

Note: S_c = Circumferential Sensitivity Factor

S_r = Radial Sensitivity Factor which is either S_T for tip or S_H for hub, depending upon IDR selection.

AEROMECHANICAL RESPONSE

by

F. Sisto

Professor and Head
Department of Mechanical Engineering
Stevens Institute of Technology
Hoboken, New Jersey 07030, USA

SUMMARY

Physical mechanisms are discussed which lead to the aeromechanical response of axial-flow fan and compressor components when these machines operate with a distorted inlet flow. Steady response of blades, vanes and discs are considered briefly. Forced excitation of rotating components are treated in some detail. The specific form of the exciting gusts are elucidated. Self-excited vibrations of rotor blades and stator vanes are considered as stemming from the general degradation of flow with distortion. Shaft and disc vibrations are also discussed as possible aeromechanical responses to distorted flow. The role of various forms of damping and the use of composite materials are described with attendant problems in application through design. Remedial action available to the aeromechanical engineer is discussed with the objective of ameliorating the adverse effects of distorted-induced structural response.

INTRODUCTION

The extent to which the elastic flexibility of a turbomachine structure contributes to, or interacts with, the distortion of the throughflow is at present a moot point. Nominally the elastic deflections of blades, vanes, discs and shafts are not considered to affect the distribution of flow velocity vectors, total pressures, etc. throughout the machine. There may be important shortcomings in this assumption, but it is universally made, stemming from the extreme complexity of assuming otherwise. (An exception that may more easily be calculated relates the local setting angle of a blade or vane to the aerodynamic moment distribution radially along the member. In turn the setting angle is a determinant of the aerodynamic moment and so blade flexibility may be shown to affect the local velocity triangles and hence the modification of flow distortion within the machine; the effect is akin to the static torsional divergence of a wing. In almost every practical instance the magnitude of this flexibility effect will be negligibly small.) Hence it will be assumed as has been the case heretofore that the distortion which may be present is describable in terms of velocity, pressure, temperature and foreign gas distributions; inquiry is then made as to the consequent behavior of the structure.

In treating the aeromechanical response of structure, the nonuniformity of flows in time and space will be taken as given quantities. Other lecturers will deal with the prediction, measurement, amelioration, etc. of distorted flow. The distortion may be radial and/or circumferential, steady or nonsteady.

In the instance of nonsteady distortion it is difficult to include the nonsteadiness in the analysis or in the consideration of aeromechanical response. This is particularly true if the nonsteadiness is a random process with only a statistical description. The recourse in this situation is to treat the distortion as steady if statistically it is present more than, say, 25% or 30% of the time and to ignore it otherwise. On the otherhand, if the nonsteadiness is periodic in time, then the predicted behavior of the structure may be obtained by Fourier analysis, if a forced vibration* is implicit.

If a self-excited vibration is under consideration, then the period of the nonsteadiness of the distortion must be roughly an order of magnitude greater than the period of the characteristic vibration and the nonsteadiness of the flow may then be treated quasi-steadily. Otherwise it may be assumed that insufficient time is available for the self-excited amplitudes to build up appreciably.

GENERALIZATIONS CONCERNING EXPECTED PHENOMENA

Subject to the approximation and exceptions discussed in the foregoing Introduction, the distortion of the throughflow in an axial turbomachine may be treated as steady for the purposes of analysis and prediction. This steadiness is with respect to a reference frame fixed to the housing, hence stator vanes will never be subject to forced excitation directly from distorted flow; the possibility of self-excited vibration (flutter) remains, as well as indirect excitation from the wakes and potential disturbances attributable to adjacent rotor blades.

---

*By this description turbulent flow defined by its power spectrum is analyzed as a forced vibration problem.

By similar reasoning one may rule out radial distortion as a source of forced vibration for either stator vanes or rotor blades. Unquestionably a major potential source of vibration is the passage of ro or blades through strong circumferential distortion patterns.

A periodic or transient time dependence of the flow distortion has the potential for affecting blades and vanes equally; surge and hammershock (because of their low frequency of reoccurrence) foreign gas ingestion, foreign object ingestion are phenomena which may be treated as aperiodic. The excitation may be important due to the suddenness of change in loading or else the operating condition after the change may be conducive to self excitation. Structural component typical natural frequencies are measured in hundreds and even thousands of Hertz. Hence any distortion which, although technically periodic, has a frequency of reoccurrence of 10 Hertz or less (typical for surge) may practically be treated as aperiodic in terms of its effect on the structure.

The rotating structure in axial turbomachines consists not only of the rotor blades, but the drums and discs as well to which they are attached and the supporting shafts and bearings. Periodic loading and unloading of rotor blades in distorted flow may under certain circumstances provide circumferentially asymmetric loading to the entire rotating assembly; this type of system may then in turn develop instabilities of its own related to excitation of its characteristic modes. Small wall thicknesses of both stationary and rotating structural members, characteristic of lightweight aircraft gas turbine design may resonate directly when subjected to pulsating pressure loading of sufficient magnitude at the proper frequency.

Finally, the harmful nature of any of these aeromechanical instabilities will usually be related to the amplitude of oscillatory strains in the structural elements. These equilibrium amplitudes, in turn, will be dependent not only on the strength of the excitation (or self-excitation if such a term may be used) but also on the aerodynamic and structural damping in the system.

INDIRECT EFFECTS OF INLET DISTORTION

A thick annulus boundary layer is a form of inlet distortion that may stall the rotor blade tips and give rise to a rotating stall pattern of limited radial extent. More general, or severe distortion may stall or surge an axial compressor giving rise to periodically reversing throughflow. Surge refers to the case where the reversal is not only local, but the net integrated massflow reverses sign. In the latter case the sudden forward release of the compressor discharge pressure (coexisting with the flow reversal) implies a pressure wave or moving shock travelling through the compressor into the inlet, the so-called hammerwave or hammershock.

The degradation of flow quality implicit with a distorted inlet may give rise to unusually high turbulence levels and a migration of local incidence on stators and rotor such that thick wakes with sizable momentum defects are produced by the respective airfoils. Effective blockage by low energy regions of the inlet distortion pattern may force radial redistribution of the throughflow producing unnaturally low or negative incidences in some stages of an axial compressor.

All of the foregoing are examples of the <u>indirect</u> effects of inlet distortion in producing potentially harmful aerodynamic environments for blading at operating conditions that would be free of these phenomena in the absence of distortion. For this reason not only must the direct effect of inlet distortion on aeromechanical response be considered, but for a complete assessment of unstable behavior the subsidiary effects of distortion must be considered as well.

RESPONSE OF STRUCTURE TO STEADY LOADS

Stator vanes in steady distortions or rotor blades in purely radial distortion can effectively be analyzed for their aeromechanical responses by employing the strip hypothesis and the parallel compressor hypothesis. At each radius the local upstream flow properties of pressure, temperature and vector velocity can be converted to downstream values using the known local cascade geometry and its incidence-deviation characteristic. Some form of radial equilibrium consideration will also be necessary for the prediction of flow properties of a buried stage where these properties may not be known or measurable. However that is a problem of steady performance prediction under conditions of distorted inflow; the aeroelastician must presume the local flow properties are known and the local lift, drag and moment* are derivable from chordwise pressure distribution and/or static pressure and vector momentum changes across the blade row.

With steady local loads applied to the blade, considered to be a tapered twisted beam of variable cross-section, and due consideration of centrifugal loads if any, the deflected position of the airfoil may be predicted by straightforward structural analysis. The results of such calculations, generally in accord with experience, are such that no untoward problems are commonly encountered. The so-called "gas loads" are not

---

*It is an interesting fact that steady aerodynamic moment coefficients are rarely, if ever, calculated for cascaded airfoil either theoretically or from experimental data.

sufficiently different from undistorted design conditions as to create new problems. Tip rubbing, or other interference of fixed and moving members cannot usually be attributed to this type of inlet distortion. A subsidiary reason for this is probably due to the fact that at the aerodynamic match point rotor blades are usually "leaned" in the centrifugal field to remove one half of the gas bending stress. Hence, for normal blades, either doubling or else entirely removing the gas loads would not normally have a strong effect on changing the tip deflection of the rotor blade; its equilibrium deflected position is largely dominated by the intense centrifugal loading measured in the tens of thousands of g's.

As noted previously this severe centripetal acceleration of each rotor blade may account for an unexpected shift in steady aerodynamic performance due to the amount of untwist produced in the initially "as manufactured" twisted blade [1]. But the modification of untwist attributable to aerodynamic moment is generally negligible by comparison.

Changes in axial shaft and thrust bearing loads attributable to steady radial distortion are also of small consequence.

RESPONSE OF STRUCTURE TO TRANSIENT LOADS

Significant transient loading of compressor or fan structure will usually be associated with a gross change in the throughflow that is either truly aperiodic or of very low frequency. Examples may be related as noted previously to compressor stall, surge, hammershock [2], bistable inlet operation, foreign gas ingestion. Additionally integrated operating experience over the years has indicated the need to consider in the mechanical design phase of an aircraft engine the possibility of ingesting solid objects including birds. These latter considerations are frequently based on fracture mechanics including estimates of impact energy absorption and will usually include, at least in the case of bird ingestion, a subsequent experimental proofing phase. Other than to note that aerodynamic or other forms of damping are not significant in limiting the first peak excursion strains imposed by this type of "mechanical" loading there will be no further consideration here of this problem; structurally safe foreign object ingestion is routinely provided by engine designers.

The sudden changes in throughflow, however, have really not been adequately treated either analytically or experimentally. The problem is closely related to the aeroelastic problem of a single airfoil passing through a sharp-edge gust front in the atmosphere, such as might be produced by a remotely originated blast wave. As in Fig. 1, the blast front can have any orientation θ relative to the airfoil flight direction so that both chordwise u_g and normal w_g components of the gust are experienced and the velocity (and direction) of gust penetration U_p can have any value. For this situation the rate of penetration U_p and the gust components are given by

$$U_p = U_f + U_b \csc \theta$$

$$U_g = V_b \sin \theta$$

$$w_g = V_b \cos \theta$$

where U_f is the flight speed and V_b is the increment of fluid velocity experienced by particles as they are overtaken by the blast front. The two-dimensional lift and moment responses to w_g calculated for this example [3] show that the asymptotic steady state is approached more or less rapidly as a direct function of the speed of penetration (or speed of overtaking if the gust approaches from the trailing edge). A lift overshoot is obtained soon after gust encounter provided U_p is large enough.

The largest two dimensional lift overshoot is obtained for example with infinite speed of penetration and an incompressible fluid (Wagner's problem); the impulse imparted to the airfoil is equal to that of a mass of a cylinder of air (diameter equal to the chord) travelling with the gust velocity w_g. By assuming this impulse is applied to a linear oscillator simulating the elastically mounted airfoil it may be shown that the maximum oscillatory excursion that may be expected will be of the order of

$$h = w_g \, m_{air}/(\omega_o m_{foil})$$

where m_{air} is the mass of the aforesaid cylinder of air and m_{foil} the mass of the airfoil, each for unit span. The quantity ω_o is the circular natural frequency of the vane or blade in bending. This result is modified by the assumption that "inasmuch as the lift response to a horizontal gust is approximately $2\alpha_o$ times the response to a vertical gust of the same intensity, a combined effective gust intensity, which takes into account both components, is " [3]

$$w = (\cos\theta + 2\alpha_o \sin \theta)V_b$$

where α_o is the steady angle of attack. The same conclusion is reached in [4].

Replacing w_g in the previous expression by w and relating α_o to lift coefficient through

$$C_L = 2\pi K \sin\alpha_o$$

where K is a lattice-effect coefficient [5] it is found that

$$2\pi\omega_o h = 2\pi \frac{m_{air}}{m_{foil}} (\cos\theta + \frac{C_L}{\pi K} \sin\theta) V_b$$

This peak value of the "tip" velocity is a parameter used as a criterion for predicting fatigue failure in bending. For typical values in the hammershock situation the velocity may easily exceed the nominally dangerous values in the range of 1 to 3 feet/second [6]. Factors which exacerbate the problem are low thickness ratio profiles and low density materials such as Titanium, high density air such as in rear stages at high flight speed and low altitude, heavy loading such as high pressure ratio per stage and large gust velocities on the order of 10 to 100 feet per second. The analysis could be extended for large finite gust penetration velocities U_p, but the infinite value seems to yield the most dangerous initial impulse.

An important shortcoming in the foregoing analysis is related to the treatment of a single [7] airfoil rather than the cascade; another improvement that is needed is the inclusion of compressibility of the fluid in the analysis. Both these effects have been formulated by a number of investigators in terms of the behavior of a plane acoustic wave propagating either upstream or downstream into an infinite cascade. These infinitesimal perturbation analyses [8] [9] [10] would suffice to give the first order effects being sought except that none have conducted extensive studies of the resulting blade loadings; the emphasis has been on the reflection and transmission of the acoustic waves although presumably the blade loadings could have been extracted from the theory.

No studies of any kind, either experimental or analytical, are known to have been made on the aerodynamic moment resulting from aperiodic forcing and the resulting torsional blade or vane response.

Most likely the entire phenomenon, whether torsion or bending, is not important when the disturbance is truly aperiodic since the vibration would soon damp out due to aerodynamic and other forms of damping. However, if a compressor or fan were to be operated unintentionally in a cyclic surging or stalling condition, the required number of cycles for fatigue and consequent failure could be amassed in a short period of time. With the exceedingly high centrifugal stresses in modern fan and front compressor rotor blades one may even encounter situations conducive to low cycle fatigue.

Since the excitation tends to be rotationally symmetric and to impose purely axial loads on rotors and shafts the response of these structures is usually quite safe; they are very stiff in the axial direction with exceedingly high natural frequencies in their longitudinal modes. An exception might be the "umbrella mode" of a bladed disc assembly, particularly when a very light disc is used or else when a low hub/tip ratio implies long, limber rotor blades with minimal root restraint.

PERIODIC LOADS

By far the most significant aeromechanical response attributable to inlet distortion is the periodic forcing experienced by a rotor blade operating in a circumferential distortion. The relative inflow condition to a specific rotor blade will consist of a superposition of terms with harmonic time variation. The frequency of a general term will be 60 nN Hertz where n is an integer and N is the rotational speed in rpm. In theory one may conceive of completely rotationally periodic distortion patterns with two, three or more distortion patches about the flow annulus. However, in practice this periodicity will not be exact and so n = 1 and all higher n are always present to some degree.

The periodic inflow conditions at a specific radius will be defined by the circumferential distributions of pressure, temperature and vector velocity of the absolute flow. A transformation to rotor coordinates will, in turn, define the inflow conditions relative to the individual rotor blades. Theoretical analysis or interpretation of experimental data for the aeromechanical response must then recognize the centrifugal and Coriolis accelerations to which the arbitrary vibrating turboblade is subject. In other words the mode shapes, stresses and natural frequencies of rotating rotor blades will be different from their static (non-rotating) values and this factor must be clearly recognized in theoretical and experimental work.

The absolute distorted flow at any radius may be expressed in terms of periodic functions of the circumferential coordinate. Referring to Fig. 2, it may be seen that the expressions

$$u' = -u_o - \sum_{n=1}^{\infty} u_n \cos[n\eta(x - y \tan\phi_o) + \psi_n]$$

$$v' = -v_o - \sum_{n=1}^{\infty} v_n \cos[n\eta(x - y \tan\phi_o) + \zeta_n]$$

(where η is the wave number equal to the inverse radius measured from the compressor axis of rotation) satisfy the conditions of circumferential periodicity of absolute flow magnitude and direction. Furthermore, exactly the same distortion exists at another axial station except for being indexed circumferentially to account for the mean swirl angle of the flow, ϕ_o. The latter statement is known to be an approximation in distorted flow; the distortion varies with axial direction so as to satisfy boundary or end conditions

associated with the presence of a bounding cascade [11]. However the variation is small for distances associated with axial depth of one blade row. In effect the influence of upstream and downstream blade rows are neglected insofar as they attenuate the distortion with axial distance.

Under these assumptions the application of the two dimensional incompressible continuity equation reveals that $\Psi_n = \chi_n$ and $u_n = \tan \phi_o v_n$ for $n \geq 1$. Hence $-u' = u_o + \tan \phi_o \tilde{v}$ and $-v' = v_o + \tilde{v}$ where

$$\tilde{v} = \sum_{n=1}^{\infty} v_n \cos[n\eta(x - y \tan \phi_o) + \chi_n]$$

Fixing ξ, ζ coordinates to the chord of a particular rotor blade, the field position of a point ξ on the chord depends on time and is given by

$$x = c\zeta \sin\beta - Ut$$

$$y = -c\xi \cos\beta$$

where ξ is dimensionless with respect to the chord, c. By direct resolution of the components u', v' and $-\vec{U}$ the components of relative velocity along and normal to the airfoil chord are

$$\Xi = (U - u_o) \sin\beta + v_o \cos\beta - \tilde{v}(\tan\phi_o \sin\beta - \cos\beta)$$

$$Z = (U - u_o) \cos\beta - v_o \sin\beta - \tilde{v}(\sin\beta + \tan\phi_o \cos\beta)$$

where

$$\tilde{v} = \sum_{n=1}^{\infty} v_n \cos\{n\eta[(\sin\beta + \tan\phi_o \cos\beta)c\xi - Ut] + \chi_n\}$$

The disturbance is seen to sweep over the airfoil chord with a celerity, or gust penetration velocity

$$U_p = \frac{U}{\sin\beta + \tan\phi_o \cos\beta} = \frac{U \cos\phi_o}{\sin(\beta + \phi_o)}$$

The components of the gust velocity are

$$u_g = \tilde{v} \sec\phi_o \cos(\phi_o + \beta)$$

$$w_g = \tilde{v} \sec\phi_o \sin(\phi_o + \beta)$$

where

$$\tilde{v} = \sum_{n=1}^{\infty} v_n \cos[n(\omega t - 2k_p \xi) - \chi_n]$$

and

$$k_p = \omega c/(2U_p), \quad \omega = \eta U$$

The lift response of an airfoil to gusts* in the oncoming flow consisting of any one of the Fourier harmonics appearing in v has been studied extensively [12] [13] [14] [15] [16]. The effect of cascading has been considered [17] [18] [19] [20] as has the effect of thickness and camber [21] [22]. The more important and difficult influence of compressibility of the fluid has also been tackled [23] [24].

The net result of these theoretical studies and developments indicate that the lift and moment are in effect given by the quasisteady values for very low frequency $n\omega$ of the transverse gust and low wave number $2nk_p$ of the chordwise gust. As the frequency and wave number increase the magnitudes diminish and nonzero phase angles develop between the gust excitation and the lift or moment. The phasing can be either positive or negative.

What would appear to be an exception to the previous general statement occurs when the compressibility of the fluid is taken into account [25] [23]. For certain combinations of frequency, cascade geometry and relative Mach number the so-called condition of aerodynamic resonance is defined (in acoustic studies this is termed "cut-off"). At these conditions the oscillatory lift and moment on the rotor blade vanish; however at Mach numbers very close to resonance rather larger magnitudes of the lift and moment may be obtained. Thus near cut-off conditions it is not clear that the effect of increasing frequency or wave number will account for decreased magnitudes of lift and/or moment. A specific study of this point would seem to be important.

---

*It is interesting that for $\phi_o + \beta = 90$ degrees no chordwise gust is experienced independently of the value of U.

VIBRATORY RESPONSE

The specific reduction in magnitude is not so important as the phasing of the oscillatory lift or moment response. This is because the vibration that is set up by the oscillating force (moment) is subject to a second complete set of lift and moment reactions attributable to that oscillatory motion. Thus the forcing is of aerodynamic nature due to the inlet distortion; the aerodynamic response to the ensuing oscillatory motion can be estimated by considering the relative upwash associated with the vibration in a main stream that is to the first order undistorted. By such a consideration, equilibrium oscillatory amplitudes will obtain when lift and moment amplitudes and phasings are such as to feed the same amount of energy in from the distortion as is fed out in aerodynamic damping. In the entire consideration the frequency is a known quantity.

There is in the literature a great paucity of such resonant amplitude studies of a quantitative nature. Some incompressible results [26] [27] [4] are available for single airfoils* and none for cascades. It would seem, again, that such parametric investigations would be extremely interesting and valuable using the rudimentary theories that are already available. A gross approximation valid for blade bending oscillations in transverse gusts of small wave number (wave length large compared to the chord) is the assumption [28] that the vibratory bending velocity will be equal at each instant to the gust velocity. This theory gives crude correlation with experience under certain conditions, but is powerless to predict torsional oscillations.

For the transverse gust and bending oscillation these theories [27] [4] predict velocity ratios as displayed in the following table,

		Maximum Bending Velocity / Maximum Gust Velocity				
Mass Ratio**	Reduced Frequency	0.05	0.1	0.2	0.5	1.0
0.0015		1.01	1.0	0.94	0.90	-
0.0020		-	1.01	1.00	0.88	0.70

TABLE 1

These results show a modest departure at the higher frequencies from the rule-of-thumb tip velocity rule. Some results for forced torsional oscillations [26] in a stream with fluctuating incidence show that the angular amplitude of the blade motion may be several times the angular amplitude of the incidence variation for low reduced frequencies.

Reference [28] is an excellent review of the practical aspects of distortion-induced blade vibrations. In addition to the diagnostic technique of constructing an interference diagram (plotting blade natural frequencies and engine order lines against rotational speed to observe the potentially dangerous intersections) it is noted therein that the most important intersections are associated with the first six engine orders and that the blade failures which do occur are usually confined to the lower modes of vibration. Thus, the interference diagram which may be drawn for each rotor, is an alert that dangerous forced vibrations may be present at the lower mode-lower order intersections. The actual harmonic content of the distortion at the order of the intersection, for the particular circumferential distortion existing, will determine the actual danger of fatigue-producing vibrations. The means of assessing the harmonic content is of course by direct Fourier decomposition of the measured or predicted distortion pattern. However, most Fourier series have coefficients which decrease inversely with the order n of the harmonic after the first few leading terms. It is for this reason that the lowest engine orders of forcing frequency are most important.

The discussion up to this point has been quasi-two-dimensional. Physical reasoning has been confined to consideration at some radius where both distortion and blade vibratory displacement are in some sense representative. In fact the resonant amplitude which will be attained by a rotor blade will depend on the integrated energy input all along the radius from root to tip and its equalization with a similar integral for the energy consumed in damping [29]. These integrals, in turn, will depend on the radial distribution of the circumferential distortion and on the vibratory mode shape of a typical blade. A particular harmonic of the circumferential distortion will tend to be in phase with itself radially (i.e. in the previous analytic description χ_n would tend not to vary radially). Excepting fundamental bending and fundamental torsion, a particular radial portion of a rotor blade vibrates out of phase with adjacent radial portions. Hence in the higher modes energy input cancellation tends to occur at different radii; the integrand of the energy input integral changes sign. It is by reasoning of this nature that the higher vibration modes tend not to be so dangerous.

---

* With penetration velocity equal to flow velocity

**Mass of a cylinder of air, diameter equal to the chord, as a fraction of the mass of the airfoil.

Conversely, consideration of radial variations illuminates the possibility of a different kind of forced excitation of a rotor blade. When the phase angle of a particular harmonic of a circumferential distortion does vary with radius (χ_n not constant) the peak excitation will be experienced at successive instants of time at successive radii. A kind of travelling load on a beam will resonate the beam if the speed of travel attains certain critical values. This effect [29] [30] [31] can be the cause of those few higher mode vibrations that do occur infrequently since this skewing of the distortion pattern may account for a threefold, or more, amplifications of the blade response, assuming a linear damping law. The phenomenon may be particularly important as one of the indirect effects of inlet distortion; thick rotor wakes of high momentum defect may "stroke" the following stator vanes to resonance in a higher mode. For a radial trailing edge the wake leaving the rotor will also be initially radial. As the wake is convected downstream, however, it will become non-radial and therefore develop the capability of applying a travelling load to succeeding stators. The effect is equally applicable to either bending or torsional vibrations. The travelling load phenomenon should be kept in mind by the aeromechanical engineer as a potential cause for unusually high resonant stresses in a higher vibration mode.

The previous analytical considerations have described inlet distortions in terms of velocity perturbations in the absolute flow. This was for illustrative purposes and because the aerodynamics of unsteady flow is available as a tool for analysis. For distortions consisting of either temperature or molecular composition distortion, no such analytical tool is available. In these instances the best that can be done for the moment is to treat the compressor or fan according to the "parallel compressor" theory. This will give the extreme values of quasisteady lift and moment to be experienced by a rotor blade; the frequency may be supplied by the number of distortion zones or their integer multiples taken together with the compressor speed. Unsteady flow effects may then be estimated (reduction of lift and moment amplitudes and phasing with respect to flow disturbances) using equivalent reduction and phase for the velocity disturbance problem. This latter procedure is highly approximate but seems to be the only obvious correction that can be reasonably applied. A theory which connects total pressure, total temperature and foreign gas distortions by expressing each of these in terms of a vorticity [32] distortion appears to be too esoteric for practical applications at present.

TURBULENCE

Under the assumption that turbulent excitation of a compressor or fan blade is random, it is possible to relate the power spectrum of the resulting vibration to the power spectrum of the excitation. Having the vibration record of a blade excited by turbulence it is possible to process the signal in a spectrum analyzer and deduce the total damping of the system. Some tentative results of such a procedure on a running compressor [33] have indicated that the total damping, aerodynamic plus mechanical, may typically be of the order of 0.10 in fundamental bending, of the order of 0.03 in second bending and of the order of 0.02 in fundamental torsion, all values expressed as logarithmic decrements. A further deduction is that the damping factor is not appreciably affected by stalling of the blades, and in either event, stalled or unstalled, the factor is chiefly of aerodynamic nature. Hence, increased amplitudes, or stresses, in the stall should be associated with increased levels of turbulence and consequent turbulent excitation.

These results must be considered very provisional since stall flutter, a phenomenon that is known to occur, is entirely attributable to negative aerodynamic damping in the blade stall regime. It is probable that the amplitude and frequency conspire to govern the effective aerodynamic damping, particularly if periodic stalling and unstalling occur during a cycle of vibration; the latter is a nonlinear phenomenon, exhibiting hysteresis, entrainment of frequency, etc.

There seems to be no reason why the aeromechanical responses for gusts of the form of u_g and w_g described previously should not be worked out. Then parametric studies of turbulent forcing may be conducted in which the excitation as well as the damping may be formulated. This theory would parallel the analysis of [20] [34] for attached flow and [35] for stalled flow and would allow the lift and moment for each frequency component in the turbulence spectrum to be computed as an input to the response calculation.

SELF-EXCITED INSTABILITIES

In addition to the possibility of increased levels of turbulence attributable to inlet distortion, the degradation of flow in an axial turbomachine may lead to the onset of self-excited blade vibration (stall flutter) or self-excited fluid oscillation (stall propagation) at operating conditions where the phenomenon would not be observed in the absence of distortion. Typically the stall limit line on the compressor map is lowered by distortion, bringing it closer to the operating line and reducing the so-called stall margin. Thick annular boundary layers, or annular regions of outright separation, are particular inlet distortion characteristics that give rise to premature or particularly severe self-excitation.

The effects of propagating stall may be treated from an aeromechanical point of view exactly as any other periodic gust. The frequency, however, is not an integer multiple of the rotational speed; the nonintegral speed is usually between 40 and 60 percent of the rotor speed and the number of stall patches in the annulus may vary between one and ten. Since the latter number may not be predicted analytically with any certitude, the

interference diagram may not be constructed before experimental data on a particular machine have been obtained. An important point to note is that both rotor blades and stator vanes [36] must be analyzed for resonance, probably the major instance where this must be done. (The other case that comes to mind is the rotor-stator wake interaction that always occurs, but at exceedingly high excitation frequencies compared to rotating stall.) Some progress toward predicting the fine grain details of stall patterns - number, intensity, extent and frequency - has been made recently [37] but the only reliable analysis must still rest on the procurement of experimental information.

Stall flutter has been a major concern of jet engine designers and users for three decades. It has so far defied analysis and successful prediction of the phenomenon is confined to the presence or absence of flutter based upon empirical correlation. Oscillatory strain amplitudes cannot be forecast. Since stalling of the front stages is involved, the premature stall attributed to distortion will aggravate the manifestation of flutter.

The correlation which has been and continues to be used is illustrated in Fig. 3. Here, the experimentally determined (or at best empirically correlated) flutter boundary and the blade row operating line are shown in coordinates of blade incidence or flow angle and reduced relative velocity, $W/(b\omega)$ each taken at some characteristic radius. The nondimensionalization factor $b\omega$ is the product of blade or vane semichord and frequency of the vibration. The lower limit of the flutter boundary tends to lie in the neighborhood of reduced velocity equal to 1.0 to 1.3 for torsional motion and 7 to 10 for bending motion. However, the lateral extent and exact shape tend to vary and be a function of the many geometrical and aerodynamic parameter defining the physical blade row and its environment. Hence, the need for empiricism.

Recently, some progress has been made in modeling the unsteady aerodynamics of an airfoil with time-varying extent of separation on the suction surface [35]. This analysis now being extended to cascade flow holds promise of guiding the systematic correlation of governing parameters if the analytic results can be shown to display all the essential features of stall flutter behavior.

An interesting manifestation of stall flutter may occur during compressor surge. The period during which the flow is reversed is two or three orders of magnitude greater than the period of natural blade vibrations. Consequently, sufficient time is available for the vibrations to build up to appreciable magnitude during periods of reverse flow. Examining the velocity triangles in a compressor with reversed throughflow, see Fig. 4, it becomes quite clear that the combination of high incidence and sharp trailing (now leading) edge conspire to assure fully separated flow from the suction surface. An analytical theory is available for predicting the oscillatory lift and moment on the cascade airfoils [38] under these circumstances. The theory affords satisfactory predictive capability for this rather special case.

ROLE OF DAMPING

Three forms of damping are usually discriminated: aerodynamic, material and structural.

The aerodynamic damping arises from the vibratory motion of a blade or vane in an airstream; the out-of-phase component of lift or moment will damp out a bending or torsional vibration if the reaction lags the motion. The theoretical formulation of aerodynamic damping has exactly the same physical model as for the impressed loads due to gusts. In the former case the boundary condition requires annihilation of the upwash due to the blade vibratory velocity; in the latter the boundary condition requires annihilation of the upwash due to the gust velocity. In this sense the results of aerodynamically forced resonance calculations may be expected to be more accurate than the particular choice of aerodynamic assumptions might be; the same assumptions govern both the impressed lift (moment) and the damping lift (moment). This general concept is lent additional credulity by the well established fact that the aerodynamic damping is in most cases the predominant contribution to the total damping.

A characteristic of aerodynamic damping that is not universally appreciated is its role in self-excited instability, or flutter. Since there is no forcing present it is the very fact of negative aerodynamic damping which explains the presence of vibration.

As already noted material damping, the hysteretic dissipation of frictional energy stemming from cyclic straining of the blade material, is usually small compared to the aerodynamic component of damping. Some metals have higher damping factors than others; the chromium stainless steels have higher than usual damping, particularly at elevated temperatures.

Appreciably higher values of material damping are available from composite materials. In particular graphite and boron whiskers and other high strength fibers are laid up in metal or plastic matrices of many kinds (e.g., aluminum or epoxy). Blade and vane constructions employing these new materials have been under sporadic development for at least two decades. While they have apparently been perfected in several instances, particularly with graphite fibers, their introduction into wide scale manufacturing has not been forthcoming. Where these composites have been introduced it has been chiefly with the objective of reducing fan or compressor weight. However, due to the ubiquitous blade vibration environment, the high damping which these blades and vanes exhibit are

essential to their practical application. A problem with rotor blading has been the transference of high centrifugal and bending loads from the fiber rovings to the blade attachments in the discs or drums. There has also been considerable concern over the possible delamination or relative movement between fiber and matrix during vibratory straining. Should this happen in service the endurance limit of these parts become unacceptably low.

Structural damping is thought to occur at joints and interfaces between blades or vanes and their attachments. Microscopic motion between the parts leads to frictional dissipation of energy, hence damping. The implication is that fretting must also occur unless the joint is lubricated; hence if tolerances at the joint are critical as in the root attachment of a cantilever rotor blade, fretting cannot be permitted. If the interface is not critical as in a lacing wire or a part-span shroud, some slight amount of wear may be permitted to occur over a long period of time. Other intentionally designed dampers, in which interfacial motion is induced by vibration, but not in a critical load bearing path, are usually classified as structural damping promoters. Damper design is an exacting exercise where optimum results are desired, but the results are worth the efforts [30].

SHAFT AND DISC RESPONSE

Periodic aerodynamic and inertia blade loadings may have serious consequences with respect to the discs and shafts to which these blades are attached.

Flutter with either random or uniform phasing between adjacent blades may be expected to exert oscillatory root reactions that integrate or sum out to zero for the entire disc. Inlet distortion, on the other hand may always be expected to have an appreciable first engine order component. A distortion that is purely radial or a distortion from a bifurcated inlet that exhibits symmetry about both vertical and horizontal diameters are two exceptions. In propagating stall resonance the stall patches are neither equal in extent nor equiangularly spaced about the annulus. Appreciable departure from such a periodic arrangement have been noted [40].

It follows from the previous consideration that with inlet distortion as far as the shaft is concerned there will be in effect an unbalanced pulsating force exerted at one point on the rim of each rotor disc. The force will have axial and tangential components and will pulsate with the frequency of the fundamental component of blade excitation. In the case of forcing by distortion the point of application of the force will move relative to a point on the rim of the disc in a direction opposite to the direction of rotation and at the tangential speed of the disc. In r, θ coordinates fixed to the disc the net effect is a travelling wave of force excitation whose time and space dependence is given by a sinusoidal function whose argument is $\omega t-\theta$ where ω is the rotor angular velocity. The tangential component of this force is of no consequence to shaft or disc response; the axial component may excite a shaft resonance since the force exerts a bending moment on the shaft with the same temporal dependence. These resonances, where the rotational speed ω coincides with the rotor natural frequency are the so-called critical speeds of rotation. Although their appearance is usually attributed to residual amounts of rotor unbalance, the previous consideration shows that the degree of aerodynamic excitation has also some effect on the expected response and may explain why some criticals are "rougher" than others.

With rotating stall present and exhibiting an angular velocity ω_p the argument of the rotor excitation function becomes $(\omega-\omega_p)t-\theta$ where again θ is an angular coordinate fixed to the rotor. Hence it becomes possible for the rotor to resonate at a frequency different from (lower than) the rotational speed. Such unbalanced aerodynamic excitation may be the cause of otherwise unexplained "minor criticals" that are frequently observed.

Massive rotating assemblies with gyproscopic forces, coulomb friction, trapped fluids, compliant bearings, etc., have a rich variety of vibration phenomena which can certainly couple with the special excitation afforded by operating in distorted, or non-uniform, throughflow. It is not possible to consider the many possibilities in a short review such as this. Suffice it to say that the necessary stimuli at rotation frequency and all higher harmonics can be counted upon to be present with distortion; the presence of rotating stall expands the possibilities to frequencies of nonintegral engine orders and their harmonics.

The beam-like vibrations of the shaft described in the perultimate paragraphs had as their genesis the presumed excitation by the fundamental component of either a circumferential distortion or of a rotating stall pattern, a possible indirect effect of inlet distortion. When the disc is considered as a separate entity the higher harmonics of the excitation may provoke important flexural modes of forced vibration.

These disc modes, or blade-and-disc modes of bladed disc assemblies, consist of alternating patterns of axial displacements with increasing numbers of diametral nodal lines and circular nodal lines for higher natural frequencies. The dangerous modes are evidently [41] the so-called unsymmetrical modes which have no nodal circles, or at most one nodal circle, and one or more nodal diameters [42]. By use of sophisticated computing programs these complex modes and their frequencies may be calculated under rotating conditions. At resonance with an engine order line (or a "stall" order line) the energy input which is through the rotor blades can be assessed by the gust function analysis

described previously. Failure prediction could then be conducted by comparing with the results of rotating disc fatigue testing under controlled conditions of energy input. This degree of refinement has not been approached in design phases, probably due to the cost of obtaining parametric fatigue limit data of discs, including variations in disc geometry, material, etc. (A similar program involving just blade vibrations has been conducted by a number of manufacturers, using production or preproduction lots of blades held in bench type fixtures.)

REMEDIAL ACTIONS

Presupposing unacceptable aeromechanical response of some structural element from a stress or deflection point of view, steady or oscillatory, the corrective options that are open to consideration are i) removal of the stimulus or ii) redesign of the structure to withstand the excitation.

Under the first category we may consider cleaning up the inlet to lessen or remove the distortion. The inlet designer and/or the engineer charged with airframe-engine integration may have some control over this factor, although there always exists the strong possibility that the distorted flow will reappear at some other system operating condition. In the case of periodic forcing of the structure it may be that the distortion may be retained but its frequency content changed (converting a distortion pattern, for instance, with one axis of symmetry to one with two axes of symmetry with the objective of reducing the energy content of any odd engine order excitation).

Stall phenomena (which lead to forced excitation by rotating stall or to self-excitation by stall flutter) may be modified, or pushed out of the operating range by changes in turbine nozzle throat area, variable guide vane schedules, etc. Casing treatments such as honeycombing or grooving have been found to be beneficial in delaying rotor tip stall, etc. The specification of means of avoiding or delaying stall will be the function of the aerodynamics engineer. The aeromechanical engineer must be prepared to assess the change in structural response expected for any proposed change in the aerodynamic environment.

The most common situation is one in which the stimulus cannot be changed and structural changes must be contemplated to achieve acceptable life. It is clear that changing mass and stiffness distribution in the structure will change its eigenfunctions and eigenfrequencies. Thus a particular harmful resonance may be moved out of the operating range. Although theoretically this may be done by either reducing or increasing the structural natural frequency, the choice taken is almost always to increase the frequency; blade chords are increased with a consequent reduction in number of blades per row to maintain constant solidity. This kind of change can also be justified to avoid self-excited vibrations (stall flutter). See Fig. 3, for the effect on the operating line of increasing the natural frequency ω. However, one might argue that for forced excitation where the tip amplitude of vibration is in some sense determined, the more limber lower frequency cantilever blade might sustain the lower root bending stresses.

This is not the only case of contradictory action being indicated depending on whether forced or self excitation is being guarded against. The case of mistuning blades in given row to lower the peak stress expected [43] will depend on the specific phenomenon. Mistuning is beneficial in the case of flutter; precise tuning is beneficial if pure forcing is expected with no chance of encountering flutter. Hence another tool open to the structural designer is not only to change the frequency level of the blades in a row, but to specify the distribution of frequencies of blades within a row by, say, selective assembly of blades manufactured to wide dimensional tolerances.

Application of a lacing wire or part-span shroud (clapper) will raise the frequency of a blade because of the additional restraint thereby imposed. More importantly perhaps, it will change the vibration mode, typically converting an antinode into a node. This form of "node control" can be very effective in reducing drastically the energy input from the airstream into the blade. The integrand of the energy input integral consists of the product of the oscillating lift (moment) and vibratory velocity (angular velocity) both being functions of radius. The vibratory velocity distribution is strongly effected by the mode shape, being essentially ω times the nodal displacement. Thus control of input forcing energy - the integral from root to tip of the force x velocity product - is obtained by such modification of mode shape. In the case of self-excited vibration one may conceivably create a node at the radial location where stalling is expected and thereby physically prevent stall flutter from occurring.

Damping, of course, is an important means of reducing blade amplitudes. The phenomenon implies the dissipation of energy and care must be taken that such dissipation does not also result in excessive wear of a critical part in the case of structural damping or the generation and propagation of microscopic cracks along the internal grain boundaries of metallic alloys. Changing material specifications to improve damping has been effective in marginal cases to improve fatigue life, as has shot-peening, heat treatments etc. Radical changes in damping may be obtained with composites as noted earlier. It seems that long development phases will be necessary due to problems mentioned previously and the subleties of designing with nonorthotropic materials. The chief characteristic would seem to be the uprating of axial machines to withstand more severe vibration environments by the change to composites; the fans and compressors must operate with metallic materials in service while the improvements are being sought in the development laboratories.

CONCLUSION

In short the possibilities for prediction and corrective action are quite numerous. The specific suggestions discussed here have been illustrative in nature and not exhaustive by any means. The aeromechanical design of axial turbomachines continues to be a demanding discipline with improving physical understanding leading to more and more effective avoidance or control of harmful aeromechanical response.

REFERENCES

1. M. Ohtsuka, "Untwist of Rotating Blades", ASME Paper No. 74-GT-2, April 1974.

2. J.S. Alford and I.W. Victor, "Dynamic Measurements of Forward Gas Expulsion during High Speed Stall of Jet Engines", SAE Paper No. 650840, October 1965.

3. F.W. Diederich and J.A. Drischler, "Lift and Moment Responses to Penetration of Sharp-Edged Travelling Gusts, with Application to Penetration of Weak Blast Waves", NACA TN 3956, May 1957.

4. F. Sisto, Discussion of Reference 27, J. Applied Mechanics, v. 22, n. 4, December 1955, pp. 597-598.

5. G.F. Wislicenus, Fluid Mechanics of Turbomachinery, Dover Publications, New York, 1965, p. 234.

6. E.K. Armstrong, "Recent Blade Vibration Techniques", ASME J. Engrg. for Power, v. 89, n. 3A, July 1967, pp. 437-444.

7. L.C. Woods, "On Unsteady Flow Through a Cascade of Aerofoils", Proc. Royal Society (A), v. 228, n. 1172, 1955, pp. 50-65.

8. S. Kaji and T. Okazaki, "Propagation of Sound Waves Through a Blade Row II. Analysis Based on the Acceleration Potential Method", J. Sound Vib., v. 11, n. 3, 1970, pp. 355-375.

9. R.K. Amiet, "Transmission and Reflection of Sound by a Blade Row", AIAA Paper No. 71-181, January 1971.

10. R. Mani and G. Harvey, "Sound Transmission Through Blade Rows", J. Sound Vib., v. 12, 1970, pp. 59-83.

11. A.H. Stenning and G.A. Plourde, "Attenuation of Circumferential Inlet Distortion in Multistage Axial Compressors", J. Aircraft, v. 5, n. 3, May-June 1968, pp. 236-242.

12. J.M. Greenberg, "Some Considerations on an Airfoil in an Oscillating Stream", NACA TN 1372, August 1947.

13. J.H. Horlock, "Fluctuating Lift Forces on Aerofoils Moving Through Transverse and Chordwise Gusts", ASME J. Basic Engrg., v. 90D, n. 4, 1968, pp. 494-500.

14. C.L. Morfey, "Lift Fluctuations Associated With Unsteady Chordwise Flow Past an Airfoil", ASME J. Basic Engrg., v. 92D, n. 3, September 1970, pp. 663-665.

15. G.L. Commerford and F.O. Carta, "Unsteady Aerodynamic Response of a Two-Dimensional Airfoil at High Reduced Frequency", AIAA Journal, v. 12, n. 1, January 1974, pp. 43-47.

16. J.P. Giesing, W.P. Rodden and B. Stahl, "Sears Function and Lifting Surface Theory for Harmonic Gust Fields", AIAA J. Aircraft, v. 7, n. 3, 1970, pp. 252-255.

17. B. Schorr and K.C. Reddy, "Inviscid Flow Through Cascades in Oscillatory and Distorted Flow", AIAA Paper No. 70-131, January 1970.

18. R.E. Henderson and J.H. Horlock, "An Approximate Analysis of the Unsteady Lift on Airfoils in Cascade", ASME J. of Engrg. for Power, v. 94, October 1972, pp. 233-240.

19. H. Yeh and H. Naumann, "Unsteady Induced Velocities in a Cascade", Proc. 2nd Int. JSME Symposium, Tokyo, September 1972, pp. 201-207.

20. D.S. Whitehead, "Force and Moment Coefficients for Vibrating Aerofoils in Cascade", Aero. Res. Council Reports & Memoranda R&M No. 3254, February 1960.

21. H. Atassi and M. Goldstein, "Unsteady Lift Forces on Highly Cambered Airfoils Moving Through a Gust", AIAA Paper No. 74-88, January 1974.

22. H. Naumann and H. Yeh, "Lift and Pressure Fluctuations of a Cambered Airfoil Under Periodic Gusts and Applications in Turbomachinery", J. of Engrg. for Power, ASME Trans., v. 95A, n. 1, January 1973, pp. 1-10.

23. R. Mani, "Compressibility Effects in the Kemp-Sears Problem", International Symposium on the Fluid Mechanics and Design of Turbomachinery, Penn State University, August 31-September 3, 1970.

24. D.S. Whitehead, "Aerodynamic Aspects of Blade Vibration", Proc. Inst. of Mech. Engrgs., v. 180, part 3I, 1965-66.

25. R.E. Henderson, "The Unsteady Response of a Blade Row From Measurements of the Time Mean Total Pressure", ASME Paper No. 73-GT-94.

26. F. Sisto, "Resonance and Flutter", Lecture No. 13, ASME Course Fluid Dynamics of Turbomachinery", Iowa State University, August 1968.

27. J.R. Schnittger, "The Stress Problem of Vibrating Compressor Blades", J. Applied Mechanics, Trans. ASME, v. 77, pp. 57-64.

28. E.K. Armstrong and D.D. Williams, "Some Intake Flow Maldistribution Effects on Compressor Rotor Blade Vibration", J. Sound Vib., v. 3, n. 3, 1966, pp. 340-354.

29. C.E. Danforth, "Distortion Induced Vibration in Fan and Compressor Blades", AIAA Paper 74-232, January 1974.

30. C.E. Danforth, "How to Reduce Wake-Driven Vibrations in Light Turbojets", Aviation Age, February 1956.

31. W. Traupel, "Stresses on Blades Oscillating under Resonance Conditions". Brown Boveri Rview, n. 415, 1971, pp. 138-147.

32. C. Farmer, M. Iverson and A. Fuhs, "A New Approach to Distortion Induced Compressor Stall--Vorticity Maps", AIAA Paper No. 72-1116, November 1972.

33. D.S. Whitehead, "The Analysis of Blade Vibration due to Random Excitation", Aero. Res. Council Reports & Memoranda R&M No. 3253, August 1960.

34. S.N. Smith, "Discrete Frequency Sound Generation in Axial Flow Machines", Cambridge University Dept. of Engrg. Rept. CVED/A-Turbo/TR29, 1971.

35. F. Sisto and P.V.K. Perumal, "Lift and Moment Prediction for an Oscillating Airfoil with a Moving Separation Point" ASME Paper No. 74-GT-28, March-April 1974.

36. M.C. Huppert, D.F. Johnson and E.L. Costilow, "Preliminary Investigation of Compressor Blade Vibration Excited by Rotating Stall", NACA RME52J15, Washington, December 1952.

37. H. Takata and S. Nagano, "Nonlinear Analysis of Rotating Stall", ASME 72-GT-3, 1972.

38. F. Sisto, "Linearized Theory of Nonstationary Cascades at Fully Stalled or Supercavitated Conditions", ZAMM, v. 47, n. 8, 1967, pp. 531-542

39. E.J. Williams, S.W.E. Earles, "Optimization of the Response of Functionally Damped Beam Type Structures with Reference to Gas Turbine Compressor Blading", Trans. ASME, J. Eng. for Industry, vol. 96B, n. 2, May 1974, pp. 471-476.

40. John A. Rockett, "Modulation Phenomena in Stall Propagation", Trans. ASME, J. Basic Eng., v. 81D, September 1959, pp. 417-425.

41. S. Timoshenko, "Vibration Problems in Engineering", 3rd ed., New York, Van Nostrand, 1955, pp. 455-457.

42. F.O. Carta, "Coupled Blade-Disk-Shroud Flutter Instabilities in Turbojet Engine Rotors", Trans. ASME, J. Eng. for Power, v. 89A, n. 3, July 1967, pp. 419-426.

43. D.S. Whitehead, "Effect of Mistuning on the Vibration of Turbomachine Blades Induced by Wakes", J. Mech. Engrg. Sci., v. 8, n. 1, 1966, pp. 2-21.

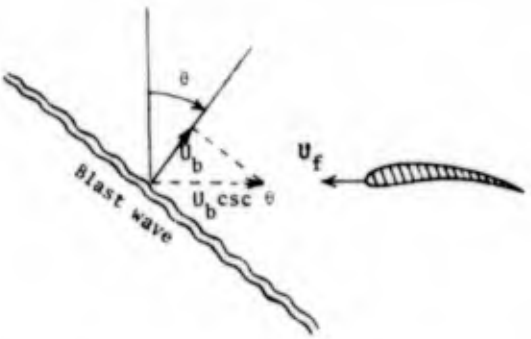

Fig.1 Orientation of blastwave and airfoil.

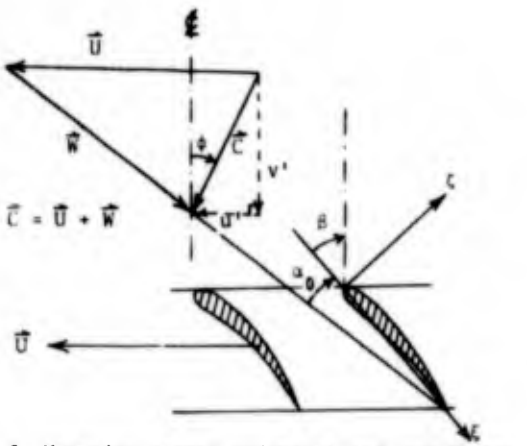

Fig.2 Velocity vector triangles and coordinate conventions for circumferentially periodic distortions.

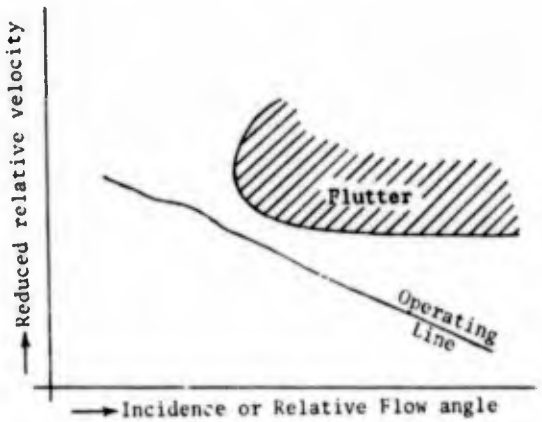

Fig.3 Stall Flutter Boundary

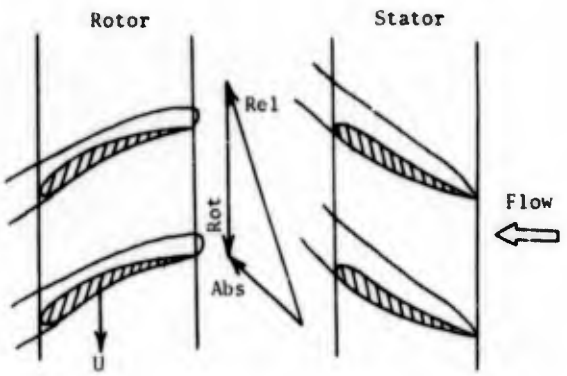

Fig.4 Full separation as a consequence of reversed flow.

PREDICTION TECHNIQUES

by

H. Mokelke

Motoren- und Turbinen-Union München GmbH, München, Germany

SUMMARY

An outline is presented on mathematical modelling for prediction of the aerodynamic response of aircraft engine compressors to steady-state and time-dependent pressure and temperature distortion. A detailed review is made of various models. In particular their assumptions, their limitations for practical applications and their scope for further development are discussed. Results predicted with the models (as far as possible compared with experimental evidence) are selected from published works.

SYMBOLS

A	area, constant
a	tangent of mean swirl angle $\bar{\alpha}$, Eq. (32)
B	rate of change of body force with axial velocity, constant
c_x, c_Θ, c_r	axial, tangential, radial velocity
g	axial gap between blade rows
K	circumferential resistance factor, Section 3
K	constant defined by Eq. (60 b)
k	reduced frequency parameter, Eq. (13)
L	length of compressor
l_c	chord length
M	mass flow
Ma	Mach number
n, j	circumferential harmonic number
P	total pressure
PRS	stall pressure ratio
P_n	complex harmonic coefficient of total pressure
P_a	atmospheric pressure
p	static pressure
r	radial coordinate, mean radius of annulus
$S\Theta$	circumferentail distortion sensitivity
$[S_v]$	state vector, defined by Eq. (38)
T	total temperature
t_s	static temperature
t	time
$t^* = \Omega t/2\pi$	dimensionless time
U_n	complex harmonic coefficient of axial velocity
u_b	rotor wheel speed
V_n	complex harmonic coefficient of tangential velocity
X	axial body force
x	axial coordinate
α, β	flow angle relative to stator, rotor
γ	ratio of specific heats
Δ	difference, change, loss
δ	amplitude
ζ, η, ξ	axial, tangential, radial vorticities
η_{is}	isentropic efficiency
Θ	circumferential coordinate
$\bar{\Theta}$	angle of spoiling
Θ_s	ratio of inlet total temperature to standard ambient temperature
ρ	density
$\phi = c_x/u_b$	flow coefficient
Φ	velocity potential
$\psi = \Delta P/\rho u_b^2$	pressure rise coefficient
$\bar{\psi}' = d\psi/d\phi$	slope on $\psi = f(\phi)$ at the flow coefficient $\bar{\phi}$
Ψ	stream function
Ω	rotor wheel speed, rad/sec
ω	disturbance circular frequency

Subscripts

1	at inlet to compressor
2	at outlet of compressor
M	at constant corrected mass flow
N	at constant corrected speed
min	minimum
max	maximum
c	critical, corrected, chord
$-\infty$	for upstream
n	harmonic number
ov	overall
st	stage
t	tip
P	total pressure
T	total temperature

Superscripts

~	flow quantities in spoiled section
^	flow quantities in unspoiled section
–	circumferential average
e	effective
'	pertubation (except ψ')
av	blade passage average

Location of planes in 4-stage sample compressor (Fig. 6, 20, 22, 24)

plane 1	1.9" upstream of compressor
plane 2	behind IGV blade row
plane 4, 6, 8, 10	behind 1st, 2nd, 3rd, 4th stage
plane 11	2" downstream of plane 10 and 1" upstream of OGV s

1. INTRODUCTION

Mathematical models have been developed to predict the response of axial compressors to distorted inlet flow.

A survey of the various types of inlet distortions, configurations of compressors and compressor responses to inflow distortions is given below.

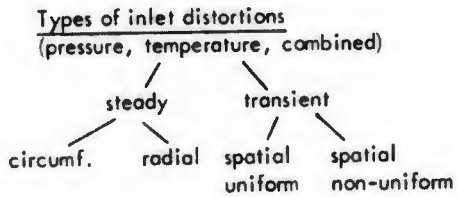

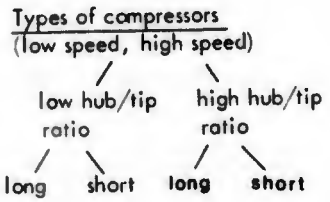

Compressor responses to inlet distortions

a) Loss in performance
b) Loss in stability (surge)
c) Attentuation of distortion
d) Perturbed flow fields
e) Unsteady blade forces

No mathematical model exists which would predict all listed responses for every compressor and every distortion. Instead, specialized models with different prediction capabilities are available for specific types of inlet distortions and configurations of compressors. These models will be reviewed in the main body of the paper.

2. PARALLEL COMPRESSOR MODEL

2.1 DESCRIPTION OF THE MODEL

The compressor-in-parallel model is used to predict the effects of steady circumferential total pressure and/or total temperature distortions on the performance and stability of compressors. The model divides the distorted compressor into sections, which are treated as hypothetical compressors working in parallel. The following assumptions are made:

(a) All parallel compressors discharge to the same exit static pressure
(b) There is no connection between the parallel compressors
(c) All parallel compressors operate on the undistorted characteristic.

It should be noted that the model is only suitable for circumferential inlet distortions, because radial distortions induce a great amount of radial flow redistribution which is in contradiction to the second assumption.

For the case where the circumferential inlet distortion can be described in the form of a square wave, the compressor

is divided into two sectors as shown in Fig. 1. As an input for the analysis, the total pressures and total temperatures across the inlet of the two sectors and the angle of spoiling, Θ^*, are required (Fig. 2). In addition, the performance map of the undistorted compressor in the form of "total pressure ratio" and "isentropic efficiency" as functions of "corrected mass flow" for different corrected speeds are needed (Fig. 3). With the definition of the isentropic efficiency (ratio of isentropic to real total enthalpy rise across the compressor), the total temperature at the exit of sector A can be derived as

$$\tilde{T}_2 = \tilde{T}_1 \left[1 + \frac{(\tilde{P}_2/\tilde{P}_1)^{\frac{\gamma-1}{\gamma}} - 1}{\tilde{\eta}_{is}} \right] \tag{1}$$

Further, the following well-known gas dynamic relationship is employed together with the assumption of axial discharge

$$\frac{\tilde{P}_2}{\tilde{P}_2} = f\left(\frac{\tilde{M}\sqrt{\tilde{T}_2}}{\tilde{P}_2 \quad A_2} \right) \tag{2}$$

Combining Eq. (1) and (2) yields, after rearranging:

$$\tilde{P}_2 = \left(\frac{\tilde{P}_2}{\tilde{P}_1}\right) \tilde{P}_1 \; f\left[\frac{\tilde{M}\sqrt{\tilde{T}_1}}{\tilde{P}_1} \; \frac{\sqrt{1 + \frac{(\tilde{P}_2/\tilde{P}_1)^{\frac{\gamma-1}{\gamma}} - 1}{\tilde{\eta}_{is}}}}{(\tilde{P}_2/\tilde{P}_1) \; A_2} \right] \tag{3}$$

A corresponding expression is found for the parallel compressor representing sector B

$$\hat{P}_2 = \left(\frac{\hat{P}_2}{\hat{P}_1}\right) \hat{P}_1 \; f\left[\frac{\hat{M}\sqrt{\hat{T}_1}}{\hat{P}_1} \; \frac{\sqrt{1 + \frac{(\hat{P}_2/\hat{P}_1)^{\frac{\gamma-1}{\gamma}} - 1}{\hat{\eta}_{is}}}}{(\hat{P}_2/\hat{P}_1) \; A_2} \right] \tag{4}$$

The operating points of the two parallel compressors on the undistorted performance map have to be determined so that $\tilde{P}_2 = \hat{P}_2$. In the case of different total temperatures at the inlet of sectors A and B, care has to be taken that the appropriate speed lines are used, (Fig. 3). Once the uniform exit static pressure is obtained, unknown pressures and temperatures at inlet and outlet of the two sections can also be determined. The rate of attenuation of the disturbance is thus established. In addition, the overall performance of the distorted compressor can be obtained by suitably averaging the inlet and outlet pressures and temperatures of the parallel compressors. Parallel compressor operation in the h-s-diagram is shown in Fig. 4.

The above described method of calculation is considerably simplified if a performance map is available in which the ratio of outlet static pressure to inlet total pressure is plotted against corrected mass flow. The method is also simpler in the case of low-speed compressors, where the flow can be considered as incompressible.

2.2 PREDICTION OF DISTORTION ATTENUATION AND LOSS IN PERFORMANCE

The parallel compressor model has been used in Ref. (1) to predict the attenuation of a 120°-square wave total pressure inlet distortion in a low-speed, four-stage, axial flow compressor. (A description of the experimental apparatus and the test procedure can also be found in Ref. (2).) The performance characteristic of the compressor is presented in the form of overall total pressure rise coefficient, $\Delta P / \rho u_b^2$, plotted versus flow coefficient, c_x/u_b, (Fig. 5). A least square approximation of the measured characteristic by a polynomial of second order simplifies the application of the parallel compressor model. As input to the analysis, the difference in high and low total pressure at compressor inlet, the angle of spoiling, the mean flow rate $\bar{c}_x/u_b$ of the distorted compressor and the coefficients of the least square polynomial are required.

Results of the computation are shown in Fig. 5. The flow coefficients $\tilde{c}_x/u_b$ and $\hat{c}_x/u_b$ of the two parallel compressors, representing the distorted and undistorted sections, are found to the left and right of the mean flow coefficient $\bar{c}_x/u_b$. The figure further shows the experimentally and theoretically obtained total pressure rise indicating the loss in performance compared with the undistorted compressor.

The circumferential distributions in total and static pressure are presented in Figs. 6a, b. The analytical profiles describing the flow within the compressor are calculated by assuming equal performance for all stages. Experimental results are also introduced into the figures. As shown, the magnitude of the distortions is well predicted. Differences in shape can be attributed mainly to circumferential cross flow, which has the effect of decreasing the relative rotor incidence angle on one side of the distortion and increasing it on the other, thus causing an asymmetry in the profiles.

Roberts, Plourde and Smakula (3) measured the attenuation of a 180°-square wave total pressure inlet distortion in a low-speed axial compressor which was operated in a single-stage, two-stage and three-stage configuration. They also utilized the parallel compressor model and compared the experimental and analytical results. As shown in Fig. 7, they obtained a reasonable agreement between experiment and theory.

In a further experiment, Roberts, Plourde and Smakula measured the performance characteristics of a three-stage configuration subjected first to a mild and then to a severe total pressure inlet distortion and compared the results with

predictions obtained with the parallel compressor model. As shown in Fig. 8, they found a good agreement between experiment and theory for the mild distortion. The agreement is poor for the severe distortion near the peak pressure coefficient. As pointed out by Roberts et al, the assumption of parallel compressor operation on undistorted characteristic is invalid under these operating conditions. (As shown in Ref. (4) and 5), compressor operation with high mean rotor blade loading produces significant dynamic stall at circumferential location: where the rotor blades leave the distortion.)

2.3 MODEL PREDICTIONS OF COMPRESSOR STALL

The main merit of the parallel compressor model is its capability of predicting the loss in stall pressure ratio of compressors with pressure and/or temperature inlet maldistribution.

Two definitions for the loss in stall pressure ratio are in use, depending on whether it is evaluated at constant corrected mass flow or constant corrected speed. Using the same notation as in Ref. (6), the two definitions are (Fig. 9):

$$(\Delta PRS)_M = \frac{PRS_b - PRS_e}{PRS_b} \tag{5}$$

$$(\Delta PRS)_N = \frac{PRS_c - PRS_e}{PRS_c} \tag{6}$$

where PRS_e = stall pressure ratio of the distorted compressor

PRS_b = stall pressure ratio of the undistorted compressor at the same corrected mass flow

PRS_c = stall pressure ratio of the undistorted compressor at the same corrected rotor speed

From an inspection of Fig. 9, it is apparent that the difference between $(\Delta PRS)_M$ and $(\Delta PRS)_N$ decreases as the speed line steepens.

To predict the loss in stall pressure ratio, it is assumed in the parallel compressor model that the inlet distorted compressor stalls, if one of the parallel compressors operates on the clean stall line. On this assumption, a simple relationship between the loss in stall pressure ratio $(\Delta PRS)_N$ and the distortion parameter $(\bar{P} - P_{min})/\bar{P}$, Fig. 10, can be established in the case of an inlet total pressure distortion. For its derivation, the additional assumption is made that the total pressure P_2 at the exit of the distorted compressor is constant. (This assumption is somewhat contradictory to the more correct assumption of constant exit static pressure.) With these assumptions it follows from Eq. (6):

$$(\Delta PRS)_N = \frac{\frac{P_2}{P_{min}} - \frac{P_2}{\bar{P}}}{\frac{P_2}{P_{min}}} = 1 - \frac{P_{min}}{\bar{P}} \tag{7}$$

In Ref. (7), Reid investigated the effect of increasing the circumferential extent of total pressure inlet distortions on the stability of a six-stage axial flow compressor. His experiments showed that the surge delivery static pressure fell rapidly as the angle of spoiling was increased from 0° to 90° and then levelled out at a constant value from 90° to 360°. Reid concluded from his results that a critical angle of spoiling exists, which had a value between 60° and 90° in the case of the compressor he investigated.

A similar experiment was performed by Calogeras, Mehalic and Burstadt (8) with an eight-stage axial flow compressor. The compressor stall pressure ratio, defined as $PRS_e/PRS_b = 1 - (\Delta PRS)_M$, fell rapidly as the angle of spoiling was increased from 0° to 60° and then stabilized at a nearly constant value between 90° and 180°. Defining the critical angle of spoiling as the minimum distortion angle to which the compressor responds quasi-steadily, Calogeras et al concluded that 60° was the critical angle for the compressor investigated.

For the case of 100 % corrected rotor speed and 8 1/2 mesh/inch spoiler gauze densitiy, the experimental points obtained by Calogeras et al have been replotted in Fig. 11 in the form $(\Delta PRS)_M = f(\Theta^-)$. The solid curve through these points rises first to a maximum and then falls to zero at $\Theta^- = 360^\circ$. The assumption of zero loss in stall pressure ratio at $\Theta^- = 360^\circ$ is based on the fact that a spoiler screen of 360° extent acts as an upstream throttling device which should not affect the compressor stall limit. An inspection of this curve shows that the critical angle of spoiling might also be defined as that distortion angle which causes the maximum loss in stall pressure ratio at a constant P_{min}/P_{max}.

Returning now to the model prediction of the loss in stall pressure ratio, Eq. (7), introduction of the area-averaged total pressure at compressor inlet

$$2\pi\bar{P} = (2\pi - \Theta^-)\,P_{max} + \Theta^-\,P_{min} \tag{8}$$

into Eq. (7) yields

$$(\Delta PRS)_N = 1 - \frac{P_{min}/P_{max}}{1 - \frac{\Theta^-}{2\pi}\,(1 - P_{min}/P_{max})} \tag{9}$$

With a constant ratio of $P_{min}/P_{max} = 0.86$ for the case of 100 % corrected speed and a screen density of 8 1/2 mesh from Fig. 19a of Ref. (8), the theoretical loss in stall pressure ratio $(\Delta PRS)_N$ has been computed from Eq. (9) as a function of the circumferential extent of spoiling, Θ^-. Results are introduced in Fig. 11 as the dashed-dotted curve. Since the 100 % corrected rotor speed line of the eight-stage compressor is almost vertical, the experimental loss in stall pressure ratio evaluated at constant corrected mass flow is comparable with the theoretical loss determined at constant

corrected speed.

Fig. 11 shows that as the angle of spoiling decreases, from a certain critical value onwards the discrepancy between theory and experiment grows rapidly. This discrepancy can be explained by an unsteady response of the compressor to the disturbed flow, contradicting the assumption of quasi-steady parallel compressor operation on the undistorted characteristic. In order to overcome this difficulty, Reid suggested combining the concepts of "parallel compressor model" and "critical angle of spoiling". Consider, for example, an inlet total pressure distortion of a circumferential extent smaller than the critical angle, Θ_c^-, as shown in Fig. 10. An effective distortion may now be defined having a width equal to the critical angle and a minimum effective total pressure P^e_{min} defined by the following equation:

$$\Theta_c^- \ (P_{max} - P^e_{min}) = \Theta^- \ (P_{max} - P_{min}) \tag{10}$$

Eq. (10) rearranged yields

$$\frac{P^e_{min}}{P_{max}} = 1 - \frac{\Theta^-}{\Theta_c^-} \ \left(1 - \frac{P_{min}}{P_{max}}\right) \tag{11}$$

For a distortion of a width smaller than the critical angle, $\Theta^- < \Theta_c^-$, the ratio P_{min}/P_{max} in Eq. (9) is replaced by the effective total pressure ratio, P^e_{min}/P_{max}. Introduction of Eq. (11) into (9) yields

$$(\Delta PRS)_N = 1 - \frac{1 - \frac{\Theta^-}{\Theta_c^-} \ \left(1 - \frac{P_{min}}{P_{max}}\right)}{1 - \frac{(\Theta^-)^2}{2\pi\Theta_c^-} \ \left(1 - \frac{P_{min}}{P_{max}}\right)} \qquad \text{for } \Theta^- < \Theta_c^- \tag{12}$$

Results of Eq. (12) for a constant value of $P_{min}/P_{max} = 0.86$ and a critical angle of $\Theta_c^- = 90^\circ$ are presented in Fig. 11 (dashed line) and show a considerable improvement in the prediction of the loss in stall pressure ratio.

The critical angle of spoiling (which is required for the prediction) is unfortunately not a universal constant but changes with the design of the compressor. The design parameter, which significantly influences the critical distortion angle, may be deduced from experiments by Roberts, Plourde and Smakula. In one of their tests, they determined the effect of varying rotor and stator blade chord length on the loss in peak pressure rise coefficient for a three-stage compressor with a 180° total pressure inlet distortion. They also utilized the parallel compressor model to predict the loss in peak pressure rise coefficient. The ratio of experimental to theoretical loss coefficient is replotted in Fig. 12 against rotor chord length. The figure shows that a good agreement between experiment and theory is obtained for rotor blades with short chord length. However, as the chord length increases, a growing discrepancy can be observed. The reason for this behaviour is the capability of the flow around blades with a short chord to adjust to changes in flow environment more rapidly than around blades with a long chord. For short chord blades the assumption of quasi-steady parallel compressor operation is therefore more justified and the theory yields better results. As a conclusion, the critical distortion angle should be small for compressors with short rotor blade chords and large for compressors with long rotor blade chords.

Instead of attempting to predict the critical distortion angle, Korn (9) correlated the difference between experimental loss in stall pressure ratio and that predicted with the parallel compressor model with the reduced frequency parameter k. For the prediction, the usual assumption is made that stall occurs when one of the parallel compressors operates on the clean compressor stall line. The reduced frequency parameter is defined as

$$k = \frac{\omega \, l_c / 2}{u_b} \tag{13}$$

where l_c is the chord length of the rotor blade, u_b the rotor speed and ω the disturbance circular frequency. The period of the disturbance as assumed by Korn is the time required for a rotor blade to travel through the distortion

$$t = \frac{\Theta^-}{\Omega} \tag{14}$$

where Θ^- is the circumferential extent of the distortion and Ω the angular velocity of the rotor. Introduction of

$$\omega = \frac{2\pi}{t} = \frac{2\pi}{\Theta^-} \Omega \tag{15}$$

and

$$u_b = \Omega \, r \tag{16}$$

into Eq. (13) yields

$$k = \frac{\pi \, l_c}{r \, \Theta^-} \tag{17}$$

It may be noted that the reduced frequency parameter k contains the two parameters "circumferential distortion extent" and "rotor chord length" which have been identified above (Fig. 11, 12) as major influences on the loss in stall pressure ratio of a compressor. The difference in test data and model prediction (also referred to in Ref. (9) as circumferential distortion sensitivity, $S\Theta$) is determined by Korn for several single-stage compressors and plotted against the reduced frequency parameter (Fig. 13). The data correlate well and show the same tendency as predictions by Melick (10,11).

The parallel compressor model was used in conjunction with the established correlation $S\Theta = f(k)$ by Korn to predict the degradation in compressor stall and performance of a single-stage compressor with a 90° circumferential distortion. A good agreement between experiment and theory was obtained (Fig. 14).

The effect of 180° total temperature, total pressure and combined pressure and temperature inlet distortions on the loss in stall pressure ratio of an eight-stage compressor has been determined by Braithwaite, Graber and Mehalic in Ref. 6.

The distortion configurations employed are shown schematically on the left of Fig. 15. Braithwaite et al also used the parallel compressor model to predict the loss in stall pressure ratio. In order to simplify the calculations, they made the assumption of constant total pressure instead of constant static pressure at the exit of the compressor. The distorted compressor was again considered to stall when any of the parallel compressors operated on the clean compressor stall line.

The case of a pure total pressure inlet distortion is presented schematically in Fig. 15a. The two parallel compressors operate on the same speed line. The stall point of the distorted compressor is located on a straight line connecting the operating points of the two parallel compressors.

Fig. 15 b shows the case of a pure total temperature inlet distortion. The two parallel compressors operate on different corrected speed lines. Operating points of the parallel compressors and the predicted stall point are located on a horizontal line, since the total pressure is constant at the inlet and exit of the temperature distorted compressor.

A 180° overlap of total pressure and total temperature distortion is shown in Fig. 15 c. The section with a low inlet total pressure and a high inlet total temperature, represented by parallel compressor 2, will cause stall of the distorted compressor.

The case of a 90° overlap is presented in Fig. 15 d. Four parallel compressors operate on the undistorted performance map. Stall of the distorted compressor will be initiated in section 1, for which the inlet total pressure is low and the inlet total temperature high.

Fig. 15 e shows the case of 0° overlap in pressure and temperature. Here, both sections may be responsible for stall of the distorted compressor, depending on whether the temperature or the pressure inlet disortion is more severe. Two separate solutions were therefore presented by Braithwaite et al to decide which of the two sections is the critical one.

A comparison between measured and predicted loss in stall pressure ratio for the various cases is presented in Fig. 16 and shows a reasonable agreement between experiment and theory.

With the aid of the parallel compressor model, Braithwaite et al further established a simple mathematical relationship between the loss in stall pressure ratio $(\Delta PRS)_N$ and the pressure and temperature distortion parameters $\Delta P/P$ and $\Delta T/T$. (The parameters are defined as $\Delta P/P = (P_{max} - P_{min})/\bar{P}$ and $\Delta T/T = (T_{max} - T_{min})/\bar{T}$.) Three cases of pressure and temperature overlap are considered:

(1) Stall is initiated by the sector with low pressure and low temperature (Fig. 15 e)
(2) Stall is initiated by the sector with high pressure and high temperature (Fig. 15 e)
(3) Stall is initiated by the sector with low pressure and high temperature (Fig. 15 c)

Assuming that the stall pressure ratio can be expressed as a linear function of the corrected speed, $PRS = A(N/\sqrt{\Theta_s}) + B$, A, B = constants, and that $\Delta T/T$ and $\Delta P/P$ are small, the loss in stall pressure ratio for the three cases has been derived in Ref. 6 as

$$(1) \qquad (\Delta PRS)_N = \frac{\Delta P}{P}\left(1 - \frac{\bar{\Theta}_P}{2\pi}\right) - \frac{1}{2}\,\frac{\Delta T}{T}\left(\frac{\bar{\Theta}_T}{2\pi}\right) \Big/ \left(1 + \frac{B}{A(N/\sqrt{\bar{\Theta}_s})}\right) \qquad (18)$$

$$(2) \qquad (\Delta PRS)_N = -\frac{\Delta P}{P}\left(\frac{\bar{\Theta}_P}{2\pi}\right) + \frac{1}{2}\,\frac{\Delta T}{T}\left(1 - \frac{\bar{\Theta}_T}{2\pi}\right) \Big/ \left(1 + \frac{B}{A(N/\sqrt{\bar{\Theta}_s})}\right) \qquad (19)$$

$$(3) \qquad (\Delta PRS)_N = \frac{\Delta P}{P}\left(1 - \frac{\bar{\Theta}_P}{2\pi}\right) + \frac{1}{2}\,\frac{\Delta T}{T}\left(1 - \frac{\bar{\Theta}_T}{2\pi}\right) \Big/ \left(1 + \frac{B}{A(N/\sqrt{\bar{\Theta}_s})}\right) \qquad (20)$$

Results of these equations for a corrected speed of 97 % and 180° distortion showing the loss in stall pressure ratio as a function of $\Delta T/T$ with $\Delta P/P$ as parameter are presented in Fig. 17. The figure shows the importance of the relative position of pressure and temperature distortion. The highest loss in stall pressure ratio is caused by a 180° overlap, Fig. 15c, Eq. (20). For a distortion with 0° overlap, Fig. 15 e, either of the two sections may cause stall, the highest of the two losses predicted by Eqs. (18) and (19) being the valid one. It may also be noted from Fig. 17 that for some combinations of $\Delta P/P$ and $\Delta T/T$, no loss in stall pressure ratio occurs.

3. TWO-DIMENSIONAL LINEAR BODY-FORCE MODEL

It is not immediately apparent from the parallel compressor analysis what steps in compressor design should be taken to achieve a rapid attenuation of steady circumferential inlet distortions through the compressor. It is also of interest to determine the impact of the parallel compressor assumption of zero circumferential crossflow and to obtain an idea of the flow redistribution upstream of the distorted compressor.

Answers to the above questions can be obtained from an analysis presented by Plourde and Stenning in Ref. (12). The theory is restricted to compressors of high hub/tip ratio, so that the flow field can be regarded as two-dimensional. Further, the assumption is made that the flow is inviscid and incompressible. The compressor is assumed to consist of a large number of small stages, and the effect of these stages on the increase in pressure is simulated by an appropriate distribution of axial body forces, X.

Circumferential redistribution of the perturbed flow within the compressor can only occur in the gaps between the blade rows. Compared with a blade-free flow field, resistance to crossflow is therefore encountered within the compressor, and this is taken into account in the analysis by means of a resistance factor, K.

The perturbed flow is assumed to consist of a mean flow with superimposed perturbations

$$c_x = \bar{c}_x + c'_x(\Theta, x) \qquad (21\,a)$$

$$c_\Theta = \bar{c}_\Theta + c'_\Theta(\Theta, x) \qquad (21\,b)$$

$$p = \bar{p} + p'(\Theta, x) \tag{21 c}$$

$$X = \bar{X} + X'(\Theta, x) \tag{21 d}$$

The significant assumption is made that the axial and tangential velocity perturbations are small compared with the mean axial velocity, i.e., $c'_x \ll \bar{c}_x$ and $c'_\Theta \ll \bar{c}_x$. Substitution of Eqs. (21) into the two-dimensional equations of momentum and continuity yields (after neglecting terms of second order) a set of linear partial differential equations. Assuming also the mean flow to be purely axial, i.e. $\bar{c}_\Theta = 0$, these equations simplify to

$$K r \rho \bar{c}_x \frac{\partial c'_\Theta}{\partial x} = - \frac{\partial p'}{\partial \Theta} \tag{22 a}$$

$$\rho \bar{c}_x \frac{\partial c'_x}{\partial x} = - \frac{\partial p'}{\partial x} + X' \tag{22 b}$$

$$\frac{1}{r} \frac{\partial c'_\Theta}{\partial \Theta} + \frac{\partial c'_x}{\partial x} = 0 \tag{22 c}$$

It is shown in Ref. (12) that (assuming the local total pressure rise across a portion of the compressor to be a function of c_x and x) the change of X' with c'_x is proportional to the slope of the undistorted pressure rise charachteristic. Therefore,

$$\frac{\partial X'}{\partial \Theta} = \frac{\partial X'}{\partial c_x} \frac{\partial c'_x}{\partial \Theta} = - B \frac{\partial c'_x}{\partial \Theta} \tag{23}$$

where

$$B = - \frac{1}{L} \frac{d \Delta \bar{p}}{d \bar{c}_x} , \tag{24}$$

$d \Delta \bar{p} / d \bar{c}_x$ = slope of undistorted characteristic, $\bar{p} = f(\bar{c}_x)$.

Introduction of Eq. (23) into (22 b) yields

$$\rho \bar{c}_x \frac{\partial^2 c'_x}{\partial x \, \partial \Theta} + B \frac{\partial c'_x}{\partial \Theta} = - \frac{\partial^2 p'}{\partial x \, \partial \Theta} \tag{25}$$

A solution of Eqs. (22a), (25), and (22 c) may be attempted in the form

$$p' = \rho \bar{c}_x \sum_{n=1}^{i} W_n(x) \, e^{in\Theta} \tag{26 a}$$

$$c'_x = \sum_{n=1}^{i} S_n(x) \, e^{in\Theta} \tag{26 b}$$

$$c'_\Theta = \sum_{n=1}^{i} T_n(x) \, e^{in\Theta} \tag{26 c}$$

Introduction of these expressions into Eqs. (22a), (25) and (22 c) yields a system of three simultaneous, ordinary differential equations in $W_n(x)$, $S_n(x)$ and $T_n(x)$, which is readily solved. The solutions for $W_n(x)$, $S_n(x)$ and $T_n(x)$, contain three unknown constants. Six further unknown constants are included in the solutions of the upstream and downstream flow fields (for which $K = 1$ and $B = 0$). Consequently, there are altogether nine unknown constants which have to be determined from the boundary conditions.

These boundary conditions are listed below:

1. Specified axial velocity far upstream of the compressor
2. Zero static pressure perturbation far upstream of the compressor
3. Matched axial velocity at compressor inlet
4. Matched static pressure at compressor inlet
5. Reduction of the circumferential velocity at compressor inlet due to resistance to crossflow within the compressor
6. Matched axial velocity at compressor exit
7. Zero tangential velocity at $x = L$ just inside the compressor
8. Zero tangential velocity just downstream of the compressor
9. Zero static pressure perturbation far downstream of the compressor

The total pressure perturbations may be found from the relationship

$$P = p + \frac{1}{2} \rho (c_x^2 + c_\Theta^2) \tag{27}$$

which yields, for small dusturbances and axial mean flow, $\bar{c}_\Theta = 0$,

$$P' = p' + \rho \bar{c}_x c'_x \tag{28}$$

Numerical examples have been presented by Plourde and Stenning showing the attenuation rates of first order sinusoidal inlet distortions in a compressor with $L/r = 1.615$. In Fig. 18 a, the decay rates of total pressure disturbances are plotted against axial location. The figure shows that for a constant crossflow factor, $K = 3.88$, the attenuation grows with increasing values of $Br/(\rho \bar{c}_x)$. Since

$$\frac{Br}{\rho \bar{c}_x} = - \frac{1}{L/r} \frac{\bar{\psi}'}{\bar{\phi}} \tag{29}$$

(where $\bar{\psi}'$ is the slope of the undistorted pressure rise characteristic $\psi = f(\phi)$ at a mean flow coefficient $\bar{\phi}$) it can be deduced that a steep slope and a low mean flow coefficient are beneficial for the attenuation of a total pressure inlet distortion.

The decay of the axial velocity perturbations for a constant K = 3.88 and variable values of $Br/(\rho \bar{c}_x)$ is shown in Fig. 18 b. The figure demonstrates the marked redistribution of the flow upstream of the compressor.

Fig. 19 shows the effect of varying the circumferential crossflow factor (between unity for very large gaps and infinity for very small gaps) on total pressure, static pressure, and axial velocity at a constant $Br/(\rho \bar{c}_x)$. Experimental results obtained by Plourde and Stenning are also introduced into Fig. 19 a. As shown, the prediction assuming a high resistance to circumferential crossflow is closest to the experiments.

A similar result has been obtained in Ref. (1) in which the body-force analysis is used to predict the attenuation of a 120° square wave distortion in a four-stage compressor with $L/r = 2.318$, Fig. 20. (The experimental results are the same as those presented in Fig. 6). The square wave approximation (dashed line in Fig. 20 a) of the measured circumferential total pressure distribution 1.9" upstream of the compressor (plane 1) serves (in the form of a Fourier series with 30 harmonic components) as an input for the analysis. The slope of the undistorted pressure rise characteristic at a flow of $\bar{\phi} = 1.251$ is found from the polynomial in Fig. 5 as $\bar{\psi}' = -2.56$. The predicted total and static pressure perturbations shown in Fig. 20 are superimposed upon the mean experimental pressures obtained by circumferentially averaging the appropriate curves. The closest prediction is obtained for a high value of K, indicating again that little circumferential crossflow occurs within a compressor.

Discrepancies between experiment and theory, which are particularly evident for the static pressure (Fig. 20 b), can be mainly attributed to the effect of the (small) circumferential crossflow on the pressure increase across the stages, which is neglected by the model.

4. TWO-DIMENSIONAL LINEAR ACTUATOR DISC MODEL

4.1 REVIEW OF THE BASIC MODEL

Compressor stall at high rotor speeds is generally initiated in the later stages of a multi-stage machine. To deal with a steady circumferential total pressure inlet distortion, it is therefore of importance to design the front stages for rapid distortion attenuation. The body-force analysis is not very suitable to provide guidelines for such a design, since (in the form presented) it assumes all stages to have an equal performance. Better guidelines may be obtained from a model (Ref. (13), (14), (15)) which replaces the blade rows of the compressor individually by actuator discs.

In this section the model will be described for compressors with a high hub/tip ratio. As has been noted before, this allows the flow field to be regarded as two-dimensional. It is further assumed that the flow outside the discs is inviscid and incompressible. The axial spacing of the discs corresponds to the gaps between the blade rows since (as mentioned above), circumferential flow redistribution can only occur in these gaps. As for the case of the body-force analysis, the perturbed flow is regarded as consisting of a mean flow with superimposed perturbations and the velocity perturbations are assumed small compared with the mean axial velocity. The equations of motion may therefore be linearized. Results are listed below together with the equation of continuity.

$$\rho \bar{c}_\Theta \frac{\partial c'_\Theta}{\partial \Theta} + r \rho \bar{c}_x \frac{\partial c'_\Theta}{\partial x} = - \frac{\partial p'}{\partial \Theta} \tag{30 a}$$

$$\rho \bar{c}_\Theta \frac{\partial c'_x}{\partial \Theta} + r \rho \bar{c}_x \frac{\partial c'_x}{\partial x} = - r \frac{\partial p'}{\partial x} \tag{30 b}$$

$$\frac{1}{r} \frac{\partial c'_\Theta}{\partial \Theta} + \frac{\partial c'_x}{\partial x} = 0 \tag{30 c}$$

A comparison between Eqs. (22) and (30) reveals the differences between the body-force model and the actuator disc model:

1. There is no resistance to circumferential crossflow between the actuator discs, therefore K = 1
2. No body forces are acting on the flow between the discs, therefore X' = 0
3. The mean flow between the discs may swirl, i.e. $\bar{c}_\Theta \neq 0$.

In the flow fields upstream and downstream of the compressor (for which in general $\bar{c}_\Theta = 0$), Eqs. (22) and (30) reduce to the same expressions.

It is convenient to replace the static pressure perturbations in Eqs. (30a, b) by total pressure perturbations. From Eq. (27) for small perturbations:

$$p' = P' - \rho \bar{c}_x c'_x - \rho \bar{c}_x a c'_x \tag{31}$$

where

$$a = \tan \bar{\alpha} = \bar{c}_\Theta / \bar{c}_x \tag{32}$$

Eq. (31) introduced into Eqs. (30 a, b) yields, after normalizing x by r,

$$a \rho \bar{c}_x \left(\frac{\partial c'_x}{\partial \Theta} - \frac{\partial c'_\Theta}{\partial x} \right) = - \frac{\partial P'}{\partial x} \tag{33 a}$$

$$\rho \bar{c}_x \left(\frac{\partial c'_x}{\partial \Theta} - \frac{\partial c'_\Theta}{\partial x} \right) = \frac{\partial P'}{\partial \Theta} \tag{33 b}$$

Normalizing x by r in the equation of continuity

$$\frac{\partial c'_\Theta}{\partial \Theta} + \frac{\partial c'_x}{\partial x} = 0 \qquad (33\ c)$$

A solution of Eqs. (33) may be attempted in the form

$$p' = \rho\, \bar{c}_x \sum_{n=1}^{i} R_n(x)\, e^{in\Theta} \qquad (34\ a)$$

$$c'_x = \sum_{n=1}^{i} S_n(x)\, e^{in\Theta} \qquad (34\ b)$$

$$c'_\Theta = \sum_{n=1}^{i} T_n(x)\, e^{in\Theta} \qquad (34\ c)$$

Introduction of Eqs. (34) into Eqs. (33) yields a system of three simultaneous, ordinary differential equations which is readily solved.
The results are

$$p' = \rho\, \bar{c}_x \sum_{n=1}^{i} \left((1 + a^2)\, A_3\, e^{-inax} \right) e^{in\Theta} \qquad (35\ a)$$

$$c'_x = \sum_{n=1}^{i} \left(A_1\, e^{nx} + A_2\, e^{-nx} + A_3\, e^{-inax} \right) e^{in\Theta} \qquad (35\ b)$$

$$c'_\Theta = \sum_{n=1}^{i} \left(A_1\, i\, e^{nx} + A_2\, i\, e^{-nx} + A_3\, a\, e^{-inax} \right) e^{in\Theta} \qquad (35\ c)$$

With different values for the complex constants A_1, A_2, A_3, Eqs. (35) apply to each gap between the discs. They also apply to the flow fields upstream and downstream of the compressor, for which, as noted before, the mean flow will generally be axial, $a = 0$.

The as yet unknown complex constants have to be determined from the boundary conditions. There are three boundary conditions for each blade row to be satisfied. They have to be derived from

(1) continuity of axial velocity
(2) specified fluid outlet angle
(3) specified total pressure change

Results for either rotor or stator blade row may be written in the form

$$(c'_x)_{Ex} = (c'_x)_{In} \qquad (36\ a)$$

$$(c'_\Theta)_{Ex} = \sigma\, (c'_x)_{In} + \tau\, (c'_\Theta)_{In} \qquad (36\ b)$$

$$(P')_{Ex} = (P')_{In} + \rho\, \bar{c}_x\, \gamma\, (c'_x)_{In} + \rho\, \bar{c}_x\, \epsilon\, (c'_\Theta)_{In} \qquad (36\ c)$$

where σ, τ, γ and ϵ are functions of the mean inlet and outlet angles, the mean flow coefficient and cascade loss and deviation data. The indices In and Ex refer to the inlet and exit of the blade row, respectively.

As an example, consider a compressor with 10 blade rows, Ref. (5). There are 27 constants for the 9 gaps and 3 constants for each of the upstream and downstream flow fields. The requirement of finite velocity perturbations for upstream and downstream of the compressor eliminates two of the constants. One constant will be determined from the specification of the inlet distortion, i.e., the circumferential total pressure variation upstream of the compressor. The remaining 30 complex constants can be determined by matching the flow fields at the 10 discs. Introduction of Eqs. (35) into Eqs. (36) yields a system of 30 linear equations in 30 unknowns which may be solved by a standard computational procedure. A separate solution of the system is required for each harmonic number n. Once the constants are determined, the velocity and pressure perturbations at all axial locations can be found from Eqs. (35).

4.2 DUNHAM'S METHOD OF SOLUTION

The number of linear equations to be solved increases in proportion to the number of compressor stages. Since most of the elements of the coefficient matrices are zero, the above mathematical procedure is not very efficient. A more efficient technique to determine the perturbed flow field has been presented by Dunham in Refs. (16), (17). This technique will be outlined below.

The pressure and velocity perturbations at any x may be expressed by

$$p' = \bar{c}_x \sum_{n=1}^{i} P_n\, e^{in\Theta} \qquad (37\ a)$$

$$c'_x = \sum_{n=1}^{i} U_n\, e^{in\Theta} \qquad (37\ b)$$

$$c_\Theta = \sum_{n=1}^{j} V_n \, e^{\quad \text{in } \Theta} \tag{37 c}$$

where P_n, U_n, V_n are complex harmonic coefficients. With Eqs. (37) the n-th harmonic component of the perturbed flow may be described at any x by a state vector in form of a column matrix

$$\left[S_v\right] = \begin{bmatrix} P_n \\ U_n \\ V_n \end{bmatrix} \tag{38}$$

The relationship between the state vector at exit of a blade row and that at inlet to the blade row is then found by introduction of Eqs. (37) into Eqs. (36). Dropping the index n gives:

$$\begin{bmatrix} P_{Ex} \\ U_{Ex} \\ V_{Ex} \end{bmatrix} = \begin{bmatrix} 1 & \gamma & \epsilon \\ 0 & 1 & 0 \\ 0 & \sigma & \tau \end{bmatrix} \begin{bmatrix} P_{In} \\ U_{In} \\ V_{In} \end{bmatrix} \tag{39}$$

Matrices for rotor, stator, IGV and OGV rows may be found in Table 1 of Ref. (5). They will be referred to as $[R]$, $[S]$, $[IGV]$, $[OGV]$ matrices respectively.

The relationship between the components of the state vector at inlet to a gap (or at inlet to the upstream or downstream flow field) and the complex constants A_1, A_2 and A_3 is found from Eqs. (37) and Eqs. (35) with $x = 0$:

$$P_{In} = (1 + a^2)\, A_3 \tag{40 a}$$

$$U_{In} = A_1 + A_2 + A_3 \tag{40 b}$$

$$V_{In} = i A_1 + i A_2 + a A_3 \tag{40 c}$$

Resolving Eqs. (40) with respect to A_1, A_2, A_3 yields

$$A_1 = -\frac{1}{2}\left(P_{In}(1 - i a) / (1 + a^2) - U_{In} + i V_{In} \right) \tag{41 a}$$

$$A_2 = -\frac{1}{2}\left(P_{In}(1 + i a) / (1 + a^2) - U_{In} - i V_{In} \right) \tag{41 b}$$

$$A_3 = P_{In} / (1 + a^2) \tag{41c}$$

The relationship between the components of the state vector at exit of a gap of length g and the complex constants A_1, A_2 and A_3 is found from Eqs. (37) and Eqs. (35):

$$P_{Ex} = (1 + a^2)\, A_3 \, e^{\quad - inag} \tag{42a}$$

$$U_{Ex} = A_1 \, e^{\quad ng} + A_2 \, e^{\quad - ng} + A_3 \, e^{\quad - inag} \tag{42 b}$$

$$V_{Ex} = A_1 \, i \, e^{\quad ng} + A_2 \, i \, e^{\quad - ng} + A_3 \, a \, e^{\quad - inag} \tag{42 c}$$

Introduction of Eqs. (41) into Eqs. (42) yields the relationship between the state vector at exit of a gap (index Ex) to the state vector at inlet to that gap (index In). The relationship may be written in the form

$$\begin{bmatrix} P_{Ex} \\ U_{Ex} \\ V_{Ex} \end{bmatrix} = \begin{bmatrix} G_{11} & G_{12} & G_{13} \\ G_{21} & G_{22} & G_{23} \\ G_{31} & G_{32} & G_{33} \end{bmatrix} \begin{bmatrix} P_{In} \\ U_{In} \\ V_{In} \end{bmatrix} \tag{43}$$

where G_{11}, G_{12} ... are the elements of the gap transfer matrix $[G]$. The gap matrix for a gap with a length g in which the mean flow swirls with an angle $\bar{\alpha}$ is presented in Table 1 of Ref. (5).

As an example, consider a four-stage compressor. The state vector at the exit of a stage consisting of gap, rotor, gap, stator can be related to the state vector at inlet to that stage by

$$[S_v]_{Ex} = [St][S_v]_{In} \tag{44}$$

where

$$[St] = [S][G_S][R][G_R] \tag{45}$$

The four stages may be preceded by inlet guide vanes and followed after some gap by outlet guide vanes. The state vector at the exit of the compressor is then related to the state vector at the inlet to the compressor by

$$[S_v]_{Ex} = [T][S_v]_{In} \tag{46 }$$

where

$$[T] = [OGV][G_B][St_4][St_3][St_2][St_1][IGV] \tag{47}$$

Eq. (47) allows the compressor transfer matrix to be calculated. Eq. (46) is equivalent to the following set of equations:

$$P_{Ex} = t_{11} P_{In} + t_{12} U_{In} + t_{13} V_{In} \tag{48 a}$$

$$U_{Ex} = t_{21} P_{In} + t_{22} U_{In} + t_{23} V_{In} \tag{48 b}$$

$$V_{Ex} = t_{31} P_{In} + t_{32} U_{In} + t_{33} V_{In} \tag{48 c}$$

where t_{11}, t_{12}, ... are the complex elements of the matrix $[T]$. As mentioned above, the requirement exists that the velocity perturbations remain finite even if the upstream flow field extends to minus infinity. Combining Eq. (41 b) with Eq. (35 b) (together with the assumption of axial mean flow, $a = 0$) yields the following condition for the harmonic coefficients at inlet of the compressor:

$$P_{In} - U_{In} - i V_{In} = 0 \tag{49}$$

Correspondingly, for the downstream flow field, Eq. (41a) combined with Eq. (35 b) yields the condition for the harmonic coefficients at exit of the compressor (note the change in indices)

$$P_{Ex} - U_{ex} + i V_{Ex} = 0 \tag{50}$$

By introducing Eqs. (48) into Eq. (50), a second relation between the harmonic coefficients at compressor inlet is obtained which may be combined with the first relation, Eq. (49), to eliminate V_{In} and U_{In}, respectively. The result is

$$U_{In} = -\frac{t_{11} - t_{21} + t_{33} + i\,(t_{31} - t_{13} + t_{23})}{t_{12} - t_{22} - t_{33} + i\,(t_{32} + t_{13} - t_{23})}\; P_{In} \tag{51}$$

and

$$V_{In} = -\frac{t_{11} - t_{21} + t_{12} - t_{22} + i\,(t_{31} - t_{32})}{t_{13} - t_{23} + t_{32} + i\,(t_{33} - t_{12} + t_{22})}\; P_{In} \tag{52}$$

With the harmonic coefficients P_{In} determined from a Fourier series approximation of a given total pressure distribution at the inlet to the compressor, the corresponding axial and tangential velocity perturbations are determined from Eqs. (51) and (52), respectively. With the transfer matrix of the first blade row and the known coefficients P_{In}, U_{In} and V_{In} at the inlet of the compressor, the perturbed flow at the exit of the first blade row can be found. Applying the same procedure through the whole compressor using the appropriate matrices for the various gaps and blade rows, the total pressure and velocity perturbations may be calculated everywhere. The static pressure perturbations can then be determined from Eq. (31).

It is demonstrated by Eq. (47) that the essential mathematical procedure of Dunham's method for prediction of the perturbed flow is the successive multiplication of 3 by 3 complex matrices as opposed to the first described method, where a system of simultaneous linear equations had to be solved.

4.3 REPLACEMENT OF THE STAGES BY ACTUATOR DISCS

The above analysis (which will be referred to as a "blade row model") replaced rotor and stator blade rows separately by actuator discs and required as an input the appropriate cascade loss and turning characteristics. Alternatively, the stages of a compressor may be replaced by actuator discs, using input data from the stage characteristics. This model will be referred to as a "stage model". A stage of the model is assumed to consist of rotor and stator without a gap. The gap which in reality exists between the blade rows is added to the gap preceding the rotor. The length of the resulting gap therefore represents the axial distance between two actuator discs. The transfer matrix through a stage is then found from

$$[St] = [S][R] \tag{53}$$

where $[S]$ and $[R]$ are the stator and rotor matrix, respectively. The resulting stage transfer matrix may be simplified by assuming the outlet angles of the rotor and stator blade rows to be independent of the inlet angle. In addition, the relationship between the slope of the stage characteristic $\bar{\psi}'_{St}$ and the blade row characteristics (Ref. (2) or (17)) may be used. With the final assumption of constant rotor losses independent of inlet angle, the stage transfer matrix takes the simple form

$$[St] = \begin{bmatrix} 1 & (1/\bar{\phi})\,(\bar{\psi}'_{St} + \tan\bar{\alpha}_{In}) & -1/\bar{\phi} \\ 0 & 1 & 0 \\ 0 & \tan\bar{\alpha}_{Ex} & 0 \end{bmatrix} \tag{54}$$

where the indices In and Ex refer to the inlet and exit of the stage, respectively. Once all stage matrices of the compressor have been determined, Eq. (55) may be used to calculate the transfer matrix through the 4-stage sample compressor.

$$[T] = [OGV][G_B][St_4][G_4][St_3][G_3][St_2][G_2][St_1][G_1][IGV] \tag{55}$$

The remaining procedure to determine the pressure and velocity perturbations is analogous to that given in Section 4.2.

4.4 DISCUSSION OF ASSUMPTIONS

For the development of the actuator disc model, a number of assumptions have been made which will be discussed below.

(a) The model is restricted to compressors of high hub/tip ratio which allowed the flow field to be regarded as two-dimensional. Extensions of the linearized model to low hub/tip ratio compressors will be reviewed in Section 5.

(b) The assumption that the velocity perturbations are small compared with the mean axial velocity permitted the equations of motion to be linearized. Suitable non-linear models for the prediction of large disturbances are the parallel compressor analysis and the finite-difference flow field analysis to be discussed in Section 6.

(c) The assumption of incompressible flow is not strictly necessary but has been made to simplify the analysis. Extension to compressible flow is possible by utilizing the linearized compressible (instead of the incompressible) flow equations. An extension of Ehrich's (13) single blade row analysis to compressible flow has been presented by Krzywoblocki in Ref. (18).

A simple approach to account for compressibility effects is to assume a constant density in any one gap of a multi-stage compressor but to allow for changes in densities between different gaps. Changes in flow coefficient may be taken into account correspondingly.

(d) In the above analysis it has been assumed that the rotor blades respond quasi-steadily to the change in flow as the rotor blades travel through the steady distortion. In Ref. (19), Seidel extended Rannie and Marble's (14) actuator disc analysis to allow for an unsteady blade response of a single, unstalled rotor. For this, Seidel considered the rotor blades as isolated airfoils operating in transverse and streamwise gusts. Unsteady lift fluctuations due to these gusts were calculated from Sears' (20) and Isaac's (21) analyses. The results were then used to modify a matching condition at the rotor row.

A similar approach has been followed in Ref. (1) with the exception that the litt fluctuations due to streamwise gusts have been determined from Horlock's (22) unsteady analysis on isolated airfoils.

Numerical examples show that there are no great differences between results from quasi-steady and unsteady versions of the small perturbation theories. This is not surprising, since reduced frequency parameters based on the first harmonic of single lobe distortions are generally low.

Experimental and theoretical investigations on isolated airfoils demonstrate that (at least for low reduced frequency parameters) unstalled unsteady effects are small compared with unsteady stalling effects. These latter effects, involving boundary layer separation and reattachment at high mean blade loadings, are included in an unsteady blade passage analysis which is coupled with a non-linear flow field analysis. This model will be reviewed in Section 6.

4.5 NUMERICAL EXAMPLES

The stage model has been used in Ref. (2) to predict the total pressure attenuation ratio of sinusoidal inlet distortions through a hypothetical 10-stage compressor. (The additional assumption is made in Ref. (2) that the effect of the tangential velocity perturbations on the pressure rise across a stage may be ignored). Prediction results for different harmonic numbers are shown in Fig. 21a and the corresponding axial velocity attenuation ratios are presented in Fig. 21 b. The figures demonstrate the remarkable influence of the order of the distortion on the decay rate of the distortion.

The stage model has further been used in Ref. (1) to predict the development of a 120°-square wave total pressure inlet distortion in a 4-stage compressor. Experimental results and input to the analysis correspond to those used in connection with the parallel compressor and body-force analysis. The required stage slopes are assumed equal to a quarter of the slope on the overall characteristic at $\bar{\phi} = 1.251$, Fig. 5. Fig. 22 shows the comparison between predicted and measured total and static pressure perturbations.

Katz (15) used his small perturbation analysis to predict the attenuation of a circumferential distortion through a rotor belonging to a singlestage compressor with IGV s and OGV s. The blade rows of the compressor were arranged far apart from each other. Katz therefore considered the rotor as isolated and replaced it by a single actuator disc in the analysis. The circumferential total pressure variation measured upstream of the rotor served as an input for the analysis. This is shown in Fig. 23 a, together with the predicted and experimental profiles downstream of the rotor. Corresponding measured and predicted circumferential variations in flow angle and flow coefficient are shown in Fig. 23 b. Two predictions have been made, with losses and outlet angle variations included in one case and excluded in the other. Considerably better agreement between experiment and theory was obtained, when losses and outlet angle variations were considered.

The blade row model has been used in Ref. (1) to predict the development of a 120° square wave inlet distortion through a 4-stage compressor (10 blade rows). Experimental results and input to the analysis correspond to those used in connection with the stage model predictions. The required cascade loss and deviation characteristics have been determined from a semi-empirical analysis by Carter (23). The measured and predicted circumferential variations in total and static pressure are presented in Fig. 24. A comparison between Fig. 22b and Fig. 24b shows the improvement in the prediction of the static pressure distribution with the blade row model. This improvement can be attributed to the inclusion of loss and outlet angle variations with inlet angle, both effects being neglected by the stage model.

5. THREE-DIMENSIONAL LINEAR ACTUATOR DISC MODEL

5.1 GENERAL REMARKS

The two-dimensional small perturbation analysis discussed in the previous section is restricted to compressors with a high hub/tip ratio. Extensions of the model to predict the development of steady distortions in compressors with a low hub/tip ratio will be reviewed below.

For the three-dimensional model, the blade rows of the compressor are again replaced by discs. Since radial flow redistribution is not restricted by the blades, it is not realistic to contract the blade row to a disc as in the two-dimensional case. Instead, the disc has to be located within the blade row, preferably at the mid-axial plane, Ref. (24).

As before, the flow outside the discs is considered to consist of a mean flow with superimposed perturbations

$$\begin{aligned} c_x &= \bar{c}_x + c'_x \quad (r, \Theta, x) \\ c_\Theta &= \bar{c}_\Theta + c'_\Theta \quad (r, \Theta, x) \\ c_r &= \bar{c}_r + c'_r \quad (r, \Theta, x) \\ p &= \bar{p} + p' \quad (r, \Theta, x) \\ \rho &= \bar{\rho} + \rho' (r, \Theta, x) \end{aligned} \tag{56}$$

For the mean flow it may be assumed at present that

$$\bar{c}_r = 0 \tag{57}$$

$\bar{c}_\Theta$, $\bar{c}_x$ functions of the radius only,

and for the perturbations

$$c'_x << \bar{c}_x \; ; \; c'_\Theta << \bar{c}_x \; ; \; c'_r << \bar{c}_x \; ; \; \rho' << \bar{\rho}$$

With these assumptions, linearization of the three-dimensional compressible flow equations yields:

Eq. of motion

$$\frac{\bar{c}_\Theta}{r}\frac{\partial c'_r}{\partial \Theta} + \bar{c}_x \frac{\partial c'_r}{\partial x} - \frac{2\,\bar{c}_\Theta c'_\Theta}{r} = -\frac{1}{\bar{\rho}}\frac{\partial p'}{\partial r}$$

$$\frac{\bar{c}_\Theta}{r}\frac{\partial c'_\Theta}{\partial \Theta} + \bar{c}_x \frac{\partial c'_\Theta}{\partial x} + \frac{c'_r}{r}\frac{d}{dr}(r\,\bar{c}_\Theta) = -\frac{1}{\bar{\rho}\,r}\frac{\partial p'}{\partial \Theta} \qquad (58)$$

$$\frac{\bar{c}_\Theta}{r}\frac{\partial c'_x}{\partial \Theta} + \bar{c}_x \frac{\partial c'_x}{\partial x} + c'_r \frac{d\bar{c}_x}{dr} = -\frac{1}{\bar{\rho}}\frac{\partial p'}{\partial x}$$

Eq. of continuity

$$\frac{1}{r}\frac{\partial}{\partial r}(r\,c'_r) + \frac{1}{r}\frac{\partial c'_\Theta}{\partial \Theta} + \frac{\partial c'_x}{\partial x} + \frac{\bar{c}_x}{\bar{\rho}}\frac{\partial \rho'}{\partial x} = 0 \qquad (59)$$

A comparison between Eqs. (30) and Eqs. (58), (59) indicates one increase in complexity of the linearized model by the extension from two-dimensional, incompressible to three-dimensional, compressible flow. It is believed that no general solution to Eqs. (58), (59) has been obtained so far.

5.2 FREE VORTEX MEAN FLOW (INCOMPRESSIBLE)

Dunham (16), (17) considered the case where the mean flow is a free vortex. He also made the assumption that the flow is incompressible. Hence

$$\bar{c}_x = \text{constant} \qquad (60\,a)$$

$$\bar{c}_\Theta = \frac{K\,\bar{c}_x}{r}, \quad K = \text{constant} \qquad (60\,b)$$

$$\rho' = 0$$

Introduction of Eqs. (60) into Eqs. (58) and elimination of the pressure yields

$$\left(\frac{K}{r^2}\frac{\partial}{\partial \Theta} + \frac{\partial}{\partial x}\right)\xi = 0$$

$$\left(\frac{K}{r^2}\frac{\partial}{\partial \Theta} + \frac{\partial}{\partial x}\right)\eta = -\frac{2\,K\,\xi}{r^2} \qquad (61)$$

$$\left(\frac{K}{r^2}\frac{\partial}{\partial \Theta} + \frac{\partial}{\partial x}\right)\zeta = 0$$

where ξ, η, ζ are the radial, tangential and axial vorticities, respectively, (Ref.(16)). The equation of continuity rewritten in terms of vorticity becomes

$$\frac{1}{r}\frac{\partial}{\partial r}(r\,\xi) + \frac{1}{r}\frac{\partial \eta}{\partial \Theta} + \frac{\partial \zeta}{\partial z} = 0 \qquad (62)$$

Eqs. (61), (62) were utilized by Dunham to determine closed form expressions for the velocity (and pressure) perturbations, satisfying the condition of zero radial flow at the inner and outer casing.

An isolated blade row is now considered with the upstream flow field extending to minus infinity and the downstream flow field to plus infinity. The upstream and downstream solutions of the perturbed flow have to be matched at the disc. Four independent matching conditions have to be satisfied:

(1) continuity of axial velocity
(2) continuity of radial velocity
(3) specified flow leaving angle
(4) specified total pressure change

These conditions, together with the requirement that the perturbations remain finite far upstream and far downstream of the blade row, allow (for a, say, specified inlet total pressure distortion) the harmonic coefficients for the flow fields upstream and downstream of the blade row to be determined. Once these are known, the velocity and pressure perturbations can be calculated.

A numerical example using the above analysis is presented by Dunham in Ref. (17). A free vortex stator blade row is installed in a cylindrical duct. Upstream of the blade row a steady total pressure distortion is assumed to extend in the outer half of the annulus 90° around the circumference. The ideal square wave shape of the distortion, as well as the representation by Fourier-Bessel harmonics which serves as an input for the analysis, are shown in Fig. 25 a. The three-dimensional analysis is used to determine the axial velocity perturbation induced at the blade row. The analytical results are shown in Fig. 25 b. A comparison of the theory with experimental data may be found in Ref. (16).

5.3 AXIAL MEAN FLOW (COMPRESSIBLE)

Callahan and Stenning (25) restricted the three-dimensional small perturbation analysis to the prediction of the distorted flow fields upstream and downstream of the compressor. In these flow fields, the mean flow is (normally) axial, so that $\bar{c}_x$ = constant and $\bar{c}_\Theta = 0$. (Introduction of $\bar{c}_x$ = const and $\bar{c}_\Theta = 0$ into Eqs. (58) indicates the simplification of the analysis due to the assumption of axial mean flow.) Since, from Eq. (60 b), $\bar{c}_\Theta = 0$ is equivalent to $K = 0$, it

follows from Eqs. (61) that the perturbation velocity fields upstream and downstream of the compressor are irrotational. A perturbation velocity potential ϕ may therefore be defined. The continuity equation, in which the velocity perturbations are now replaced in terms of the velocity potential, together with an appropriate substitution of the perturbation density change, $\partial\rho'/\partial x$, yields the Laplace equation for the determination of ϕ as function of Θ, r and $x_c = x/\sqrt{1 - \bar{M}a^2}$, where $\bar{M}a$ is the local Mach number. From the Laplace equation, solutions describing the perturbed flow upstream and downstream of the compressor can be determined. These solutions have to be matched at the compressor, which is replaced by a single actuator disc.

Two cases were considered by Callahan and Stenning. In the first case, the compressor was assumed to be short enough to preserve the radial velocities. The boundary conditions are therefore comparable with those at a single blade row, Section 5.2. In the second case, the compressor was considered sufficiently long to reduce the radial velocities to zero. When the tangential velocities are also zero due to a high solidity last stator blade row, the exit static pressure is constant.

The condition of constant static pressure at the exit of a "long" compressor was utilized by Callahan and Stenning to determine the harmonic coefficients for the perturbed flow upstream of the compressor in terms of the slope of the compressor characteristic (expressed as static pressure rise vs. axial velocity) and the amplitude of a given sinusoidal axial velocity distortion far upstream. Once the harmonic coefficients were known, velocity and pressure perturbations could be calculated in the entire upstream flow field.

Experiments by Callahan (26) on a single-stage compressor showed that for a distortion introduced far upstream, the compressor exit static pressure was almost constant. Consequently, the "long compressor hypothesis" was adopted for the analysis.

Figs. 26a, b compare the analytical and experimental axial velocity perturbations determined at the tip and hub just ahead of the compressor for a specified cosine-wave axial velocity distortion far upstream of the compressor. Fig. 26c shows the decrease of the axial velocity perturbation amplitude at the tip and hub as the flow approaches the compressor. The corresponding measured and predicted tangential velocity perturbations at the hub and tip just ahead of the compressor are presented in Fig. 26 d. A good agreement between experiment and theory is shown in all results.

6. TWO-DIMENSIONAL NON-LINEAR ACTUATOR DISC MODEL

6.1 GENERAL REMARKS

For the linear models reviewed in the previous sections, the assumptions were small perturbations and quasi-steady rotor response. Extensions to include an unsteady response were limited to unstalled unsteady effects. In the case that the inlet-distorted compressor operates near its undistorted stalling point, unsteady stalling effects with large distortion amplitudes contradict the above assumptions, even if the external upstream distortions are not severe.

A non-linear model which accounts for large disturbances and unsteady stalling effects is presented by Adamczyk and Carta in Ref. (27). The flow fields upstream and downstream of a blade row are described by the time-dependent, two-dimensional, inviscid and incompressible flow equations. The numerically obtained solutions are matched at the blade row, using matching conditions obtained from an unsteady blade passage analysis.

6.2 UNSTEADY BLADE ROW ANALYSIS

Application of the continuity equation to the two-dimensional incompressible flow through a blade passage revealed that the axial velocities averaged across the passage are constant. Under the assumption that the blade pitch is small compared with the circumferential extent of the distortion, gap-averaged quantities can be replaced by local quantities. Hence

$$(c_{x_1})_{av} = (c_{x_2})_{av} = c_x \tag{63}$$

Adamczyk and Carta further applied the unsteady energy equation to the flow in the passage, obtaining the following expression for the difference in total pressure across the blade row

$$\Delta P = -\frac{1}{2}\rho c_1^2 \chi - \rho l_{ax} \Xi_m \frac{\partial c_x}{\partial t} \tag{64}$$

where

χ = unsteady loss parameter defined by

$$\frac{l_{ax}\, a_T}{\bar{c}_x}\frac{\partial \chi}{\partial t} + \chi = \chi_{SS} \tag{65}$$

$$\chi_{SS} = \frac{P_1 - P_2}{\frac{1}{2}\rho c_1^2} = f(\alpha_1); \quad \text{steady-state total pressure loss coefficient depending on inlet angle} \tag{66}$$

l_{ax} = axial length of cascade

a_T = dimensionless time constant derived experimentally

Ξ_m = constant determined from cascade geometry

For testing the validity of the unsteady blade row analysis, a modified form of Eq. (64) was used by Adamczyk and Carta to predict the circumferential variation in static pressure just downstream of both rotor and stator for a specified upstream variation. Agreement between experiment and unsteady theory was considerably better than that for prediction results assuming a quasi-steady cascade response.

6.3 FLOW FIELD ANALYSIS

The flow upstream and downstream of a blade row is described by the flow equations

$$r\frac{\partial c_x}{\partial t} + c_x\frac{\partial c_x}{\partial x} + c_\Theta\frac{\partial c_x}{\partial \Theta} = -\frac{1}{\rho}\frac{\partial p}{\partial x} \tag{67a}$$

$$r\frac{\partial c_\Theta}{\partial t} + c_x\frac{\partial c_\Theta}{\partial x} + c_\Theta\frac{\partial c_\Theta}{\partial \Theta} = -\frac{1}{\rho}\frac{\partial p}{\partial \Theta} \tag{67 b}$$

$$\frac{\partial c_x}{\partial x} + \frac{\partial c_\Theta}{\partial \Theta} = 0 \tag{68}$$

(The axial coordinate in these equations is normalized by the radius). Eq. (68) shows that a stream function may be defined such that

$$c_x = \frac{\partial \psi}{\partial \Theta} \tag{69 a}$$

$$c_\Theta = -\frac{\partial \psi}{\partial x} \tag{69 b}$$

Introduction of Eqs. (69) into the expression for the radial vorticity

$$\xi = \frac{\partial c_\Theta}{\partial x} - \frac{\partial c_x}{\partial \Theta} \tag{70}$$

yields

$$\frac{\partial^2 \psi}{\partial x^2} + \frac{\partial^2 \psi}{\partial \Theta^2} = -\xi \tag{71}$$

By eliminating the pressure from Eqs. (67) and introducing Eqs. (69), (70) it is found that

$$r\frac{\partial \xi}{\partial t} + \frac{\partial \psi}{\partial \Theta}\frac{\partial \xi}{\partial x} - \frac{\partial \psi}{\partial x}\frac{\partial \xi}{\partial \Theta} = 0 \tag{72}$$

A numerical method is required for a simultaneous solution of Eqs. (71), (72). Adamczyk and Carta used a standard center differencing scheme for solving Eq. (71) and Arkawa's (28) vorticity conservation algorithm and the Crank-Nicholson scheme for solving Eq. (72). The solution has to satisfy the boundary conditions specified below.

6.4 BOUNDARY CONDITIONS

Consider a blade row located at plane EB in a flow field ADFC as shown in Fig. 27. Inlet plane AD and exit plane CF are chosen sufficiently far upstream and downstream, respectively, to be unaffected by the blade row.

A circumferential variation in axial velocity may be specified at the inlet plane AD. Eq. (69a) then yields the stream function

$$\psi(x, \Theta, t) = g\ (\Theta, t) \text{ for } x \text{ at plane AD} \tag{73}$$

Since, at plane AD, the stream function is independent of x, the vorticity along AD is found from EQ. (71) as

$$\xi(x, \Theta, t) = -\frac{\partial^2 \psi(x, \Theta, t)}{\partial \Theta^2} \qquad x \text{ at plane AD} \tag{74}$$

The flow at $\Theta = 0$ is identical to that at $\Theta = 2\pi$. The condition for this periodicity in terms of stream function and vorticity is

$$\psi(x, 2\pi, t) = \psi(x, 0, t) + 2\pi \bar{c}_x \tag{75}$$

$$\xi(x, 2\pi, t) = \xi(x, 0, t) \tag{76}$$

From Eq. (63) it follows that there is no change in the stream function across the actuator disc. The change in vorticity is given below. Eq. (67 b) can be expressed in terms of total pressure by

$$\frac{\partial}{\partial \Theta}\left(\frac{P}{\rho}\right) = -r\frac{\partial c_\Theta}{\partial t} - c_x\xi \tag{77}$$

This equation applied just behind and just ahead of the blade row yields for the difference in total pressure

$$\frac{\partial}{\partial \Theta}\left(\frac{\Delta P}{\rho}\right) = -\frac{r\,\partial c_{\Theta 2}}{\partial t} + \frac{r\,\partial c_{\Theta 1}}{\partial t} + c_x(\xi_1 - \xi_2) \tag{78}$$

By taking the derivative of Eq. (64) w.r.t. Θ and combining the result with Eq. (78), it is found after introduction of

$$c_{\Theta 2} = c_x \tan a_2(a_1) \tag{79}$$

that the change in vorticity across the blade row is

$$r\frac{\partial c_{\Theta 1}}{\partial t} - \frac{r\partial}{\partial t}(c_x \tan a_2) = -\frac{1}{2}\frac{\partial}{\partial \Theta}(c_1^2 x) - I_{ax}\,\Xi_m\frac{\partial^2 c_x}{\partial \Theta\,\partial t} - c_x(\xi_1 - \xi_2) \tag{80}$$

In this equation, $a_2 = f(a_1)$ is the steady-state relationship between blade row outlet and inlet angle.

A condition for the vorticity at the blade row exit can be found by introducing Eq. (79) into Eq. (70):

$$\xi_2 = \frac{\partial}{\partial x}(c_x \tan a_2) - \frac{\partial c_x}{\partial \Theta} \tag{81}$$

(It should be noted that the above blade row matching conditions are derived for a stator. For a rotor, the change in total pressure from the relative to the absolute system has to be accounted for.)

At the exit plane of the flow field, CF, the boundary condition of constant static pressure has to be satisfied. From Eq. (67 b), this condition is given by

$$r\frac{\partial c_\Theta}{\partial t} + c_x \frac{\partial c_\Theta}{\partial x} + c_\Theta \frac{\partial c_\Theta}{\partial \Theta} = 0 \qquad x \text{ at plane CF} \tag{82}$$

6.5 NUMERICAL EXAMPLES

In a first numerical example, Adamczyk and Carta determined the condition for the onset of rotating stall in an isolated rotor operating in undistorted flow. This was achieved by a momentary introduction of an axial velocity cosine-wave distortion 1/2 circumference upstream of the blade row. The limit between growth and decay of the disturbance was found to be at an inlet angle of 35° (measured against the circumference). This was regarded as the critical angle at which rotating stall would develop.

In a further example, the effect of a 30 percent steady axial velocity cosine wave distortion on the performance of the rotor was investigated at an inlet angle of 42 degrees. Fig. 28 a shows the specified upstream distortion together with the (attenuated and circumferentially displaced) disturbance predicted at the rotor inlet at a non-dimensional time $t^* = 2.94$. (Note that a time interval of $t^* = 1$ corresponds to one rotor revolution.) No change in the profile at rotor inlet was found for other values of t^*, indicating stability of the flow.

Reduction of the inlet angle to 40° resulted in flow instability as evident from the different velocity disturbances predicted at three different times (Fig. 28 b). Further reduction of inlet angle to 38° increased the unsteadiness, as shown in Fig. 28 c.

It was found by Adamczyk and Carta that the axial velocity profiles predicted for rotor inlet angles of $\beta_1 = 38°$ and 40° re-occured periodically after time intervalls of approximately $\Delta t^* = 2$. This result indicates that the observed velocity profiles at rotor inlet are generated by the superposition of the forced external distortion and a self-induced rotating disturbance.

A comparison between the undistorted and distorted case shows that the critical inlet angle at which rotating stall develops increases from 35° without a distortion to about 41° with a distortion. This capability of the non-linear model to predict the reduction in stable operating range due to distorted inflow is a major improvement compared with the linear model, which is only capable of predicting incipient rotating stall in undistorted flow.

The non-linear model is not only capable of predicting the reduction in stable operating range, it also predicts the reduction in performance. Contrary to the linear model, which calculates only pressure perturbations, the non-linear model determines the perturbed pressure so that circumferential averages upstream and downstream of, say, a rotor may be calculated. The reduction in total pressure rise across the rotor due to inlet maldistribution is therefore predictable.

7. ONE-DIMENSIONAL LUMPED VOLUME MODEL

7.1 GENERAL REMARKS

The non-linear, incompressible analysis reviewed in the previous section was shown to be capable of predicting (for both clean and distorted inflow) a flow instability in blade rows known as rotating stall.

In this section, a model will be discussed which allows (for undistorted flow and for flow with a time-variant total pressure and/or temperature inlet distortion) the prediction of a system instability known as surge or compressor stall. The model assumes one-dimensional compressible flow, thus only spatially uniform flows are included (for an extension see Section 7.5). The stages (or stage groups) of the compressor are replaced by actuator discs followed by lumped volumes equal to the stage (or stage group) volume. Conservation laws of mass, momentum and energy are applied separately or in combination to the lumped volumes, accounting thus for the dynamic behaviour of the system. The required pressure and temperature increase across the actuator discs is normally obtained from steady-state stage characteristics presented in the form of pressure and temperature rise coefficients against flow coefficient. The upper frequency limit of inflow oscillations for which the assumption of quasi-steady stage characteristics is still justified is given in Ref. (34) for unstalled flow. Deviations from the steady-state characteristic due to unsteady stalling effects are considered in Ref. (40) as discussed in Section 7.4. The volume and nozzle downstream of the compressor are also included in the model. Choked flow is normally assumed for the nozzle, so that a simple relationship exists between nozzle inlet pressure, temperature and mass flow. The nature of the mathematics involved favours an analog simulation to a digital simulation.

The model is generally applied to predict

(a) system instability (compressor stall) for undistorted inflow
(b) compressor discharge conditions for inflow osciallations or pulses in pressure and/or temperature (compressor response characteristics)
(c) system instability for time-variant inflow

Different types of models will be reviewed below. The names of the models are derived from the conservation laws applied to the lumped volumes.

7.2 CONTINUITY MODEL

Gabriel, Wallner, and Lubick (30), (31) have used the continuity model to predict the dynamic response of a 15-stage axial compressor to inflow pressure transients. For this, the stages of the compressor were grouped into four parts for which steady-state group characteristics were available. The equation of continuity was applied to the four grouped stage volumes.

Fig. 29 shows the experimentally determined compressor discharge pressure during sinusoidal inlet pressure oscillations. At low frequency, little change in amplitude and phase between inlet and exit can be observed. At high frequencies,

the outlet pressure no longer follows the inlet pressure. Compressor pressure amplitude ratios and phase shifts measured for various frequencies are presented in Fig. 30 together with predictions with the continuity model.

The model was further used to predict surge for the compressor operating with sinusoidally varying inlet pressures of various amplitudes and frequencies. Surge in this analysis was assumed to occur when one of the calculated instantaneous stage group pressure ratios reached the corresponding steady-state stall pressure ratio. A comparison between experimental and predicted stall limits is shown in Fig. 31.

A detailed description of the continuity model analog simulation technique may be found in Ref. (32), (33).

7.3 CONTINUITY - MOMENTUM MODEL

Kuhlberg, Sheppard, King and Baker (35) replaced individual stages rather than stage groups by actuator discs and lumped volumes. They also noted that, for many stable operating conditions of the compressor, certain compressor stages operate stalled, i.e., they operate on the positively sloped branch of their characteristic. A model simulation therefore has to include this effect. Since in the basic continuity model the stage characteristic is entered with the pressure rise coefficient, two values for the flow coefficient are found from the two branches of the characteristic. This difficulty has been overcome in Ref. (35) by applying the momentum equation (in addition to the continuity equation) to the lumped volumes of the stages.

The continuity-momentum model was used in Ref. (35) to predict speed and surge lines of a seven-stage compressor with undistorted inflow, Fig. 32. For the speed line prediction, no dynamics are involved and the simulation becomes a stage stacking procedure, Ref. (36). The good accuracy of the speed line prediction is an indication for the quality of the stage characteristics employed. The situation is different for the surge line prediction, where surge is indicated by an instability in the dynamic simulation. (The important difference may be noted between the conclusion that surge is an instability phenomenon and the assumption made in Ref. (31) that surge occurs if one stage or a group of stages operates stalled.)

The continuity-momentum model was further used in Ref. (35) to predict the ratio of exit to inlet pressure amplitudes in a fan with sinusoidally oscillating inlet pressure. Results are shown in Fig. 33.

Stall limit predictions for a five-stage compressor with sinusoidal inflow pressure oscillations of different amplitude and frequency are predicted in Fig. 34. The figure shows the marked sensitivity of the compressor to frequencies of about 500 cps. Compressor stall limits were also predicted for square-wave inlet pressure pulses of variable amplitude and duration. As shown, stall risk increases with increasing pulse amplitude and duration, Fig. 35.

7.4 CONTINUITY- MOMENTUM - ENERGY MODEL

For this model, the energy equation (in addition to the continuity and momentum equations) is applied to the lumped stage volumes.

Model predictions of surge for an eight-stage compressor with undistorted inflow using steady-state stage characteristics have been performed by Willoh and Seldner in Ref. (37). Two different cases were considered. In the first, grouped stage volumes were employed for the simulation, but no satisfactory result was obtained. A remarkable improvement in the prediction was achieved by employing an individual stage volume representation, Fig. 36. It was also noted in Ref. (37) that the stability limit in the simulation is strongly influenced by the stage characteristics. The quality of the surge line prediction is therefore very dependent on the accuracy of the stage characteristics employed. (The accuracy of the different model types in predicting the clean surge line is investigated in Ref. (38) and a summary of the results is given in Ref. (39).)

The continuity-momentum-energy model was used in Ref. (40) to determine the effect of pressure and/or temperature transients on the performance of axial flow compressors. Here, however, the steady-state stage characteristics are extended to include unsteady stalling effects. The method is outlined with the aid of Fig. 37. The unstalled branch of the stage characteristic was determined in Ref. (40) from a separate calculation procedure, since experimental data from isolated stages are unreliable due to interference and distortion effects in the actual multi-stage compressor. The pressure ratio $(P_2/P_1)_A$ at which rotating stall is initiated in steady flow, was determined from a small perturbation analysis. The assumption was then made in Ref. (40) that due to rotating stall, the pressure ratio drops from $(P_2/P_1)_A$ to $(P_2/P_1)_B$, $(P_2/P_1)_B$ being 80 % of $(P_2/P_1)_A$. By introducing a rotating stall "growth-decay" rate, a hysteresis loop in stage pressure ratio is predicted during a rapid decrease and increase in corrected airflow.

The model was used in Ref. (40) to determine the effect of square-wave pressure pulses of different amplitude and duration on the reduction in stable compressor operating range. Occurrence of reversing flow anywhere in the compressor was adopted as the criterion for surge. The three nominal operating points at which upstream pressure pulses were introduced are shown on the overall compressor performance map (Fig. 38). Prediction results of the stable operating limits are presented in Fig. 39. As might be expected, sensitivity to pulses grows rapidly as the nominal operating point approaches the steady-state compressor surge point.

7.5 PARALLEL LUMPED VOLUME MODEL

Extensions of the lumped-volume model are presented in the literature to include the important practical case of time-variant distortions extending only over a certain section of the compressor inlet. Parallel operation of three continuity models is considered in Ref. (32), (33). The three lumped volumes which replace each stage are circumferentially interconnected. The effect of tangential flow on the pressure rise across a stage is accounted for by an appropriate shift of the steady-state characteristic curve to higher or lower mass flows.

Parallel operation of two continuity-momentum-energy models is considered in Ref. (40). The effect of a rotating stall cell that grows or decays as it moves from one sector into the neighbouring one is included in the model by an appropriate computation of the required stage characteristic.

8. REFERENCES

(1) Mokelke, H. — Circumferential inlet flow distortions in multi-stage axial compressors
Dissertation submitted for the Ph.D degree to the University of Cambridge, (1974)

(2) Mokelke, H. — The development of inlet flow distortions in multi-stage axial compressors of high hub-tip ratio
ICAS Paper 72-20, (1972)

(3) Roberts, F., Plourde, G.A. and Smakula, F. — Insights into axial compressor response to distortion
AIAA Paper No. 68-565, (1968)

(4) Mokelke, H. — The unsteady response of an axial flow compressor with a distorted inlet flow
A.R.C. C.P. No. 1203, (1972)

(5) Mokelke, H. — Dynamic stall detection and design aids for distortion tolerant compressors using quasi-steady actuator disc analysis
Paper presented at the Project SQUID/AFOSR/UARL Workshop on Unsteady Flows in Jet Engines, held at UARL, July (1974)

(6) Braithwaite, W.M., Graber, E.J., Mehalic, C.M. — The effect of inlet temperature and pressure distortion on turbojet performance
AIAA Paper No. 73-1316, (1973)

(7) Reid, C. — The response of axial flow compressors to intake flow distortion
ASME Paper 69-GT-29, (1969)

(8) Calogeras, J.E. Mehalic, C.M. and Burstadt, P.L. — Experimental investigation of the effect of screen-induced total-pressure distortion on turbojet stall margin
NASA TMX-2239, (1971)

(9) Kom, J.A. — The effect of inlet distortion on the performance and stability of the low-speed spool of a turbofan engine
AIAA Paper No. 74-233, (1974)

(10) Melick, H.C. and Simpkin, W.E. — A unified theory of inlet/engine compatibility
AIAA Paper No. 72-1115

(11) Melick, H.C. — Analysis of inlet flow distortion and turbulence effects on compressor stability
NASA CR 114577, (1973)

(12) Plourde, G.A. and Stenning, A.H. — The attenuation of circumferential inlet distortion in multi-stage axial compressors
AIAA Paper No. 67-415

(13) Ehrich, F. — Circumferential inlet distortions in axial flow turbomachinery
J. Aero.Sci. Vol. 24, No. 6, June (1957)

(14) Rannie W.D. and Marble, F.E. — Unsteady flows in axial turbomachines
C.R. des Journées Internationales de Sciences Aérnoautique, O.N.E.R.A. (1957)

(15) Katz, R. — Performance of axial compressors with asymmetric inlet flows
Ph. D. thesis, Daniel and Florence Guggenheim Jet Propulsion Center, California Institute of Technology, Pasadena, California (1958)

(16) Dunham, J. — Non-axisymmetric flows in axial compressors
Mechanical Engineering Science Monograph No. 3, (1965)

(17) Dunham, J. — Non-axisymmetric flows in axial compressors
Ph.D. thesis, Cambridge University, (1962)

(18) Krzywoblocki, M.Z.v. — Compressibility effects in circumferential inlet distortion in axial compressors
Österr. Ing.-Archiv, Part I: Vol. 13, No. 4, p. 214 (1959)
Part II: Vol.14, No. 2, p. 79, (1960)

(19) Seidel, B.S. — Asymmetric inlet flow in axial turbomachines
Trans. of the ASME, J. of Eng. for Power, Vol. 86, No. 1, (1964)

(20) Sears, W.R. — Some aspects of nonstationary airfoil theory and its practical application
Journal of Aeronautical Sciences, Vol. 8, No. 3, (1941)

(21) Isaacs, R. — Airfoil theory for flows of variable velocity
Journal of Aeronautical Sciences, Vol. 12, No. 1, (1945)

(22) Horlock, J.H. — Fluctuating lift forces on aerofoils moving through transverse and chordwise gusts
ASME Paper 68-FE-28 , (1969)

(23) Carter, A.D.S. — The low speed performance of related aerofoils in cascade
N.G.T.E. Report No. R 55, (1949)

(24) Horlock, J.H. and Deverson, E.C. — An experiment to determine the position of an equivalent actuator disc replacing a blade row of a turbomachine
A.R.C. C.P. 426

(25)	Callahan, G.M. and Stenning, A.H.	Attenuation of inlet flow distortion upstream of axial flow compressors J. of Aircraft, Vol. 8, No. 4, April (1971)
(26)	Callahan, G.M.	Attenuation of inlet flow distortion upstream of axial flow compressors Ph.D. thesis, Lehigh University, (1968)
(27)	Adamczyk, J.J. and Carta, F.O.	Unsteady fluid dynamic response of an axial-flow compressor stage with distorted inflow Project SQUID Technical Report UARL-2-PU, (1973)
(28)	Arkawa, A.	Computational design for long-term numerical integration of the equations of fluid motion: Two-dimensional incompressible flow Part I: Journal of Computational Physics, Vol. I, (1966)
(29)	Richtmyer, R.D. and Morton, K.W.	Difference methods for initial-value problems Interscience Publishers, New York (1967)
(30)	Gabriel, D.S., Wallner, L.E. Lubick, R.J., Vasu, G.	Some effects of inlet pressure and temperature transients on turbojet engines Aeronautical Engineering Review, Vol. 16, Sept. (1957)
(31)	Lubick, R.J. and Wallner, L.E.	Stall prediction in gas-turbine engines Journal of Basic Engineering, Sept. (1959)
(32)	Kimzey, W.F.	The effects of unsteady, nonuniform flow on axial flow compressor stall characteristics University of Tennessee Master s Thesis, Knoxville, Tennessee, (1966)
(33)	Goethert, B.H. and Kimzey, W.F.	Effect of high frequency fluctuations of inlet flow on compressor stall Paper presented at the 32nd Meeting of the Propulsion and Energetics Panel of AGARD, Toulouse, September, (1968)
(34)	Goethert, B.H. and Reddy, R.C.	Unsteady aerodynamics of rotor blades of a compressor under distorted flow conditions AGARD, CP 71-71
(35)	Kuhlberg, J.F., Sheppard, D.E., King.E.O.	The dynamic simulation of turbine engine compressors AIAA Paper No. 69-486, June (1969)
(36)	Johnson, I.A. and Bullock, R.O.	Aerodynamic design of axial-flow compressors NASA SP-36 (1965)
(37)	Willoh, R.G. and Seldner, K.	Multi-stage compressor simulation applied to the prediction of axial flow instabilities NASA TMX-1880, (1969)
(38)	Elder, R.	Mathematical modelling of axial flow compressors University of Leicester Engineering Department, Report 72-6 (1972)
(39)	Williams, D.D. and Yost, J.O.	Some aspects of inlet/engine flow compatibility ICAS Paper No. 72-19, (1972)
(40)	Jansen, W., Swarden, M.C. and Carlson, A.W.	Compressor sensitivity to transient and distorted transient flows AIAA Paper No. 71-670, (1971)

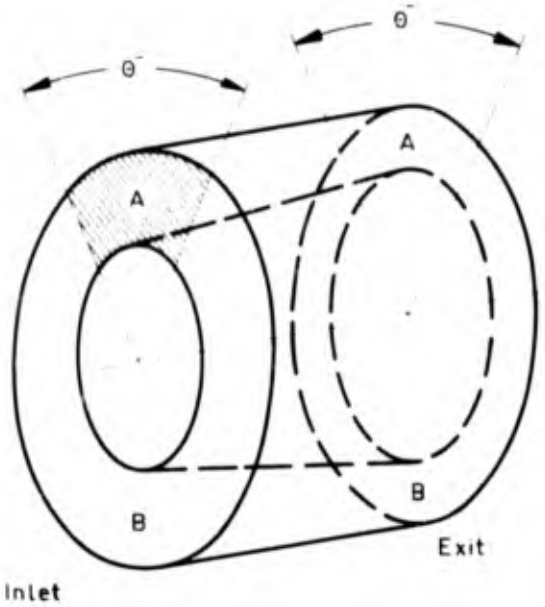

Sector A distorted
Sector B undistorted

FIG. 1 SCHEMATIC REPRESENTATION OF TWO-COMPRESSOR-IN-PARALLEL MODEL

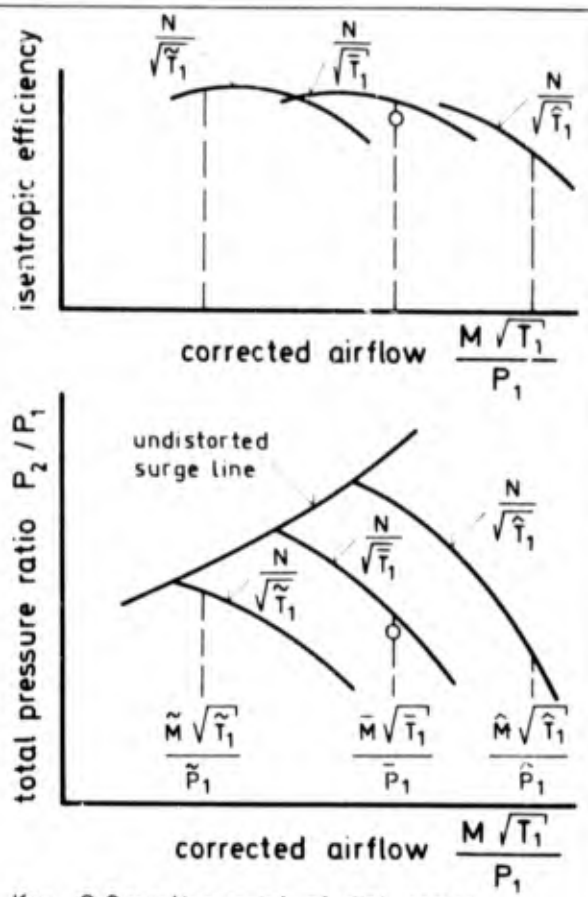

Key O Operating point of dist. compr.

FIG. 3 OPERATING POINTS OF PARALLEL COMPRESSORS ON UNDISTORTED OVERALL PERFORMANCE MAP (SCHEMATIC)

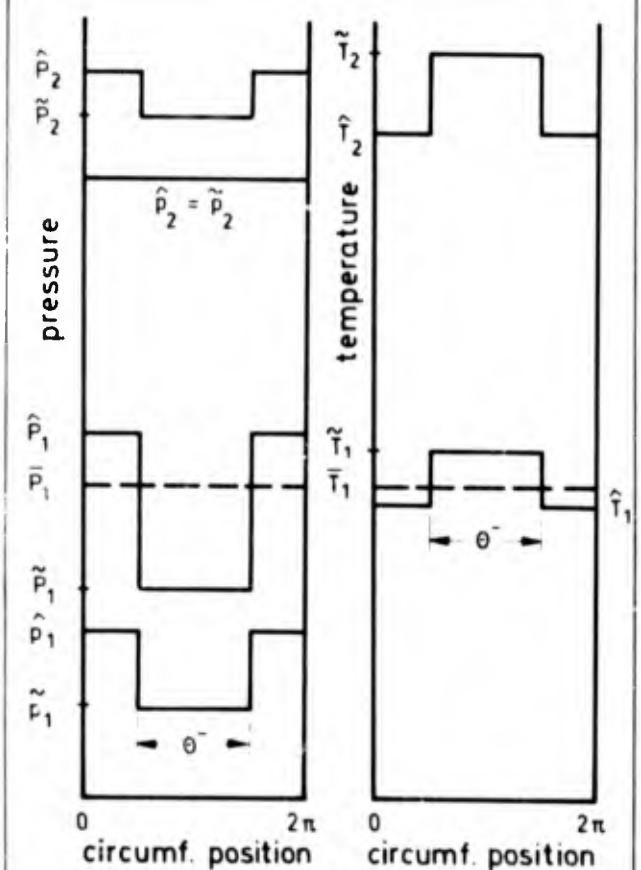

FIG. 2 CIRCUMFERENTIAL PRESSURE AND TEMPERATURE DISTRIBUTION AT COMPRESSOR EXIT FOR A SPECIFIED INLET DISTRIBUTION (SCHEMATIC)

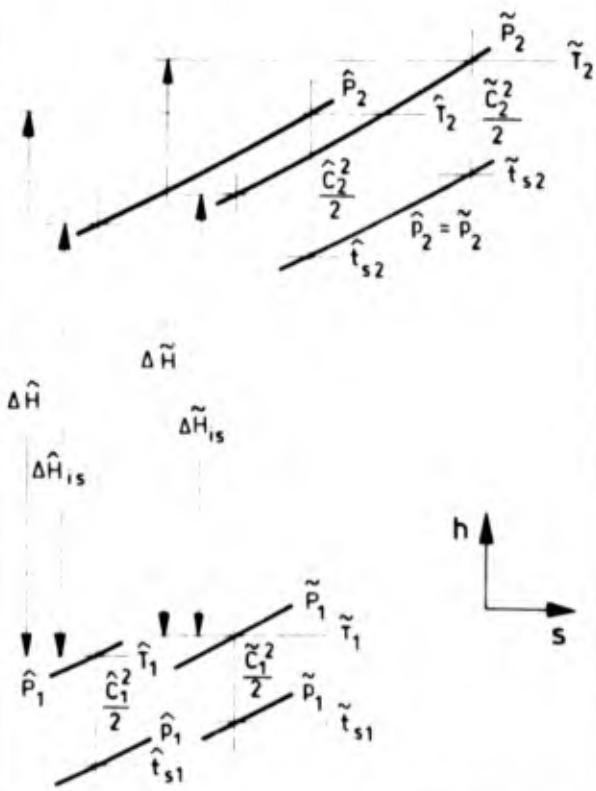

FIG. 4 PARALLEL COMPRESSOR OPERATION IN THE ENTHALPY-ENTROPY DIAGRAM (SCHEMATIC)

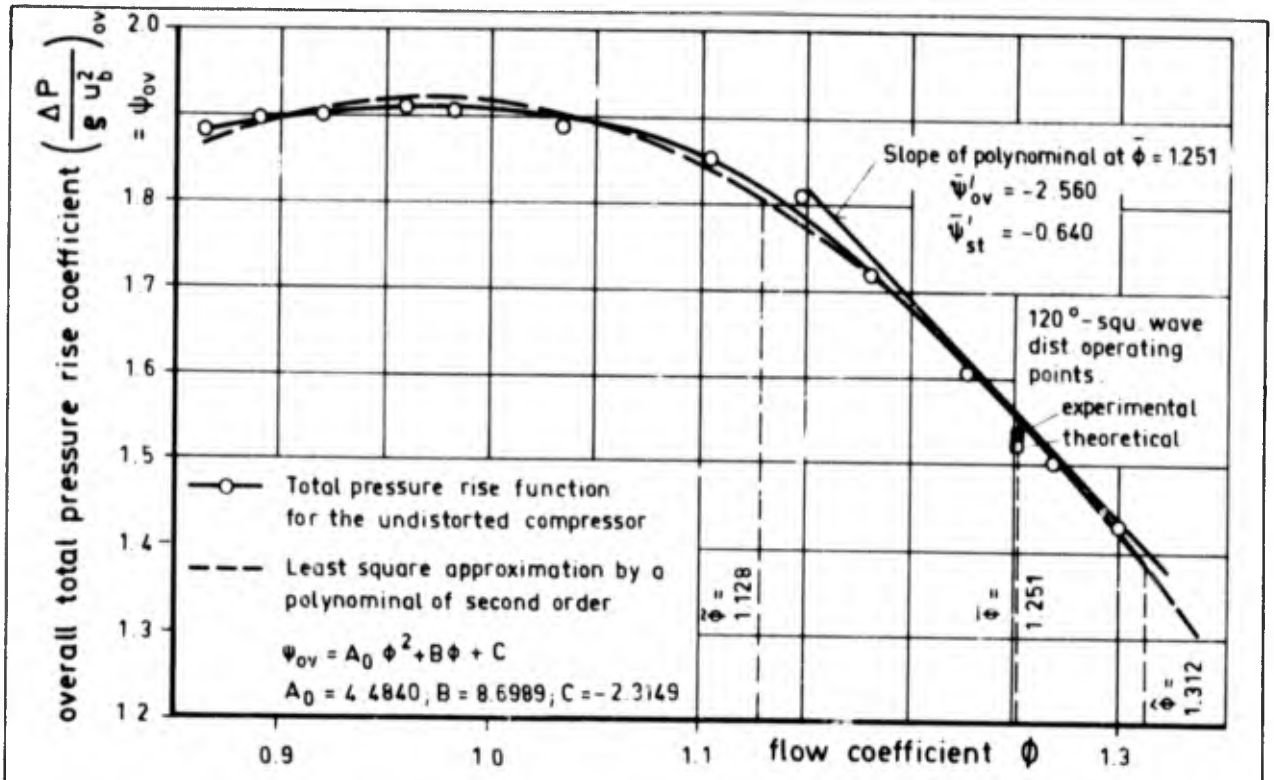

FIG. 5 PREDICTION OF 120°-SQUARE WAVE DISTORTION ATTENUATION - PARALLEL COMPRESSOR OPERATION ON UNDISTORTED TOTAL PRESSURE RISE CHARACTERISTIC

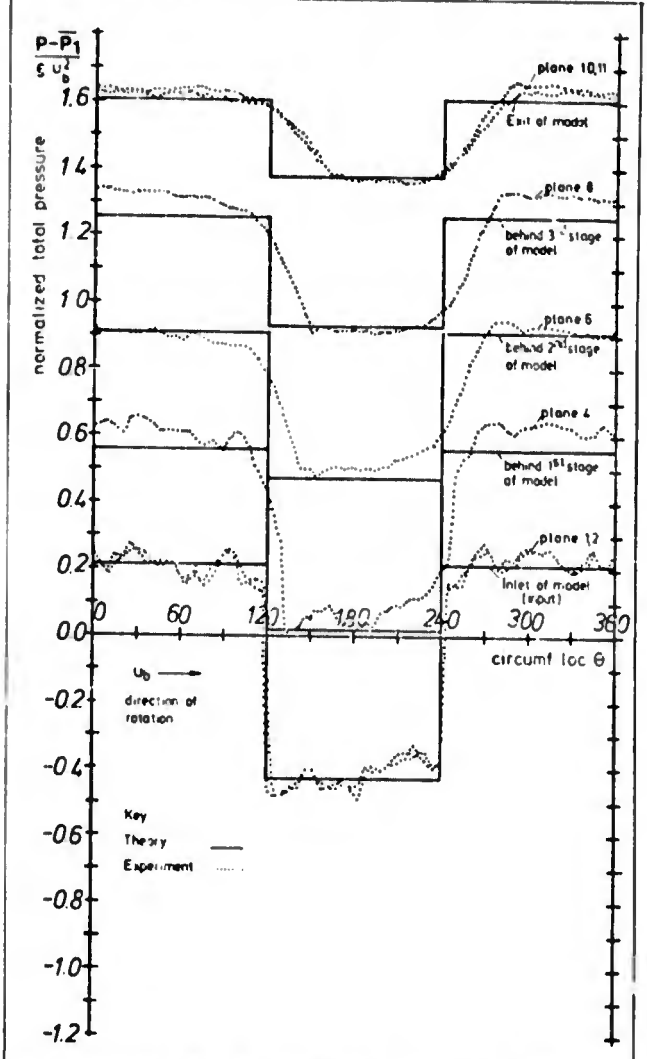

FIG. 6a MEASURED AND THEORETICAL TOTAL PRESSURE PROFILES OF 120°-DISTORTION PREDICTION WITH TWO-COMPR.-IN-PARALLEL MODEL

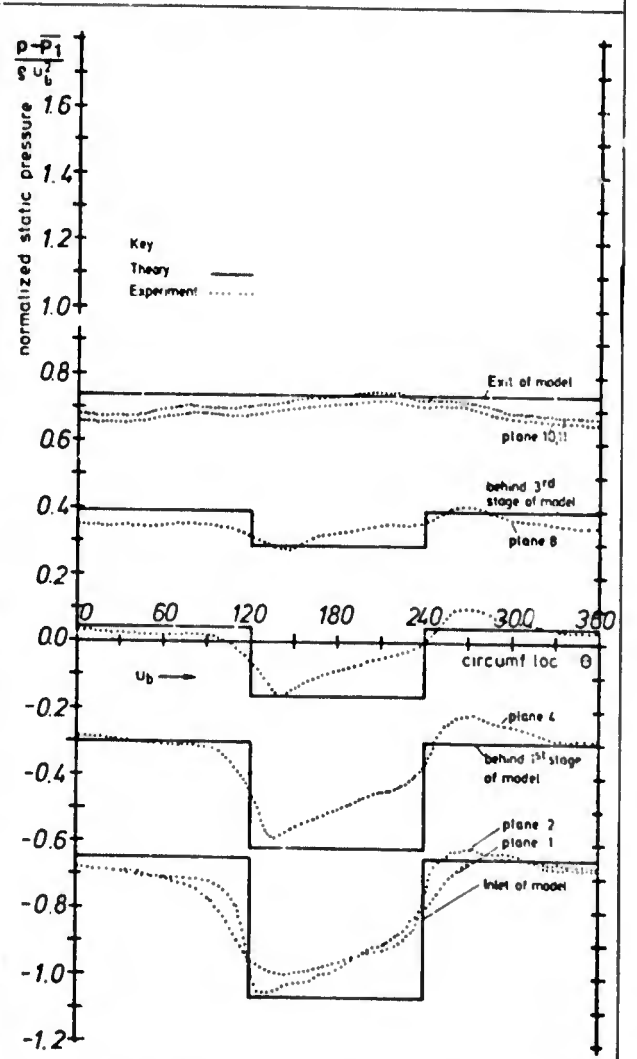

FIG. 6b MEASURED AND THEORETICAL STATIC PRESSURE PROFILES OF 120°-DISTORTION PREDICTION WITH TWO-COMPR.-IN-PARALLEL MODEL

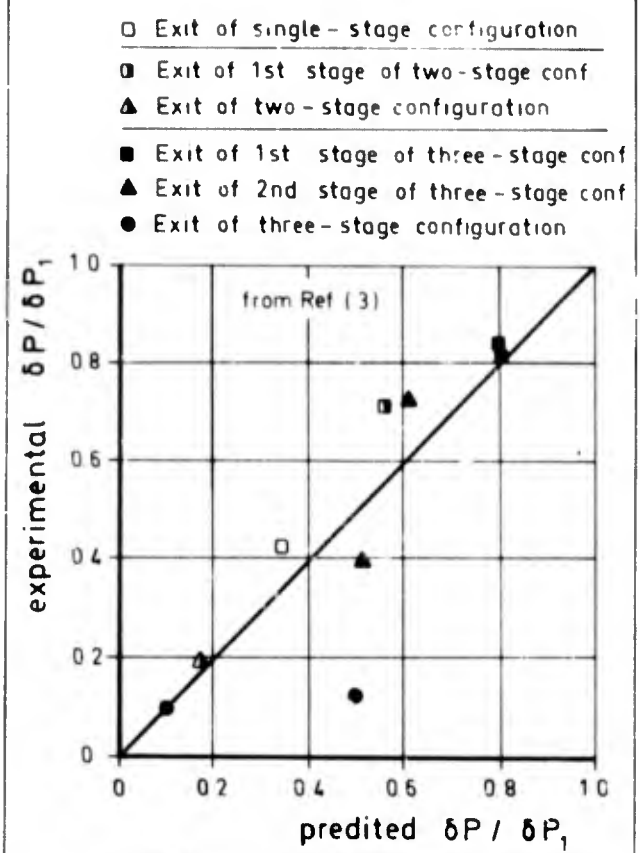

FIG. 7 COMPARISON OF MEASURED AND PREDICTED ATTENUATION RATE FOR 180°-TOTAL PRESSURE INLET DISTORTION

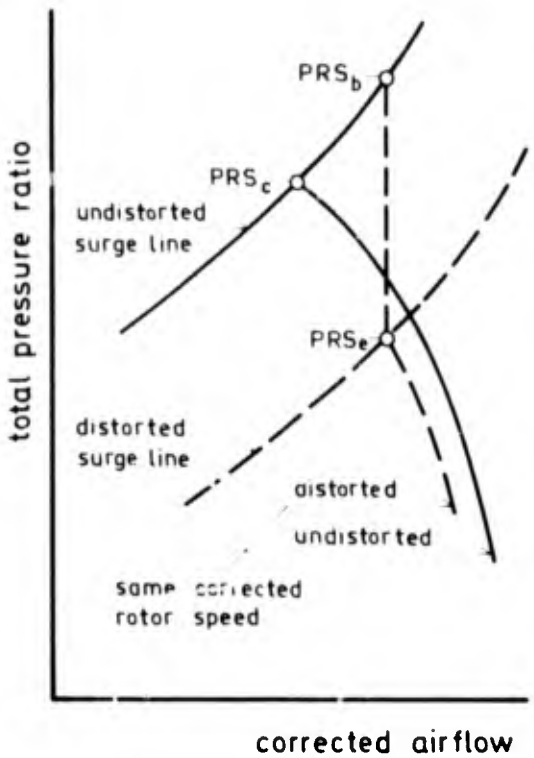

FIG. 9 LOSS IN STALL PRESSURE RATIO

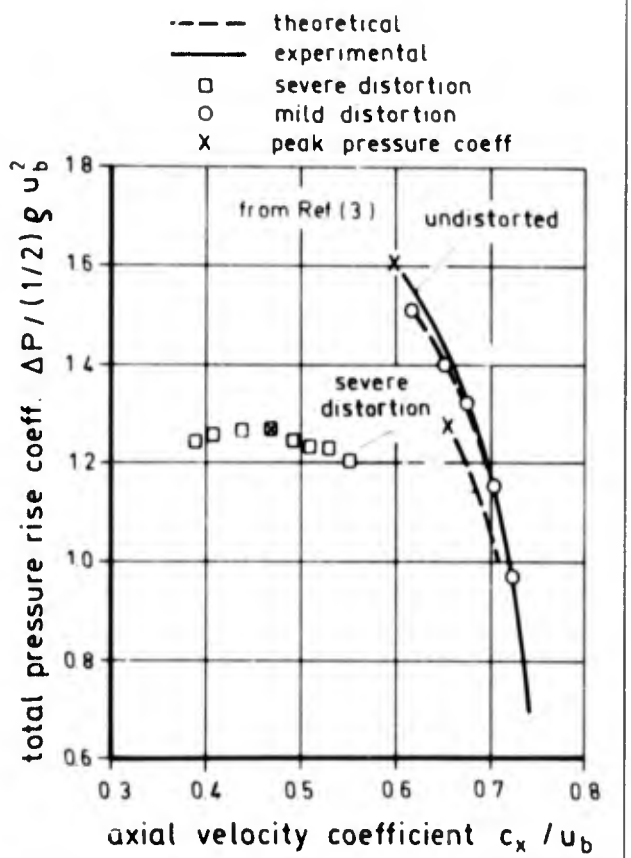

FIG. 8 MEASURED AND PREDICTED LOSS IN PERFORMANCE DUE TO MILD AND SEVERE 180°-TOTAL PRESSURE INLET DISTORTION

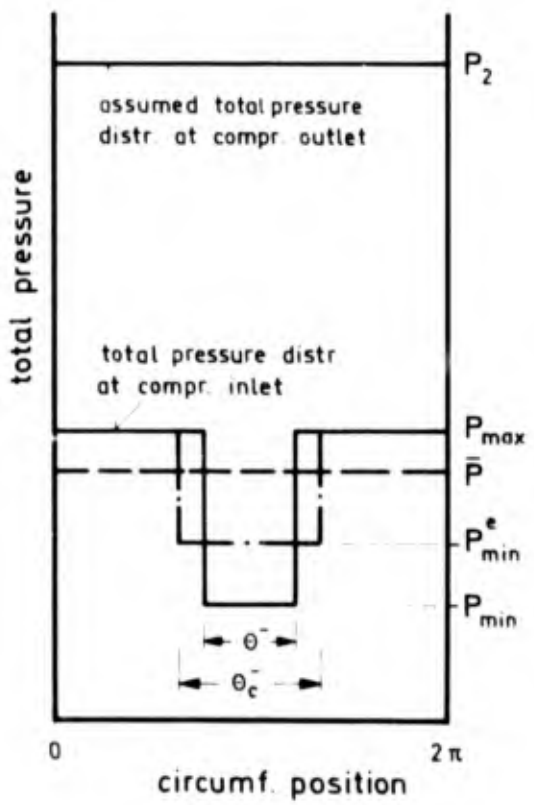

FIG. 10 DISTRIBUTION OF TOTAL PRESSURES AT COMPRESSOR INLET AND OUTLET WITH EFFECTIVE MINIMUM TOTAL PRESSURE

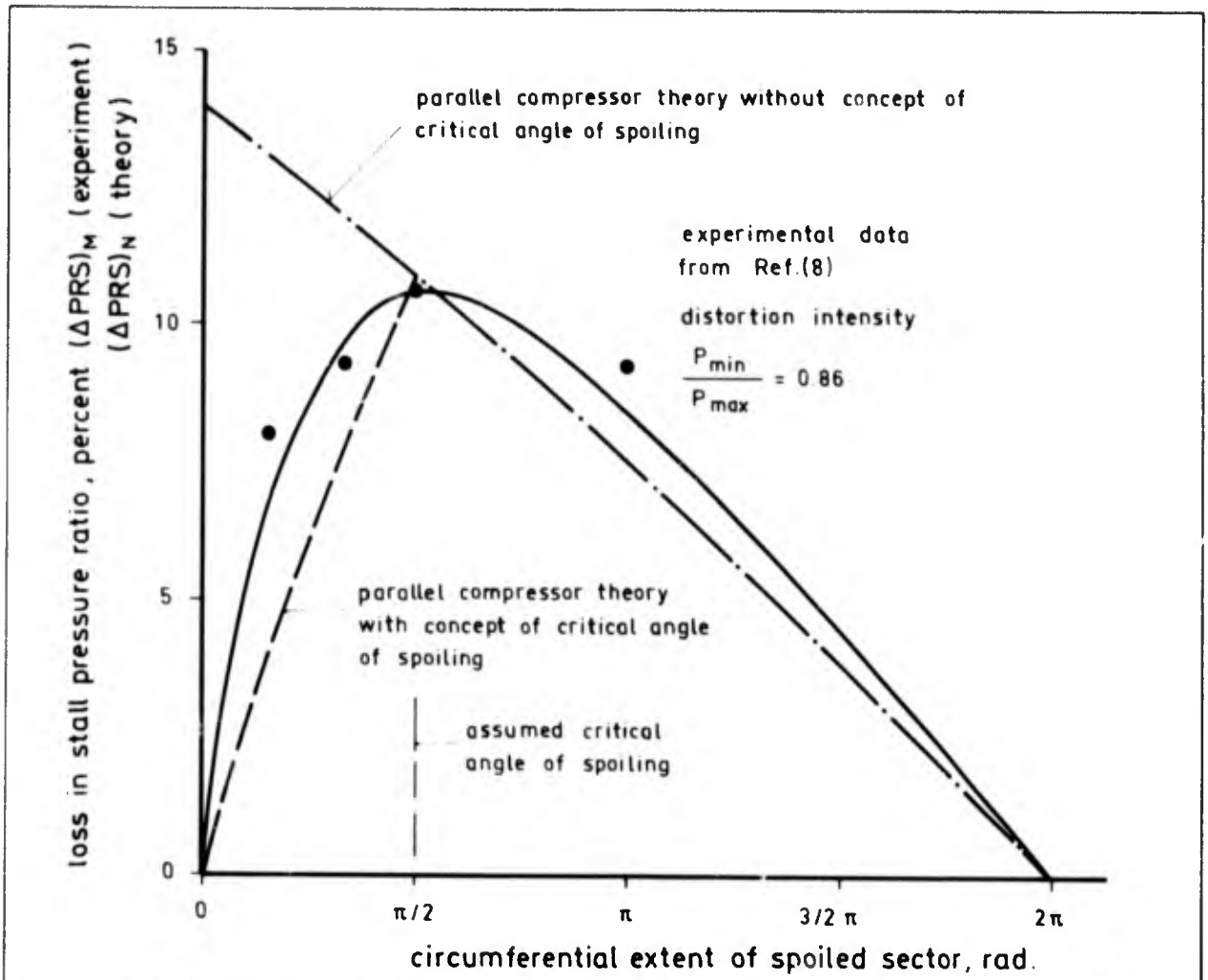

FIG. 11 EXPERIMENTAL AND THEORETICAL LOSS IN STALL PRESSURE RATIO AS A FUNCTION OF DISTORTION ANGLE

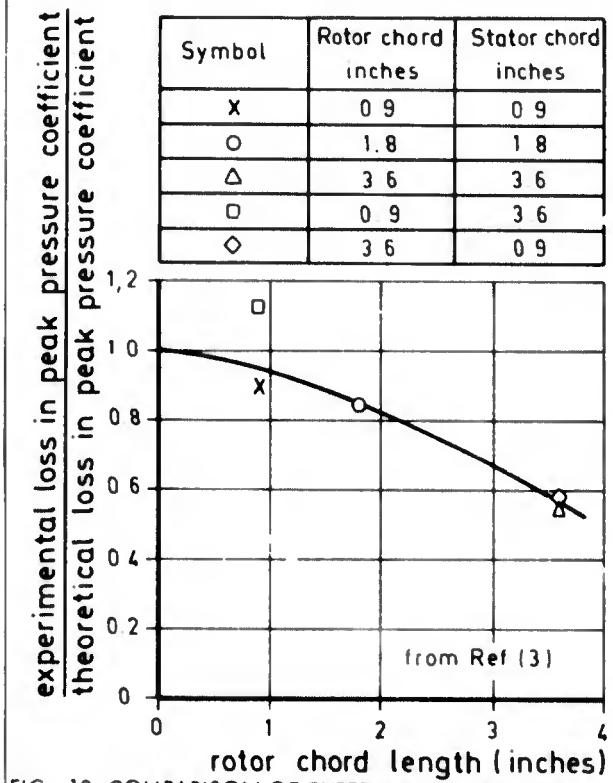

FIG. 12 COMPARISON OF EXPERIMENTAL AND THEORETICAL LOSS IN PEAK PRESSURE COEFFICIENT AS A FUNCTION OF ROTOR CHORD LENGTH

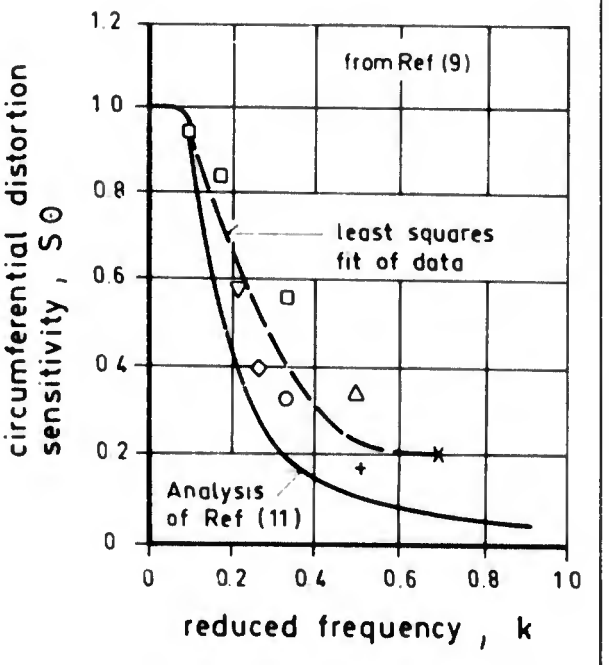

FIG. 13 CIRCUMFERENTIAL DISTORTION SENSITIVITY CORRELATED WITH REDUCED FREQUENCY

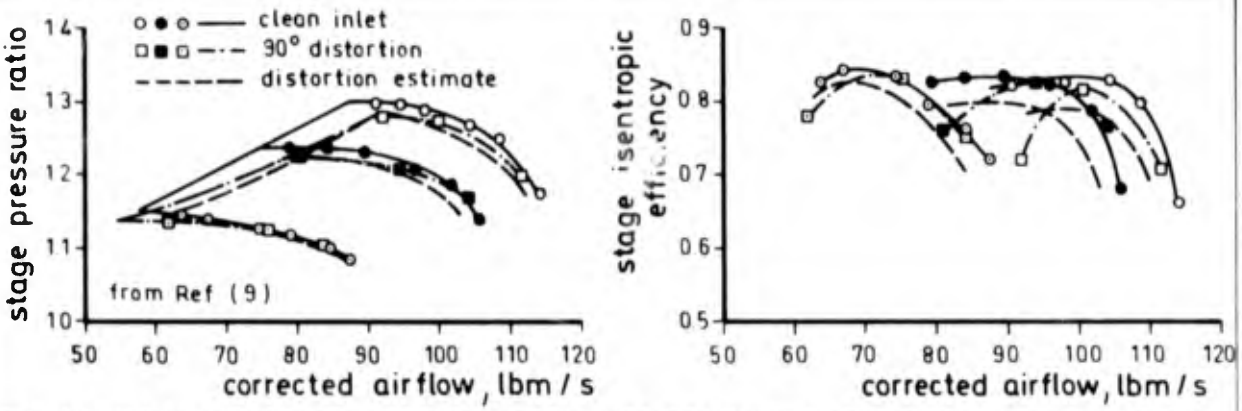

FIG. 14 PARALLEL COMPRESSOR MODEL PREDICTION INCORPORATING RELATIONSHIP BETWEEN DISTORTION SENSITIVITY AND REDUCED FREQUENCY

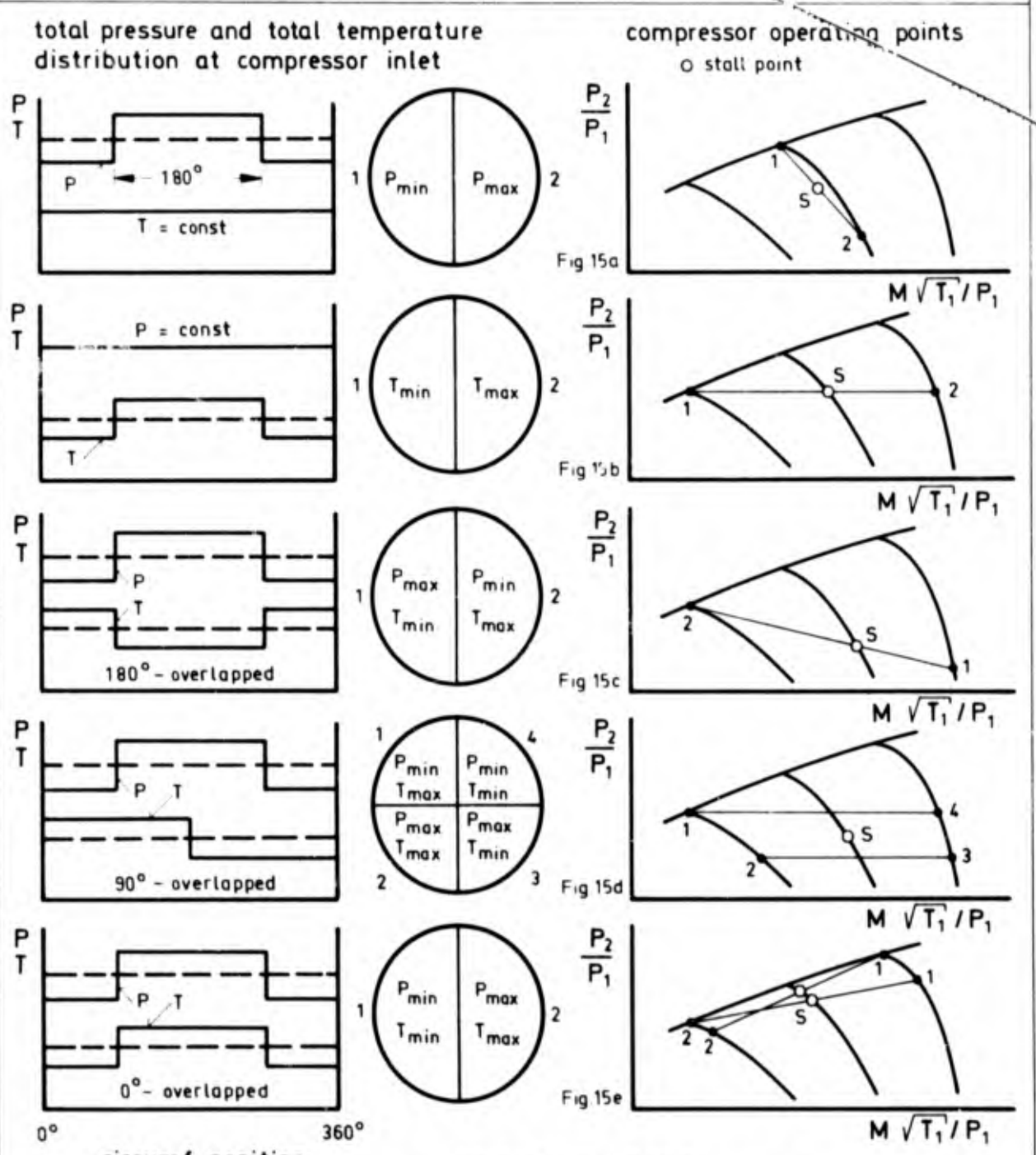

FIG. 15 APPLICATION OF PARALLEL COMPRESSOR MODEL TO COMBINED TOTAL PRESSURE AND TOTAL TEMPERATURE INLET DISTORTIONS (SCHEMATIC)

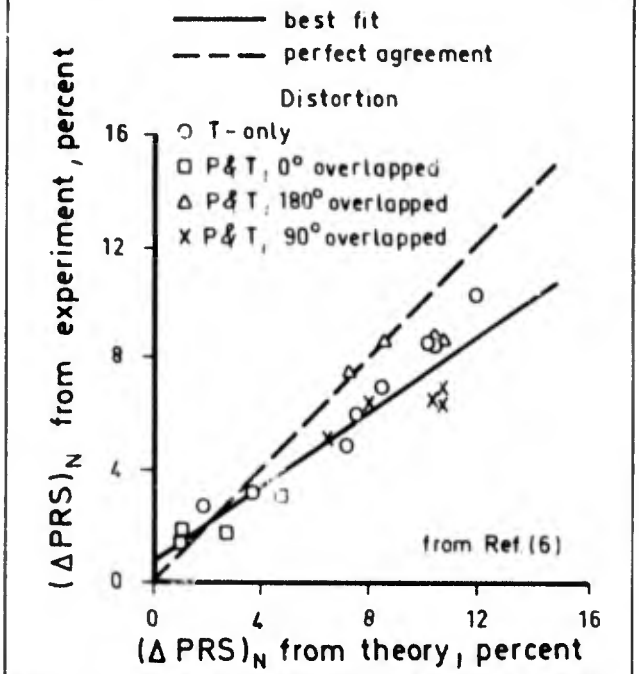

FIG. 16 COMPARISON BETWEEN MEASURED AND PREDICTED LOSS IN STALL PRESSURE RATIO USING PARALLEL COMPRESSOR THEORY

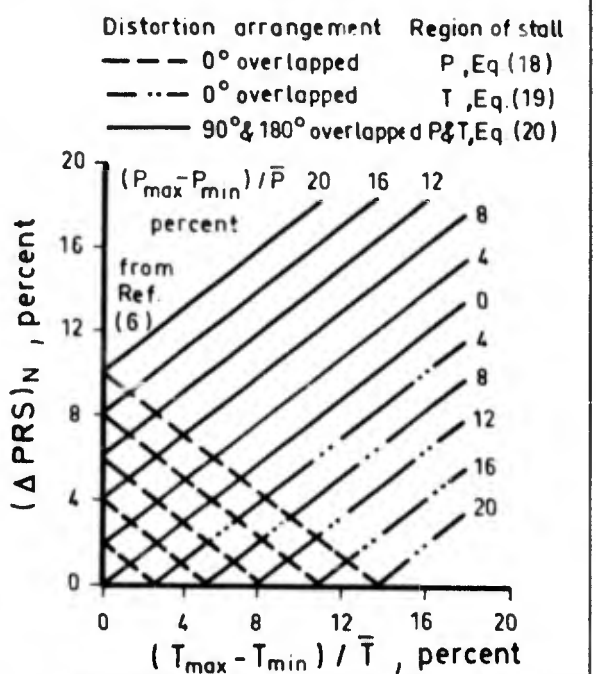

FIG.17 PREDICTIONS OF LOSS IN STALL PRESSURE RATIO FOR COMBINED INLET PRESSURE AND TEMPERATURE DIST. WITH SIMPLIFIED MODEL

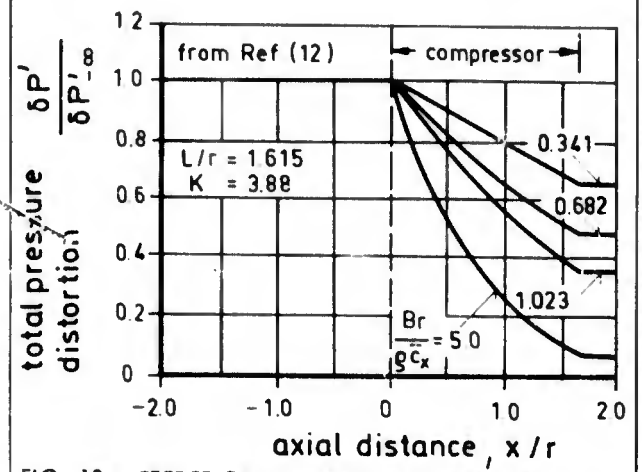

FIG. 18 a EFFECT OF COMPRESSOR CHARACTERISTIC ON ATTENUATION RATE OF TOTAL PRESSURE DISTORTION

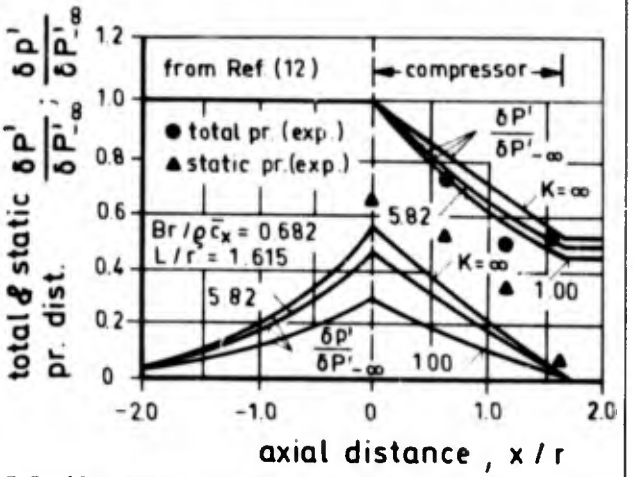

FIG. 19 a EFFECT OF RESISTANCE TO CROSSFLOW ON ATTENUATION RATES OF TOTAL AND STATIC PRESSURE DISTORTIONS

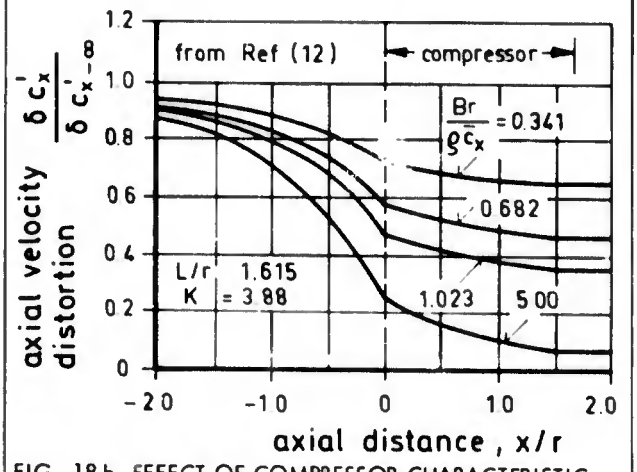

FIG. 18 b EFFECT OF COMPRESSOR CHARACTERISTIC ON ATTENUATION RATE OF AXIAL VELOCITY DISTORTION

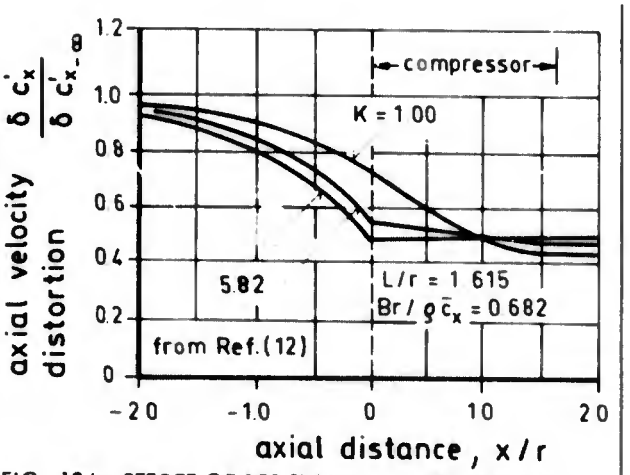

FIG. 19 b EFFECT OF RESISTANCE TO CROSSFLOW ON ATTENUATION RATE OF AXIAL VELOCITY DISTORTION

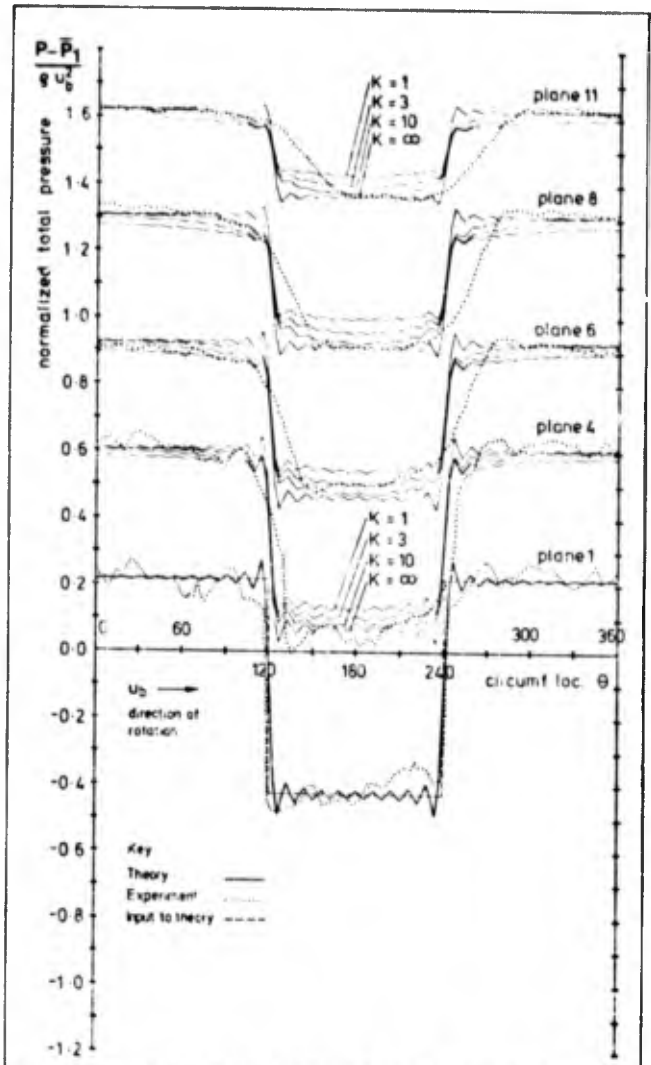

FIG. 20 a MEASURED AND THEORETICAL TOTAL PRESSURE PROFILES OF 120°-DISTORTION PREDICTION WITH LINEAR BODY-FORCE MODEL

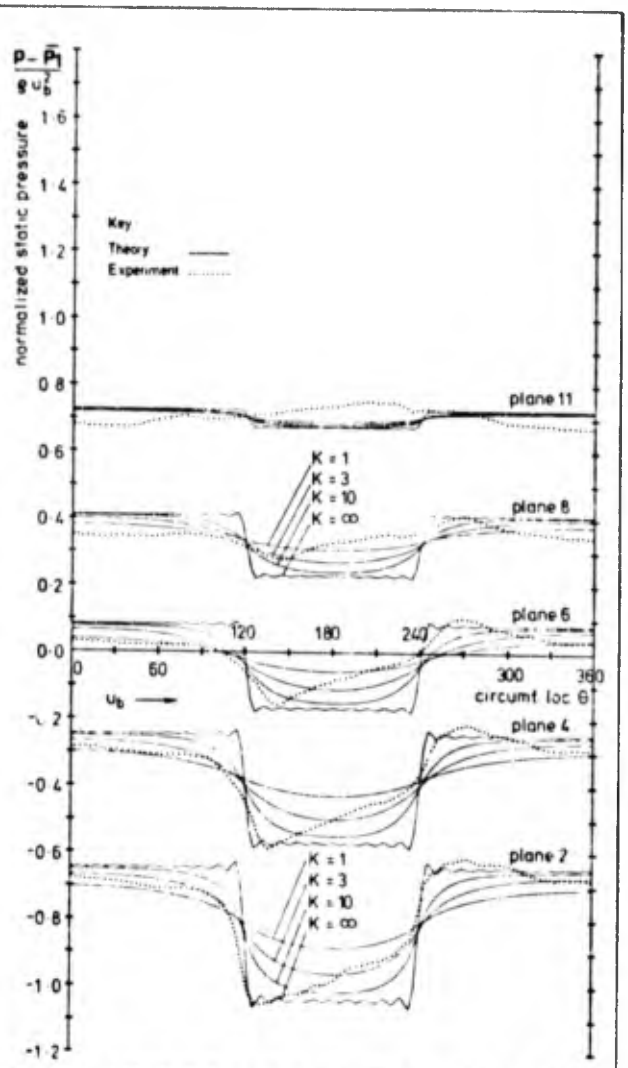

FIG. 20 b MEASURED AND THEORETICAL STATIC PRESSURE PROFILES OF 120°-DISTORTION PREDICTION WITH LINEAR BODY-FORCE MODEL

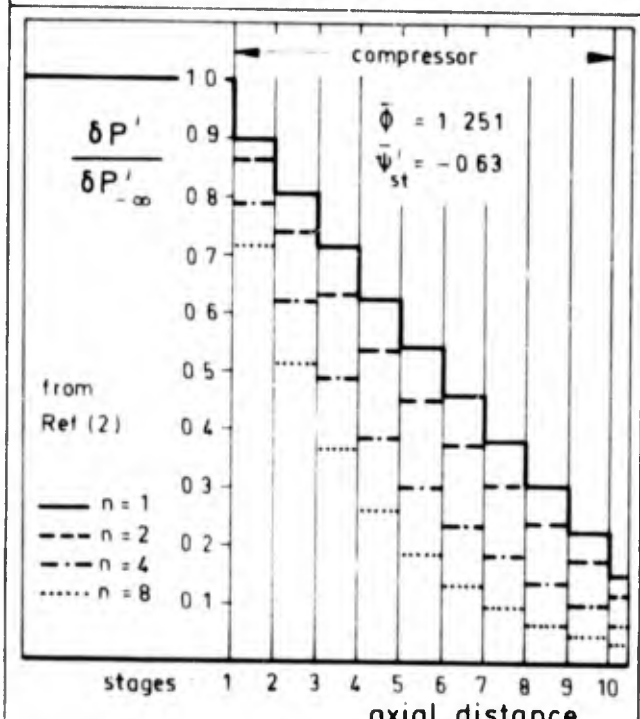

FIG. 21a STAGE MODEL PREDICTIONS OF EFFECT OF HARMONIC NUMBER ON TOTAL PRESSURE DISTORTION IN 10-STAGE COMPRESSOR

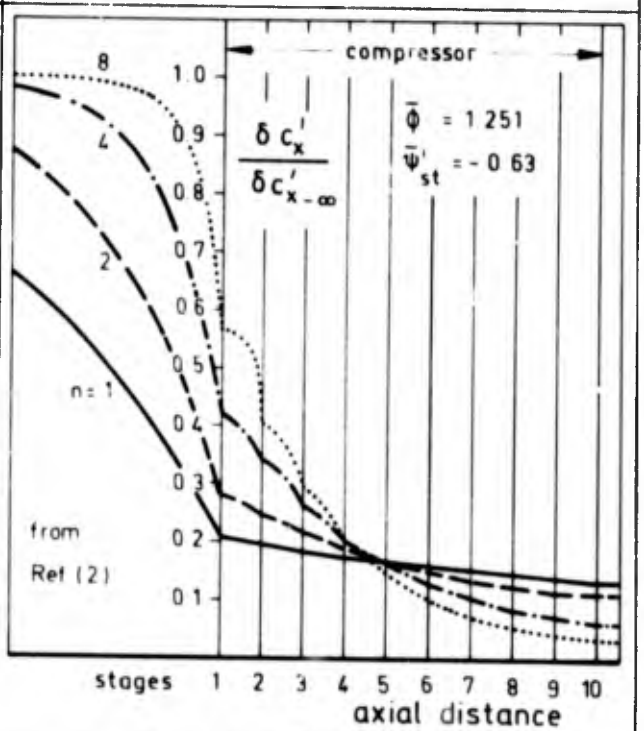

FIG. 21b STAGE MODEL PREDICTIONS OF EFFECT OF HARMONIC NUMBER ON AXIAL VELOCITY DISTORTION IN 10-STAGE COMPRESSOR

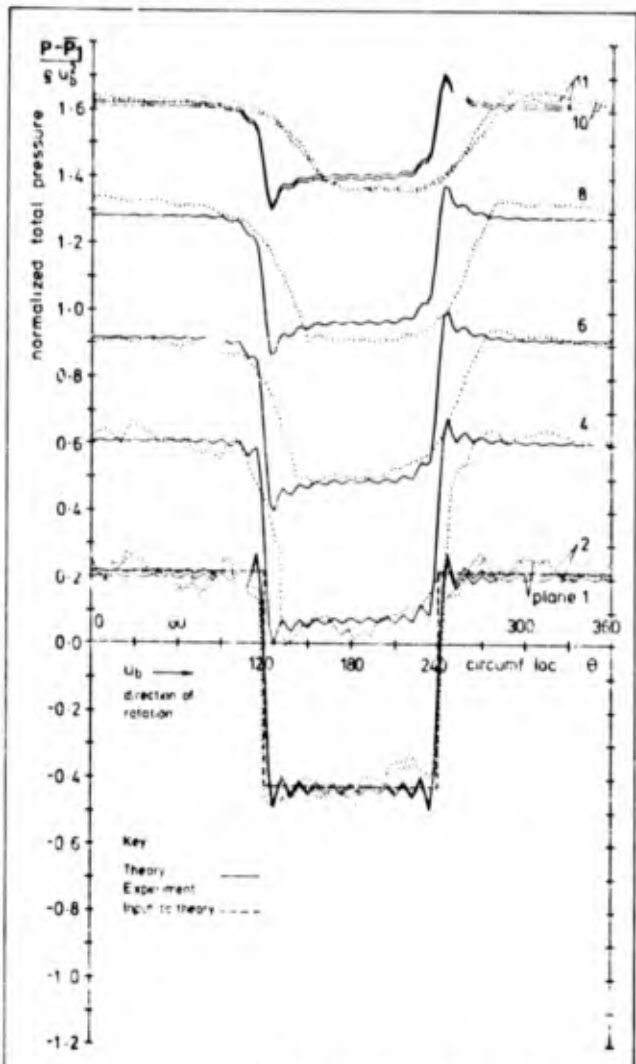

FIG. 22a MEASURED AND THEORETICAL TOTAL PRESSURE PROFILES OF 120°-DISTORTION PREDICTION WITH LINEAR ACTUATOR DISC STAGE MODEL

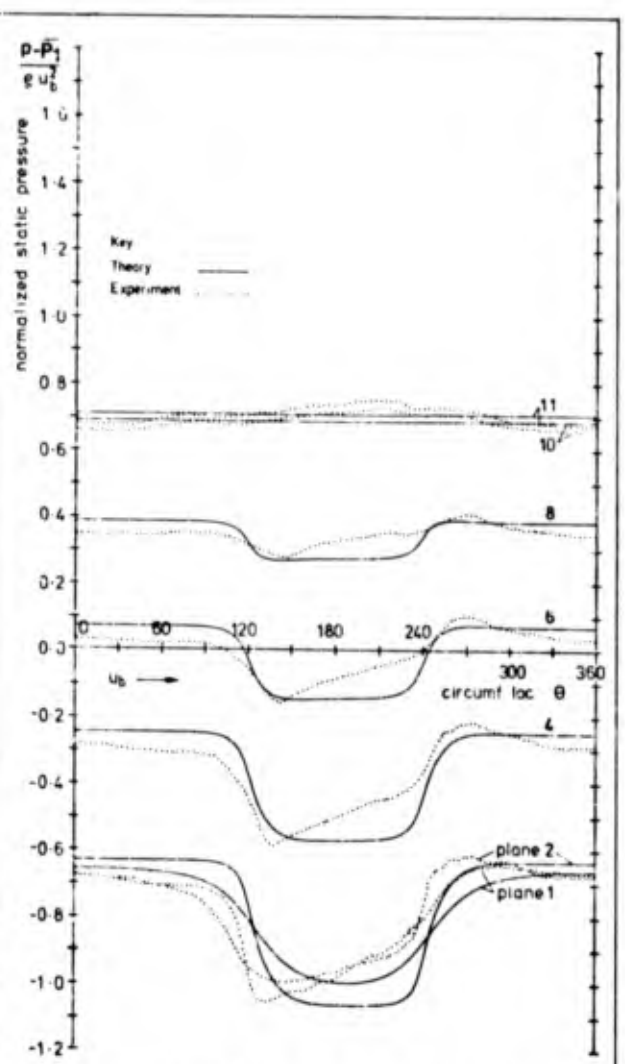

FIG. 22b MEASURED AND THEORETICAL STATIC PRESSURE PROFILES OF 120°-DISTORTION PREDICTION WITH LINEAR ACTUATOR DISC STAGE MODEL

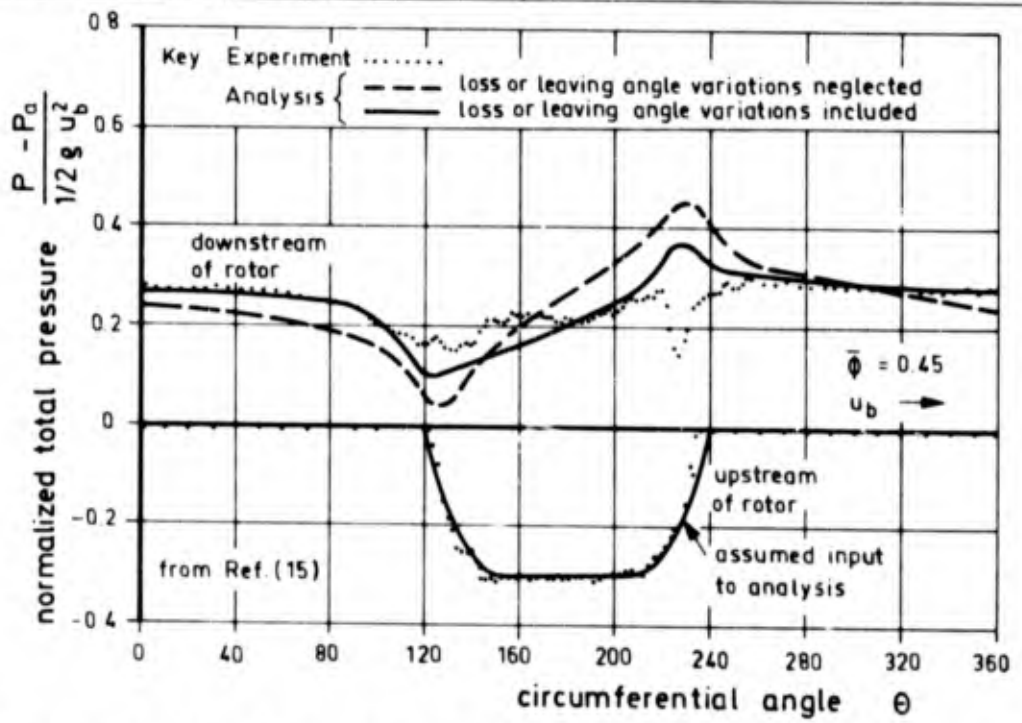

FIG. 23a MEASURED AND THEORETICAL TOTAL PRESSURE PROFILES UPSTREAM AND DOWNSTREAM OF A ROTOR; PREDICTION WITH LINEAR ACTUATOR DISC MODEL

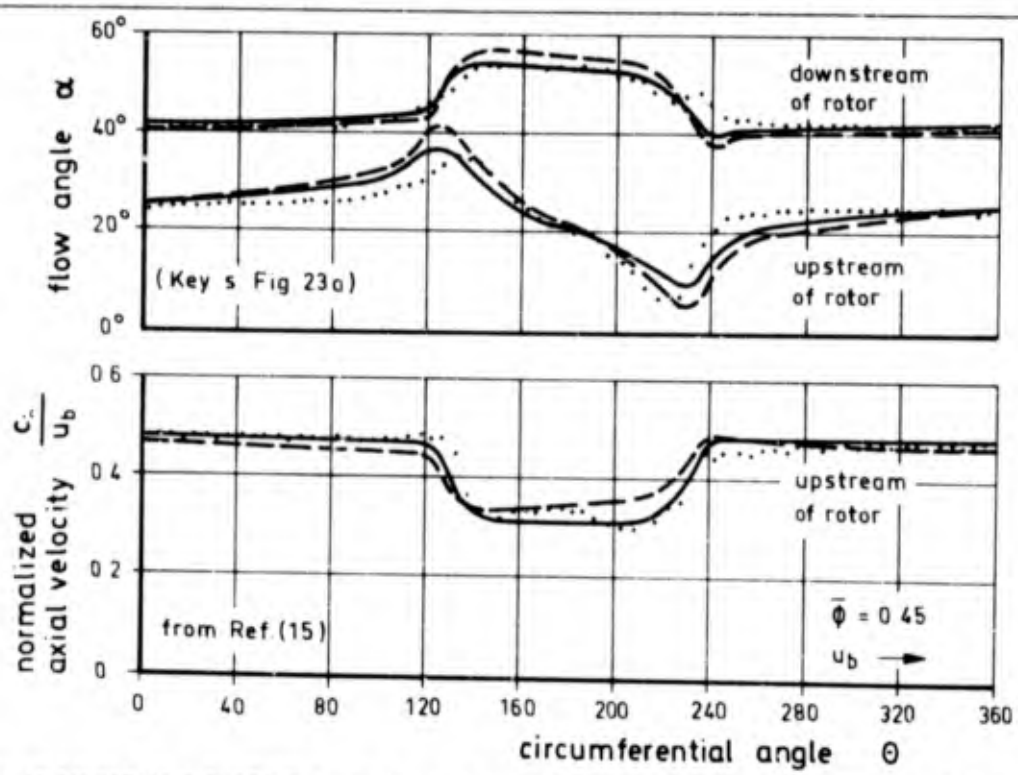

FIG. 23b MEASURED AND THEORETICAL FLOW ANGLE AND AXIAL VELOCITY PROFILES UPSTREAM AND DOWNSTREAM OF A ROTOR - PREDICTION WITH LINEAR ACTUATOR DISC MODEL

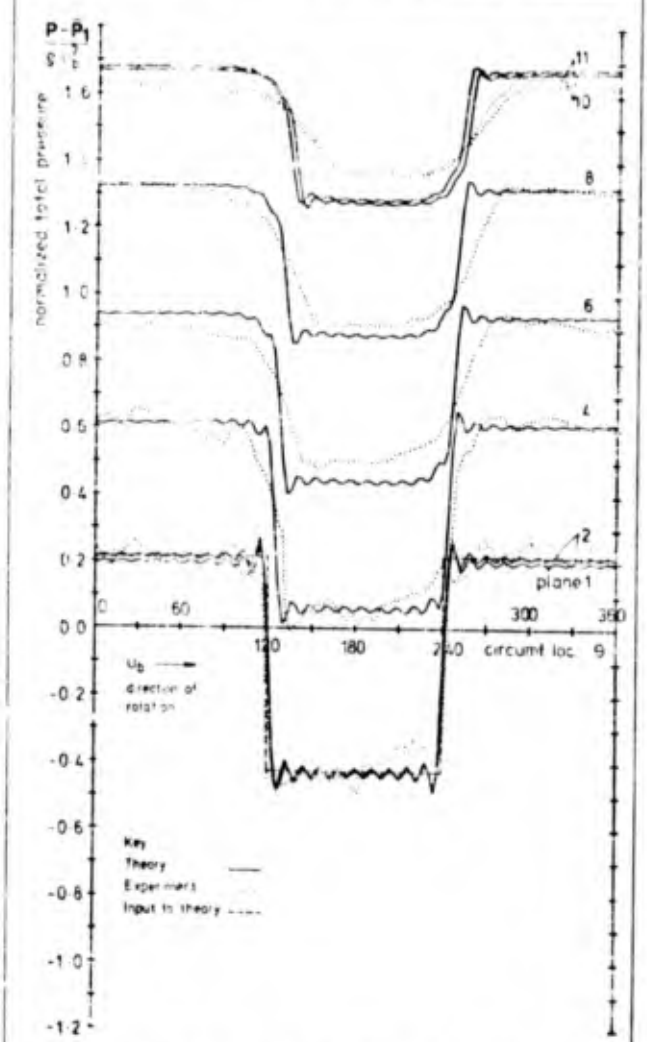

FIG. 24a MEASURED AND THEORETICAL TOTAL PRESSURE PROFILES OF 120°-DISTORTION; PREDICTION WITH LINEAR ACTUATOR DISC BLADE ROW MODEL

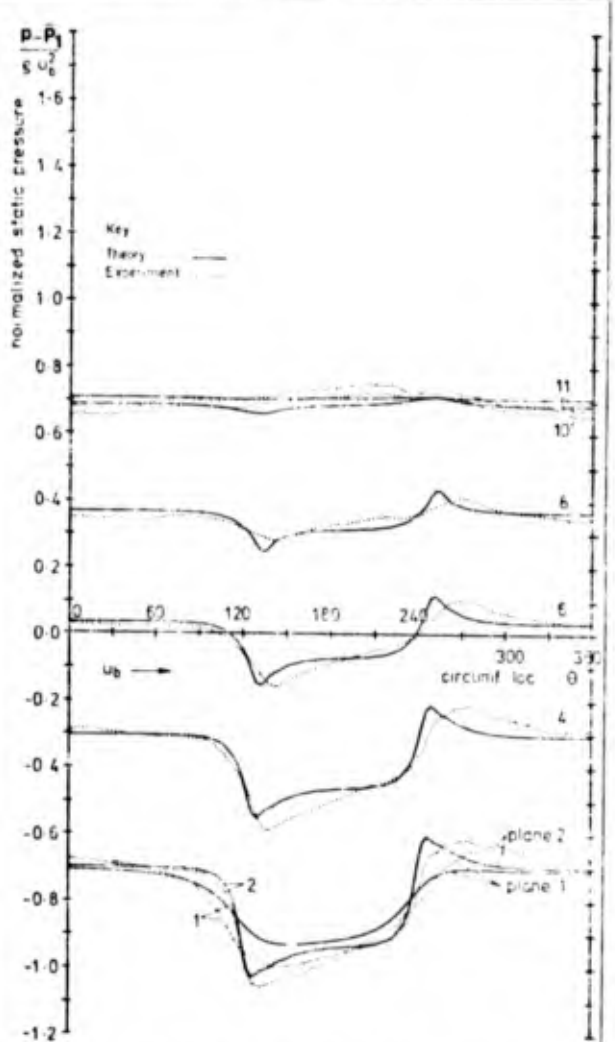

FIG. 24b MEASURED AND THEORETICAL STATIC PRESSURE PROFILES OF 120°-DISTORTION; PREDICTION WITH LINEAR ACTUATOR DISC BLADE ROW MODEL

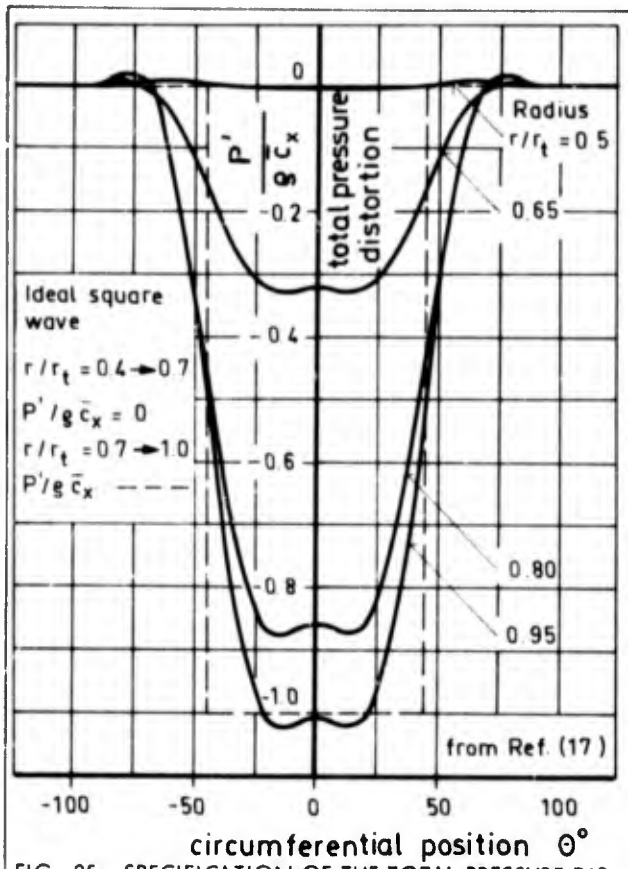

FIG. 25a SPECIFICATION OF THE TOTAL PRESSURE DISTRIBUTION AT INLET TO FREE VORTEX STATOR BLADE ROW

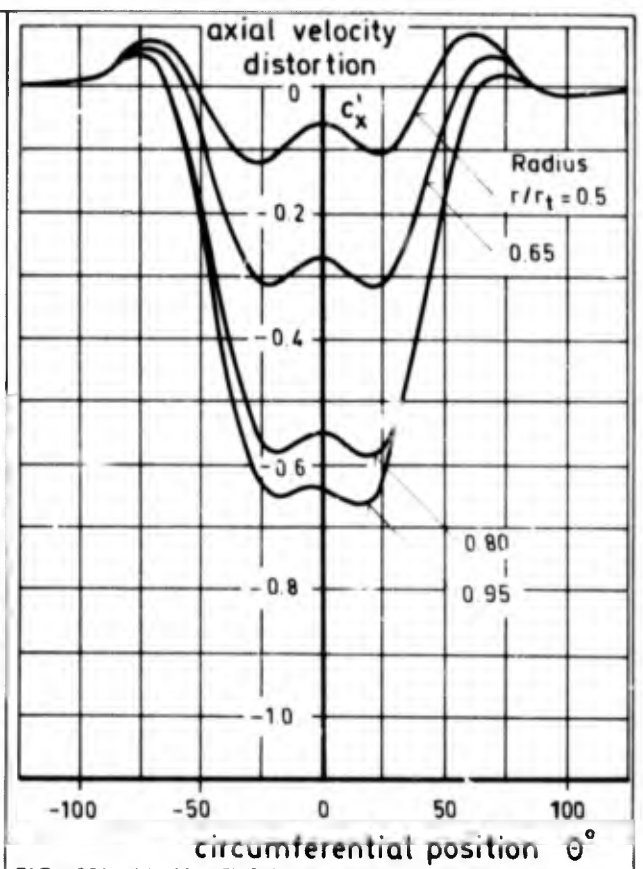

FIG. 25b AXIAL VELOCITY INDUCED AT STATOR; PREDICTION WITH THREE-DIMENSIONAL LINEAR ACTUATOR DISC MODEL

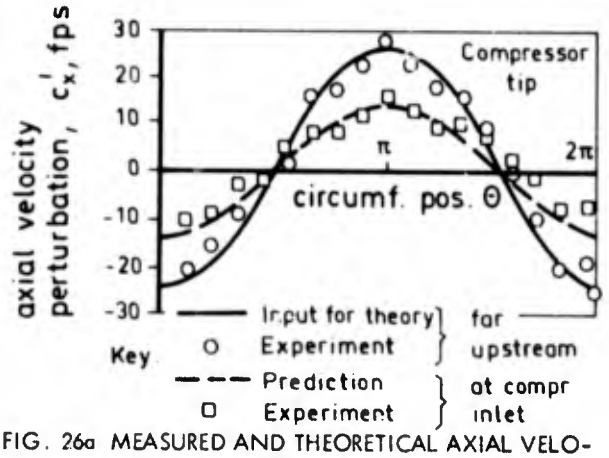

FIG. 26a MEASURED AND THEORETICAL AXIAL VELOCITY DISTORTION AT COMPRESSOR TIP

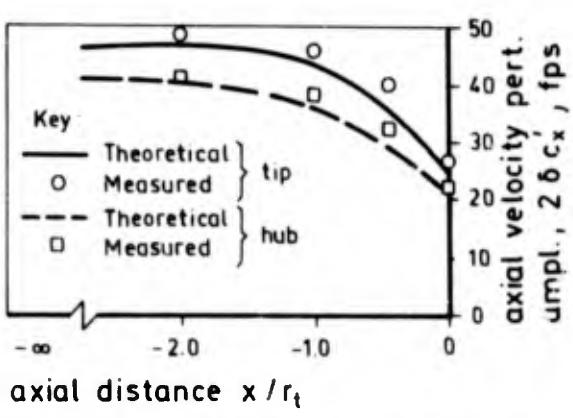

FIG. 26 c MEASURED AND THEORETICAL AXIAL VELOCITY PERTURBATION AMPLITUDE VS. AXIAL DISTANCE

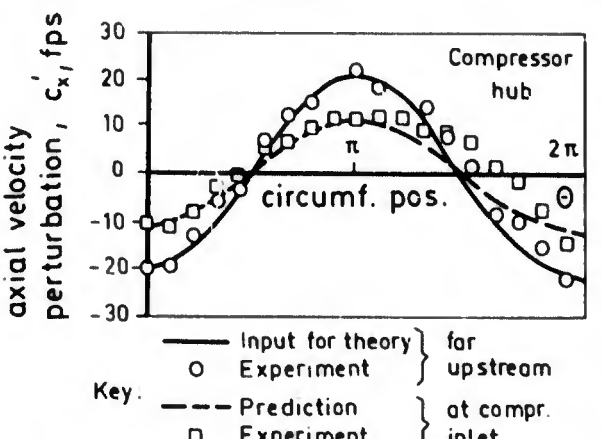

FIG. 26 b MEASURED AND THEORETICAL AXIAL VELOCITY DISTORTION AT COMPRESSOR HUB

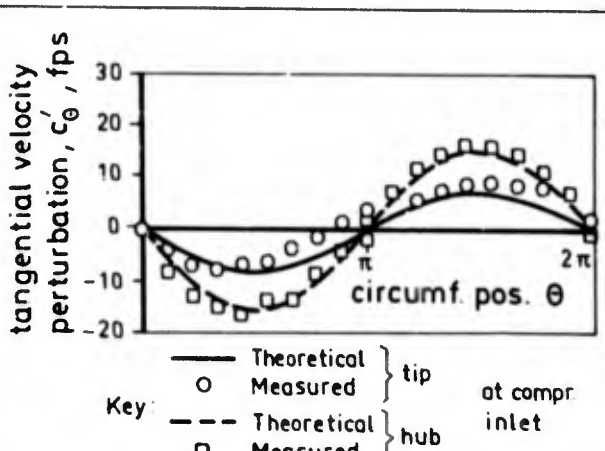

FIG. 26 d MEASURED AND THEORETICAL TANGENTIAL VELOCITY DISTORTION AT COMPR. INLET

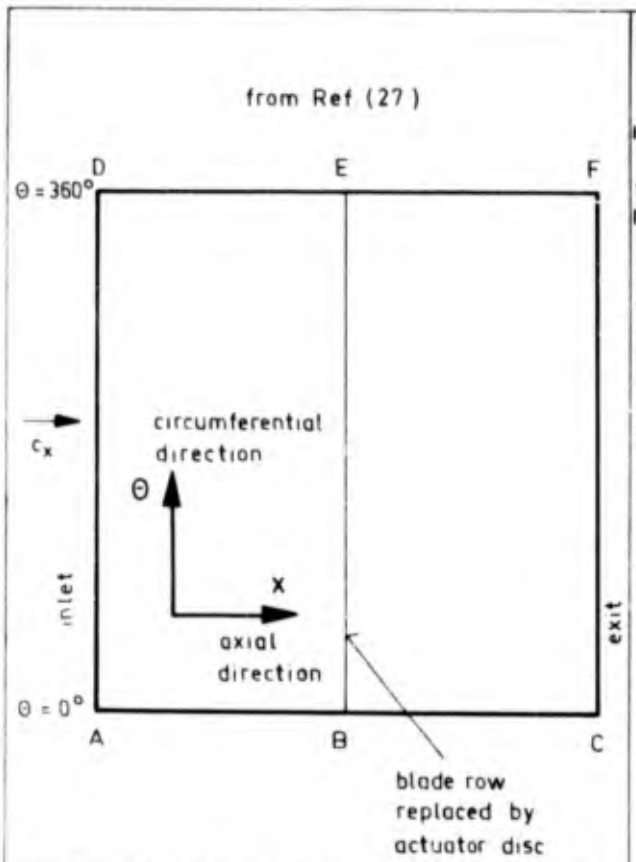

FIG. 27 FLOW FIELDS UPSTREAM AND DOWNSTREAM OF A BLADE ROW (SCHEMATIC)

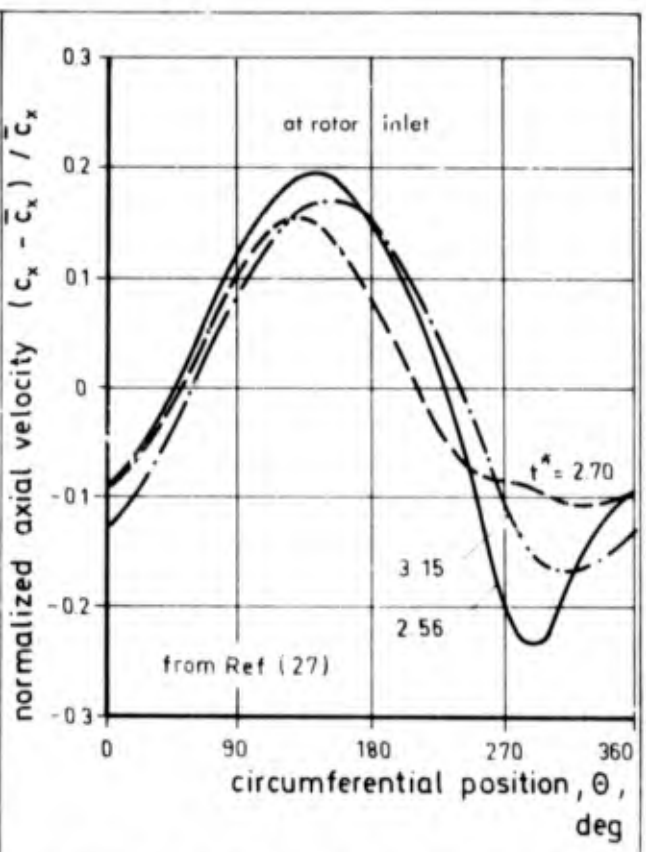

FIG. 28 b DEVELOPMENT OF A 30 PERCENT COSINE WAVE AXIAL VELOCITY INLET DISTORTION FOR $\beta_1 = 40^\circ$

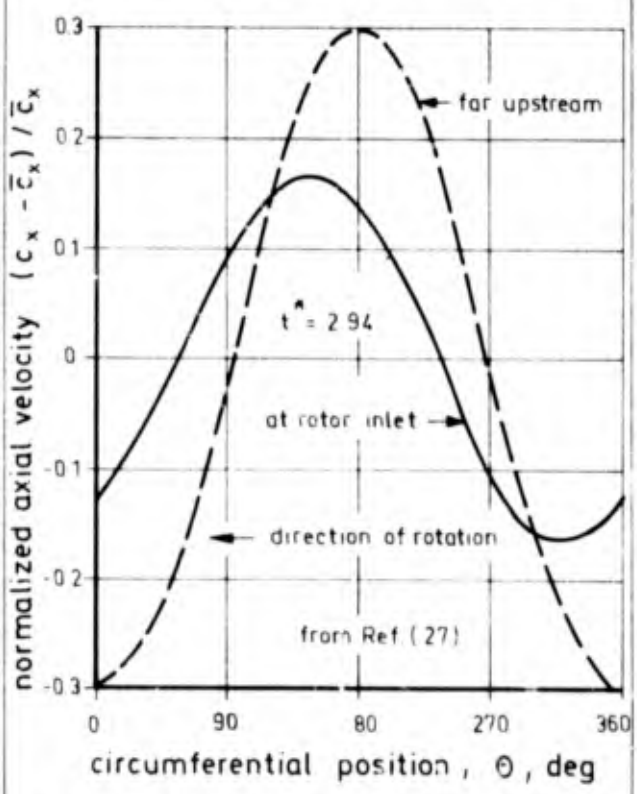

FIG. 28 a DEVELOPMENT OF A 30 PERCENT COSINE WAVE AXIAL VELOCITY INLET DISTORTION FOR $\beta_1 = 42^\circ$

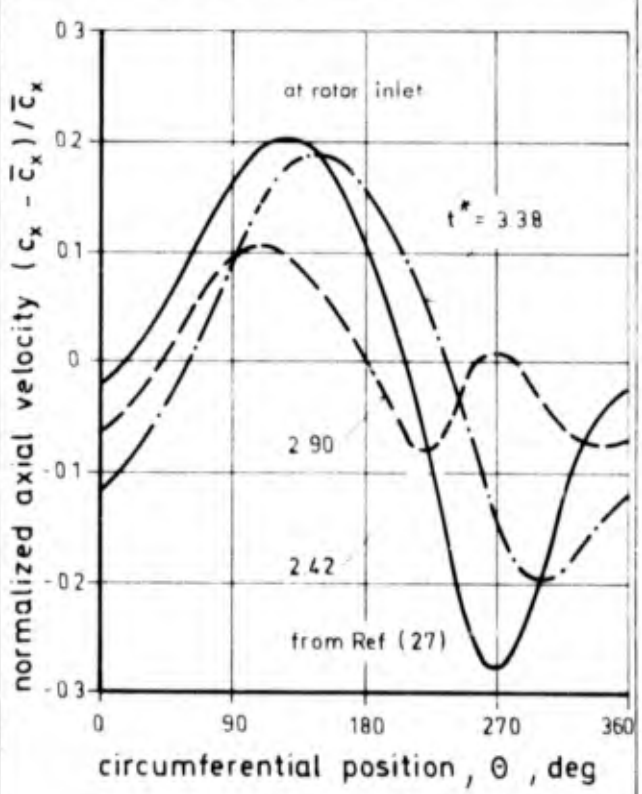

FIG. 28 c DEVELOPMENT OF A 30 PERCENT COSINE WAVE AXIAL VELOCITY INLET DISTORTION FOR $\beta_1 = 38^\circ$

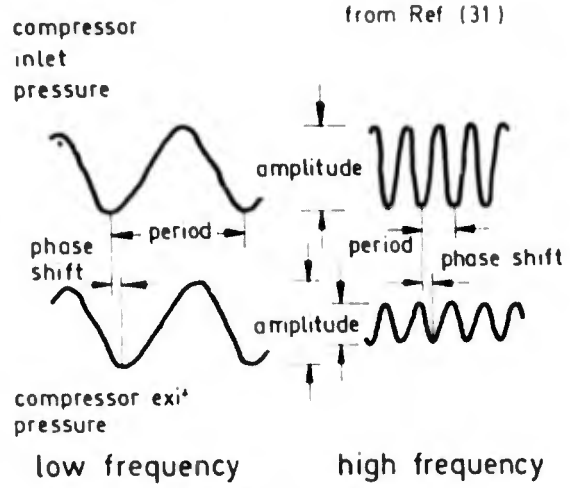

FIG. 29 OUTLET PRESSURE IN RELATION TO A SINUSOIDALLY OSCILLATING INLET PRESSURE

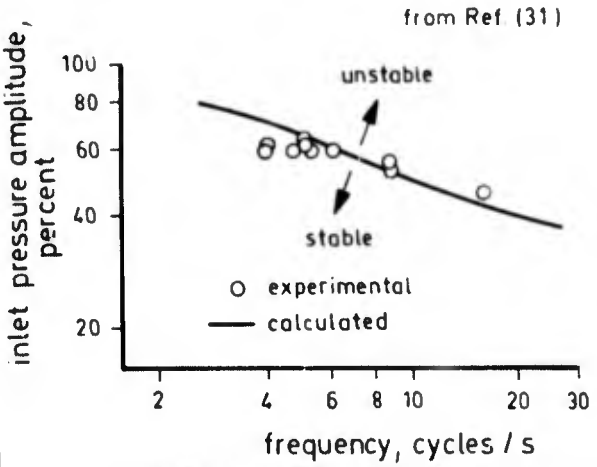

FIG. 31 MEASURED AND PREDICTED SURGE LIMIT AS FUNCTION OF INLET PRESSURE OSCILLATION FREQUENCY

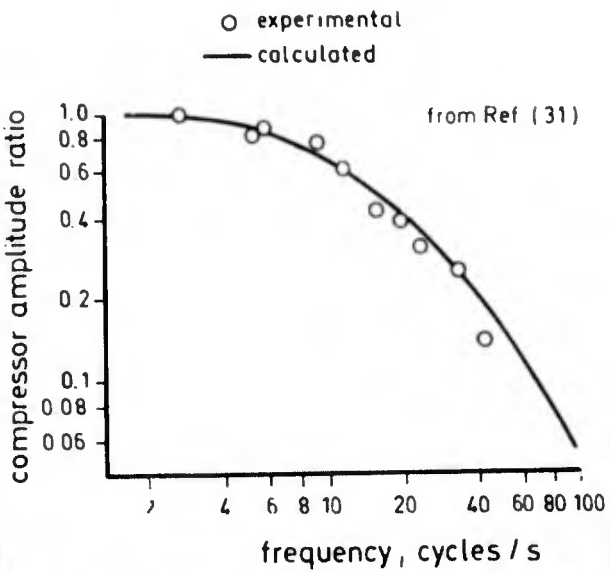

FIG. 30a COMPRESSOR FREQUENCY RESPONSE FOR INLET PRESSURE OSCILLATIONS; AMPLITUDE RATIO VS. FREQUENCY

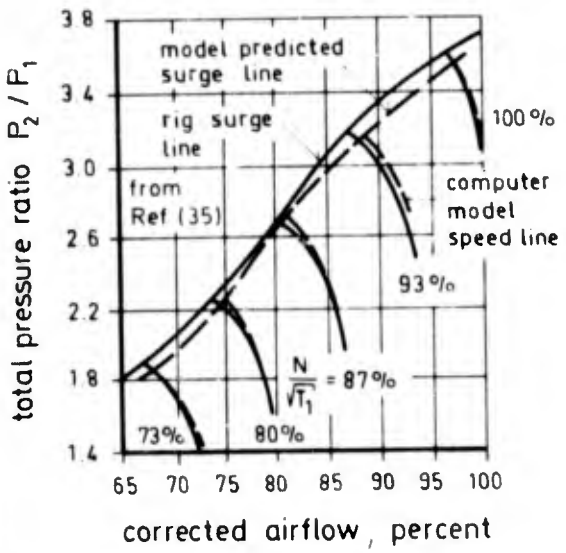

FIG. 32 MEASURED AND PREDICTED PERFORMANCE MAP OF A SEVEN-STAGE COMPRESSOR

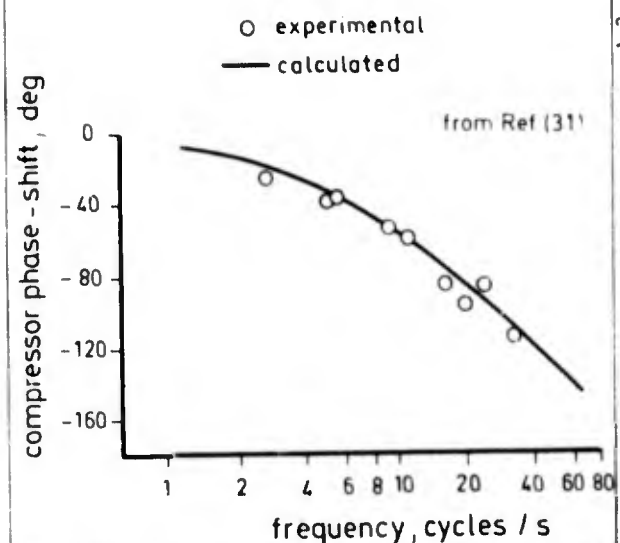

FIG. 30b COMPRESSOR FREQUENCY RESPONSE FOR INLET PRESSURE OSCILLATIONS; PHASE SHIFT VS. FREQUENCY

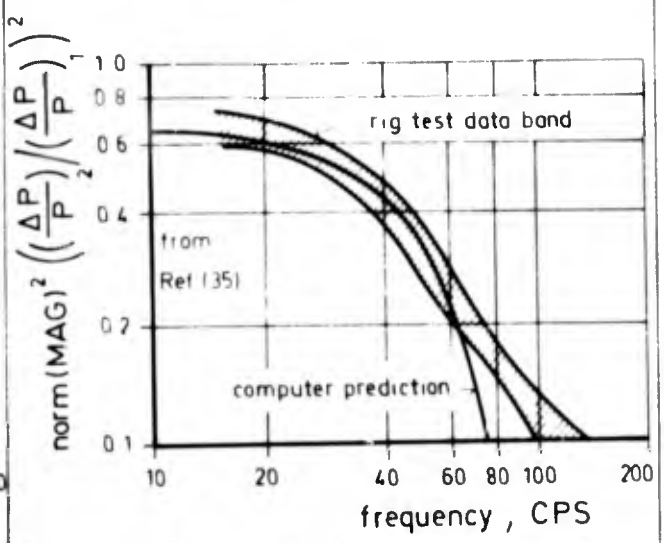

FIG. 33 FAN FREQUENCY RESPONSE FOR INLET PRESSURE OSCILLATIONS; SQUARE OF NORMALIZED AMPLITUDE RATIO VS. FREQUENCY

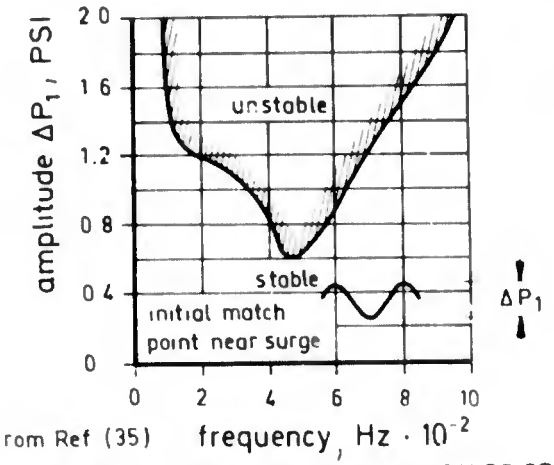

from Ref (35)

FIG. 34 PREDICTED STABILITY LIMIT OF 5-STAGE COMPRESSOR FOR SINUSOIDAL INLET PRESSURE OSCILLATNS.

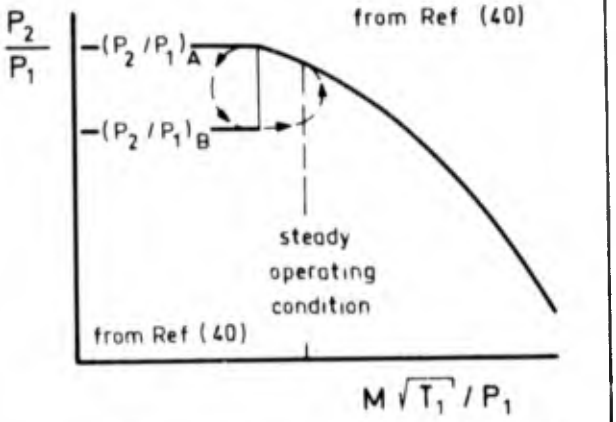

FIG. 37 STAGE CHARACTERISTIC SHOWING AN UNSTEADY STAGE RESPONSE TO A FLOW TRANSIENT (SCHEMATIC)

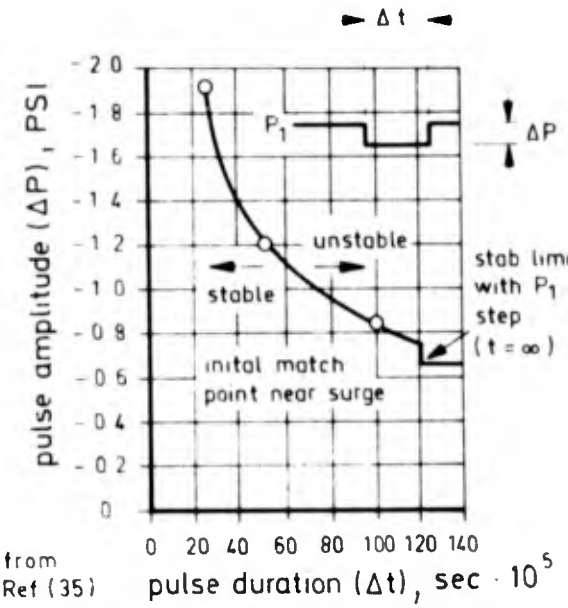

from Ref (35)

FIG. 35 PREDICTED STABILITY LIMIT OF 5-STAGE COMPRESSOR FOR SQUARE-WAVE INLET PRESSURE PULSES

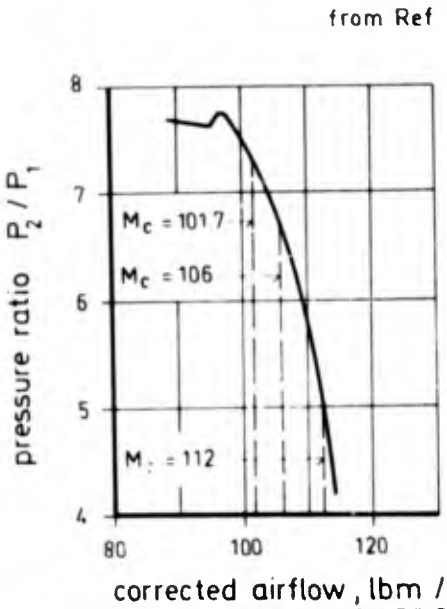

FIG. 38 PERFORMANCE MAP OF 6-STAGE COMPRESSOR SHOWING 3 OPERATING CONDITIONS AT WHICH UPSTREAM PRESSURE PULSES ARE INTRODUCED

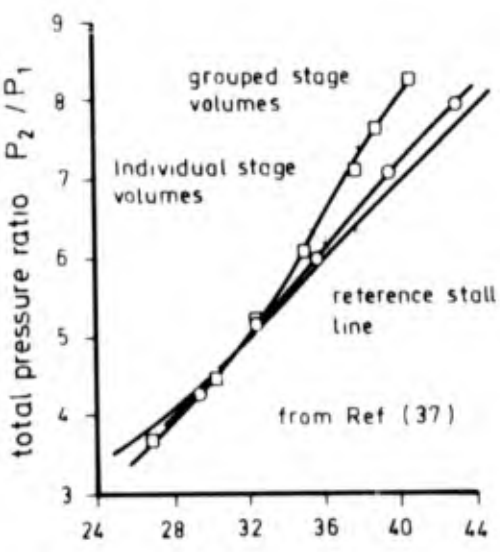

FIG. 36 PREDICTED COMPRESSOR STALL LINE USING GROUPED STAGE VOLUMES AND INDIVIDUAL STAGE VOLUMES

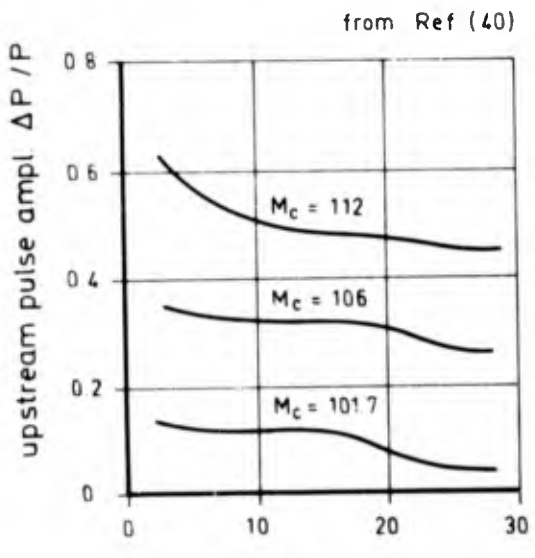

FIG. 39 PREDICTED SURGE LIMITS FOR UPSTREAM SQUARE-WAVE PRESSURE PULSES AT 3 OPERATING CONDITIONS (TRANSIENTS ABOVE CURVE LEAD TO SURGE)

TEST TECHNIQUES, INSTRUMENTATION, AND DATA PROCESSING

by

William G. Schweikhard
Deputy Director, Propulsion Research
NASA Flight Research Center
P. O. Box 273
Edwards, California 93523
USA

SUMMARY

Ever since the effects of dynamic distortion on engine stability were first realized, much effort has been expended in developing techniques for simulating these effects in ground facilities, instrumentation for measuring these effects both on the ground and in flight, and data analysis methods and facilities for processing the large quantity of data that is generated. This paper surveys test techniques, methods and types of instrumentation, and data analyses and processing methods that have been used most successfully and evaluates their strengths and shortcomings. It is emphasized that ground facility tests are only a simulation of the flight environment, that instrumentation provides only a partial representation of the physical phenomena, and that poorly organized and poorly understood data processing procedures can seriously impede and even distort the final result.

SYMBOLS

b	distortion weighting factor (Eq. (11))
D	distortion coefficient (Eq. (14))
F_1, F_2, F_3, F_4	recorded data samples
F_x	interpolated data sample
f	frequency
Δf	frequency bandwidth
K_{RAD}	radial distortion coefficient
K_θ	circumferential distortion coefficient
L	length of resonant cavity
L_c	coil inductance
L_p	plate inductance
M	Mach number
P	steady-state pressure and time ratio (figs. 39 and 40)
ΔP	root mean square turbulence pressure disturbance or differential pressure
P_{abs}	absolute pressure
P_{in}	input pressure
P_{out}	output pressure
P_{ref}	reference pressure
P_{ss}	steady-state absolute pressure
P_t	total pressure
P_{to}	free-stream total pressure
P_{t_2}	diffuser exit total pressure
$P(x)$	probability density function
R_c	resistance of coil
R_p	resistance of plate
RMS	root mean square value
r	radius
s	Laplace transform variable
T	temperature or analog-to-digital cycle time (fig. 39)
t	time
V	volume
γ	ratio of specific heats
ζ	damping ratio
λ	wavelength
ν	kinematic viscosity
ρ	density
φ	phase angle
ω	frequency
ω_n	natural frequency

Subscripts:

av	average
max	maximum
min	minimum

1.0 INTRODUCTION

In the general sense, our ability to understand a particular phenomenon is based on our ability to observe and measure each pertinent variable as precisely as possible. How well these observations and measurements are made depends on the experimental techniques used to identify and isolate unique factors. Through analysis of the data generated, theories can be developed from which predictions can be made. Depending on the success of these predictions in representing the real world behavior, this process is repeated in a never-ending cycle which we call advances in technology. It is important to realize that the key elements in this cycle are measurement or instrumentation test techniques and analysis or data processing. The failure or shortcomings of either element weakens the final result.

Theories are no better than the information from which they are drawn. Thus, in the past few years, much effort has been directed toward developing the measurement, experimental, and analytical tools necessary to identify and predict the critical factors which cause distortion-induced instabilities in aircraft propulsion systems. The problem is so complex, nonlinear, and interactive that isolation of the individual variables is virtually impossible even in ground test facilities. This has caused investigators to take either an empirical or a statistical approach in analyzing their data. When the propulsion system is projected into the flight environment, the problem of instrumenting an aircraft, designing a test procedure, and acquiring and processing the data becomes more difficult. This paper surveys the experimental techniques, methods and types of instrumentation, and data processing and analysis approaches that have been used.

2.0 TEST TECHNIQUES

The ultimate goal in the design of a propulsion system is to derive the maximum performance from the system. This requires that every element be pushed to its maximum efficiency.

Years of experience have shown that certain margins are necessary to prevent instabilities such as stalls and surges. Recently, direct relationships have been established between these margins and inlet flow dynamics or turbulence. The problem has been one of simulating in ground facilities the dynamic pressures produced by the inlet, the atmosphere, the aircraft motion, and the flow field. Also, it has been difficult to obtain the quantity and quality of flight data needed to validate the simulation results.

In the flight environment (fig. 1), the engine must contend with disturbances due to atmospheric turbulence and the aircraft flow field as well as internal disturbances caused by the inlet and its controls. It is the task of the ground test facilities to simulate these dynamic effects as accurately as possible. This is difficult because the nature of atmospheric turbulence is not well defined, especially at high altitudes. Also, the effects of the flow field surrounding the wing and fuselage forward of the inlet depend on the boundary layer and vortex flows generated. Turbulence and fluctuating flows reaching the inlet are dependent both on the model scale, which is a function of the Reynolds number, and the turbulence dissipation, which is a function of the linear distance between the disturbance source and the inlet. Hence, results from wind-tunnel-model tests may not represent the full-scale dynamic flow characteristics.

2.1 External Disturbance Simulation

Simulation of upstream turbulence entering an inlet can be approached in several ways. Disturbances generated by the wing and fuselage can be simulated by tests in subsonic and supersonic wind tunnels with small-scale models which represent the aircraft forward of the inlet (ref. 1).

Atmospheric turbulence can be simulated by using screens and vortex generators in subsonic wind tunnels; however, supersonic simulation is not so easy. A schematic drawing of some proposed approaches is shown in figure 2. An oscillating wedge mounted near the wall of a supersonic wind tunnel has been used (ref. 2) to generate a variable strength shock wave ahead of the model. The flow field induced by oscillation of the vane had two shortcomings: It was not uniform across the inlet, and the flow parameter changes were not truly representative of flight transients. Studies have been made to investigate the feasibility of injecting pulses of high-pressure air upstream of a model to generate fluctuating shocks and vorticity. Also, a rotating ellipse located in the throat of a supersonic wind tunnel has been considered. The success of these devices at supersonic speeds is questionable at this time because of uncertainties about what is to be simulated. A good model of atmospheric turbulence at high altitude and supersonic speeds is not available.

It is evident, then, that even a full-scale inlet engine test in a wind tunnel is only a partial simulation of the flight environment and is done only as a final demonstration of compatibility after the engine and inlet have undergone years of development.

2.2 Developmental Approach

It is essential that indications of incompatibilities between an engine and inlet be identified early in the development program. The current approach is to conduct a large-scale wind-tunnel test of an inlet model and to determine the steady-state and dynamic pressure distortion patterns. The frequency of the dynamic data is scaled to the model scale. The steady-state distortion patterns are then simulated in an engine test facility by using screens which also generate pressure fluctuations approximating the expected frequency and amplitude (typically 5 percent to 15 percent of the measured pressure). In this way, it is hoped that incompatibilities can be discovered and dealt with early. Ultimately, full-scale engine—inlet tests are performed.

2.3 Total Pressure Distortion Simulation

Many dynamic distortion generating devices have been developed. References 1, 3, and 4 describe the development and improvement of a choked-throat turbulence generator (fig. 3) for use in an engine test facility. With this device, turbulence is generated by the interaction of the shock with the boundary layer downstream of the throat. The power spectral density characteristics of this system are shown in figure 4. The power for the unmodified turbulence generator drops off sharply with increased frequency, but the insertion of a grid of 1/2-inch square rods and 3-inch pipes upstream of the compressor face amplifies the power at the high

frequencies and reduces the power at the low frequencies. Spikes that occur at several frequencies with the 3-inch pipes are caused by vortex shedding in the wake.

But, how well do the simulated spectra represent the flight environment? Results from flight tests of the F-111 airplane for frequencies from 0 to 200 hertz (ref. 5) are also shown in figure 4. Comparison of these results indicates that the power spectral density characteristics of the unmodified choked-throat turbulence generator closely approximate the flight results, especially at Mach 2.4. Though the trends with frequency are the same at the lower Mach numbers, the amplitudes are significantly less except for flight measurements made downstream of the spike cone. At a flight Mach number of 2.4, the entire compressor face is affected because the terminal shock is inside the duct and produces more uniform levels of turbulence over the whole duct. This may be particularly true of mixed-compression inlets for which the terminal shock is inside the inlet.

Although the choked-throat turbulence generator matches the spectral characteristics of a flight vehicle reasonably well, it does not necessarily represent the dynamic distortion patterns. A pulsating jet device (ref. 6) has been developed to simulate both the spatial and temporal characteristics of the flow entering an engine. This device is being used to create controllable dynamic or steady-state pressure disturbances at the inlets of engines being tested in altitude facilities. The technique uses many small air jets upstream of the engine inlet. Figures 5(a) and 5(b) show the main features of the air jet system. Primary airflow passes through the bellmouth and inlet duct to the engine. The air jet system includes an array of small nozzles in the inlet duct. These nozzles are uniformly distributed in an axial plane and arranged in a pattern which repeats every 60°. As indicated, secondary airflow is injected from these nozzles and directed counter to the primary airflow. Flow control of the secondary airflow is provided for each 60° sector of air jet nozzles by six valves external to the inlet duct. These are high-response valves of NASA design for operation over an oscillatory frequency range from 0 to approximately 200 hertz. Separate matched flow lines are provided from each of the valves to each of the air jet nozzles of a 60° sector. Secondary air is supplied to the valves at pressures up to 10 atmospheres. By controlling the secondary air distribution and the flow rate with these valves, a variety of basic dynamic or steady-state inlet pressure disturbances can be created for engine tests.

As shown in figure 6, power spectra developed by this device indicate that large quantities of energy can be controllably put into the airstream in the low-frequency region. Tests are underway using flight distortion data from reference 5 as control inputs to the jet system and using the flight-test engine to correlate the surge and stall responses observed during the flight tests. Future applications may use some combination of the choked throat and pulsating jet techniques.

Another technique has been developed to simulate the dynamic characteristics at the engine—inlet interface of two-dimensional inlets. From free-jet model tests of an F-15-type inlet, it was observed that the flow conditions approaching the third ramp of the inlet were constant over a large range of angle of attack and that the internal flow conditions were primarily a function of the flow behind the last oblique shock wave. Thus, if the conditions on the third ramp could be simulated, the dynamic flow conditions at the compressor face would be duplicated. An inlet simulator/turbulence generator (fig. 7) which utilizes this approach has been developed at the Arnold Engineering Development Center (ref. 7). This is a semi-free-jet device designed for use in an engine test facility to simulate the compressor face turbulence and distortion of a two-dimensional inlet. It consists of a convergent-divergent nozzle section which accelerates the flow upstream of the third ramp so that the last oblique shock and the terminal shock are similar to those experienced by the flight vehicle. The remaining contours of the inlet and subsonic diffuser are those of the vehicle being tested. Thus the core flow, boundary layer, and internal vorticity closely represent those of the aircraft. Bleed is provided in the nozzle for control of the boundary layer. External vortices generated by the fuselage, forward ramps, and wing during sideslip of the aircraft are simulated by doors near the nozzle throat which are set at the desired angles. These doors are not dynamically actuated. As is typical of most free-jet tests, approximately 50 percent of the air passing through the nozzle does not enter the inlet but is collected and fed to exhausters.

2.4 Temperature Distortion Simulation

Temperature distortions caused by ingestion of hot gasses from armament firings and from reingestion of hot gasses of VTOL vehicles can cause major problems. These effects must be investigated during the development of engines that are to be subjected to this type of operational environment. A device for simulating temperature effects in an engine test facility is described in references 8 and 9.

In these studies, temperature distortions were produced at the engine face by using a gaseous hydrogen-fueled heater located upstream of the engine inlet bellmouth. A schematic drawing of the heater and the hydrogen supply system is shown in figure 8(a) and a photo in figure 8(b). The engine inlet airflow passed through and was heated in a large diameter duct which was divided into four 90° sectors. Each sector had an array of five annular V-gutters. Hydrogen was distributed through a system of tubing within the V-gutters and fed from a single supply manifold for each sector. Small holes were drilled in the tubing to inject hydrogen into the V-gutters where it was burned. Five swirl-can pilot burners were placed in each sector to provide an ignition source for the main hydrogen flow. Temperature was controlled by varying the hydrogen flow using a slow response, remote operated valve for steady-state operation and a high-speed, remote operated valve for rapid transients. Each sector had its own control system which permitted independent operation of from one to four sectors, thereby producing spatial or time-dependent temperatures over 90° to 360° of the circumference. The system was designed to produce a spatial temperature rise of 800° F and time dependent temperature rises in excess of 8000° F per second. Hydrogen was chosen as the fuel because of its good ignition characteristics and rapid flame propagation speed.

2.5 Correlation of Flight and Wind-Tunnel Results

Comparisons between propulsion flight-test and wind-tunnel results may appear to be simple; however, experience has shown this not to be true. Unless unusual care is taken, more often than not the models tested do not represent the final configuration; the instrumentation used is not the same in location, accuracy, or response; and the test conditions of Mach number, local flow angles, and inlet geometry do not match. Consequently, most comparisons of wind-tunnel and flight data are lacking in at least one of these respects.

The NASA YF-12 airplane propulsion program is a good example of a meticulous approach and of problems that can arise, nevertheless, in correlating wind-tunnel and flight results. From the onset, the objective of this program was to make both steady-state performance and dynamic distortion correlations. Full-scale and one-third-scale wind-tunnel models were built as identical scaled versions of the flight vehicle. Instrumentation was installed in identical locations and had comparable accuracy and frequency response. Test conditions were selected that could be duplicated in flight and in the wind tunnels. Wind-tunnel calibrations of the bleed and bypass airflow measurements of a full-scale inlet were made to assure the best possible airflow measurements in flight. In-flight local flow measurements were made in front of the inlet to determine the local flow conditions (Mach number, angle of attack, angle of sideslip, and Reynolds number) at which the wind-tunnel tests should be done. This proved to be the weakest link in providing precise correlations.

Wind-tunnel tests of the aircraft model indicated large flow angularities at the cowl plane, but flight measurements at the spike tip did not bear this out; however, there was a great deal of scatter in the flight results. These uncertainties have caused problems in setting the wind-tunnel conditions at the spike tip to the precise local flow conditions that exist in flight.

Although this problem may yet be resolved, the wind-tunnel tests have already been done. Therefore the aircraft must be flown to match the wind-tunnel test conditions. Again, this may appear to be a simple task except when one realizes that the pilot reads aircraft Mach number and angle of attack, not the local flow conditions. Furthermore, the local Mach number and flow angles are a function of the aircraft weight at which the flight tests are conducted. Deviations of the local flow from the nominal 1g flight condition can be attained only during quasi-steady longitudinal and sideslip maneuvers. Performing longitudinal maneuvers while holding steady sideslip angles is not a practical or safe way to obtain data at combined angle-of-attack and angle-of-sideslip conditions. It should be recognized also that the altitude and Mach number must vary somewhat from the 1g trim condition during these maneuvers. Thus in-flight external flow conditions at the inlet which match the wind-tunnel values are transient or at best quasi-steady.

A third variable in correlating flight and wind-tunnel data for mixed-compression inlets is variation in geometry, such as spikes or ramps and bypass doors, between the model and the flight vehicle. It would be desirable to fly at the Mach number, angle-of-attack, and angle-of-sideslip condition for stabilized level flight while varying the inlet geometry; however, as the inlet geometry changes, the thrust and drag of the aircraft changes, causing the aircraft to climb or descend, or accelerate or decelerate. For most tests, especially supersonic tests, it is best to hold the Mach number constant and to accept a certain amount of altitude (Reynolds number) change. Here again, flight tests are only quasi-steady. When there is a choice, flight tests should precede wind-tunnel tests because the wind-tunnel condition can be set more easily.

An even more fundamental question related to correlating results from mixed-compression inlet tests is: What variables should be matched? Obviously, the local Mach number and local flow angles must be matched, regardless of the attendant operational problems just discussed. Internally, it would appear that matching the inlet geometries would provide corresponding test conditions; however, the flight and wind-tunnel temperatures are not the same, so the mass flows are different and therefore do not represent comparable conditions. Another approach is to set the same shock position by adjusting the bypass doors as required. Although this provides the correct primary duct flow conditions, it does not necessarily provide the corresponding bleed and bypass mass flow ratios. Still another approach is to set the same bleed and bypass back pressure ratios in an effort to duplicate the mass flows. Obviously, if on-line computation of mass flows is available, matching the mass flow would provide the best correlation of steady-state performance; however, shock position matching may be best for simulating dynamic distortions.

It is evident, then, that one-for-one correlations between flight and wind-tunnel results are not possible and that procedures must be developed for correcting the results for those variables that are not precisely matched.

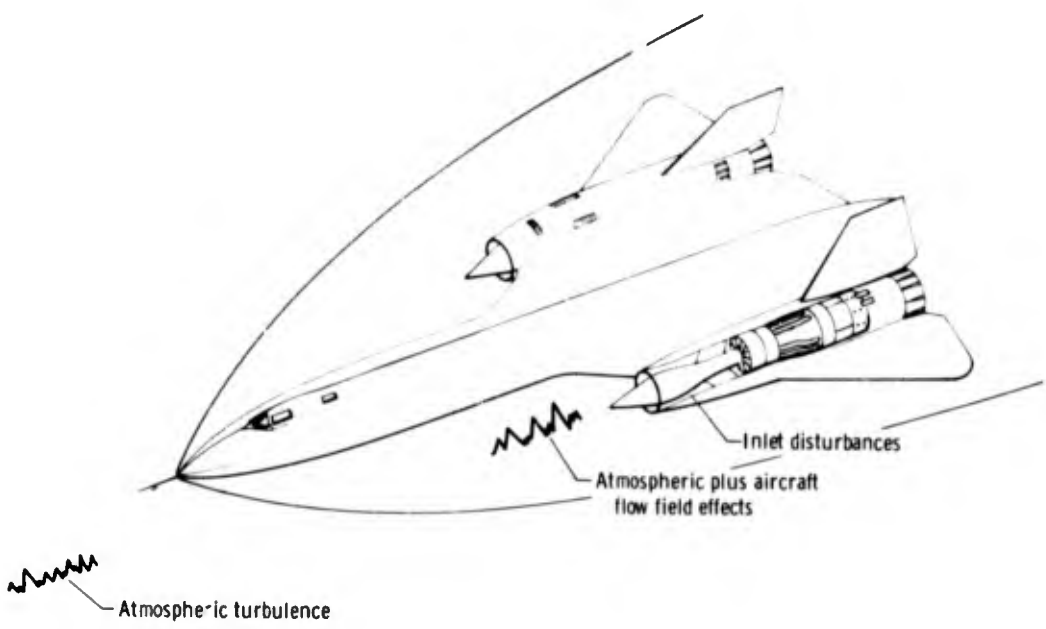

Figure 1. Disturbances which contribute to dynamic distortion in the flight environment.

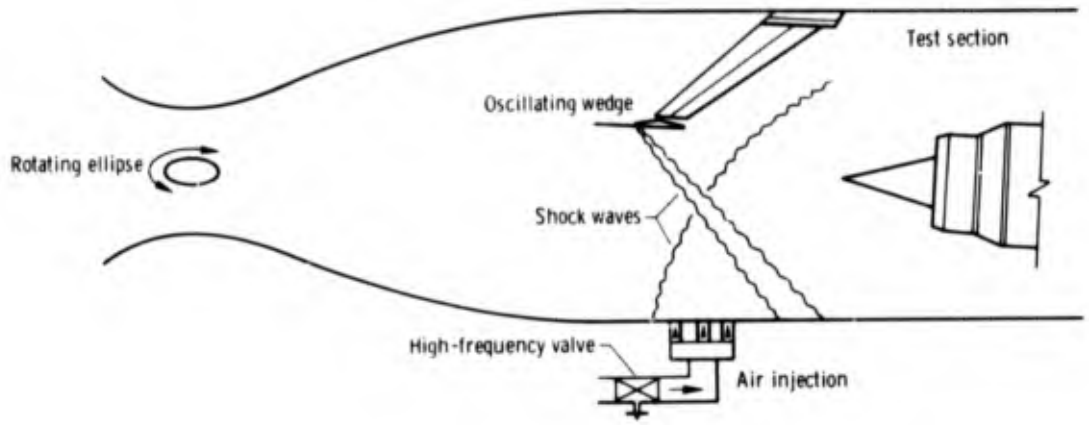

Figure 2. Free-stream turbulence simulation approaches for supersonic wind-tunnel tests.

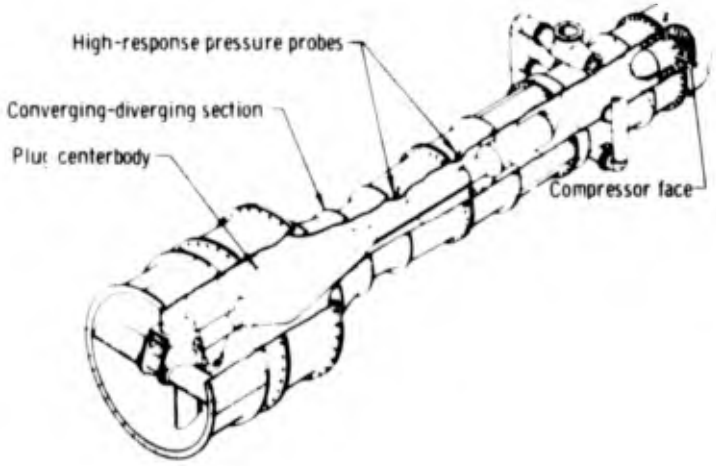

Figure 3. Choked-throat turbulence generator.

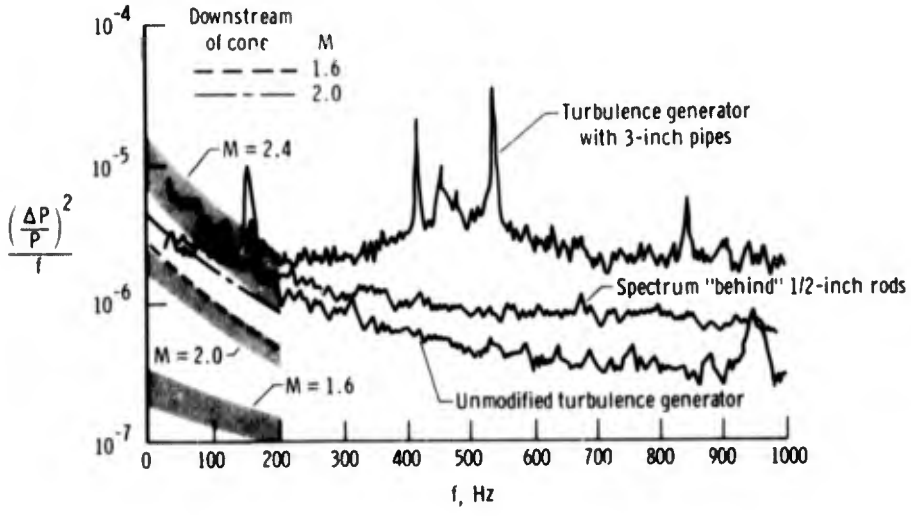

Figure 4. Comparison of turbulence generator and flight vehicle power spectral density characteristics.

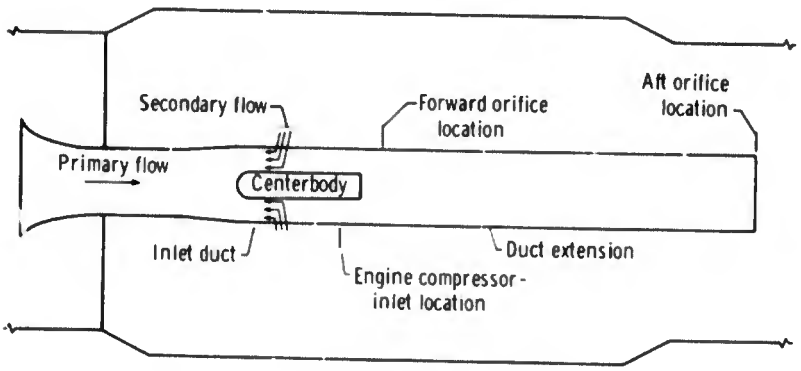

(a) Primary test installation.

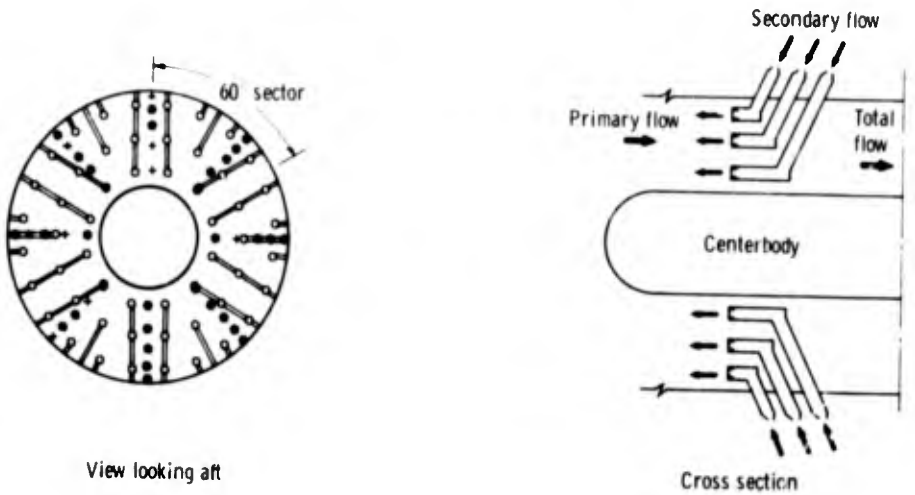

(b) Jet array.

Figure 5. Schematic drawings of pulsating jet disturbance generator.

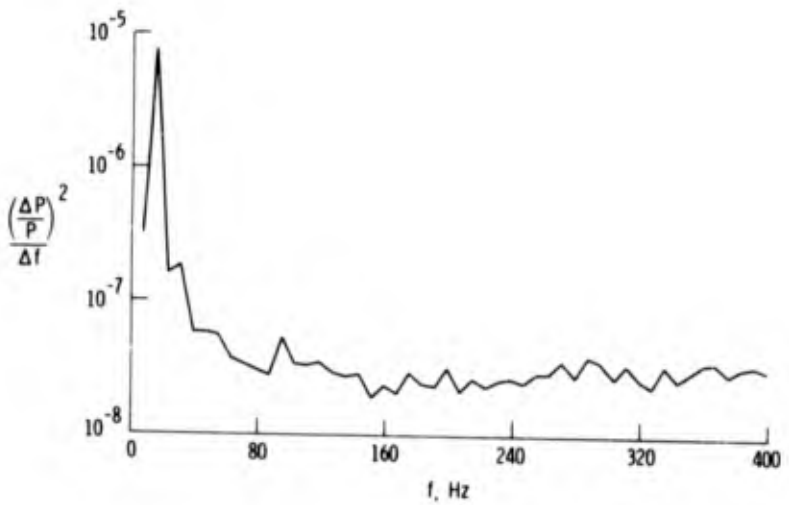

Figure 6. Power spectral density characteristics of a pulsating jet generator. Pressure oscillations induced at frequency of 15 Hz.

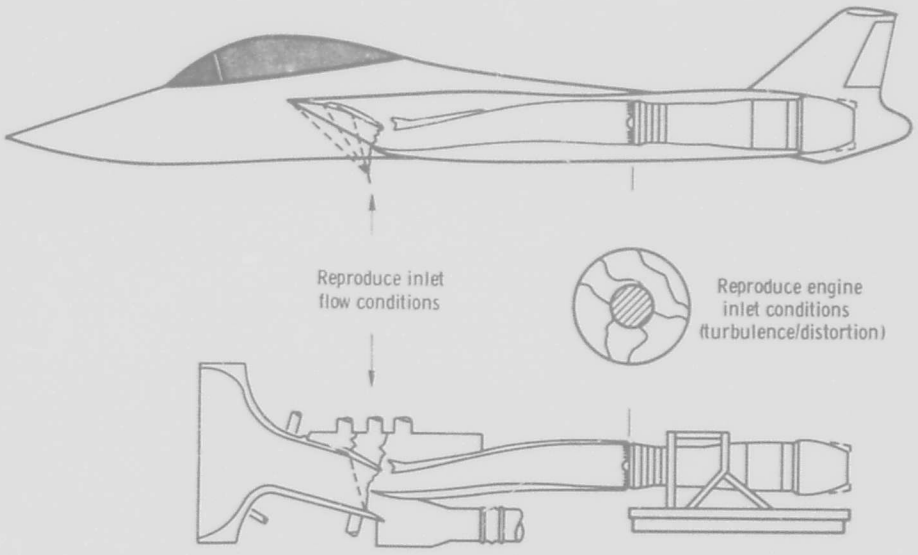

Figure 7. Inlet simulator/turbulence generator testing concept.

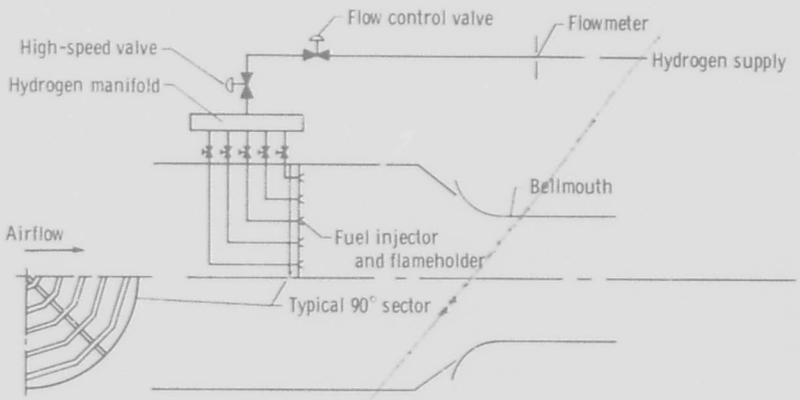

(a) Schematic drawing.

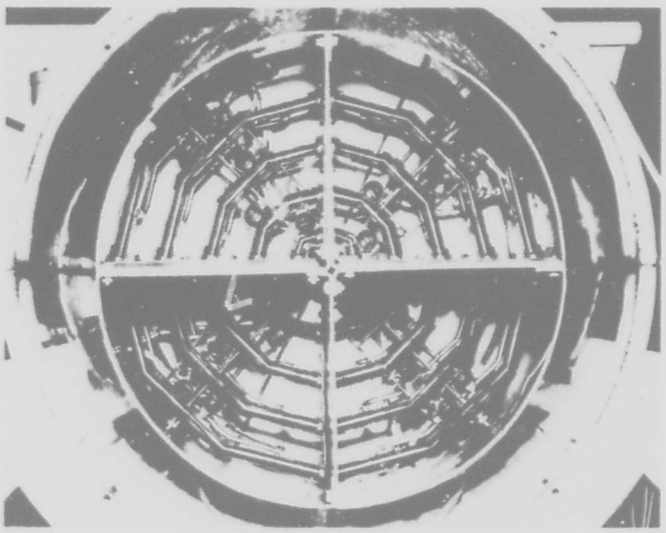

Figure 8. Hydrogen-fueled temperature distortion generator.

3.0 INSTRUMENTATION

The investigation of distortion-induced instabilities requires special instrumentation that is capable of high response as well as steady-state outputs. The parameters of primary interest are pressures, temperatures, positions or displacements, and vibrations. Rate information, such as engine speed and flow measurements, is also required for reference purposes. With this information it is possible to evaluate the temporal and spatial relationships of total pressure recovery, temperature gradients, and flow direction as well as transient response resulting from engine and inlet instabilities. These data are used to develop distortion coefficients, compressor face pressure profile maps, and time histories for transient analyses in order to gain a better understanding of dynamic interactions at the engine–inlet interface.

The following discussion treats instrumentation from the point of view of the user who is attempting to obtain valid information with which to perform his analysis.

3.1 Physical and Environmental Considerations

To make high-response measurements, the sensing elements must be as close as possible to the parameter being measured. For example, pressure and temperature must be sensed in the flow stream, and vibration and position measurements must be made at the bearing, actuator, or at particular points of interest. This requirement imposes serious size, weight, and environmental limitations on transducers because, to be in the stream, they must be within probes and rakes. The probes and sensors must be as small as possible to minimize their effect on the variable being sensed and on the flow entering the engine. Transducers used most successfully have been less than 1/8- by 1/8-inch in diameter and length, which permits conventional rake and probe designs. Mechanical problems have been experienced, such as the breaking of very fine electrical leads and hypodermic-sized reference pressure tubes leading to the differential pressure transducers. Also, transducers of this size are fragile. They must be protected against foreign objects striking the diaphragm and against physical deformations caused by mechanical pressure on the mounting retainers, which distorts the transducer and permanently modifies the calibration.

The temperature and vibration environment requires special consideration. Even in wind-tunnel and engine test facilities, a significant range of temperatures is encountered. Because of their location, the transducers are exposed directly to stagnation temperatures of 0 to 250° F or higher. Many of the transducers now in use have large temperature sensitivities for which corrections must be made. Also because of the transducer's location, vibration tests should be made with the transducer installed in the rake to assure its proper operation when probe resonances amplify the accelerations imposed at the base. For example, piezoelectric transducers have been found to be quite sensitive to vibration.

In the flight environment the problems multiply, especially for flight above Mach 2. References 10 and 11 describe F-111 flight experience with dynamic instrumentation, and reference 12 describes YF-12 Mach 3 experience. Regardless of the speed, an ever-present problem is finding space to install the propulsion flight-test instrumentation components and to route wiring through an aircraft that has been carefully designed to use every bit of internal space. Not only must the sensors be small, but the signal conditioning and recording components as well. At high speeds the problem becomes more difficult, because transducers, connectors, and wire must be inordinately large to withstand the temperature. Air-conditioned electronics bays are smaller because of limited cooling capability, and they are seldom near the propulsion system, so that long wiring runs are required. This works to the detriment of high-temperature transducers that require short, low-impedance wires to their signal conditioning units. The development of high-temperature electronics is urgently needed to alleviate this problem.

3.2 Sensing Probes

Dynamic sensing requires at least one sensor for each parameter being measured, so that a pressure commutator sampling-type system cannot be used. Thus high-frequency transient investigations necessarily involve large numbers of individual transducers and recording channels.

3.2.1 *Pressure Measurements*

Pressure measurements are of primary concern in investigations of dynamic distortion and propulsion instabilities. There are several approaches to making dynamic pressure measurements (fig. 9). The simplest and most direct is to install absolute pressure transducers in the tubes of each dynamic rake (fig. 9(a)), but this does not usually produce satisfactory results. Absolute pressure transducers must have a range of 1 or 2 atmospheres. Typically, such a transducer will have an accuracy of 2 or 3 percent and ultimately will be digitized to a 9 to 11 bit word for analysis on a digital computer. Because most inlet pressure fluctuations of interest are of the order of 2 or 3 percent of the average total pressure, these pressure fluctuations are so small that they are lost within the noise, accuracy, and resolution of the absolute pressure transducer, as illustrated in figure 10(a).

An alternate approach is to measure the small-scale pressure fluctuations with a small range differential pressure transducer and to measure the absolute steady-state pressure separately. As illustrated in figure 10(b), this provides a high resolution of the dynamic component of the pressure and a separate measure of the steady-state absolute pressure. The high-frequency absolute pressure, P_{abs}, can be obtained by adding the high-frequency differential pressure, ΔP, to the steady-state absolute pressure, P_{ss}:

$$P_{abs} = P_{ss} + \Delta P \tag{1}$$

However, dual measurements create problems. First, the number of parameters to be measured is doubled. Second, the two measurements are often spatially separated as shown in figure 9(b). If they are brought together as shown in figure 9(c), there may be interference between the probes, especially for directional flow in the plane of the two probes. If they both share the same tube as in figure 9(d), the diameter and volume of the steady-state absolute pressure tube could affect the dynamic measurements of the differential pressure

transducer. These types of probes have been used successfully in test facilities in which the steady-state pressure can be stabilized. But in flight, where only quasi-steady absolute pressures are experienced, the accuracy of the high-frequency absolute pressure measurement cannot be assured because of lag in the steady-state absolute pressure.

A third approach is to use a reference pressure system (fig. 9(e)) such as is used frequently in wind-tunnel pressure tests. The reference pressure is established at the level required to keep the low range differential pressure on scale. The high-frequency absolute pressure is obtained by adding the high-frequency differential pressure to the reference pressure:

$$P_{abs} = P_{ref} + \Delta P \tag{2}$$

This method does not significantly increase the number of parameters to be measured if a common reference pressure can be used for many ΔP transducers. A significant improvement in the accuracy of the absolute pressure measurement is possible with this method if a very precise measurement of reference pressure can be made. This improvement in accuracy can be shown by a numerical example: Assuming a 20 psi absolute pressure to be measured, the 2.5-percent absolute pressure transducer would provide a 0.5 psi accuracy. On the other hand, a reference pressure transducer with an accuracy of 0.5 percent would provide 0.1 psi accuracy plus the accuracy of the small range differential pressure transducer. Using instead a 2.5-percent differential transducer with a 6 psi range, the accuracy of the differential measurement is 0.15 psi, which, when root-summed with the reference pressure, still provides an accuracy of 0.18 psi or approximately three times the accuracy of the direct pressure measurement technique. Even better accuracy can be obtained if lower range differential transducers can be used.

In flight, where pressures change over a wide range, a floating reference pressure system has been the most successful. In this system (fig. 9(f)) a reference pressure tank is connected to a port in the duct which has a pressure that closely follows the other pressures being measured. This permits very low range differential pressure transducers to be used, thus improving the accuracy of the absolute pressure measurement. In designing the system, care must be taken to select the tank volume and tubing and orifice sizes so that the differential transducers do not go off range and the tank plus reference line pressures change at essentially the same rate for all normal and most emergency transients that can occur during flight operations.

3.2.2 *Frequency Response*

Knowledge of the amplitude and phase relationships of the input and output pressures is essential in the analysis of high-frequency data. Although this applies to the entire data acquisition system, from sensor to playback, it is especially important to understand the pneumatic response of the sensing probe and tubing ahead of the transducer. This is usually the limiting factor. As discussed in reference 13, dynamic pressure may be measured by a resonant system such as that shown in figure 11(a). If the mounting length is short and the frequencies to be measured are low compared to the resonant frequency of the mounting tube, these measurements will be reasonably accurate. However, in some types of tests, a long mounting length is required because of space or environmental restrictions of the transducer. With long mounting lengths, a pressure wave entering the tube and traveling to the transducer is reflected back toward the source and continues to oscillate in the tube. This organ pipe effect causes a tube resonance with a wavelength of approximately four times the tube length, depending on the end volume at the transducer. This causes erroneous amplitude and phase measurements, as indicated in figure 11(b). In addition, amplification of the pressure near the resonant frequency may destroy the transducer. Resonance can be prevented by providing a constant-area tube extending beyond the transducer as shown in figure 11(c). The added tube is called the termination tube, and the resulting pressure measuring system is called a nonresonant system. The amplitude response of this system is shown in figure 11(b) to be constant over a wide frequency range.

3.2.2.1 *Resonant system*

For design purposes the resonant system shown in figure 12 may be represented as a second-order differential equation if the pressure disturbance is very small compared to the average pressure, P; the tube radius, r, is small compared to the mounting length, L; the mounting length is small compared to the wavelength, λ, of the pressure oscillation being measured; and the temperature gradient along the tube is essentially constant.

The amplitude ratio, $\frac{P_{out}}{P_{in}}$, for sinusoidal inputs is

$$\frac{P_{out}}{P_{in}} = \frac{1}{\sqrt{\left[1 - \left(\frac{\omega}{\omega_n}\right)^2\right]^2 + \frac{4\zeta^2\omega^2}{\omega_n^2}}} \tag{3}$$

and the phase angle, φ, is

$$\varphi = \tan^{-1} \frac{2\zeta}{\left(\frac{\omega}{\omega_n} - \frac{\omega_n}{\omega}\right)} \tag{4}$$

where

ω = frequency, in radians per second

ω_n = natural frequency,

$$2\pi \sqrt{\frac{\gamma P}{\rho} \frac{r^2}{4\pi L\left(V + \frac{4r^3 L}{\pi}\right)}} \tag{5}$$

ζ = damping ratio,

$$\frac{4\nu}{r^3} \sqrt{\frac{L}{\pi}\left(\frac{\rho}{\gamma P}\right)\left(V + \frac{4r^3 L}{\pi}\right)} \tag{6}$$

where

P, ρ = average pressure and density of the gas within the internal volume

ν = kinematic viscosity

γ = ratio of specific heats

From Eq. (3) it is seen that an amplitude ratio of 1 is obtained when the natural frequency is high compared to the measured frequency. This occurs when tube length and volume are small and the radius is large. This configuration results in damping ratios which are typically of the order of 0.1. Because of the low damping, amplitude ratios greater than 1.2 occur when $\frac{\omega}{\omega_n}$ is greater than 0.4; however, the phase lag is less than 10°. More precise computational relationships and design criteria are included in reference 14.

Some typical experimental results for a high-temperature pressure transducer used in the XB-70 and YF-12 flight-test programs are shown in figure 13. The modifying effects of tubing length on the amplitude ratio of the basic transducer without tubing are shown in figure 13(a), and the effects of changes in tubing inner diameter are shown in figure 13(b). Figure 13(c) shows the improvement in damping due to reductions in steady-state pressure and the increased damping caused by the pressure disturbance being large compared to the steady-state pressure.

These amplitude and damping ratios shift significantly when temperatures are significantly different from those at which frequency response calibrations were made. These shifts are caused by changes in the speed of sound and viscosity with temperature, which in turn cause changes in the natural frequency and damping ratio, as shown in the following relationships:

$$\omega_n = \omega_{n_o} \sqrt{\frac{T}{T_o}} \tag{7}$$

$$\zeta = \zeta_o \sqrt{\frac{T}{T_o}\left[1 + 0.0014\left(T - T_o\right)\frac{P_o}{P}\right]} \tag{8}$$

where

ω_{n_o}, ζ_o = calibration natural frequency and damping ratio, respectively

T_o, P_o = calibration temperature and pressure, respectively

From these relationships, it is apparent that an increase in temperature increases the damping and improves the amplitude ratio of short tubes (i.e., brings them closer to 1.0). For aircraft that fly at Mach 3, the corrections (Eqs. (7) and (8)) can be as great as 40 or 50 percent and cannot be ignored when interpreting results.

3.2.2.2 *Nonresonant system*

The nonresonant system, sometimes referred to as the "infinite line system," consists of a mounting tube (fig. 11(c)) of the order of 20 inches in length with a transducer mounted on as short a "T" section as possible, followed by a termination tube approximately 50 feet long. If the termination tube is infinitely long, there will

be no resonance because the pressure pulse entering the tube will continue to travel indefinitely. As a wave travels through the termination tube, attenuation occurs because of viscous effects. This attenuation may be high enough that a reflected wave would not cause significant error and an intermediate-length termination tube could be used. The total error for the nonresonant tube system is a combination of the error due to attenuation and that due to reflection from the closed end of the tube. For the same transducer mounting length, the total error for the nonresonant system is less than the resonance error caused by terminating the tube at the transducer.

The idealized requirements for a nonresonant system are:

(1) The cross-sectional area must be constant at all points in the system.

(2) The tube internal passage must be smooth because sharp edges, burrs, steps, voids, or discontinuities create standing waves, resonance, and dynamic distortion.

(3) All joints must be carefully made to eliminate pressure leaks.

In practice, it is necessary to compromise these requirements to comply with the installation situation and to permit the use of conventional tube fittings where maintenance and removal is necessary. The effects of tube diameter, mounting length, termination tube length and enclosures, area discontinuities at the transducer, and discontinuities that occur in transitions from stainless steel to flexible tubing are discussed in reference 13. To summarize, frequency response improves with increased tube diameter and decreased mounting length. Termination tube lengths of 20 feet are sensitive to end closures (opened, closed, and orificing), but 40-foot termination lengths are not; however, closed lines cause a phase reversal. Nominal discontinuities at the transducer and at fittings and transitions to flexible tubing have negligible effect on the frequency response. Data obtained by Vernon D. Gebben of the NASA Lewis Research Center indicate some undesirable wave distortions when the mounting length is greater than half the wavelength (fig. 14).

A tubing mockup of a typical flight-test high-temperature rake installation was tested at the NASA Flight Research Center. The mockup included two right-angle turns in 0.210-inch-inner-diameter lines with the transducer located 20 inches downstream of the port and behind two right-angle bends in the 0.210-inch-inner-diameter tube. Figure 15 shows effects of terminated and nonterminated system response for a 10-percent disturbance at 15 psia, as seen by comparing figures 15(a) and 15(b). With the tube terminated at the transducer (fig. 15(a)), the primary amplitude ratio at a resonance of 10 occurs at 160 hertz followed by typical harmonics; whereas figure 15(b) shows the response to the same input when a 50-foot termination length is added. Only minor disturbances of less than 10 percent in amplitude remain. These minor resonances were not caused by the turns, for the same result was obtained when the test was repeated with 20 inches of straight tubing ahead of the transducer. The resonances disappear when the steady-state pressure is 5 psia (fig. 15(c)), but they do not increase when the pressure is increased from 15 psia (fig. 15(b)) to 25 psia (fig. 15(d)).

One major problem which prevents extensive application of nonresonant line techniques in flight is the storage space required for the termination tubing. Also, large temperature gradients which adversely affect the response can exist along the length of the tube. It may be possible to reduce the termination length by gradually reducing the tubing diameter to zero; however, neither this approach nor the effect of the termination length on the phase shifts has been verified experimentally.

3.2.3 *Frequency Response Testing*

Because of the uncertainties associated with the pneumatic response of pressure probes, it is essential that proposed designs be evaluated thoroughly in the laboratory and that the results be verified when the probes are installed to check both the probe and the data acquisition system. Several types of devices have been used (refs. 15 to 18) to check the frequency response. Several of these are illustrated in figure 16.

The piston type of device is simply a sealed piston driven by a shaker motor. Reference transducer measurements are compared with measurements from the test installation and transducer. The inlet pressure modulation device operates like a siren, in which a rotating disc with a series of holes modulates the pressure supplied to a test chamber containing reference and test transducers. The frequency is controlled by the rotational speed. The test chamber must be carefully designed to prevent unwanted resonances; however, it is small and light, thus lending itself to portable on-site applications.

The resonant fluid oscillator or whistle (ref. 18) is a resonant tube which is excited by turbulent air supplied at one end. The frequency is controlled by a movable piston at the opposite end. Three taps are provided at several stations along the tube. The tap used depends on the tuning piston position and the location of resonant nodes. This system is noisy and must be isolated from the operator.

A pressure generator must be capable of producing sinusoidal pressure disturbances that are a large fraction of the average pressure. Mechanical devices like the piston and siren meet this requirement at low frequencies, but they fall off significantly at high frequencies, as shown in figure 17. Resonant fluid oscillators perform well at very high frequencies, but have no low-frequency capability. Hence, some combination of the two types of devices is normally used.

3.2.4 *Compressor Face Rakes*

Compressor face rakes are usually designed for particular applications on the basis of the engine–inlet geometry, the technical objectives, and the transducer size, limitations, and operating characteristics. For example, the rake shown in figure 18(a) was designed for a frequency response of 400 hertz using a semiconductor strain gage transducer. The offset was provided to prevent foreign objects from striking the fragile diaphragm of the transducer. The rake shown in figure 18(b) was designed with a sliding piston that allowed zero pressure levels to be established so that corrections could be made for zero shifts of the transducer with changes in temperature. The rake shown in figure 18(c) was designed for a high-temperature flight application where transducer size could not be reduced, thus requiring a very large rake.

3.2.5 *Flow Direction Sensing Probes*

It has been suggested that time-variant flow angularity at the compressor face may be more important than time-variant total pressure. Flow angularity effects have not been extensively investigated because as many as five high-response pressure measurements are required to determine the flow direction and velocity at a single point. In addition, the phase relationships between these five measurements must be known. Several probes suitable for angularity measurements are shown in figure 19. Details of their design and calibration are given in references 12 and 19 to 21. A high-response hemispherical head probe will be used in the YF-12 flight tests. The response of this probe is shown in figure 20.

In the future the development of the laser doppler technique may improve the prospects for extensive evaluation of flow direction and velocity at the compressor face. This technique has the inherent advantage that it does not require the installation of a rake or probe in the stream.

3.2.6 *Shock Position Sensing Probes*

The position of the shock in the inlet can significantly affect the dynamic distortion observed in supersonic inlets. This is particularly true of inlets that utilize internal as well as external compression.

Shock position can be determined by sensing the pressure, temperature, or density discontinuity across the shock; however, this requires many measurements. Pressure measurements are the usual means of determining the shock position. If it were not for the interaction between the shock wave and the boundary layer, it would be easy to measure shock position; however, the sharp pressure rise across the shock causes the boundary layer to thicken or separate, as shown in figure 21. This makes it possible for high pressures to be transmitted upstream through the boundary layer so that a gradual rise in static pressure is measured rather than the abrupt jump predicted by theory.

Two static pressure shock position sensors that have been used with some success are shown in figure 22. The stiletto-type probe shown on an F-111 inlet in figure 22(a) was aft-mounted and protruded through the shock wave. Lead shot was used to damp the oscillations of the probe. The raised shock sensor strip (fig. 22(b)) was wall-mounted on a strut to isolate it from the duct boundary layer. Both sensors minimize the boundary layer thickness and thus measure a more abrupt pressure rise between pressure taps than wall statics. Both steady-state and high-frequency pressure measurements have been made using these sensors. Total pressure probe shock sensors are not desirable for shock position measurements because they disturb the supersonic stream when they protrude through the shock.

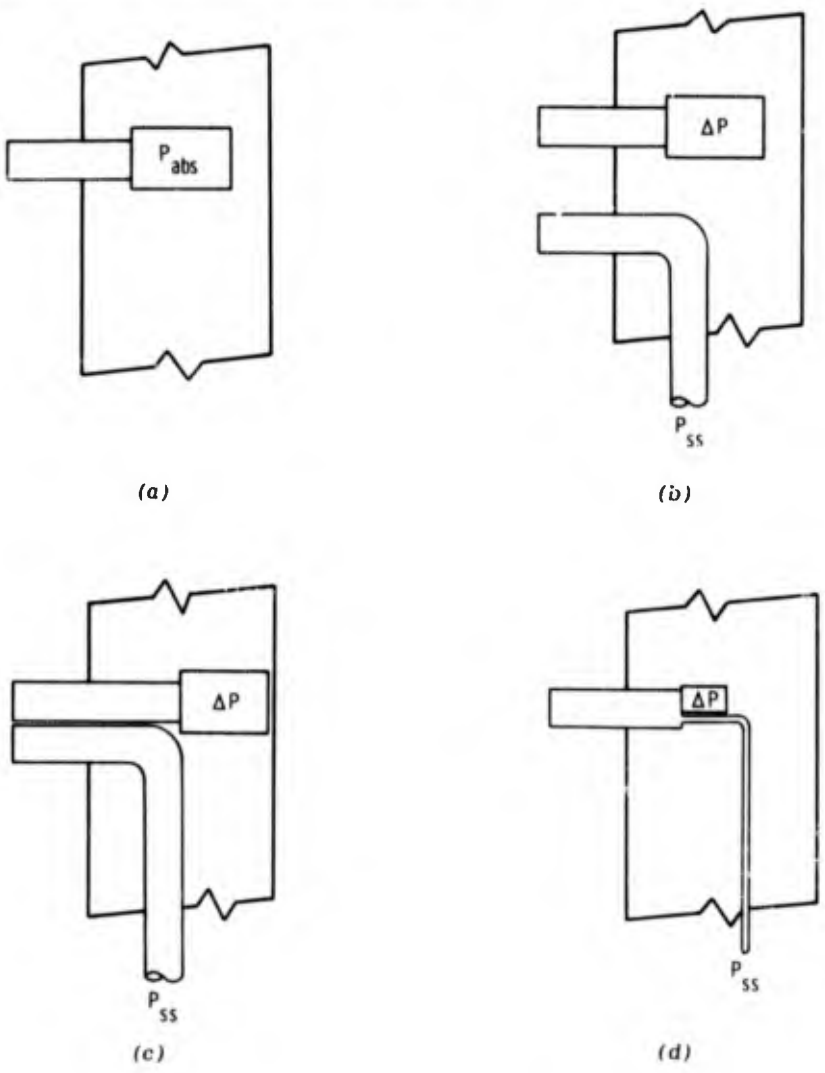

Figure 9. Schematic drawings of dynamic pressure measurement approaches.

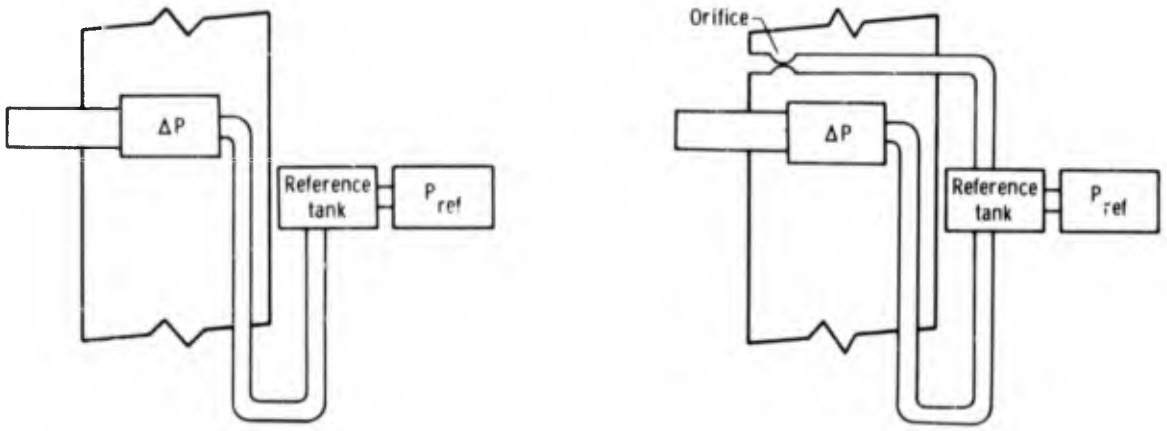

(e) (f)

Figure 9. Concluded.

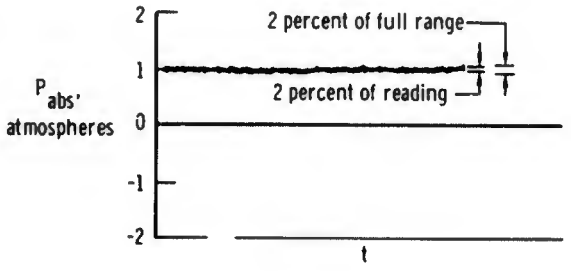

(a) Absolute pressure transducer.

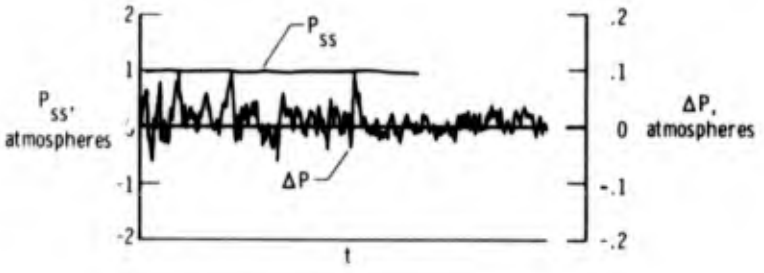

(b) Differential plus steady-state pressure transducers.

Figure 10. Illustration of dynamic pressure sensing techniques.

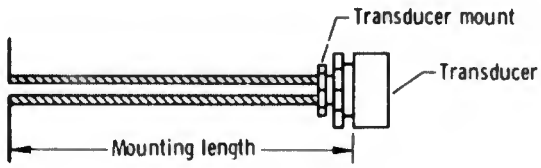

(a) Resonant system.

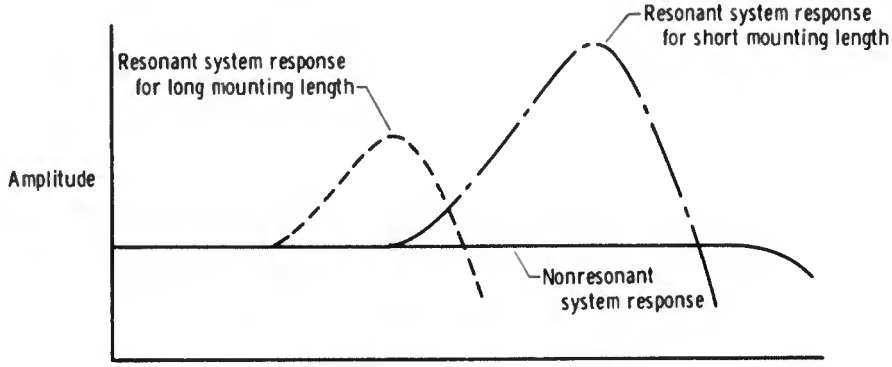

(b) Typical amplitude responses.

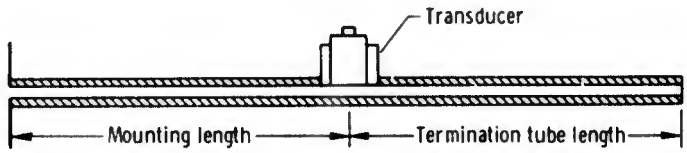

(c) Nonresonant system.

Figure 11. Resonant and nonresonant pressure sensing systems.

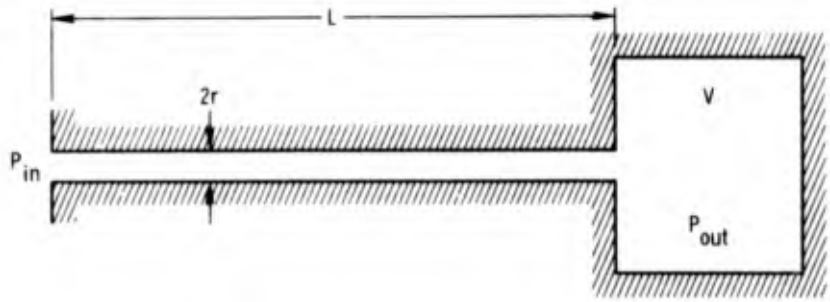

Figure 12. Diagram of typical resonant system variables.

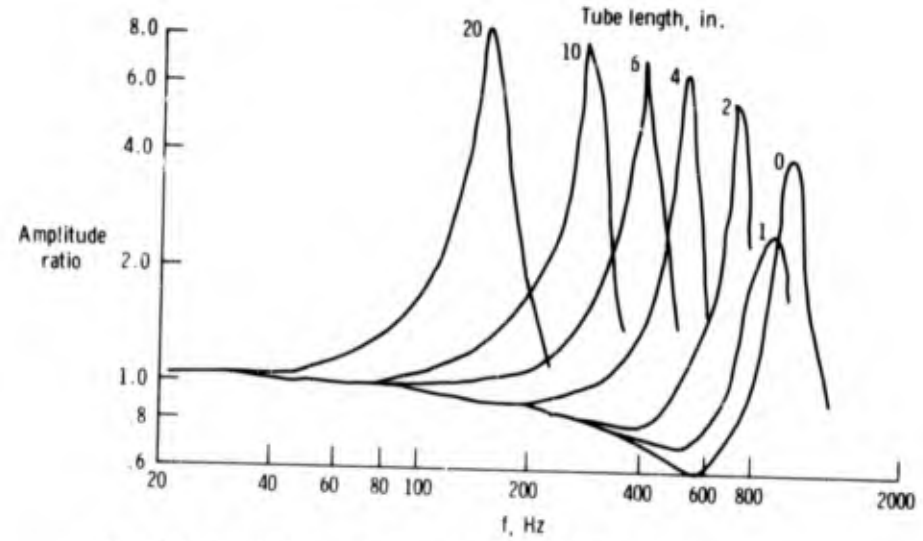

(a) Effect of tube length. P_{ss} = 25 psia, 0.210-in. tube diameter.

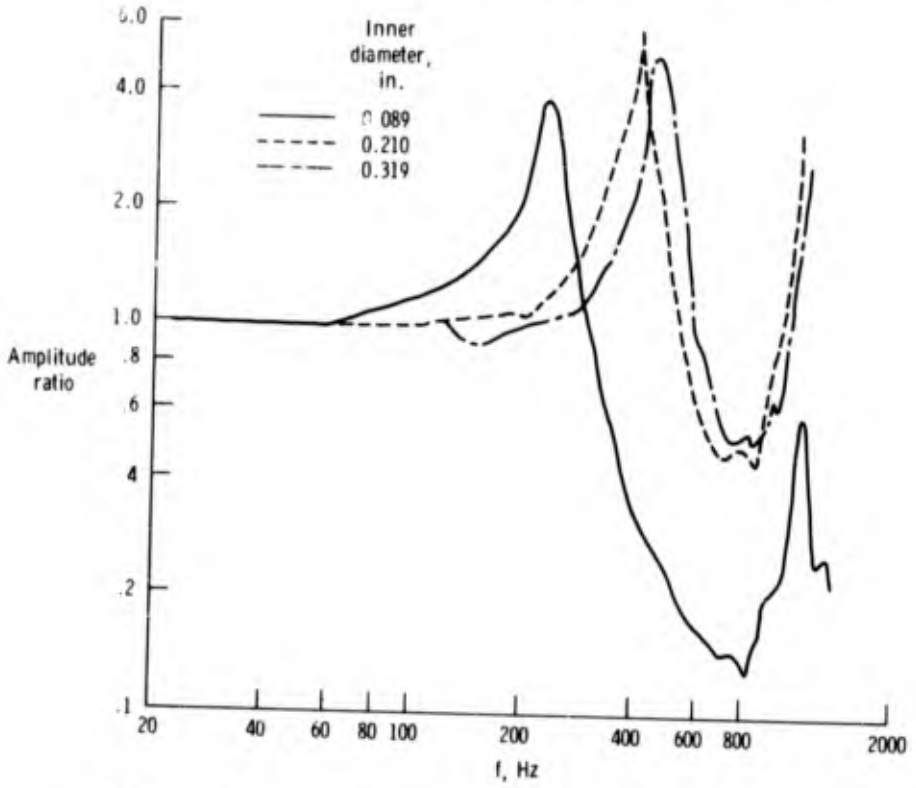

(b) Effect of tube diameter. P_{ss} = 25 psia, 6-in. tube length.

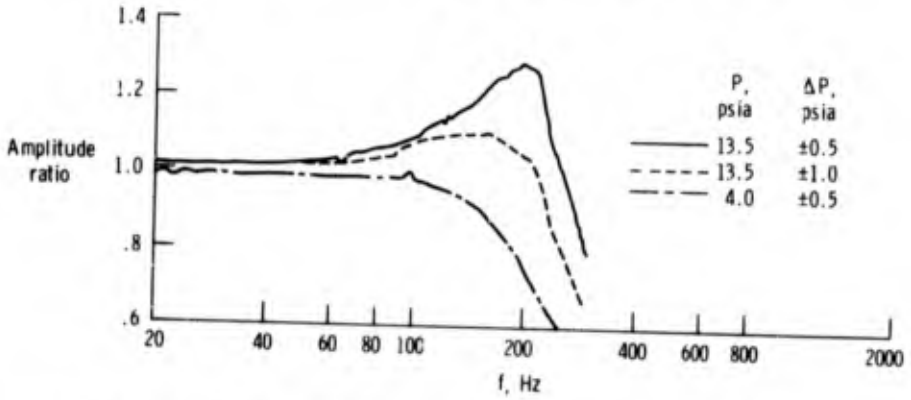

(c) Effect of steady-state pressure. 0.0385 in. inner-diameter tube, 6.6-in. tube length.

Figure 13. Effects of key variables on dynamic response of resonant systems.

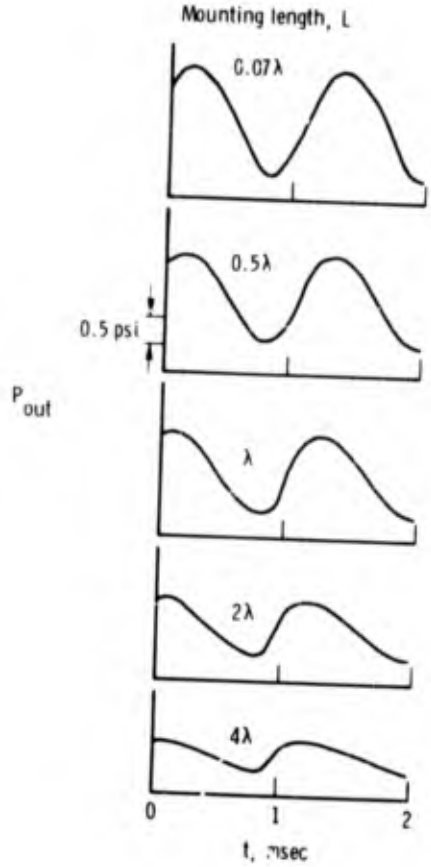

Figure 14. Effect of mounting length on waveform of nonresonant system. f = 900 Hz; P = 1.0 psi at L = 0; λ = 14.31 in.; tube inner diameter = 0.08 in.

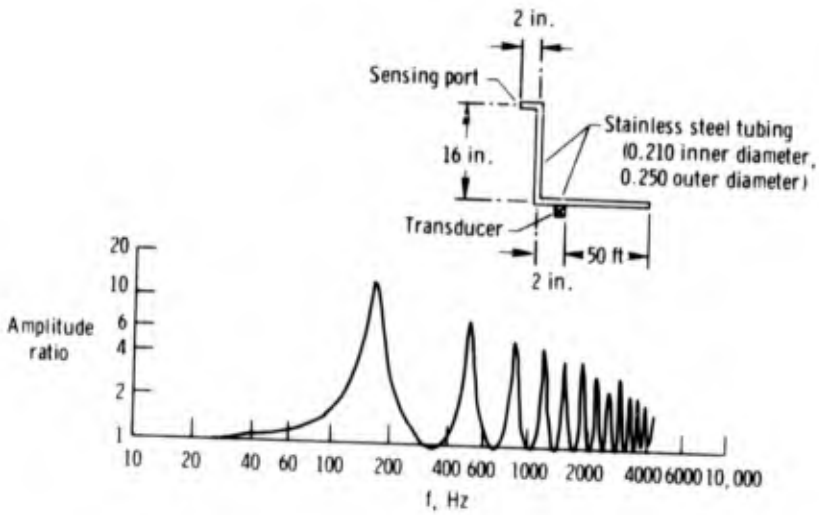

(a) Resonant system terminated at the transducer. Static pressure level = 15 psia, dynamic pressure input = ±1.5 psi.

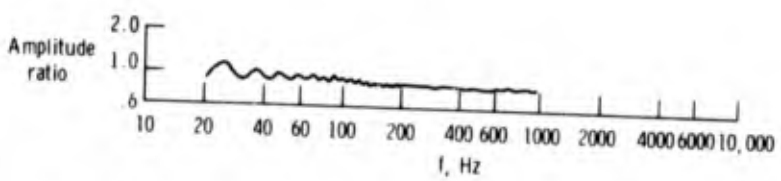

(b) Nonresonant system. Steady-state pressure level = 15 psia, dynamic pressure input = ±0.15 psi.

Figure 15. Comparison of dynamic frequency response of nonresonant and resonant systems.

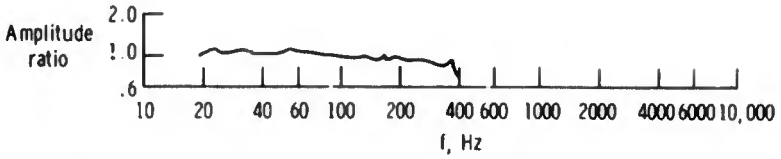

(c) Nonresonant system. Steady-state pressure level = 5 psia, dynamic pressure input = ±0.05 psi.

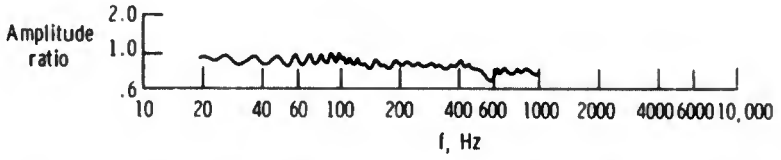

(d) Nonresonant system. Steady-state pressure level = 25 psia, dynamic pressure input = ±0.25 psi.

Figure 15. Concluded.

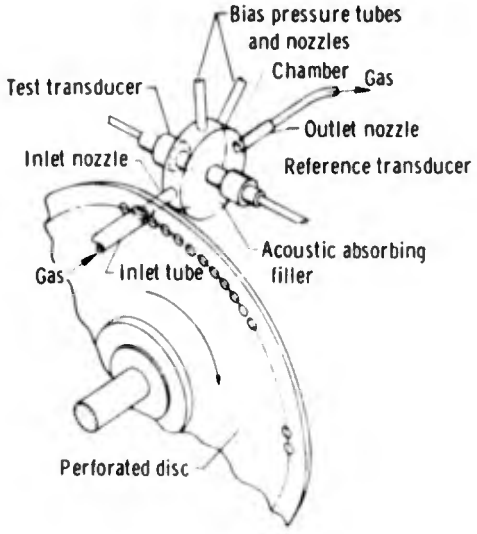

Pressure modulation type

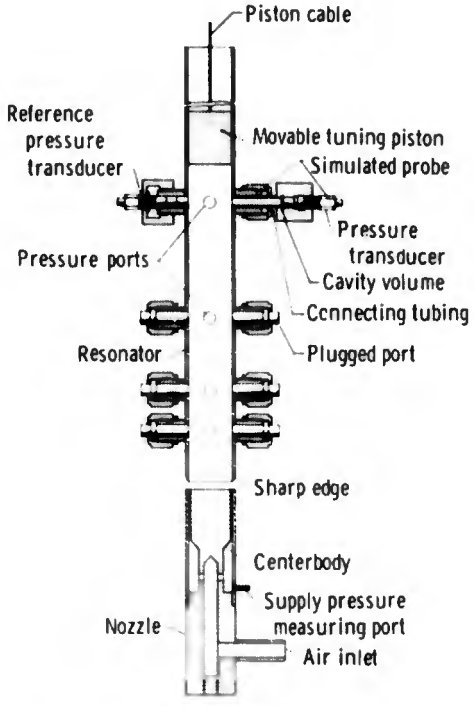

Resonant fluid oscillator

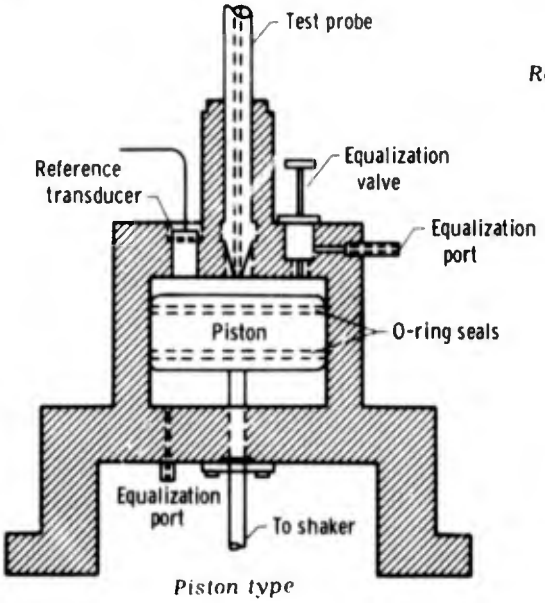

Piston type

Figure 16. Sinusoidal pressure generators.

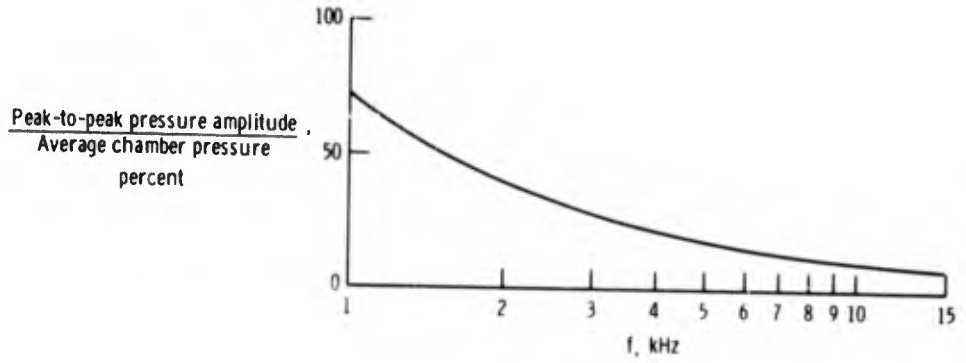

Figure 17. Sinusoidal pressure generator characteristics.

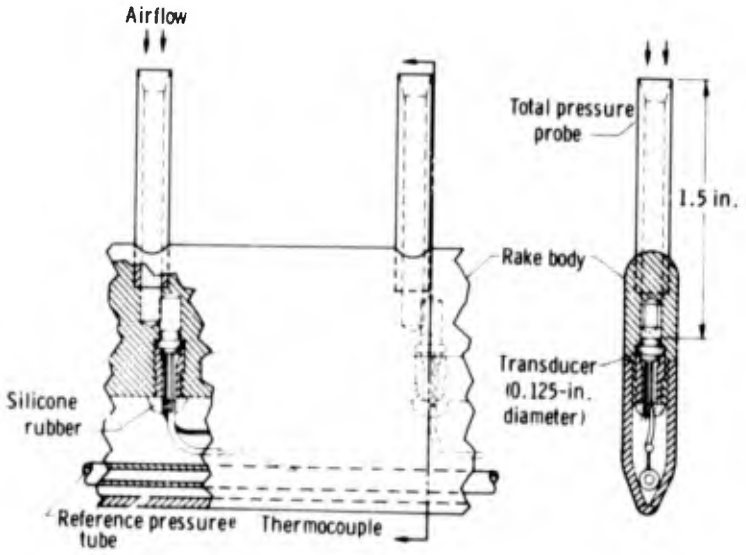

(a) Conventional compressor face rake.

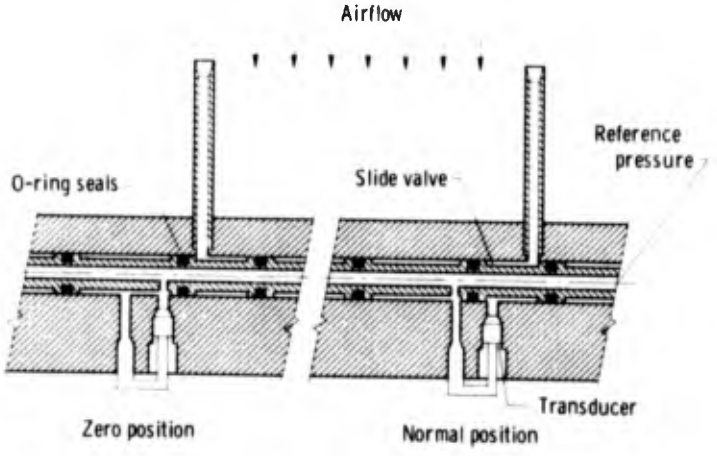

(b) Pressure-sensing rake with in-flight nulling mechanism.

Figure 18. Compressor face rakes.

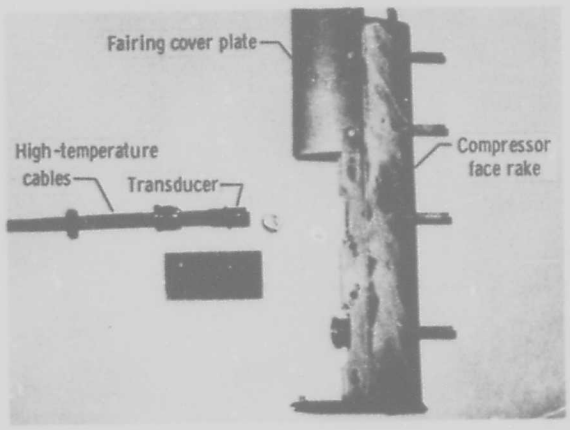

(c) Kaman rake.

Figure 18. Concluded.

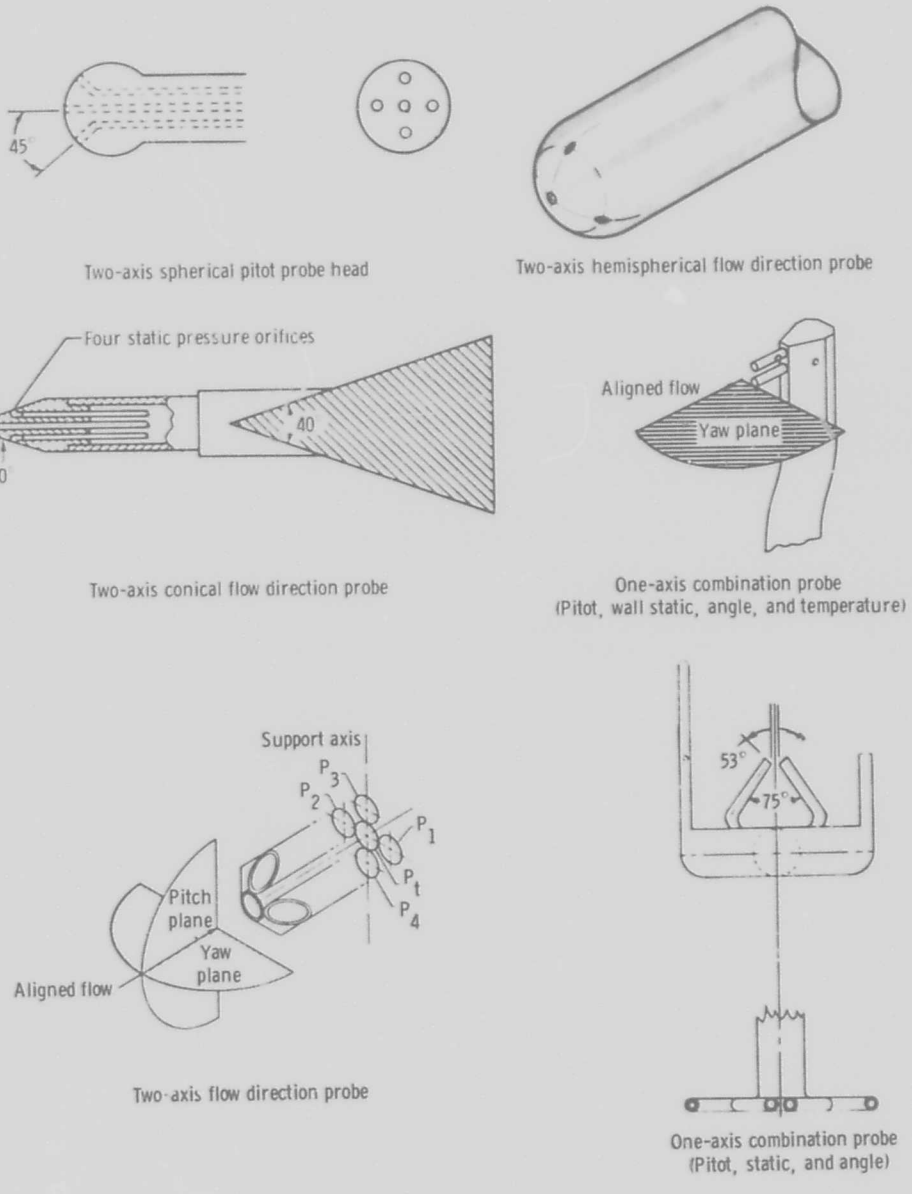

Figure 19. Flow direction sensing probes.

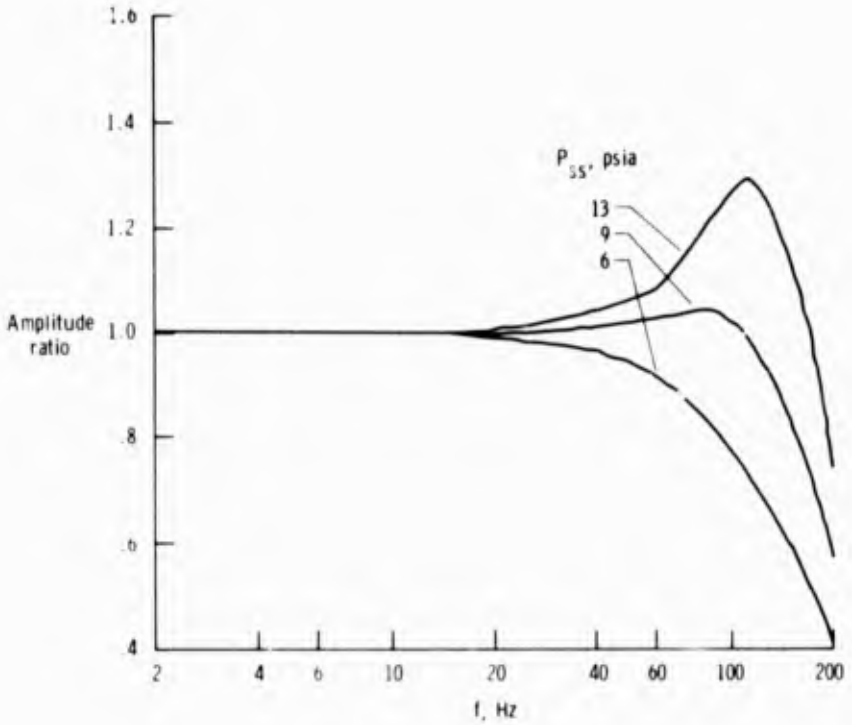

Figure 20. Frequency response of hemispherical flow direction probe. ΔP = 2 psi.

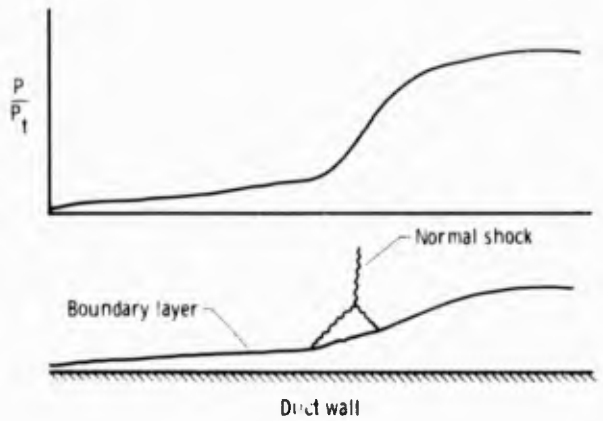

Figure 21. Boundary layer growth and sensed static pressure profiles beneath a normal shock wave.

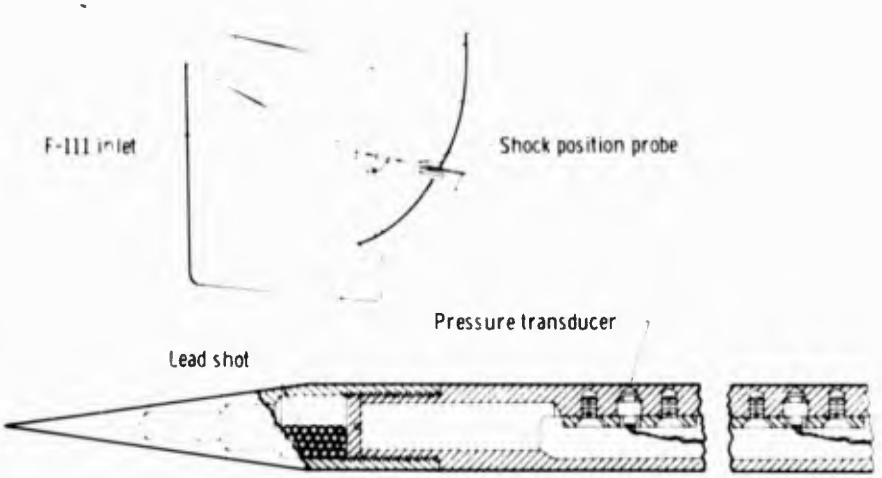

(a) Stiletto type.

Figure 22. Shock position sensors.

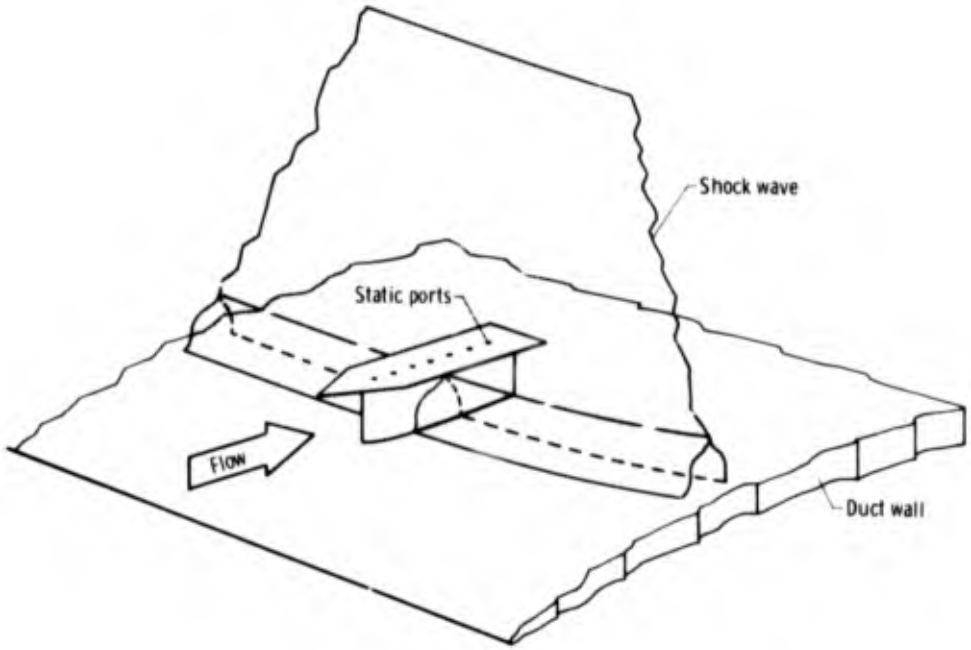

(b) Raised shock sensor strip.

Figure 22. Concluded.

3.3 Transducers

Many types of transducers have been used to investigate distortion-induced instabilities. These transducers utilize numerous measuring techniques to provide the required accuracy and response. For pressure and position measurements the most suitable techniques involve the use of strain gages (bonded, unbonded, and semiconductor), linear variable differential transformers, and capacitance, piezoelectric, and eddy current concepts. Potentiometers and synchros are suitable only for measurement of large displacements. Temperature sensors most commonly used are thermocouples, resistance conductors or semiconductors, radiation pyrometers, and fluidic resonators. Except for the fluidic resonator and eddy current displacement devices, the principals of operation of these devices are described in detail in reference 22.

3.3.1 *Fluidic Temperature Sensor*

The fluidic temperature sensor operates on the principle of an edge-tone resonator. Turbulent flow entering the inlet of the sensor (fig. 23) generates a tone with a frequency, f, that is proportional to the acoustic velocity, a, and the length of the acoustic path, L:

$$f = \frac{a}{4L} = \frac{\sqrt{\gamma RT}}{4L} = K\sqrt{T} \tag{9}$$

where

$K = \sqrt{\frac{\gamma R}{4L}}$, a constant which depends on the gas composition and the sensor geometry. Because the gas whose temperature is being measured must flow through the sensor, a certain differential pressure must exist before the sensor will operate. Typically, the sensor will begin to oscillate at pressures as low as 1 psid; however, good accuracy (±1.5 percent) is not obtained until a pressure of approximately 4 psid is reached.

A major feature of the fluidic temperature sensor is its fast and accurate transient response. The dynamic response transfer function can be represented by two first-order lags in the following form:

$$\frac{K_1}{1 - \tau_1 s} + \frac{K_2}{1 + \tau_2 s} \tag{10}$$

The first term represents the time required to flush the old gas from the sensor, and the second term results from the thermal inertia of the sensor. Typical values for these parameters are $K_1 = 0.75$, $K_2 = 0.25$, $\tau_1 = 0.03$ second, and $\tau_2 = 6.7$ seconds.

Typical sensor output responses to a step change in input temperature are shown in figure 24. The output can be compensated to provide a 0.05-second response over the complete operating range of the sensor with a simple lead-lag circuit. The response is seen to be considerably better than that of an exposed junction chromel-constantan thermocouple having a bead diameter of 0.03 inch. This response is possible because the sensor body is mounted directly in the hot gas stream.

Thermocouples and resistance wire temperature sensors with response similar to the fluidic sensor can be built, but they are short lived because they must be constructed of very fine wire that does not hold up in the severe test environment of aircraft inlets and engines.

3.3.2 *Eddy Current Displacement Sensor*

The eddy current displacement device senses the impedance change due to the generation and decay of eddy currents within a conductive plate. The conductive plate shown in figure 25 experienced a motion in response to the desired measurand (e.g., pressure, distance, force, acceleration). The coil, which is driven by an oscillator, induces eddy currents in the plate. The electromagnetic coupling between the coil and the conductive plate depends on the distance by which they are separated. Thus a measure of this coupling is a direct indication of the distance, which in turn is related to the measurand through a spring constant of the diaphragm material. The coupling is sensed as a change in the driving power of the generator in response to the load of the effective resistance and inductance of the coil. Movement of 10^{-8} inches can be resolved in this manner.

Non-contact measurement of the position of any conducting material can be made using this concept (e.g., bearings, compressor tip clearance, and components internal to controls and actuators) without drilling holes or otherwise jeopardizing the integrity of the housing. However, practical power limitations restrict its use to distances less than 1/4 inch.

The eddy current principle is closely related to that used in variable reluctance transducers (ref. 22), in that a change of magnetic coupling between a coil and a deflection member is used. It differs in that no ferromagnetic materials are used, and electromagnetic coupling is between a simple coil and the eddy currents produced by it in a nearby conductor.

In the actual construction of an eddy current transducer, two coils are used: One experiences the impedance change due to the measurand, and the other compensates for undesired environmental effects. Figure 26 illustrates schematically three types of transducers, each with two coils. Each coil is used as a component in an arm of an impedance bridge. Since two coils and a bridge are used, the transducers are insensitive to nuclear radiation and temperature.

A schematic diagram of the associated circuitry is shown in figure 27. An oscillator is used to excite both coils through a driver amplifier. An error signal from the bridge is amplified and used by the demodulator for phase detection. The detected signal constitutes an analog output that is proportional to a change of the measurand.

Transducers employing this technique have been used successfully over the wide temperature variations that occur in flight tests (ref. 12) of supersonic aircraft; however, they tend to be larger (1/2 inch in diameter) than desired, especially for pressure transducers which must be installed in rakes (fig. 18(c)). For lower temperature applications (less than 175° C), miniature pressure transducers (0.125 inch in diameter) with semiconductor strain gages have been used successfully; however, they experience zero shifts with temperature and have fragile diaphragms which must be protected from foreign objects carried in the airstream. Figure 28 shows three types of semiconductor sensing arrangements that are all incorporated in a bridge-type sensing circuit. In the first, the diaphragm itself is fabricated of semiconductor material which is part of the sensing circuit. In the others, the diaphragm is metal and a semiconductor post or bonded strain gage is used to sense displacement of the diaphragm.

Pressure transducers with unbonded wire strain gages have good sensitivity and output but too frequently fail because of vibration and shock, which may be as great as 100 g in an inlet during stalls and unstarts. Bonded strain gage transducers are more rugged but less sensitive. Although piezoelectric transducers are rugged, they do not provide a steady-state output and they tend to be unpredictably sensitive to vibration. Thus the semiconductor strain gage has been preferred for moderate temperature applications, and the eddy current and piezoelectric principles have been used at high temperatures (ref. 12).

3.3.3 *Precision Pressure Measurements*

Great advancements have been made in recent years in precision measurement of absolute pressures. It is not unusual to find devices capable of measuring to within 0.01 to 0.05 percent over the full instrument range. Transducers of this quality are being used frequently to measure reference pressures and in applications where frequency response is not required. All transducers of this type have digital encoders with a direct binary output. The earlier ones had encoders on the output shaft of a null-balance-type servo system. The response of these units was generally limited by the maximum drive rate and inertia of the gear train. Recently, more accurate transducers use frequency sensing concepts that can be electronically counted without resorting to measuring mechanical motions or turns of a servosystem. These transducers have a higher response (5 to 10 Hz) that is limited only by the counting and update cycle and the length of the tubing leading to the units. Normally, these devices must be kept in a temperature-controlled environment and are large (0.5 ft^3) and expensive. This limits their application to only the most critical measurements. Since the accuracy of these transducers approaches the accuracy of primary laboratory standards, they must be calibrated with extreme care.

3.4 Recording Systems

Analysis of distortion-induced instabilities requires permanent records for data processing after the tests. The recording system must be capable of reproducing the waveforms at very high frequencies and with good accuracy and resolution. Only magnetic tape or disc recording systems can meet these requirements. However, great care must be taken to ensure that signal conditioning, modulation, and multiplexing techniques do not distort the result when it is processed through the required analysis routines. It is extremely important that the investigator thoroughly understand the strengths and weaknesses of the recording system used.

A typical magnetic tape system accepts test data in analog form from transducers, converts the signal from analog to frequency modulation (FM) or pulse code modulation (PCM), multiplexes the FM or PCM signals, and records the multiplexed signals on a 14-track, 1-inch magnetic tape. Coded time-of-day signals, voice comments, and calibration and reference signals are mixed with the test data and recorded on tape. Details on these systems are included in reference 24.

3.4.1 *Magnetic Tape Systems*

The tape transport mechanism in a magnetic tape system consists of a tape drive system, record head assembly, and control circuitry. The unit is capable of recording 14 simultaneous tracks of data on 1-inch magnetic tape, at any one of six preselected tape speeds. Tape speeds of $1\frac{7}{8}$, $3\frac{3}{4}$, $7\frac{1}{2}$, 15, 30, and 60 inches per second may be selected.

A simplified form of tape transport is shown in figure 29. The supply reel feeds out tape and provides hold-back tension to ensure intimate contact of the tape with the heads. The tape transport is fitted with a motor for rewinding the tape and a brake to decelerate the reel rapidly and smoothly when the tape motion is stopped. Hold-back tension can be obtained by energizing the rewind motor in an opposing direction, by applying the brakes, or by a combination of the two. The inertia roller is connected to a flywheel and smooths out variations in tape speed which could be caused by uneven torque or motion of the supply reel.

The capstan is the most critical element in the tape transport because it directly controls tape speed. Any eccentricity or bearing irregularities of the capstan and shaft would introduce corresponding periodic speed variations in the tape.

Speed errors will also be introduced by variations in tape tension caused by the transition from a full to an empty reel, or they may be the result of rapid changes in tension caused by uneven winding of the tape on the reels. These speed variations are usually expressed in terms of wow and flutter. These are terms established in the audio recording field and generally used in instrumentation recording as well. Wow is defined as a momentary variation in tape speed that occurs at a rate less than 8 hertz, and flutter is defined as a momentary variation in tape speed that occurs at a rate greater than 8 hertz but generally not exceeding 100 hertz. Most recorders contain their own precision frequency source to ensure precise tape speeds, independent of the varying voltages and frequencies of the power supply. Misalignment of the tape guides and skew of the tape across the heads also cause flutter. Flutter is the dominant cause of error in FM systems.

The advantages of a magnetic tape system over other types of recording systems are:

(1) Magnetic tape has a wide frequency range from steady state to megacycles.

(2) Tape has low inherent distortion characteristics. In contrast to a galvanometer or other mechanical devices, overloading does not permanently damage the hardware.

(3) The signal information is preserved in its electrical form, so that the original event can be recreated. This lends itself to automatic reduction of data.

(4) Recordings made on tape are available for immediate playback, with no time lost in photographic processing.

(5) The tape itself is reversible, since it can be erased.

(6) The tape can be played back thousands of times, which permits every bit of useful information to be extracted from the recording.

(7) Tape provides multiple channels of information. Hundreds of channels of information may be recorded simultaneously using various multiplexing techniques (ref. 24).

(8) Tape provides the ability to alter the time base. This permits events to be recreated on playback either faster or slower than they actually occurred.

3.4.2 *Signal Conditioning and Modulation Techniques*

The primary purpose of signal conditioning is to make the output signal of a transducer compatible with the recording or modulation equipment, or both. It is also frequently used to provide some means for calibrating the instrumentation. A requirement for signal conditioning is usually generated by the type of transducer used in an instrumentation system.

Signal conditioning equipment can be designed to serve a number of purposes. Some of the more common functions are as amplifiers, filters, balance networks, FM subcarrier oscillators, and calibration circuits.

Modulation, as used here, means varying an electrical signal so that the variations convey the data in a form that is readily acceptable for recording on magnetic tape or for telemetering to a remote station. The two most practical methods are pulse code modulation and frequency modulation. Pulse code modulation represents the output data by a number composed of a series of discrete codes which are proportional to the voltage input. The data are time-sampled and recorded in digital form as a series of binary digits. In frequency modulation, changes in frequency convey the data rather than changes in amplitude. A voltage-controlled subcarrier oscillator converts changes in the data intelligence carried in the amplitude of the input signal to changes in frequency. An FM system is frequently used when a frequency response is required that is beyond the limits of the conventional PCM systems.

Even though these modulation techniques permit transmission and magnetic recording of data, the problem of simultaneously handling a large number of signals remains. That is, it must be possible to record more than one signal per track. These data input signals must be combined in such a way that the composite signal may later be separated again into the individual data input signals.

3.4.3 *Multiplexing*

There are two distinct techniques for multiplexing a number of input data signals into one data channel: time-division multiplexing and frequency-division multiplexing.

Time-division multiplexing requires an instantaneous sampling of a number of signal inputs on a sequential basis, as shown in figure 30. If the data input signal is interrupted regularly for short periods, a curve can be drawn through the recorded sampling which will be the curve which would have been recorded continuously. It has been shown experimentally that an accurate reproduction of a sine wave can be made by using five samples per sine wave cycle. Since the data input signal is being sampled at discrete intervals, it is possible to use the time between these sampling intervals to sample other data input signals (fig. 31). It should be noted that measurements cannot be recorded simultaneously by time-division multiplexing.

Time-division multiplexing is, of course, equally valid for nonsinusoidal signals if the sampling rate is at least five times the highest significant frequency component. Thus for high-frequency response, a high data sampling rate is required which generates a large quantity of data. For this reason time-division multiplexing is not normally used to record high-frequency data.

Frequency-division multiplexing makes use of one subcarrier oscillator, which has a limited frequency band around a center frequency, for each data input signal. Each band is separated so that there is no overlap or interference with adjacent channels. Figure 32 shows typical IRIG proportional- and constant-bandwidth systems. For the proportional-bandwidth system the bandwidth is 7.5 percent of the center frequency; for the constant-bandwidth system the bandwidth is fixed regardless of the center frequency. The constant-bandwidth system is well suited for recording inlet pressure measurements because all the channels have approximately the same frequency response, thus permitting direct comparison of a large number of high-frequency measurements.

The number of subcarrier oscillators cannot be increased indefinitely because the total frequency band available on a tape recorder is a function of the tape speed:

Tape speed, in/sec	Available bandwidth, Hz
60	400 to 750,000
30	400 to 375,000
15	400 to 185,000
$7\frac{1}{2}$	400 to 90,000
$3\frac{3}{4}$	400 to 45,000

The available bandwidth increase is nearly proportional to the tape speed. This directly affects the recording time and the number of channels that can be recorded per track. In selecting a system for a particular application, tradeoffs must be made between bandwidth (which affects frequency response), number of channels to be recorded, and the recording time that must be derived from a given length of tape. The recording time is important in flight testing because it is impossible to reload the tape, and continuous recording is advisable to cover unexpected events. With currently available recorders, 1 to 2 hours of recording time is possible at 15 inches per second, depending on the tape thickness and supply reel size.

3.4.4 *Recording System Requirements*

Dynamic distortion and other measurements in an inlet create unique requirements for a recording system. In general, 200 steady-state channels and 60 to 80 channels of high-frequency information are adequate for inlet–engine compatibility investigations. The highest frequency of interest is twice the blade-passing frequency of the engine. If scale models are being tested, this frequency is normally increased by dividing it by the scale (i.e., a 1/3-scale inlet would require three times the frequency response).

Steady-state measurements are required to determine the reference conditions during a dynamic event. Accuracies of 1 to 2 percent with a resolution of 0.25 percent and a frequency response of 4 hertz are adequate. The steady-state recording system should be capable of accepting the direct input of digital transducers (13 bit or more) which are used when higher accuracies are required. These requirements usually lead to the use of a PCM recording system for steady-state measurements.

The measurement of noncyclic transients like engine stall and inlet unstart requires simultaneous recording of data or a minimal time delay between various channels of recorded data. Tolerable time delays are usually in the range of 1 millisecond, which requires a sample rate of 1000 per second for time-division multiplexed systems.

Cyclic dynamic measurements present requirements that are in part dictated by the statistical analyses to be applied. The pressure fluctuations in an inlet may be as low as 1 percent of the steady-state pressure level; the resolution should be one-tenth of this for good statistical analysis, especially for digital data analysis. (See section 5.0.) For cross-correlation analyses the phase lag between two channels at the maximum frequency of interest should not exceed 5°. At 500 hertz the time discrepancy can be only 28 microseconds. For constant-bandwidth FM systems which are most frequently used for inlet dynamic recording, this lag can be achieved only for channels that are recorded on the same track. It increases by nearly an order of magnitude for data recorded on adjacent tracks of the same head stack. Thus when cross-correlations or precise transient analyses are anticipated, the pertinent channels must be recorded on the same track or at least on the same head stack.

It cannot be overemphasized that the instrumentation and data acquisition system must be carefully integrated and coordinated with the data processing system requirements.

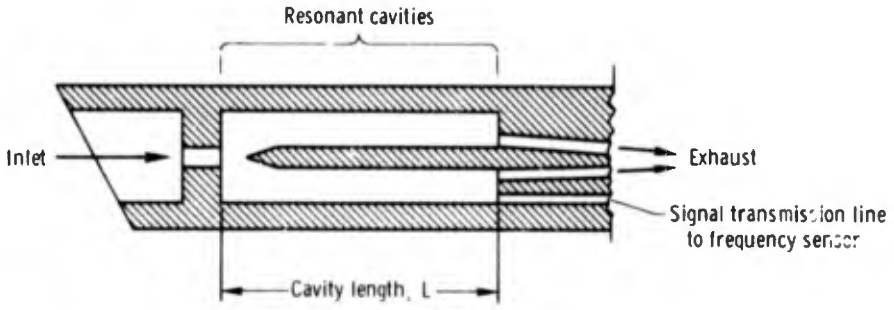

Figure 23. Fluidic temperature sensor.

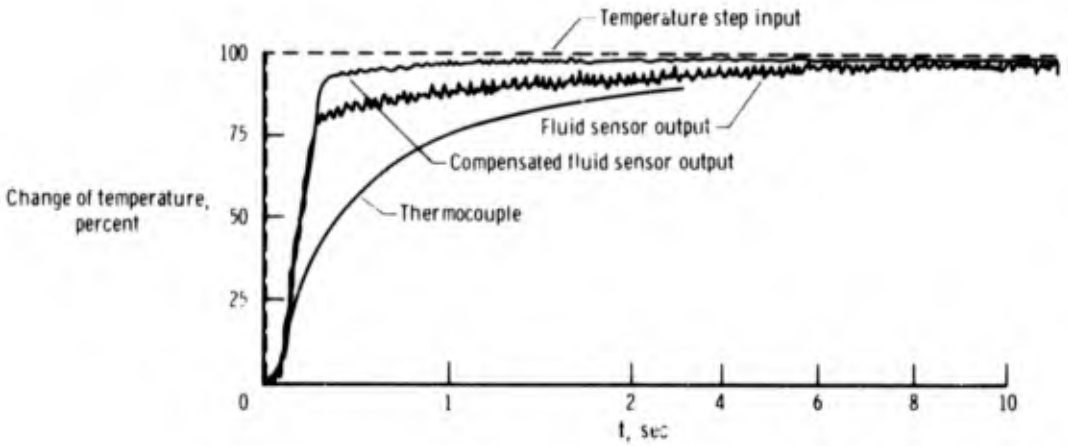

Figure 24. Transient response of temperature sensors.

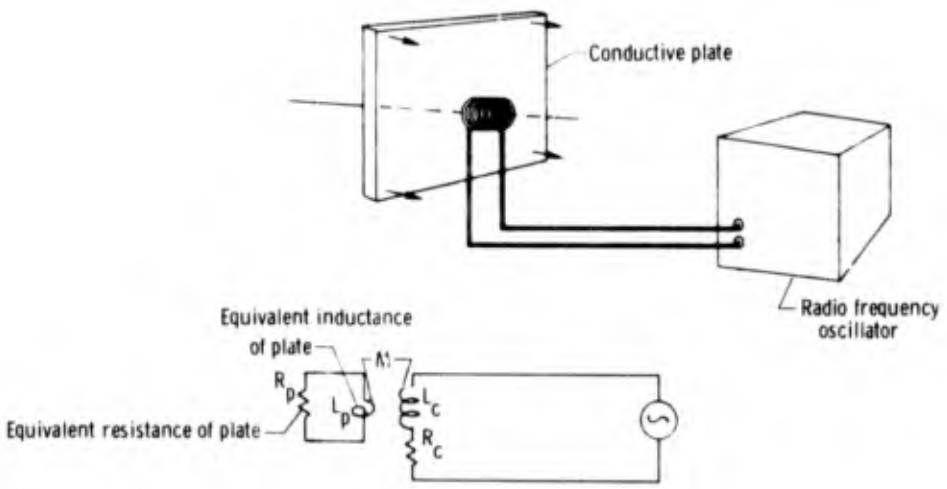

Figure 25. Variable impedance transducing principle. The impedance is a function of the conductive plate (diaphragm) position.

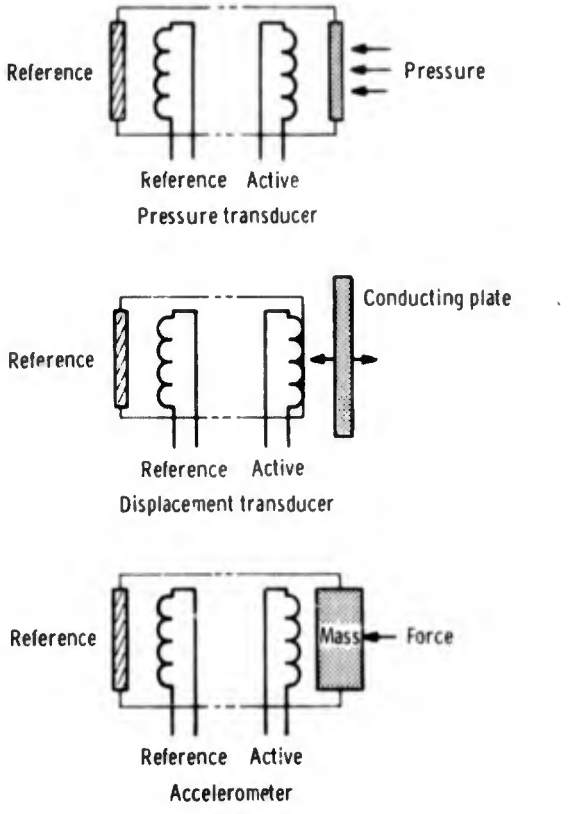

Figure 26. Eddy current transducers.

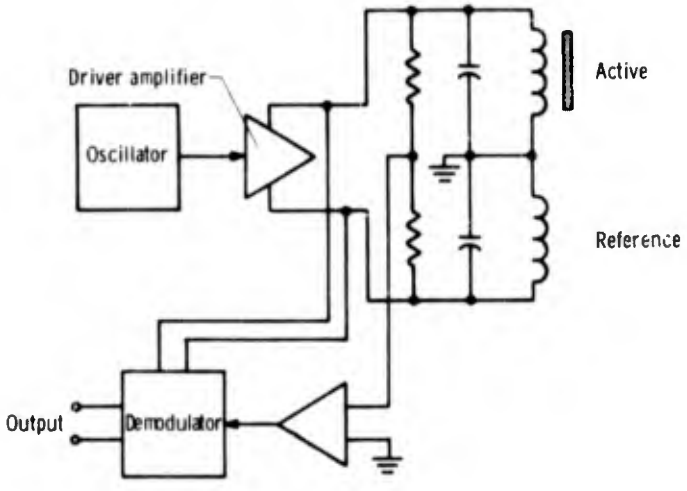

Figure 27. Sensing circuit for eddy current transducer.

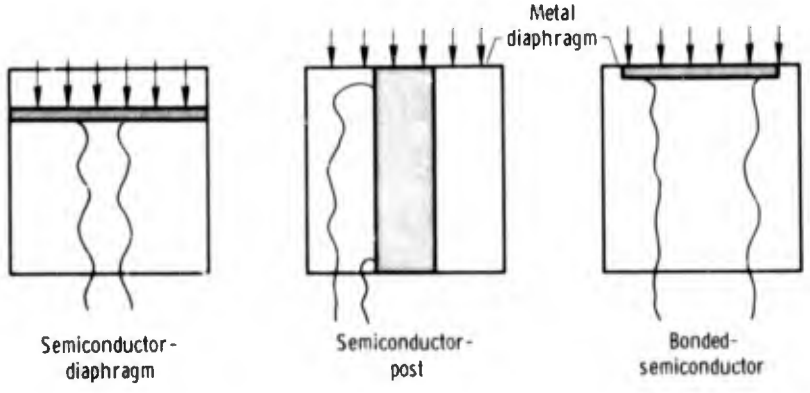

Figure 28. Miniature semiconductor strain gage pressure transducer concepts.

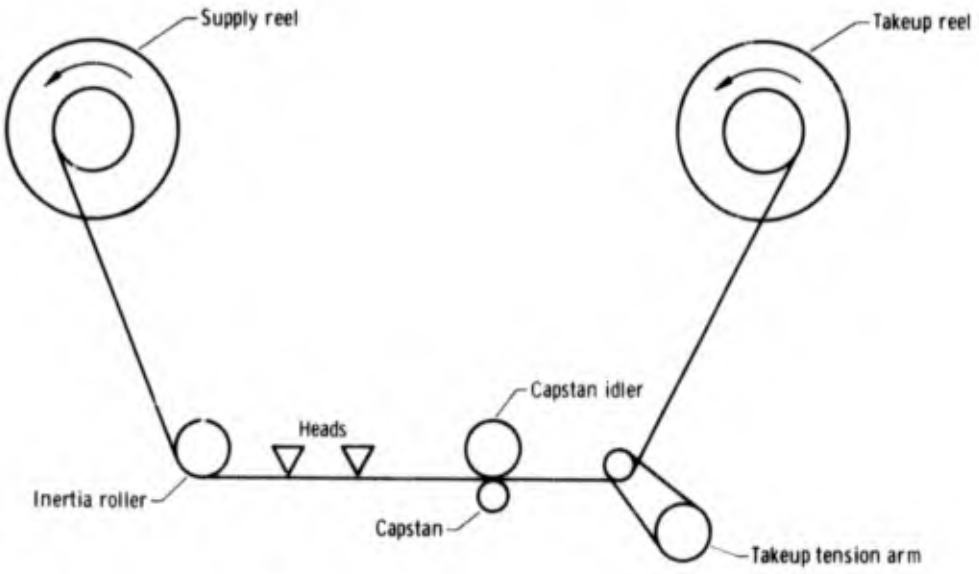

Figure 29. Simplified tape transport.

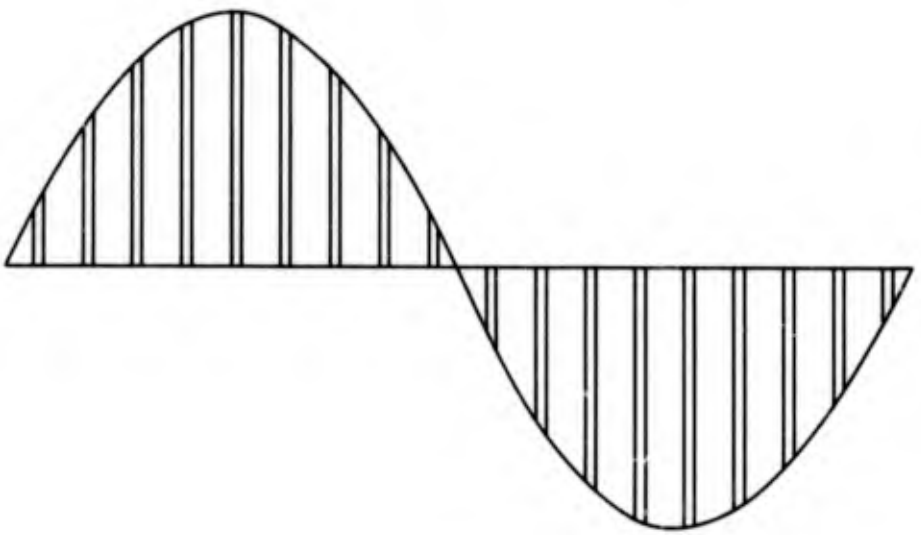

Figure 30. Time-division sampled sine wave.

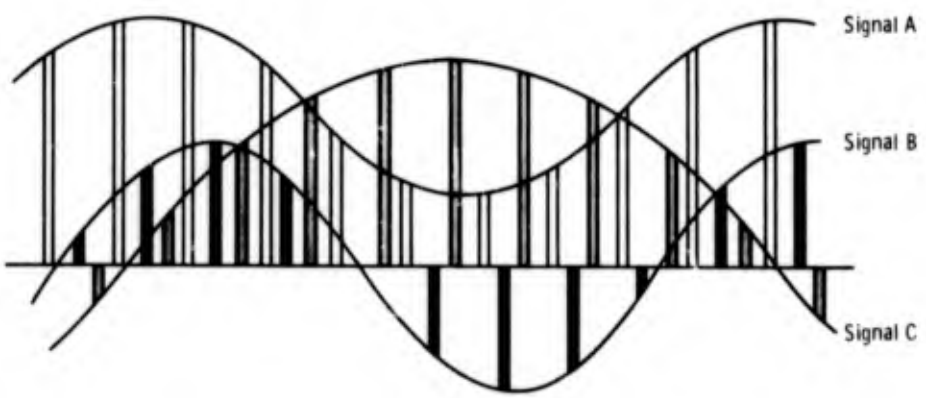

Figure 31. Time-shared samples.

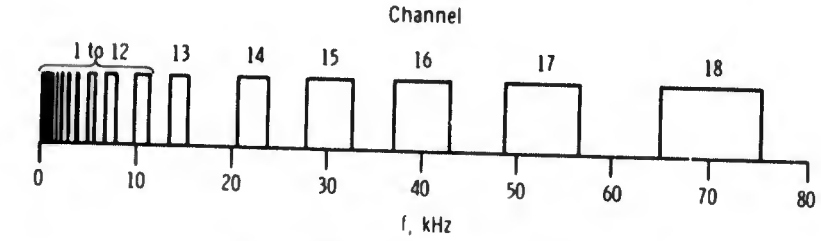

(a) Proportional-bandwidth system.

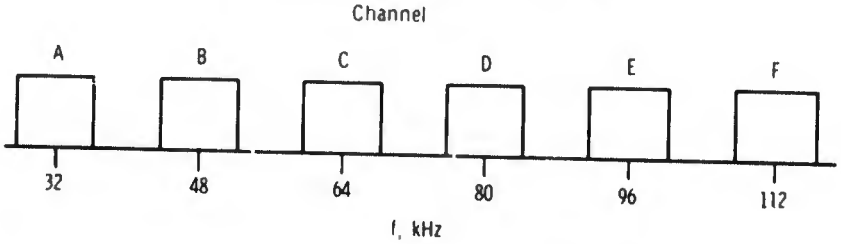

(b) Constant-bandwidth system.

Figure 32. Frequency distribution of IRIG constant-bandwidth and proportional-bandwidth channels.

4.0 INSTRUMENTATION REQUIREMENTS FOR DISTORTION DEFINITION

There is more to measuring distortion than transducers and recording systems. The number and placement of pressure probes at the compressor face are of primary importance. For precise definition of distortion it is desirable to have as many total pressure measurements as possible. However, practical considerations, such as duct blockage, rake-induced turbulence, transducer cost, and limitations on the number of high-frequency parameters that can be measured by the data system, limit the number of measurements.

4.1 Distortion Coefficients

Assuming no *a priori* knowledge of the patterns generated by an inlet, the investigator has only the engine manufacturer's information that the engine is affected most by radial, circumferential, or some hybrid area-weighted type of distortion coefficient which has been defined by the manufacturer. Several comprehensive studies on this subject have been made using distortion coefficients K_θ, K_{RAD}, and DC_{60} and the turbulence factor, $\frac{\Delta P_{RMS}}{\bar{P}}$; these quantities are defined in references 25, 26, 19, and 27, respectively. These studies generally accept a configuration with 40 probes and 8 equally spaced rakes as the standard by which others can be evaluated. As indicated in figure 33, in most instances they find that 20 judiciously placed probes adequately

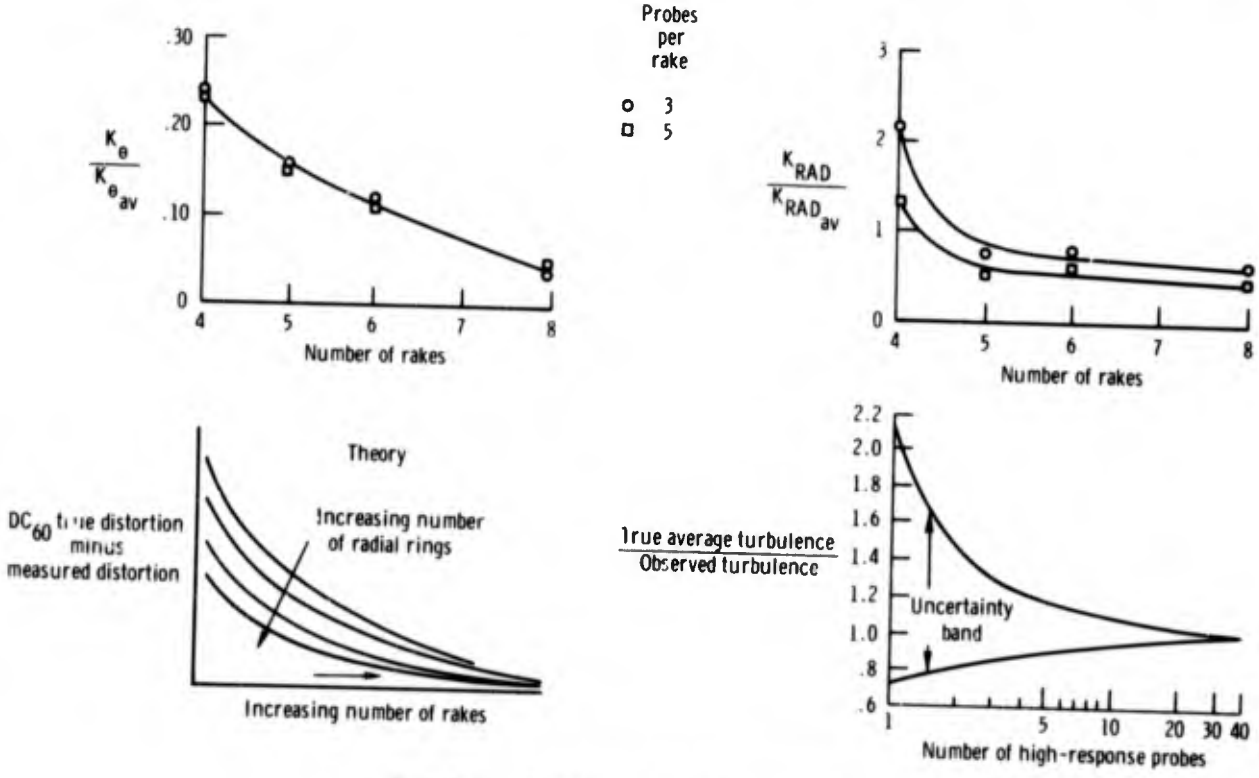

Figure 33. Probe and rake requirements.

describe the pressure patterns required for the particular distortion coefficient being considered. However, one set of results in reference 26 is unsettling to the would-be investigator and could lead him back to installing as many probes as possible. This study considers the distortion coefficients K_{RAD} and K_{θ} and the classic maximum-minus-minimum-over-average coefficient. It also considers nine pressure patterns that are typical of five different types of inlets and 12 rake configurations. Six of these configurations require analytical filling in equal area sections where measurements were not made. The filling procedures are outlined in reference 26. Sketches of 10 of the rake and probe configurations are shown in figure 34. Using these 10 rake configurations, the average

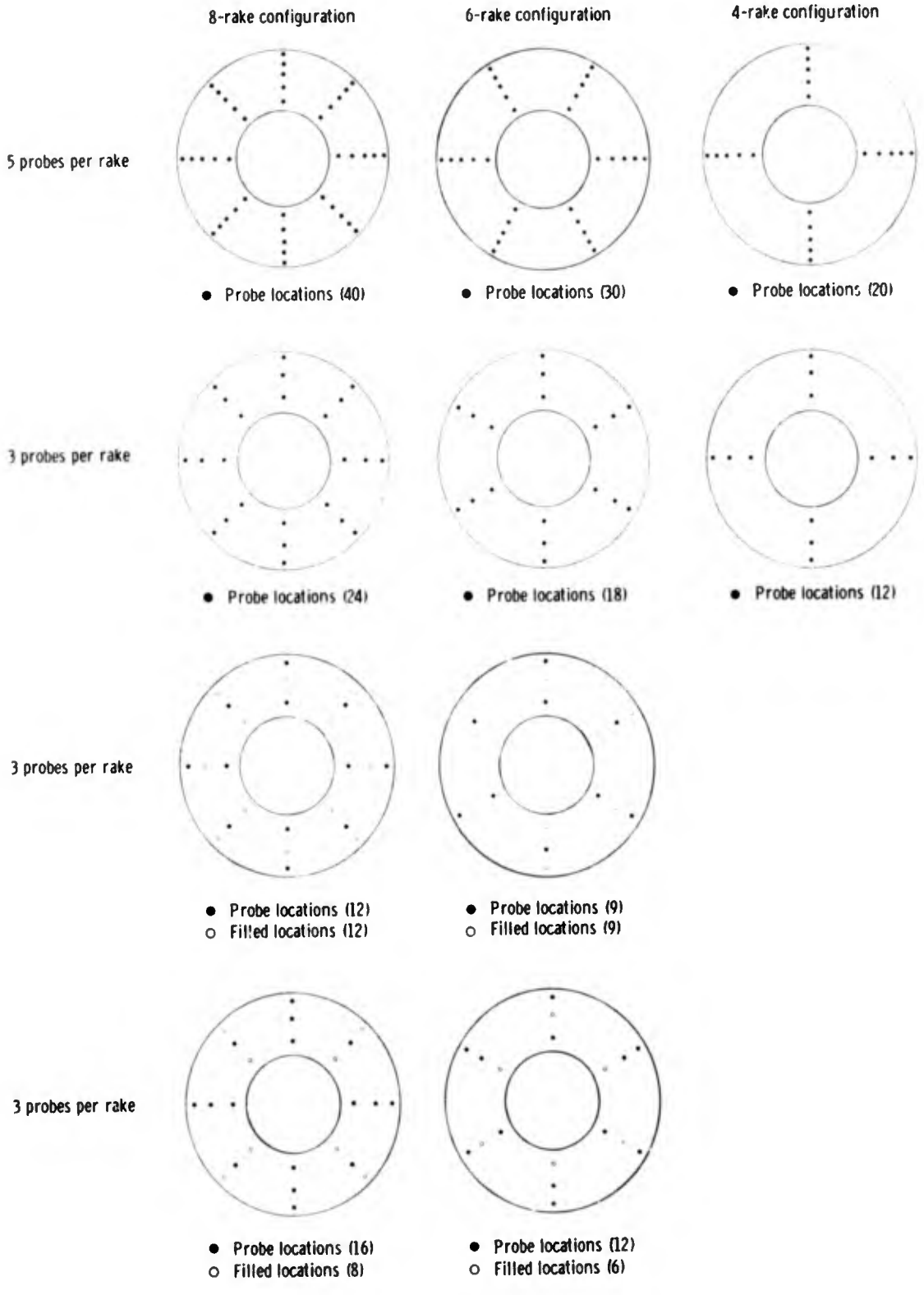

Figure 34. Rake and probe configurations.

error in calculating K_{RAD} and K_{θ} was determined for the nine pressure patterns. The results are summarized in figures 35(a) and 35(b) in terms of the total number of probes, the number of rakes, and the number of probes per rake. As expected, the accuracy of the computed distortion improves as the total number of probes and the number of probes per rake increase. What is not expected is the magnitude of the errors, which are as high as 35 percent when only four rakes are used to measure circumferential distortion and as high as 50 percent when unmeasured locations are mathematically filled on the basis of surrounding measurements. These results indicate that to achieve the best accuracy in computing circumferential and radial distortions, no fewer than 6 rakes with 3 probes per rake should be used. This provides 15 percent and 10 percent accuracy in K_{θ} and K_{RAD}, respectively. Two additional probes on each rake provide a larger increment in accuracy than the addition of two rakes. Filling should be avoided except to replace bad data and even then should be kept to a minimum.

This analysis assumes an 8-rake/40-probe configuration as the standard, but for precise computation of K_{θ} more rakes are needed. Furthermore, this analysis assumes no instrumentation error. A thorough analysis of this type should be made for other distortion coefficients being considered; otherwise, analyses and conclusions could be seriously in error.

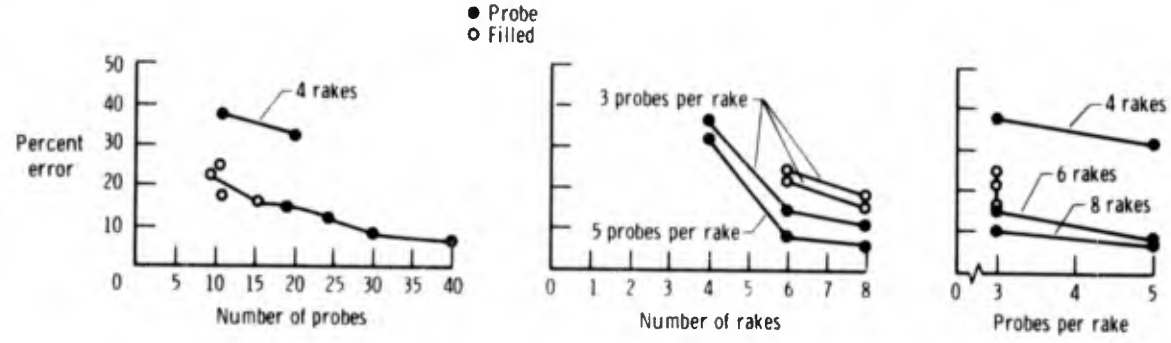

(a) K_{θ}.

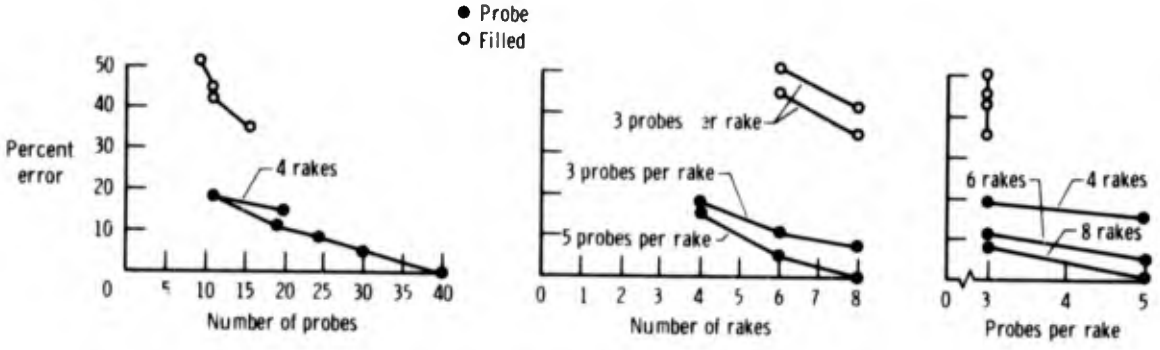

(b) K_{RAD}.

Figure 35. Distortion errors as a function of probe displacement.

4.2 Distortion Patterns

Many investigators rely extensively on distortion patterns or maps as a basis for comparing ground facility simulations and flight results. But the previous discussion indicates that caution is in order. Figure 36 shows a single distortion pattern as obtained by each of the probe configurations shown in figure 34. Using the 8-rake/40-probe configuration as the baseline, patterns developed by other probe arrays bear a decreasing resemblance to each other in almost direct proportion to the number of measurements. It would seem that to develop reasonable distortion patterns, either an 8-rake/40-probe or a 6-rake/30 probe configuration is required; however, even these may not be adequate. Figure 37 shows the effect of rotating the reference distortion pattern shown in figure 36 relative to the rake array. As indicated, rotating the 8-rake/40-probe configuration 22.5° significantly modifies the pattern. Even the classical maximum-minus-minimum-over-average distortion coefficient is drastically changed. Similar deformations of the distortion pattern occur for the 8-rake/12-probe and the 4-rake/12-probe configurations.

To summarize, the number of measurements depends on specific investigation requirements. If distortion patterns are desired, 40 probes on 8 rakes may not be enough. If 10 percent accuracy in K_{θ} and K_{RAD} is sufficient, 30 probes on 6 rakes are adequate. If other distortion coefficients are to be used, a similar study should be made before selecting the probe configuration. However, it appears that all 4-rake configurations create large uncertainties in pressure pattern and circumferential distortion measurements. Four rakes are adequate for measuring average total pressure recovery. This investigation casts a shadow over many conclusions and theories that have been developed from analyses of these types of data.

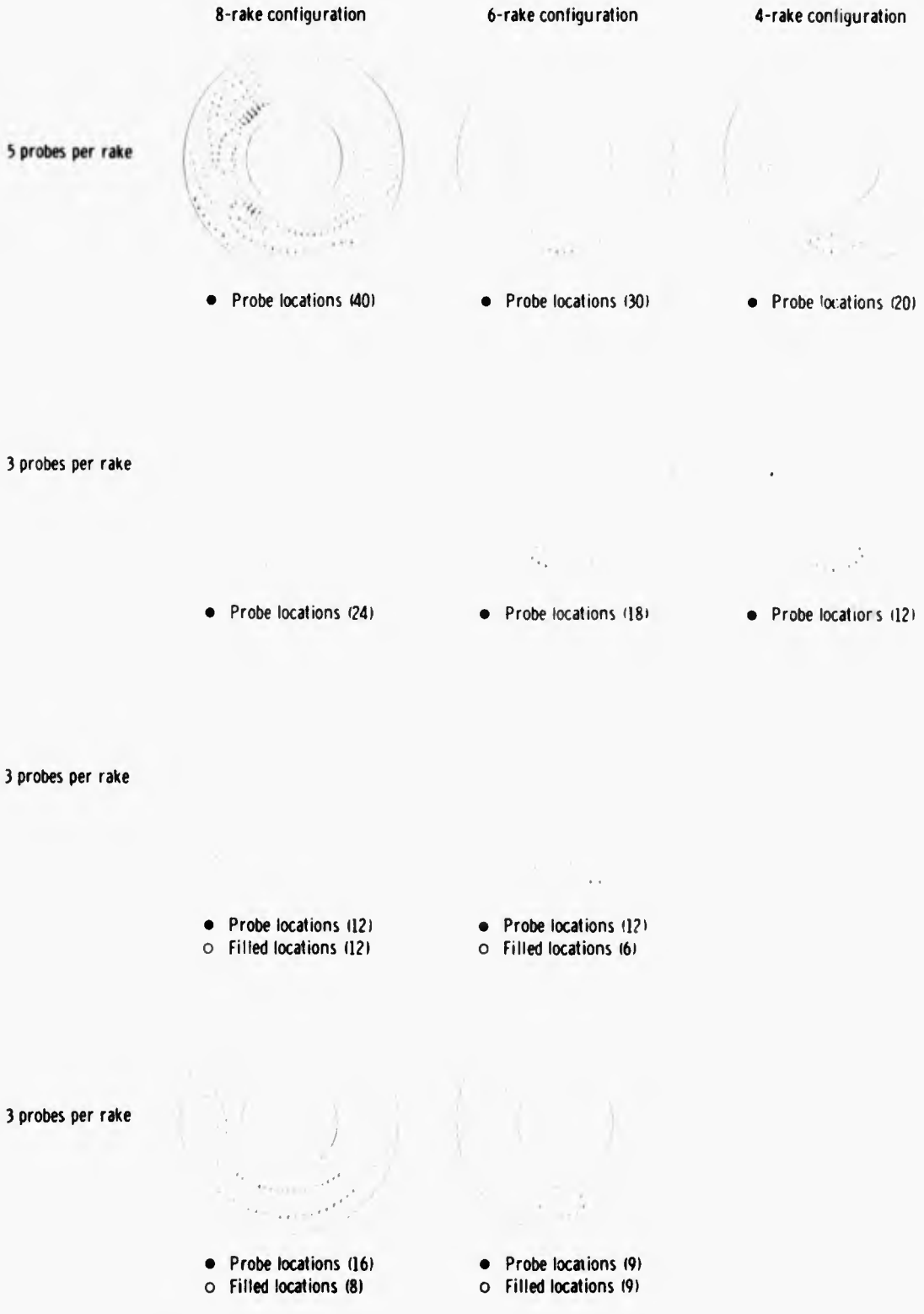

Figure 36. Measurement of a single distortion pattern by the probe configurations of figure 34.

8-rake configuration
5 probes per rake
● Probe locations (40)

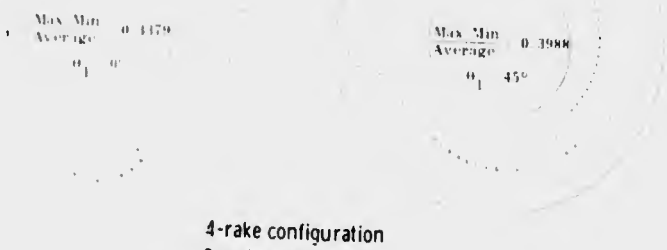

4-rake configuration
3 probes per rake
● Probe locations (12)

8-rake configuration
3 probes per rake
● Probe locations (12)
○ Filled locations (12)

Figure 37. Effect of rake rotation on distortion patterns.

5.0 DATA EDITING AND PROCESSING

If measuring and recording steady-state and dynamic parameters is classified as an engineering problem, editing and processing the data should be considered a management and decision-making problem. The sheer mass of the data collected in just a few minutes of recording time prevents detailed scrutiny by an engineer. The multiples of similar records taken during a test program would take a lifetime to evaluate. Automatic data processing and screening is essential, because both the number of parameters and the rate at which they are sampled continue to increase at an unprecedented rate. As shown in figure 38, for five typical propulsion programs conducted in an engine test facility over the past 10 years, the number of steady-state and dynamic parameters recorded has increased by a factor of five and the number of values that require processing has increased by a factor of 10 or more.

5.1 Data Processing Requirements

Three types of data analyses are required for evaluation of distortion-induced instabilities. The first is the analysis of the steady-state data, which usually represent steady or quasi-steady reference conditions of the facility or flight vehicle. These include measurements such as Mach number, angles of attack and sideslip of the air entering the inlet; bleed, bypass, and primary duct airflows; positions and control signals for variable-inlet geometries; and flow rates at various points through the engine.

The second type of data analysis involves transients measured by high-response sensors. This usually requires the time correlation of individual measurements and computed variables, such as instantaneous distortion, flow direction, and spatial visualization (e.g., instantaneous compressor face maps and duct pressure profiles). The analysis of transients requires that the wave shape be faithfully reproduced. For digital data this means high sample rates of at least 4 or 5 samples per cycle.

The third type of analysis is statistical analysis, which converts the transient data during a given time interval into a stationary set of statistical parameters that represents the physical characteristics of the data. Certain criteria concerning randomness, stationarity, and normal (Gaussian) distribution over the time interval are verified to determine the extent of the analysis that is required and its validity. The most useful statistical parameters for evaluating inlet–engine problems are root mean square values, turbulence level $\left(\frac{\text{Root mean square}}{\text{Mean}}\right)$, amplitude probability density, power spectral density, and cross spectra density or coherence.

The mathematical techniques and the attendant pitfalls of applying transient and statistical analysis are discussed in reference 28. However, some additional comments are in order on problems that have been encountered and techniques that have been developed in handling and interpreting high-frequency inlet pressure data. Care must be taken in analyzing transient data to ensure that proper time correlation and phase relationships are maintained. For example, digital data that are sequentially sampled at a given rate must be adjusted by suitable interpolation routines so that all data are presented at the same instant of time. One method which utilizes a Lagrange four-point interpolation routine is illustrated for a 24-channel system in figure 39. The Lagrange equation is

$$F_x = \frac{-P(P-1)(P-2)}{6} F_1 + \frac{(P^2-1)(P-1)}{2} F_2 - \frac{P(P+1)(P-2)}{2} F_3 + \frac{P(P^2-1)}{6} F_4$$

where F_1, F_2, F_3, F_4 represent the sampled data, F_x is the interpolated value corresponding to channel 12, and $P = \frac{t}{T}$ as illustrated in figure 39. To minimize the interpolation error, all data are aligned with channel 12, the midchannel, so that the maximum value of P is 0.5. The errors induced by this routine are shown in figure 40 as a function of frequency and the fraction of the sampling period, P. Aligning the samples to the midchannel minimizes the error, as would higher sample rates; however, higher sample rates increase the quantity of data that must be handled. Analog recording of data on a constant-bandwidth FM system is not immune to this problem. In both recording and playback, tape speed variations, tape squirm, and positioning of the read and record heads can cause similar errors.

Most data used for statistical analysis, even though originally recorded in analog form, are digitized for final analysis. During the F-111 flight tests, in which data were digitized into a 9-bit word by the onboard PCM system (ref. 5), it was found that the digital resolution and number of samples used in the analysis was critical, especially when the turbulence level was low. A 9-bit word permits resolution of one part in 256 for a differential pressure transducer having a plus and minus range. A turbulence level of 2 percent spans only 5 increments. This causes the output to have a periodic appearance when, in fact, the output is random. Figure 41 shows the amplitude probability density (APD) for a 6-increment resolution and a 10-increment resolution. The APD for the 6-increment resolution has a strong dip in the center, which is characteristic when sinusoids are present; the 10-increment APD more nearly approaches the true Gaussian distribution. This problem can be partially alleviated by increasing the number of samples or by increasing the record length when the sample rate has been fixed. The improvement that resulted from increasing the number of samples is shown in the figure. Thus statistical analyses can be tainted if the turbulence level is small relative to the digital resolution and if the number of samples is too small.

In certain instances, such as in flight tests, it is necessary to apply statistical analysis during transient or quasi-steady conditions. Also, the sample rate and digital word size is usually fixed for convenience or because of recording hardware limitations. Special analysis techniques should be incorporated to eliminate slowly varying transients, so that longer record lengths can be used during changing conditions. This can be done with high-pass or band-pass digital filtering.

Amplitude-probability-density functions provide insight into the nature of a random dynamic data trace which should ordinarily produce a Gaussian distribution. The saddleback characteristic caused by the presence of a sinusoid was observed in figure 41. Figure 42 shows some dynamic traces and their corresponding APD curves. Figure 42(a) shows a nearly Gaussian distribution, but figure 42(b) shows a skew characteristic due to the presence of more upward than downward spikes. Figure 42(c) shows the effects of a large content of nearly constant amplitude oscillations.

Since inlet turbulence amplitude is largely random, any marked departure from a normal distribution curve is a warning that parts of the data may be in error. For example, the trace shown in figure 42(d) might be considered valid, but the APD curve indicates a significant departure from a normal distribution caused by intermittent data dropouts. Instrumentation problems caused by amplifier limiting, exceeding transducer ranges, and non-random noise spikes are readily discernible from APD characteristics.

5.2 Data Editing

Although the huge quantity of data indicated in figure 38 is required to statistically capture significant events, only 1 percent is of primary interest and less than 10 percent can be reduced with a reasonable amount of time and effort. For example, the cost, manhours, and time to reduce 1000 minutes of dynamic data for an engine test program has been estimated to be 7 million dollars, including more than 80,000 manhours and approximately 1 year of full-time effort. This demonstrates the need to select only the most critical events for detailed analysis, particularly during the development of a propulsion system. Dynamic data are required not only for the engine tests but also for several sets of inlet development tests, engine–inlet compatibility tests, and the final flight-test demonstration. To reduce the quantity of data analyzed, critical events can be selected only through some fairly sophisticated procedure such as real-time monitoring or post-test editing.

The problem is to define and identify "significant events" in similar looking data such as those shown in figure 43. During early investigations of the effects of turbulence and dynamic distortion, arbitrary times were selected as a function of changes in certain steady-state parameters such as angle of attack, inlet geometry, and engine speed. These "reference conditions" were the basis for comparing wind-tunnel and flight results or for making parametric studies of nominal conditions. In general, though, they are not the critical conditions that might cause instabilities and therefore are of limited use in determining compatibility between the engine and inlet.

A second approach to reducing the amount of data to be analyzed is to select only those times preceding discrete events such as an engine surge or stall, inlet buzz or unstart, or duct roughness. Although this approach is effective for engines and inlets with serious problems, it does not identify critical conditions of engine–inlet combinations with few overt compatibility problems.

A third method for selecting critical periods to analyze is to study the turbulence activity within the inlet. This can be done by sensing RMS levels of individual measured parameters or by summing a group of RMS levels, such as the compressor face pressures, into a single RMS value. Thus data would be analyzed during periods of peak turbulence. Although peak levels of dynamic distortion are more likely to occur when the RMS levels are highest, the precise instants of peak distortion are not pinpointed. This procedure still leaves a large quantity of data to be sorted and analyzed.

Since compressor instabilities occur when distortions of a particular type, depending on the engine, reach a critical level and remain there long enough, it is desirable to compute the distortion coefficients in real time and record the times when the highest levels are attained. This can be done when the distortion is continuously computed, as in figure 44. The peak values are held until a larger value of distortion occurs which resets the threshold level against which the next peak will be compared. The location of each peak is marked on the tape, or the time of the event is recorded. The last mark or recorded time represents the largest peak during the data segment being analyzed. The times and levels of each of these peaks are recorded and data are analyzed only during the time surrounding the largest peak that occurs during the data run. Thus steady-state, transient, spatial, and statistical data would be computed only at the most critical periods.

All distortion coefficients are not time dependent (ref. 29) and therefore are not suitable for instantaneously defining critical events. Those most frequently used are K_A, K_θ, K_{RAD}, and the classic maximum-minus-minimum-over-average distortion coefficients which are rigorously defined in references 25, 26, and 29. These distortion coefficients can be adapted for conventional rake configurations having J equal-area rings and M equally spaced rakes by using Eqs. (11) to (14). For the engine distortion coefficient, K_A:

$$K_A = K_\theta + bK_{RAD} \tag{11}$$

For the circumferential distortion coefficient, K_θ:

$$K_\theta = \left(\frac{2}{MQ_{av}\sum_{r=1}^{J}\frac{1}{D_r}}\right)\sum_{r=1}^{J}\left\{\frac{1}{D_r}\left[\left(\sum_{i=1}^{M}P_{t_{2_i}}\cos\theta_i\right)^2+\left(\sum_{i=1}^{M}P_{t_{2_i}}\sin\theta_i\right)^2\right]^{\frac{1}{2}}_r\right\} \tag{12}$$

This assumes that the first harmonic of the Fourier series curve fit to the total pressures of a ring, which is the basis of the rigorous K_θ definition, is a good approximation to most physical data.

For the radial distortion coefficient, K_{RAD}:

$$K_{RAD} = \left(\frac{1}{Q_{av} \sum_{r=1}^{J} \frac{1}{D_r^2}} \right) \sum_{r=1}^{J} \frac{\left\langle \overline{P_{t_2}} - \left(\overline{P_{t_2}} \right)_r \right\rangle}{D_r^2} \tag{13}$$

where all negative values of the $\langle\ \rangle$ quantity are set equal to zero.

For the distortion coefficient, D:

$$D = \frac{P_{t_{max}} - P_{t_{min}}}{\overline{P_{t_2}}} \tag{14}$$

The symbols used in the preceding equations are defined as follows:

b = weighting factor

D_r = ring diameter

i = rake location

J = equal area rings

M = total number of equally spaced rakes

$P_{t_{2_i}}$ = individual probe total pressure

$\overline{P_{t_2}}$ = average engine face total pressure

$\left(\overline{P_{t_2}} \right)_r$ = ring average total pressure

Q_{av} = average engine face dynamic pressure

r = ring number

θ_i = angular location of rake

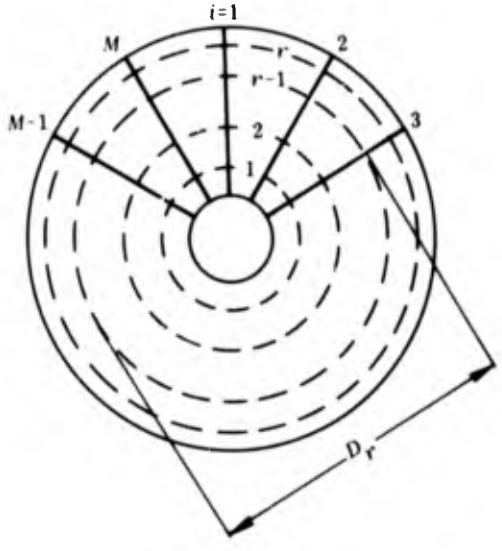

Compressor face geometry

The "reference condition" and "discrete event" approaches were used to select the data to be analyzed in reference 5 and other contemporary studies. The "RMS" and "dynamic distortion" approaches have been used in selecting significant events for F-15 and B-1 engine development (refs. 1, 29, and 30) and other research investigations.

Experience indicates that a combination of analog and digital techniques best meets the needs for speed in real-time editing and accuracy in the final analyzed data. The relative capabilities of analog and digital computation for dynamic data editing and processing are shown in the following table:

	Analog computation	Digital computation
Solution rate	Instantaneous	Not real time
Frequency requirements	High-quality components	High sample rates
Increased problem complexity requirements	More hardware	More time
Flexibility	Hardwired or patch board	Software change
Memory	No	Yes
Accuracy	2 percent to 5 percent	Less than 0.5 percent

The greatest strength of analog computation is that the solution is instantaneously available and thus lends itself to real-time computation for on-line analysis and editing. Very fast digital computers can compute in real time only when the computations can be done in a fraction of the period of the highest frequency of interest. Thus if the frequency is high and the calculations are complex, a digital computer cannot operate fast enough to keep up with the data input rate. As pointed out previously, digital analysis of high-frequency data requires high sample rates, which generate large quantities of data to be recorded or stored in memory, but current analog components can function well up to audio frequencies.

Although a digital computer requires more time to perform more complex problems, an analog computer requires more computational elements or hardware. Thus for complex operations, an analog computer will become less flexible for computational and input changes, such as inlet rake configurations, especially if it has been hardwired.

Probably the two greatest drawbacks to an analog system are lack of memory and less than desired accuracy. Since all elements of the solution of an analog computation exist in the computer at the same time, the computer immediately forgets the preceding answers; however, memory is an integral element of digital computation. Similarly, the accuracy of analog computation depends on the ability to resolve and operate on voltages, so that the accuracy is no better than 2 percent. A comparison of analog and digital results in computing dynamic distortion shown in figure 45 indicates the relative accuracy to be between 5 and 10 percent. Thus analog computation will be adequate for analysis of inlet dynamics if high accuracy is not required. (Analog techniques for computing distortion factors and turbulence are discussed in reference 29.) On the other hand, digital computation, though more accurate, requires more time, especially if high-frequency data are to be analyzed.

Because the relative strengths and weaknesses of analog and digital computers tend to be complementary, hybrid analysis is used frequently to process dynamic distortion data (refs. 1, 7, and 30). In these applications, real-time analysis, data sorting, and data screening are done by an analog computer, and digital computation is used on selected segments identified by the less accurate analog analysis.

An all-digital processing system is being developed for use in the YF-12 and B-1 flight-test programs. This system will be used for post-test data editing and screening and in the final analysis of a limited amount of data. Although this system provides improved accuracy and flexibility, the amount of data that can be processed is limited because of the large amount of computer time required per data segment. A block diagram of this system is shown in figure 46. A constant-bandwidth FM multiplexed tape containing high-frequency data is input to the computer along with the steady-state reference conditions and a list of missing or bad parameters that have been identified during the preparation of the tape. The FM data are filtered, digitized, and merged with the steady-state data. The ability to test and replace bad parameters is an important feature of the system, because transducers inevitably fail during a test, which requires either a change in the computer program or substitution of a suitable value based on adjacent parameters. This cannot be done conveniently with an analog subsystem. After bad parameters have been replaced, distortion factors and their peak values are computed for display, and all computed and measured parameters are recorded on tape. Test conditions of interest are selected for further analysis on the basis of a review of the editing data. This is done on a large, general purpose digital computer where transient and statistical analyses of selected time segments are performed.

5.3 Comments on Data Processing Systems

The major difficulty in data processing is the general low reliability of high-response measurements. In addition to their effect on the operation of real-time analog computers and displays, bad parameters have to be detected, deleted, and filled for off-line data processing. Often, costly and time-consuming reprocessing of data is required because of undetected bad transducers that failed in subtle ways. The transducer is the starting point in any measuring system, and the most sophisticated data processing system cannot produce good data from poor measurements.

The second most serious problem is the lag which can occur in off-line data processing because of the serial chain of events that is built into the data processing system. If each element in the chain is delayed overnight for any reason, the data turnaround time, which should be hours, becomes days. If the chain has to be repeated because of bad transducers not detected initially, the turnaround time becomes weeks. The solution to this lag problem is to: (1) Detect bad readings as accurately as possible in the beginning; (2) combine as many blocks as possible in the chain to minimize the number of potential delays; (3) install manual and automatic check points and procedures in the chain to check the quality of the data without creating undue delays; (4) impress the personnel involved in the chain with the importance of their jobs in the overall result and with the impact of delays, and (5) monitor closely the progress along the chain.

Other difficulties in off-line data reduction are inaccurate time-code reading and writing, abnormal operation of the program, limited computer time for long data runs, insufficient editing, and procedural and operational problems related to the status of the many data segments trapped in the chain.

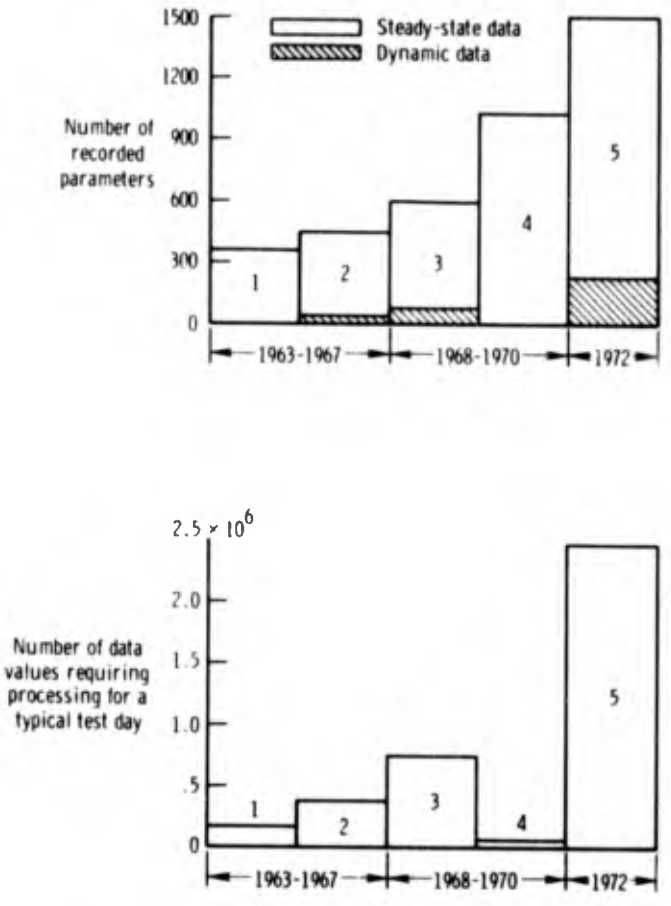

Figure 38. Increase in propulsion data processing.

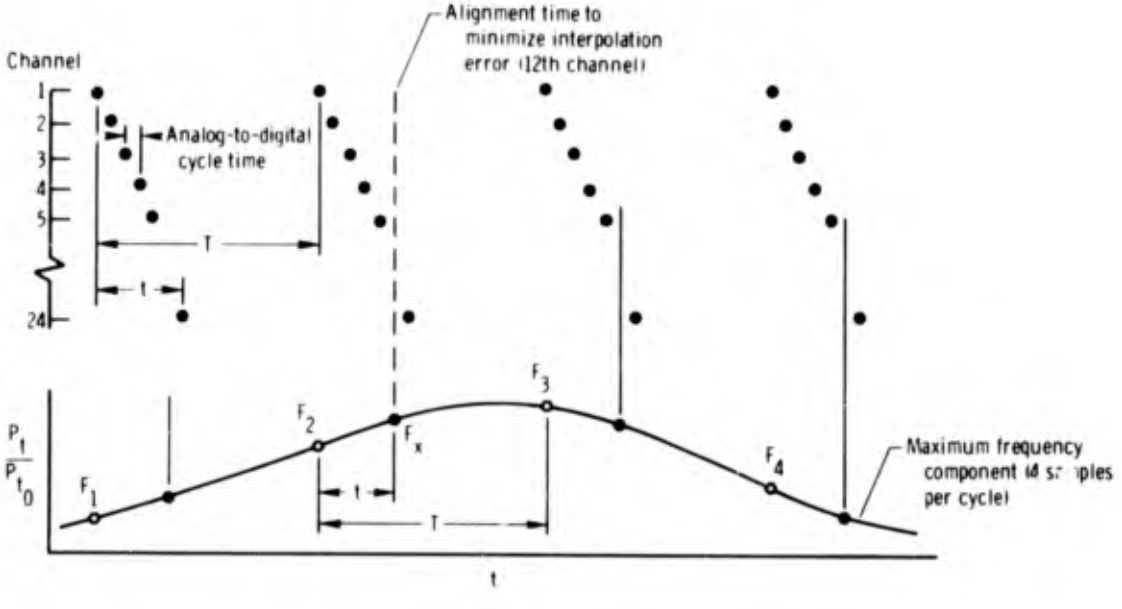

Figure 39. Illustration of analog-to-digital converter characteristics and Lagrange interpolation interpolation procedure.

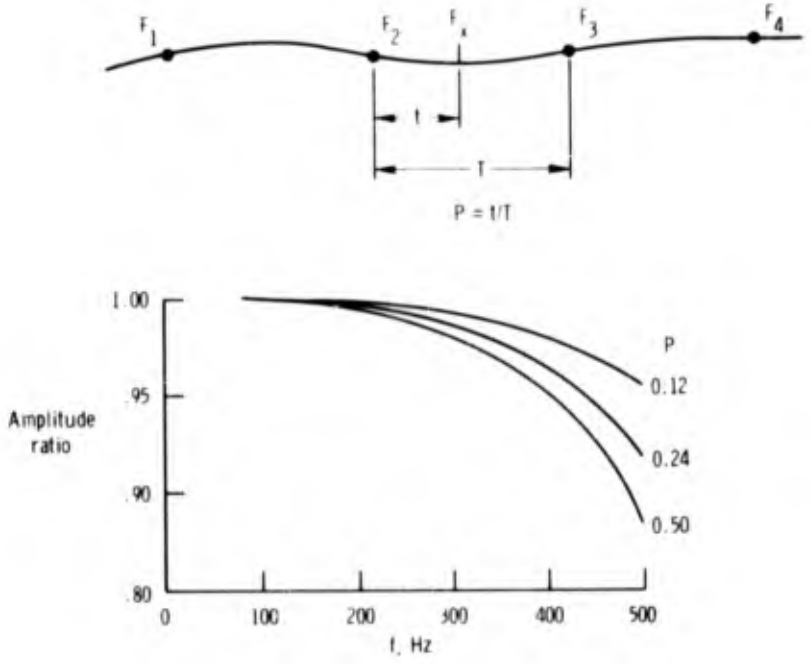

Figure 40. Attenuation characteristics of Lagrange interpolation techniques.

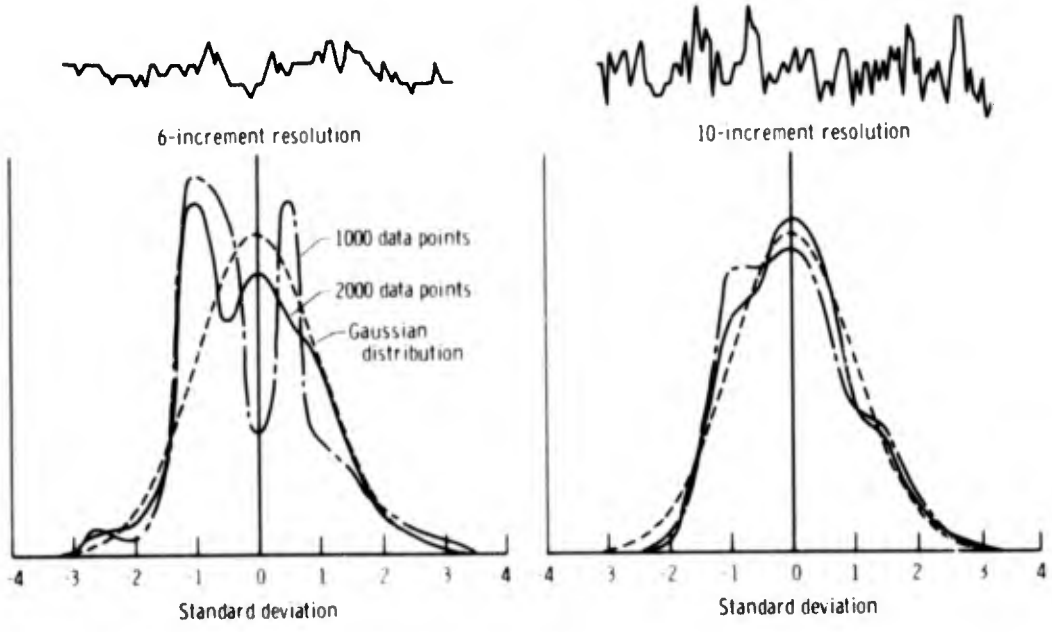

Figure 41. Amplitude probability density for a 6-increment and a 10-increment resolution.

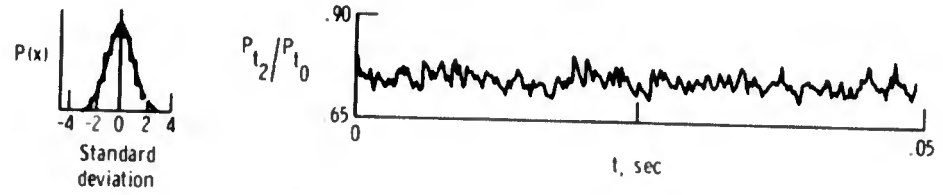

(a) Random distribution - Gaussian.

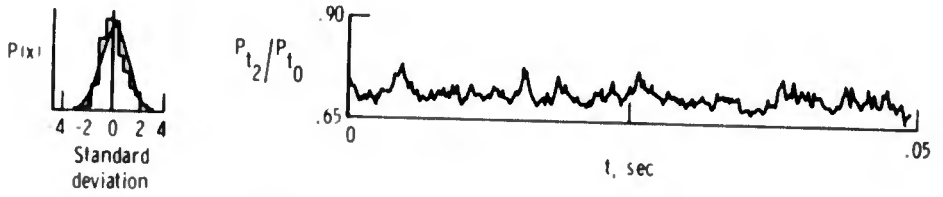

(b) Random distribution with upward spiking.

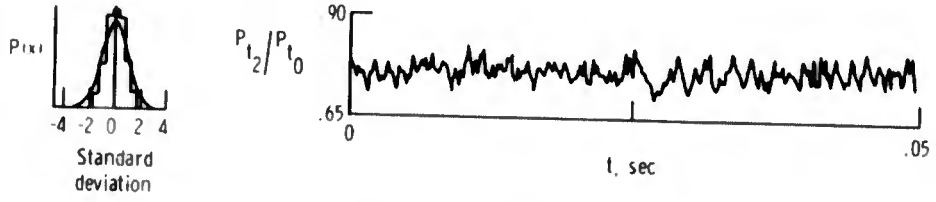

(c) Random distribution with near-constant amplitude.

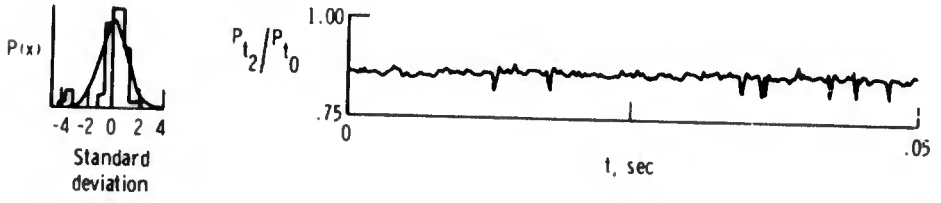

(d) Random distribution with intermittent data "dropouts".

Figure 42. Amplitude probability density for several characteristic engine face total pressure traces.

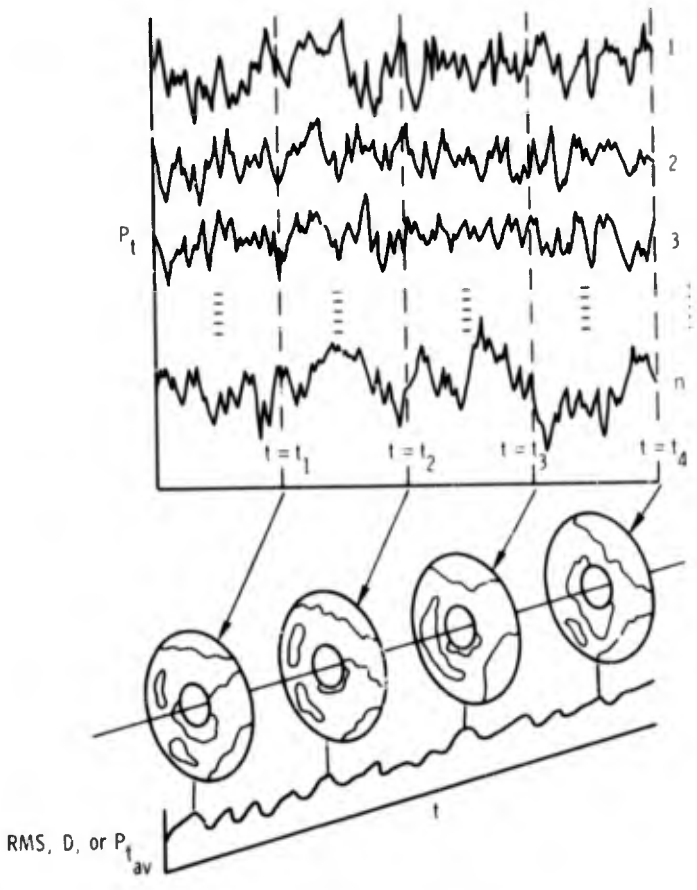

Figure 43. Contour map and distortion representation of absolute total pressure variations.

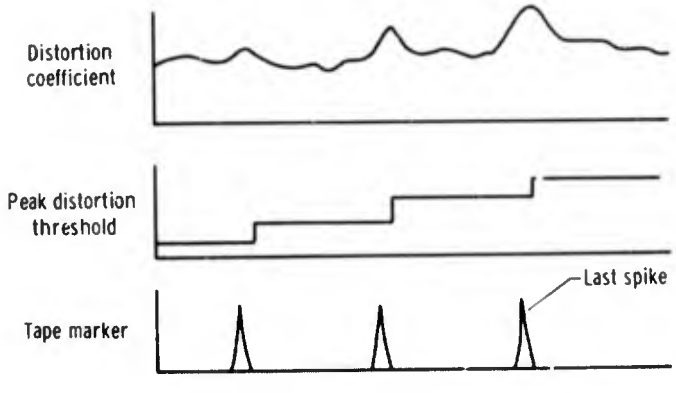

Figure 44. Continuous distortion factor monitoring system.

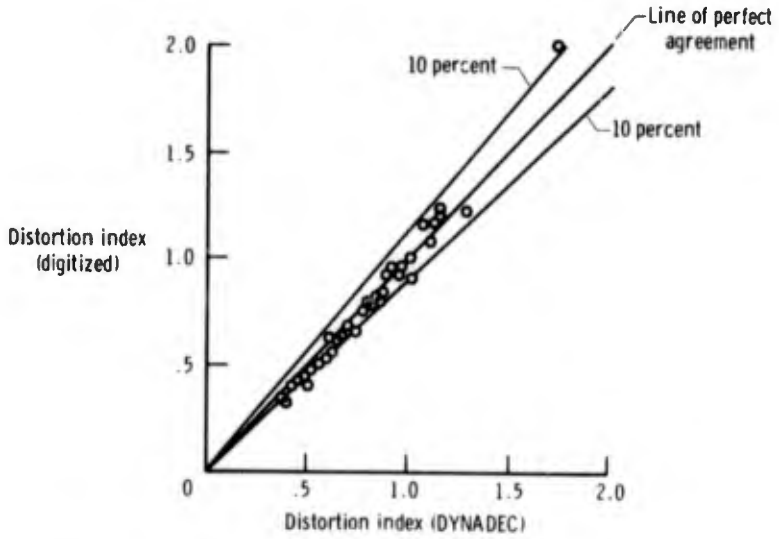

Figure 45. Comparison of peak distortions computed by digital and analog techniques.

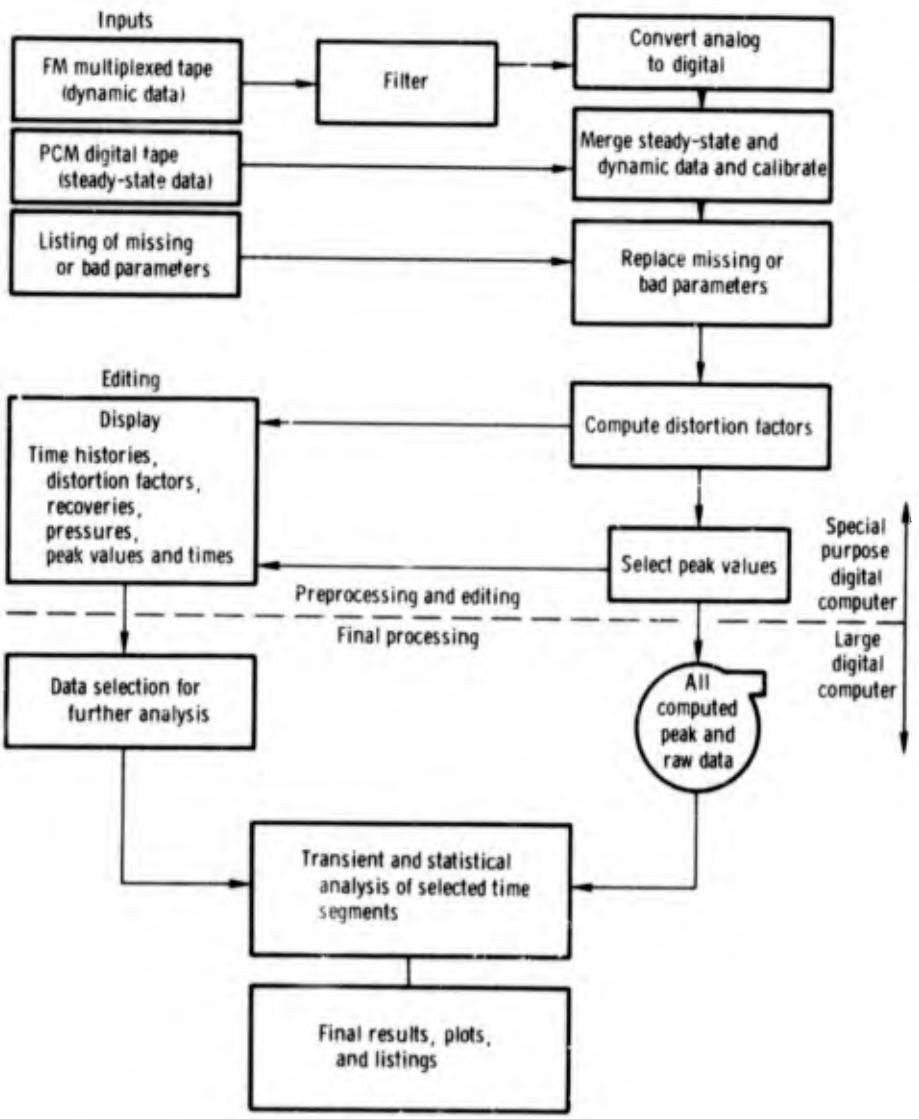

Figure 46. Block diagram of digital data editing and processing system for dynamic data.

6.0 CONCLUDING REMARKS

The success or failure of dynamic testing of inlet and inlet–engine systems depends to a great extent on detailed planning and application of proved techniques. Results produced in a wind tunnel or a test facility are only simulations of the flight environment. Their validity in many instances is yet to be verified.

The cost of operating test facilities and wind tunnels and the cost of aircraft downtime before flight tests fully justify exhaustive pre-test instrumentation checkout, using all the equipment that will be used in the test and duplicating as nearly as possible the test fixtures, such as transducers, signal conditioning equipment, pneumatic tubing runs, wiring, and connectors. The environmental conditions of each facility or aircraft are unique and should be considered when planning a program. The total data system noise level, that is, the electrical interference combined with recording system noise, should be evaluated carefully before the tests to ensure that the data recorded will meet the program requirements.

Ever since the effect of pressure dynamics on engine performance was recognized, much time, money, and effort have been spent trying to adequately measure the phenomena. The results of this effort have provided industry with new types of transducers, new data systems, and new methods of interpreting and examining data. However, considerable care and planning are required to edit and process these data. Otherwise, an investigator will be inundated with data that are impossible to analyze. It should be emphasized that automatic data processing is not automatic. It requires extreme attention to every detail of the data chain, for each element from the sensing probe to the output of the final result affects the final conclusions.

7.0 REFERENCES

1. Zonars, Demetrius: Dynamic Characteristics of Engine Inlets. Airframe/Engine Integration, AGARD-LS-53, May 1972, pp. 6-1 - 6-16.

2. Martin, Arnold W.; Kostin, Leonard C.; and Millstone, Sidney D.: Dynamic Distortion at the Exit of a Subsonic Diffuser of a Mixed Compression Inlet. NASA CR-1644, Dec. 1970.

3. Kimzey, W. F.: An Investigation and Calibration of a Device for the Generation of Turbulent Flow at the Inlet of a Turbojet Engine. AEDC-TR-65-195, Arnold Eng. Dev. Center, Oct. 1965.

4. Plourde, G. A.; and Brimelow, B.: Pressure Fluctuations Cause Compressor Instability. 60-9055, Pratt & Whitney Aircraft (East Hartford, Conn.).

5. Burcham, Frank W., Jr.; Hughes, Donald L.; and Holzman, Jon K.: Steady-State and Dynamic Pressure Phenomena in the Propulsion System of an F-111A Airplane. NASA TN D-7328, 1973.

6. Meyer, Carl L.; McAulay, John E.; and Biesiadny, Thomas J.: Technique for Inducing Controlled Steady-State and Dynamic Inlet Pressure Disturbances for Jet Engine Tests. NASA TM X-1946, 1970.

7. Kimzey, W. F.; Williams, V. O.; and Gall, E. S.: Aerodynamic Calibration and Shakedown Testing of the Full-Scale F-15 Aircraft Inlet Simulator. AEDC-TR-72-147, Arnold Eng. Dev. Center, Apr. 1973.

8. Rudey, Richard A.; and Antl, Robert J.: The Effect of Inlet Temperature Distortion on the Performance of a Turbo-fan Engine Compressor System. AIAA Paper No. 70-625, 1970.

9. Mehalic, Charles M.; and Lottig, Roy A.: Steady-State Inlet Temperature Distortion Effects on the Stall Limits of a J85-GE-13 Turbojet Engine. NASA TM X-2990, 1974.

10. Bellman, Donald R.; Burcham, Frank W., Jr.; and Taillon, Norman V.: Techniques for the Evaluation of Airbreathing Propulsion Systems in Full-Scale Flight. AGARD CP-85, Feb. 1972, pp. 7-1 - 7-15.

11. Smith, R. H.; and Burcham, F. W., Jr.: Instrumentation for In-Flight Determination of Steady-State and Dynamic Inlet Performance in Supersonic Aircraft. Instrumentation for Airbreathing Propulsion, Vol. 34 of Progress in Aeronautics and Astronautics, Allen E. Fuhs and Marshall Kingery, eds., The MIT Press (Cambridge, Mass., and London, Eng.), 1974, pp. 41-58.

12. Schweikhard, William G.; and Montoya, Earl J.: Research Instrumentation Requirements for Flight/Wind-Tunnel Tests of the YF-12 Propulsion System and Related Flight Experience. Instrumentation for Air-breathing Propulsion, Vol. 34 of Progress in Aeronautics and Astronautics, Allen E. Fuhs and Marshall Kingery, eds., The MIT Press (Cambridge, Mass., and London, Eng.), 1974, pp. 19-39.

13. Wilhelm, Walter E.: Investigation of Tubing Effects on Amplitude Frequency Response of Pressure Sensing Systems Using Nonresonant Terminations. NASA TM X-1988, 1970.

14. Nyland, Ted W.; Englund, David R.; and Anderson, Robert C.: On the Dynamics of Short Pressure Probes: Some Design Factors Affecting Frequency Response. NASA TN D-6151, 1971.

15. Robinson, R. E.; and Liu, C. Y.: Resonant Systems for Dynamic Transducer Evaluations. NASA CR-72435, 1968.

16. Robinson, Richard E.: Development of a Sinusoidal Pressure Generator for Pressure Transducer Dynamic Calibration. NASA CR-72656, 1970.

17. Robinson, Richard E.: Improvement of a Large-Amplitude Sinusoidal Pressure Generator for Dynamic Calibration of Pressure Transducers. NASA CR-120874, 1972.

18. Nyland, Ted W.; Englund, David R., Jr.; and Gebben, Vernon D.: System for Testing Pressure Probes Using a Simple Sinusoidal Pressure Generator. NASA TM X-1981, 1970.

19. Carter, E. C.: Experimental Determination of Inlet Characteristics and Inlet and Airframe Interference. Airframe/Engine Integration, AGARD-LS-53, May 1972, pp. 3-1 - 3-23.

20. Miley, Stan J.: A Catalog of Devices Applicable to the Measurement of Boundary Layers and Wakes on Flight Vehicles. NASA CR-116776, 1972.

21. Armistead, Katharine H.; and Webb, Lannie D.: Flight Calibration Tests of a Nose-Boom-Mounted Fixed Hemispherical Flow-Direction Sensor. NASA TN D-7461, 1973.

22. Doebelin, Ernest O.: Measurement Systems: Application and Design. McGraw-Hill Book Co., 1966.

23. Schneider, John C.: Measuring Instruments for Extreme Environments. Instrumentation in the Aerospace Industry, Vol. 18, ISA, 1972, pp. 289-293.

24. Bennett, G. E.: Magnetic Recording of Flight Test Data. AGARD-AG-160, Vol. 5, Feb. 1974.

25. Oates, Gordon C.; Sherman, Dale A.; and Motycka, David L.: Experimental Study of Inlet-Generated Pressure Fluctuations. PWA-3682, Pratt & Whitney Aircraft (East Hartford, Conn.).

26. Johnson, Robert H.; Bayati, Jamal E.; Lum, Evan L.; and Martin, Arnold W.: Compressor Stability Assessment Program Air Induction System Considerations. AFAPL-TR-72-30, U.S. Air Force, Aug. 1972. (Available only from Air Force Aero Propulsion Lab. (TBC), Wright-Patterson Air Force Base, Ohio 45433.)

27. Ellis, S. H.; and Brownstein, B. J.: A Procedure for Estimating Maximum Time-Variant Distortion Levels With Limited Instrumentation. AIAA Paper No. 72-1099, 1972.

28. Bendat, Julius S.; and Piersol, Allan G.: Measurement and Analysis of Random Data. John Wiley & Sons, Inc., 1966.

29. Crites, Roger C.: The Philosophy of Analog Techniques Applied to the Analysis and High Speed Screening of Dynamic Data. AIAA Paper No. 70-595, May 1970.

30. Marous, Joseph J.; and Sedlock, Dennis: Dynamic Data Editing and Computing System (DYNADEC). AFSC-TR-73-003, Vol. 1, Proceedings of the Air Force Systems Command Science and Engineering Symposium, Oct. 1973.

METHODS TO INCREASE ENGINE STABILITY AND TOLERANCE TO DISTORTION

A. A. Mikolajczak
Assistant Chief Engineer
Pratt & Whitney Aircraft Division

A. M. Pfeffer
Project Engineer
Pratt & Whitney Aircraft Division

United Aircraft Corporation
East Hartford, Connecticut 06108

SUMMARY

In this paper we discuss techniques used during engine design which ensure stable engine operation over the complete flight envelope of the aircraft in which it is installed. Adequate stability margin is required to allow for the expected levels of inlet distortion, engine to engine variations, engine aging and excursions of compressor operating lines during transients. Since the stability margin can be increased by raising the surge line of a compressor, increasing its tolerance to inlet distortion and modifying the design to reduce the sensitivity to transients, all these topics are treated in some depth. Emphasis is placed on the design for adequate stability margin and minimum penalty in engine fuel consumption, cost and weight.

1. INTRODUCTION

The prime requirement for the propulsion system of an aircraft is the production of an adequate level of thrust at all times. In addition, the engine airflow is expected to remain fairly constant, and the engine vibration to remain low. These requirements have to be met over the entire flight envelope even when the aircraft and inlet system is stalled and the engine is subjected to other transients. These requirements thus preclude engine surge or massive rotating stall. However, the engine may operate for a time with some part-span rotating stall or end-wall separation and still produce adequate thrust and flow.

The stability definition used in this paper is operational in nature and attempts to avoid the definition of the exact nature of the stability boundary. An engine is considered to operate stably if it is able to produce adequate thrust, at reasonably constant airflow, and within acceptable vibration levels. Thus, the required stability or surge margin is the margin between the engine operating line and the limit of engine stable operation.

The required stability margin of a compression system has to make allowance for a number of effects including:

(1) the expected levels of inlet distortion

(2) the compressor tolerance to inlet distortion

(3) Reynold's Number effects

(4) engine-to-engine variations and tolerances

(5) engine aging

(6) excursions of compressor operating lines during transients

For example, in a recent engine stability audit a compressor was estimated to need 20% stall margin expressed in terms of pressure ratio at constant flow. This figure was the sum of the following requirements:

Distortion	5%
Tolerances	3%
Deterioration	2%
Transients	10%

The modern engine has to satisfy a number of often conflicting requirements, such as, adequate stability, low fuel consumption, long life, low weight, and low cost. For example, stability margin could be achieved by matching the compression system below its peak pressure ratio and peak efficiency, but this would be in direct conflict with the low fuel consumption and the highest pressure ratio per stage requirement for low cost and weight. To achieve an optimum performance compromise the engine is, therefore, designed to have just enough stability margin to function adequately.

In this paper we will discuss the basic design parameters which can be varied to increase the surge margin with undistorted flow, we shall then discuss design approaches to reduce sensitivity of compressors to inlet distortions and to transients.

2. Fan and Compressor Design for Maximum Stability Margin with Undistorted Flow

2.1 Peak Efficiency on the Operating Line

The problem of providing enough margin to insure stable engine operation within the flight envelope is quite difficult and imposes a dilemma on the engine designer. A simple approach could be to match the compressor at its aerodynamic design point with the airfoils set at negative incidence. This would provide an increase in airfoil incidence range between the compressor operating line and its stability limit but would leak to an efficiency penalty along the compressor operating line. This section deals with the techniques which can be used to minimize the performance-stability trade.

The total inefficiency of a compressor can be considered to be caused by the two dimensional profile loss and endwall boundary layer loss (Fig. 1). The profile loss of conventional subsonic airfoil sections is primarily controlled by the incidence angle of the incoming flow and is a design variable (Fig. 2). A compressor designed with all airfoil sections matched at minimum loss (point A. of Fig. 2) may

not have adequate stability margin because the airfoils may have inadequate incidence range from the design point to stall. If the compressor is rematched for adequate stability by setting the airfoil sections toward choke (point B. of Fig. 2) then the increase in profile loss results in decreased operating line efficiency (Fig. 3).

A compressor matched toward choke usually has its peak efficiency between the operating line and the stall line, and is always matched on a steep portion of the pressure rise characteristic. Since the steepness of a compressor pressure rise characteristic is usually indicative of the compressor's ability to attenuate inlet distortion, the compressor designer may deliberately match the first stage of a multi-stage compressor toward choke in order to achieve an acceptable compromise between peak efficiency and distortion tolerance.

It became apparent very early in the history of compressor development that the compressor endwalls, with the complex three-dimensional boundary layers generated by blade-wall intersections, had less incidence range and pressure rise capability than the relatively two-dimensional midspan regions. It was soon recognized that midspan airfoil sections could be designed close to minimum loss while the endwall sections remained at negative incidence. The compressor was usually designed with all sections at minimum loss and then "developed" toward acceptable stability by matching the endwall sections toward choke by a trial and error process. A typical performance comparison is shown in Fig. 4.

Progress in achieving adequate stability margin with minimum performance penalty is limited by our ability to predict and control the endwall boundary layers. For example, the wall boundary layer flow must be known to allow optimum incidence angle selection throughout the compressor. Many researchers have run systematic cascade and rotating rig test programs in order to develop correlations of endwall boundary layer growth. Hanley (Ref. 1) correlated cascade exit boundary laye displacement thickness with aerodynamic loading. He shows (Fig. 5) that there exists a cascade loading limit for a given inlet boundary layer displacement thickness to chord ratio, and that an increase in chord length in a compressor should provide increased pressure rise capability. This trend has been substantiated in multi-stage compressors. It has also been shown that the range between peak efficiency and stall increases with longer chords. Engine designers are now using low aspect ratio compressors (1.0 to 1.5) in order to achieve high pressure ratio/stage and to improve the efficiency vrs. stability trade.

Direct application of the Hanley correlation (ref. 1) would indicate that the boundary layer could grow continuously through successive blade rows. However, in a turbomachine the endwall boundary layer from a stator (or rotor) is effectively re-energized (ref. 2) by the addition of wheel speed in the frame of reference of the following rotor (or stator). The succeeding blade row sees a highly skewed wall flow which has a relatively constant velocity through the boundary layer (Fig. 6). This so-called "boundary layer transformation", which is governed by the air velocity triangles, and is a function of reaction and flow coefficient, makes the existence of equilibrium boundary layers possible in downstream compressor stages. Application of the boundary layer theory allows the designer to optimize compressors for high loadings and still keep the boundary layers under control via the boundary layer transformation. Furthermore compressors can be designed with peak efficiency well away from the stability limit.

It can be seen that progress in designing compressors with adequate stability and with peak efficiency on the operating line is restricted by our knowledge and control of the endwall boundary layers. Although the designer is now able to predict the end-wall and the profile losses and can optimize his design to achieve a balance between efficiency and stability, further improvements in the performance optimization could be forthcoming from active control of boundary layer growth using suction, wall contouring, and other aerodynamic devices.

2.2 Effects of Tip Clearance

Rotor blade tip clearance and cantilevered stator root clearance play an important part in establishing the loading capability of a compressor. The work of Smith (ref. 3 and Fig. 7) illustrates the loss of pressure rise capability and hence the loss of available stability margin with rotor tip clearance and indicates the extreme importance of designing for minimum tip clearance. It is therefore not surprising that the modern engine designer uses extremely sophisticated techniques to maintain tight tip clearances. Engine transients are simulated on a computer in order to predict the running clearances accurately and the compressor materials are selected with appropriate coefficients of thermal expansion in order to maintain constant clearances during transients. Outer cases are constructed with abradable materials and blades are sometimes machined in assembly to uniform length in order to obtain the precision of construction necessary to run with absolute minimum clearance.

Increased tip clearance causes a significant reduction in compressor efficiency; however, any given compressor may respond differently because a change in clearance may also cause a change in radial flow pattern and therefore in stage matching. The reader is referred to the literature survey compiled by Reeder (ref. 4) for a review of available clearance theory. In practice a compressor is developed with a given tip clearance and rematching is usually necessary if the clearances are changed.

Approaches to reduce the effective tip clearance by modifying the blade tip or the outer casing wall to block the leakage flow between the rotor tip and outer wall have been evaluated and used in engines. Attractive modifications are discussed by Hurliman (ref. 5). Fig. 8 shows a tip modification evaluated successfully in a research fan.

2.3 Casing Treatment

It has been recognized for some time that the presence of a honeycomb casing rather than a normal smooth wall over a rotor tip could significantly increase the tip aerodynamic loading capability of the rotor. Alternative casing configurations have been evaluated (see for example ref. 6 and 7) and some of them have shown more promise than the honeycomb casing. The geometries evaluated varied from those that show large increase in stall range and a large efficiency penalty, to those that showed some increase in efficiency with very little stall range increase. A particularly attractive casing geometry is shown in fig. 9. It was applied over the rotor tip of a transonic fan and resulted in a significant increase in surge line at all fan tip speeds (fig. 10). The improvement in surge line corresponded to approximately a 40% increase in stability margin measured between the fan operating point at peak efficiency and the surge line. The application of the treatment resulted in less than 1/2% reduction in fan efficiency.

A variety of explanations have been given to clarify the fundamental fluid mechanics underlying the large changes in performance associated with the use of casing treatment. However, the explanations to date are not very satisfactory and designers are forced to use experimental results to guide their choice of configurations.

Flow mechanisms responsible for the good performance of casing treatments were investigated at Pratt & Whitney Aircraft (ref. 8) and United Aircraft Research Laboratory (ref. 9) in a water-tunnel using flow visualization. To simulate the relative motion between the outer casing and the rotor a moving belt was employed as one of the endwalls in a cascade (Fig. 11). A number of tests were run with different casing treatment geometries cut in the belt surface. To simulate compressor operation near surge, the cascade was placed at high incidence to the main flow. Figure 12 shows flow patterns obtained near the moving wall. It was observed that without belt motion there was a strong separated flow region at the intersection of the wall and the blade suction surface. With belt motion and in the presence of the casing treatment there was no separation at the suction surface intersection but now a vortex rolled off from the pressure surface.

From the observations made in the tunnel, a general description of the flow within the passage has emerged. This flow model is illustrated in Fig. 13. Near the wall a layer of fluid particles is dragged along at essentially wall speed and in the direction of belt motion. Fluid particles above this layer are entrained to various degrees depending upon the distance from the endwall and the effective roughness of the endwall. The low energy blade suction surface is aspirated and the endwall boundary layer is swept across the blade passage to the adjacent blade pressure surface where the fluid folds up into a vortex. This effect is significantly stronger with casing treatment than a smooth wall. The total entrainment and vortex formation process adds some additional loss; but it markedly reduces the total boundary layer blockage and thereby increases the loading capability of the tip.

An additional fundamental mechanism responsible for the goodness of tip treatment has been proposed by Horlock and Lakwani (ref. 10). They suggest that the treatment provides a radial relief so that the blockage associated with rotating stall cell formation is delayed

The use of casing treatment is particularly appropriate when rotor tip loading is setting the compressor stability limit. This always occurs when the fan is subjected to severe tip radial distortion and it is for this reason the fan stages of turbofan engines have been the first to benefit from the application of casing treatments. Application to other stages and refinement of the treatment to increase stability with a minimum efficiency and weight penalty can be expected in the future.

3. Design for Reducing the Influence of Engine Aging and Production Tolerances on Stability

3.1 Tip and Seal Clearance Control

It has long been recognized by engine designers that minimum compressor tip clearances and seal clearances are essential to achieve the maximum stability and performance for a given design.

However, there are other clearances in an engine that can have equally strong effect on compressor stability. High turbine tip clearances are particularly important. In a high bypass ratio turbofan of the JT9D class, a 0.010" clearance change in the first rotor of the high turbine is equivalent to 1% in turbine efficiency and turbine work. Furthermore a 1% decrease in high spool work has the effect of raising the low compressor operating line roughly 1%. Thus any increase in the first turbine blade tip clearance quickly cuts into the low compressor stability margin. Similarly any increase in the low turbine tip clearances has the effect of decreasing high compressor stability margin.

As indicated in Section 2.2 the engine designer selects materials with appropriate thermal growths and relies on close production tolerances in order to maintain tight tip clearances. Furthermore the entire bearing arrangement of an engine may have to be modified to provide tight clearance control throughout the whole life of an engine.

3.2 Blade Erosion, Foreign Object Damage and Blade to Blade Variations

It is extremely difficult to quantitatively assess the effects of eroded and damaged compressor blades on performance and stability. Generally the engine manufacturer sets limits on the amount of damage a blade can sustain before it is structurally unacceptable. However,

if the structural limits are not exceeded the engines are kept in service until hot section temperature limits start to be exceeded or until engine stalls are encountered.

A quantitative assessment of the influence of damaged airfoils on compressor stability is possible but requires information on the performance of the damaged airfoils. Such information is being acquired at P&WA for airfoils with non-standard leading and trailing edges. Figure 14 shows two leading edge modifications that were made to 400 series airfoils. The blunt leading edge contour is representative of the shape of the airfoil after impact, whereas the rounded contour is representative of a salvaged airfoil whose leading edge has been reworked to blend out the damaged region. The performance of the airfoils is shown in Fig. 15. The stall incidence range is reduced significantly for the modified airfoils and would result in a loss of stability margin in a compressor. The blunt leading edge airfoil looses positive and negative stall range and its minimum aerodynamic losses are at least double those of the nominal airfoil. The data indicates that blunt leading edges should be avoided and that some cutback and rounding of the leading edges may be tolerable.

Some airfoil-to-airfoil variation is to be expected in a compressor row due to uneven wear of airfoils in service as well as due to geometry deficiencies allowed by manufacturing tolerances. Even for seemingly identical airfoils we have observed significant airfoil-to-airfoil variation in losses, particularly at high inlet Mach numbers and when airfoils are operated near stall. To account for these variations the designer averages the airfoil properties in a compressor row and assumes that the row performance depends on this average. Intuitively we would expect that for stability predictions the average properties should be biased towards those of the worst blades. Additional work in this area is still needed.

Airfoil-to-airfoil variation can give rise to different stability margins between engines of the same design. To reduce this uncertainty the designers strive to maintain close production tolerances and the researchers attempt to develop airfoils whose performance is not sensitive to leading edge contour.

4. Design for Reduced Sensitivity to Circumferential Pressure Distortion

4.1 Shape of Compressor Characteristics

The fundamental approach to the understanding of the response of a compressor to inlet circumferential distortion has been based on the so-called "parallel compressor theory," which makes three basic assumptions:

(1) At any circumferential position the pressure rise across the compressor is only a function of the local flow coefficient at the inlet and is equal to the pressure rise of the undistorted compressor operating at that local flow.

(2) The static pressure after the last stator is circumferentially uniform.

(3) The compressor stability limit is reached when the local flow coefficient at any portion of the circumference reaches the stalling flow coefficient of the undistorted compressor.

These assumptions are shown schematically in Fig. 16. The theory is easily extended to include inlet temperature distortion by locally adjusting the corrected rotor speed for varying inlet temperature.

Since the parallel compressor theory yields a design philosophy we will give a simple example of the theory in order to make its consequences clear. If we consider two compressors, one with a steep characteristic and one with a flat characteristic (Fig. 17) operating behind the same inlet total pressure distortion then it is obvious that the distorted segment of the compressor with the flat characteristic must operate at a much lower flow than the equivalent segment of the compressor with the steep characteristic in order to generate the required total pressure ratio. The segment with the lower flow must operate at a more stalled incidence and it follows that the compressor with the flat characteristic will reach its stalling flow before the compressor with the steep characteristic. Thus parallel compressor theory implies that a compressor with a steep characteristic will have better tolerance to inlet distortion than a compressor with a flat characteristic.

The steepness of a compressor characteristic is a function of the work input or the enthalpy rise coefficient ($\Delta H/U^2$) and the flow coefficient C/U (ref. 11). Where ΔH is the enthalpy rise, U is the tangential blade speed and C is the axial velocity. If wall loss and off-design incidence considerations are neglected then for a given aerodynamic loading the steepness of the compressor characteristics (fig. 18) remains basically a free design variable. Thus to minimize compressor sensitivity to inlet distortion, the designer tries to use the highest possible blade speed to obtain the steepest compressor characteristic.

Parallel compressor theory implies that a compressor with steep characteristics attenuates more of the inlet total pressure distortion, than a compressor with flat characteristics. This can be understood by the following argument

(1) The circumferential variation in mass flow is the same at the inlet and the exit of a compressor because of the parallel compressor assumption of no circumferential crossflow.

(2) A compressor with steep characteristics has less variation in the inlet and the exit mass flow than a compressor with flat characteristic.

(3) Since the exit static pressure is circumferentially constant a compressor with steep characteristics has less variation in the exit total pressure than a compressor with flat characteristics.

Attenuation of distortion is important, especially in a multi-spool compression system, where the rear portion of the compression system sees a small total pressure distortion if the front portion of the compression system is able to attenuate the inlet distortion. For this reason, the designer attempts to limit the work level in the root sections of the front stages of a compressor in order to attenuate inlet distortion. This is particularly critical in turbofan engines where the fan root sections tend to have very flat characteristics.

4.2 Influence of External Cavities

The parallel compressor theory assumption that the pressure rise of each circumferential segment of a compressor is only a function of the local inlet flow coefficient is partly based on the observation that very little crossflow in the circumferential direction takes place within a compressor. This assumption has been examined in detail by a number of researchers (ref. 12, 13, 14, 15, 16) and has been shown to be valid for conventional compressors in which the flow is circumferentially constrained while it is within the blade rows and the axial gaps between blade rows are small compared to the compressor circumference.

However, substantial crossflow can occur when the compressor is designed with external cavities which communicate with the compressor flowpath. Figure 19 shows circumferential variations in static pressure measured at several axial locations through a research compressor. If we assume an external cavity to exist in the middle of the compressor the circumferential gradient of static pressure forces the flow into the cavity at the high static pressure segment of the circumference and out of the cavity into the low static pressure segment of the circumference (Fig. 20). In the low pressure segment the stages behind the cavity see an increased flow rate due to the crossflow mass addition. Since the stages downstream of the cavity set the match point of the front stages, the low pressure segment upstream of the cavity must match to a lower flow in order to compensate for the crossflow. The net effect of this crossflow is to reduce the axial velocity, and hence increase the stalling incidence on the blade rows in the low pressure segment in front of the cavity. By reference to figure 16 it can be seen that the distorted stall line of the upstream stages tends to be reduced. Downstream of the cavity the velocity is increased, the stalling incidence is reduced on the blade rows and the distorted stall line is increased.

A large external cavity tends to "decouple" the compressor into more highly loaded front stages and an isolated backend and in general reduces compressor tolerance to inlet distortion. Rolls-Royce experimental data (ref. 17) confirms the detrimental effect of the external cavities and verifies that distortion tolerance gains can be made by isolating cavities from the flowpath.

The importance of external cavities has been recognized by modern engine designers who attempt to minimize the external volumes and to design seal configurations which isolate the cavities from the flow.

4.3 Influence of Blading Aspect Ratio and Flow Coefficient

Certain inadequacies of the parallel compressor theory became apparent as experience was gained in checking its predictions against data. For example the theory predicts that distortions of small circumferential extent cause a greater loss in average surge line than distortions of a larger circumferential extent. This can be seen by referring to figure 16 and recalling that the circumferential segment with the lowest axial velocity is assumed to cause surge, whereas the surge pressure ratio and flow are calculated as the average for all segments. It was found, however, that experimental results were in disagreement with this prediction. Reid (ref. 18) conducted tests with distortions of varying circumferential extent (22.5°, 45°, 60°, 90° . . .) and obtained the results shown in Figure 21. It can be seen that the small extents of distortion have little effect on the pressure rise capability of the compressor. Reid's work has led to the critical segment approach to distortion prediction, which is adequately covered elsewhere in this lecture series. Our main interest in this result is that the understanding of the cause of the disagreement between the simple theory and data has very important consequences to the compressor designer. This will become apparent after a short discussion of the physics of the problem.

A rotor blade moving through a distorted flow field which is stationary in the stator frame of reference experiences time dependent incidence and velocity fluctuations. A reduced frequency parameter, k, can be defined for the rotor, where

$$k = \frac{b}{r} \cdot \frac{360}{\theta} \cdot \frac{U}{C}$$

, where b = axial projection of rotor chord
r = compressor radius at the blade section
θ = distortion extent in degrees
U = tangential blade speed
C = axial air velocity

The term $\frac{b}{r}(U/C)$ is a measure of the ratio of time a fluid particle remains in a rotor passage to the time the rotor spends in the distorted segment.

The values of the reduced frequency parameter, k, vary from nearly zero for short chord compressors subjected to large extents of distortion to well over unity for long chord compressors subjected to small extents of distortion. An analysis by Greitzer (ref. 19) shows that for low values of k a distortion can be treated on a quasi-steady basis; the rotor blade responds as if it were subjected to the local velocity at a steady incidence angle. Therefore, for low values of k the compressor should respond approximately as predicted by the parallel compressor theory. For high values of k, for example, for compressors subjected to narrow segment distortions, the rotor responds to the fluctuating conditions in a highly unsteady manner and basically responds to the average circumferential conditions. In these cases the compressor is much less sensitive to distortion than predicted by the parallel compressor theory.

We are now ready to apply the unsteady flow concepts to compressor design. Since the parameter k is proportional to rotor chord, the above discussion implies that if two compressors had identical pressure rise characteristics, and one of the compressors had X times the rotor chord of the other, it would respond to a 180° extent distortion in the same way that the second compressor would respond to a 180°/X extent of distortion. Thus the compressor with the longer rotor chords should be less sensitive to circumferential distortion than the compressor with the shorter rotor chords. Furthermore, the stator chord length should be irrelevant for distortion tolerance since the stators see only the steady inlet distortion equivalent to k = 0. However, it should be noted that the stator chord length is significant for setting the shape of the undistorted characteristic and the surge line of the undistorted compressor as discussed in section 2.1.

An experiment was carried out to verify the unsteady flow concepts outlined above (ref. 20). A series of three stage research compressors were subjected to 180° extent circumferential distortion. The results of the testing are presented in Figure 22. It is seen that the loss in surge line correlates well with rotor chord length and is basically indepent of stator chord. Thus the compressor designer should select long chord (low aspect ratio) rotors to achieve a more distortion tolerant compressor.

The parameter, k, varies inversely with flow coefficient, C/U. We can increase the distortion tolerance of a compressor by designing it at a low flow coefficient so as to benefit from the effect of unsteady rotor response. A low flow coefficient design is attractive for two other reasons:

(1) For a given pressure rise a low flow coefficient design tends to give a steep compressor characteristic which is desirable for good distortion tolerance and attenuation.

(2) Low flow coefficient design yields a favorable "boundary layer transformation" as discussed in section 2.1 and gives a strong endwall boundary layer profile.

Even though very little systematic testing has been performed on the role of the flow coefficient on distortion tolerance, modern high compressors tend to have low flow coefficients.

At this point, it seems appropriate to point out that although we are able to use unsteady flow analysis to estimate the effect rotor chords, flow coefficients and shapes of characteristics on distortion tolerance, we still cannot predict accurately the exact point of compressor instability. This still remains a difficult three-dimensional unsteady flow problem.

4.4 Exit Boundary Conditions

The importance of the major assumption that the static pressure at the compressor exit remains constant has not been adequately recognized by most researchers. It was generally felt that as long as a compressor was able to produce a relatively constant exit air angle circumferentially, and there were no obstructions behind the compressor, then the exit static pressure had to be essentially constant. This assumption was generally correct as is shown in Figure 19. However, during a series of experiments which were conducted at Pratt & Whitney Aircraft to evaluate distortion analysis models, certain anamolies were noted in the predicted exit total pressure. For some configurations the compressor attenuation of a total pressure distortion was significantly different than predicted. A study of the test data showed that in these configurations the exit static pressure was not constant circumferentially (Fig. 23) and indeed when the measured static pressure distribution at compressor exit was used as a new exit boundary condition the predicted total pressure attenuation was in close agreement with the test data.

The geometry of the test configuration described above consisted of a compressor followed by a diffuser. In its simplest form this problem can be modeled by a "parallel diffuser" technique (ref. 21), with the diffuser subjected to the compressor exit profile and the static pressure circumferentially constant at the diffuser exit (Fig. 24). If we assume that no crossflow occurs in the diffuser, then the portion of the diffuser with low inlet velocity and hence low total pressure produces a lower static pressure rise than the portion of the diffuser with high inlet velocity and high total pressure. Since the diffuser exit static pressure is constant, the diffuser inlet static pressure must be high in the low velocity region. Thus the compressor will be backpressured by the diffuser in the low velocity region. Conversely a nozzle behind a compressor will serve to unload the compressor in the low velocity region.

The presence of a diffuser behind a compressor will be detrimental to the distortion tolerance of the compressor since a portion of the compressor will simultaneously have to face low inlet total pressure and high exit static pressure. The inlet velocity distortion will be further deepened by the effect of the diffuser, and the incidences and loadings will be increased. On the other hand a nozzle will lessen the sensitivity of a compressor to inlet distortion.

The values of the reduced frequency parameter, k, vary from nearly zero for short chord compressors subjected to large extents of distortion to well over unity for long chord compressors subjected to small extents of distortion. An analysis by Greitzer (ref. 19) shows that for low values of k a distortion can be treated on a quasi-steady basis, the rotor blade responds as if it were subjected to the local velocity at a steady incidence angle. Therefore, for low values of k the compressor should respond approximately as predicted by the parallel compressor theory. For high values of k, for example, for compressors subjected to narrow segment distortions, the rotor responds to the fluctuating conditions in a highly unsteady manner and basically responds to the average circumferential conditions. In these cases the compressor is much less sensitive to distortion than predicted by the parallel compressor theory.

We are now ready to apply the unsteady flow concepts to compressor design. Since the parameter k is proportional to rotor chord, the above discussion implies that if two compressors had identical pressure rise characteristics, and one of the compressors had X times the rotor chord of the other, it would respond to a 180° extent distortion in the same way that the second compressor would respond to a 180°/X extent of distortion. Thus the compressor with the longer rotor chords should be less sensitive to circumferential distortion than the compressor with the shorter rotor chords. Furthermore, the stator chord length should be irrelevant for distortion tolerance since the stators see only the steady inlet distortion equivalent to k = 0. However, it should be noted that the stator chord length is significant for setting the shape of the undistorted characteristic and the surge line of the undistorted compressor as discussed in section 2.1.

An experiment was carried out to verify the unsteady flow concepts outlined above (ref. 20). A series of three stage research compressors were subjected to 180° extent circumferential distortion. The results of the testing are presented in Figure 22. It is seen that the loss in surge line correlates well with rotor chord length and is basically indepent of stator chord. Thus the compressor designer should select long chord (low aspect ratio) rotors to achieve a more distortion tolerant compressor.

The parameter, k, varies inversely with flow coefficient, C/U. We can increase the distortion tolerance of a compressor by designing it at a low flow coefficient so as to benefit from the effect of unsteady rotor response. A low flow coefficient design is attractive for two other reasons:

(1) For a given pressure rise a low flow coefficient design tends to give a steep compressor characteristic which is desirable for good distortion tolerance and attenuation.

(2) Low flow coefficient design yields a favorable "boundary layer transformation" as discussed in section 2.1 and gives a strong endwall boundary layer profile.

Even though very little systematic testing has been performed on the role of the flow coefficient on distortion tolerance, modern high compressors tend to have low flow coefficients.

At this point, it seems appropriate to point out that although we are able to use unsteady flow analysis to estimate the effect rotor chords, flow coefficients and shapes of characteristics on distortion tolerance, we still cannot predict accurately the exact point of compressor instability. This still remains a difficult three-dimensional unsteady flow problem.

4.4 Exit Boundary Conditions

The importance of the major assumption that the static pressure at the compressor exit remains constant has not been adequately recognized by most researchers. It was generally felt that as long as a compressor was able to produce a relatively constant exit air angle circumferentially, and there were no obstructions behind the compressor, then the exit static pressure had to be essentially constant. This assumption was generally correct as is shown in Figure 19. However, during a series of experiments which were conducted at Pratt & Whitney Aircraft to evaluate distortion analysis models, certain anamolies were noted in the predicted exit total pressure. For some configurations the compressor attenuation of a total pressure distortion was significantly different than predicted. A study of the test data showed that in these configurations the exit static pressure was not constant circumferentially (Fig. 23) and indeed when the measured static pressure distribution at compressor exit was used as a new exit boundary condition the predicted total pressure attenuation was in close agreement with the test data.

The geometry of the test configuration described above consisted of a compressor followed by a diffuser. In its simplest form this problem can be modeled by a "parallel diffuser" technique (ref. 21), with the diffuser subjected to the compressor exit profile and the static pressure circumferentially constant at the diffuser exit (Fig. 24). If we assume that no crossflow occurs in the diffuser, then the portion of the diffuser with low inlet velocity and hence low total pressure produces a lower static pressure rise than the portion of the diffuser with high inlet velocity and high total pressure. Since the diffuser exit static pressure is constant, the diffuser inlet static pressure must be high in the low velocity region. Thus the compressor will be backpressured by the diffuser in the low velocity region. Conversely a nozzle behind a compressor will serve to unload the compressor in the low velocity region.

The presence of a diffuser behind a compressor will be detrimental to the distortion tolerance of the compressor since a portion of the compressor will simultaneously have to face low inlet total pressure and high exit static pressure. The inlet velocity distortion will be further deepened by the effect of the diffuser, and the incidences and loadings will be increased. On the other hand a nozzle will lessen the sensitivity of a compressor to inlet distortion.

Although this model does provide a qualitative insight into the influence of diffusers and nozzles on compressor distortion tolerance the assumption of zero cross flow between the high and low total pressure regions gives too simple a picture of the actual non-uniform flow in the exit diffuser. To obtain a quantitative prediction of the effect of exit conditions on compressor performance with distortion, a more realistic model has been developed by Greitzer and Griswold (ref. 22), and includes the effect of cross flows.

The importance of exit boundary conditions has other significant implications for engine designers. For example, the contours of the fan exit duct in a high bypass ratio turbofan can be used to reduce the fan sensitivity to distortion. Furthermore great care must be taken in the design of test rigs to properly simulate the exit geometry actually encountered in engines.

4.5 Spool Interactions

The problem of designing multi-spool engines with minimum sensitivity to distortion is quite complex. For example, considerations of exit static boundary conditions suggest that a high compressor tends to depress the exit static pressure in the distorted region of a low compressor, and this effect should stabilize the low compressor. However, this does not always appear to be the case and this problem should be further investigated in order to clarify the required stability margin for a multispool engine.

The effect of the low spool on the high compressor seems to be theoretically clearer, although it is difficult to calculate in practice. The low compressor appears to attenuate the inlet total pressure distortion and to generate a certain amount of temperature distortion in the process. The low compressor exit conditions can be fed into the high compressor as inlet distortion and the response of the high compressor can then be predicted. It is important to note that the constant exit static condition must be taken at the high compressor exit - not at the low compressor exit. This methodology for multi-spool distortion calculation has been employed with success in stability audits. Engine designers now account for low compressor distortion attenuation in establishing the required high compressor stability margin.

5. Design for Reduced Sensitivity to Radial Inlet Distortion

5.1 Compressor Design

A compressor can be designed to operate with a known inlet radial distortion profile by including the radial profile in the design analysis. The front stage blading can then be biased to be at a minimum loss incidence in the radial profile region. Additional trailing edge camber can be added to the blading in the radially distorted region to help attenuate the distortion. It has to be recognized, however, that such a compressor might not perform adequately in an undistorted flow and that the compressor could not be used in a different installation without modifications.

A compressor with reduced sensitivity to occasional radial distortions can be conceptually designed using the available design approach for multi-stage compressors. It is well known that radial profiles are generated internally in a compressor due to endwall boundary layer growth and non-uniform radial work input; a rather extreme example of such a profile is shown in Fig. 25 taken from ref. 23. Since such profiles can be handled in a compressor design process, the influence of additional inlet distortion could conceptually be handled as an off-design problem. In practice this is quite difficult. Radial distortions cause large variations in incidence angles and stream line positions. Small portions of the span can exceed undistorted stability limits and yet the compressor as a whole can remain stable. Partial wall separations and rotating stall can occur without compressor system surge. Since we still cannot predict accurately the exact point of compressor instability, the designers tend to rely on empirical correlations of limiting loading to predict the radial distortion tolerance of compressors. Research aimed towards accurate prediction of the onset of compressor instability is still required.

5.2 Casing Treatment

The front stages of compressors, especially in turbofan engines, are frequently subjected to very local and intense tip radial distortion. This is particularly true at aircraft rotation, high angle of attack operation, and in ground running with crosswind. In these cases it is inadvisable to modify the compressor blading to accommodate the radial distortion because the local tip loading requirements are so severe that a large efficiency penalty would be incurred.

Casing treatments have been used to increase the local tip loading capability at a minimal efficiency penalty. In section 2.3 we discussed their use for increasing the stability margin with uniform inlet flow and will now show that they are also very effective in improving tolerance to radial distortion. Fig. 10 showed the performance of a fan with smoothwall casing and with casing treatment operating in uniform inlet flow. The performance of the same fan with the same casing treatment but now subjected to severe tip radial distortion is shown in Fig. 26. The fan surge line has been raised dramatically by replacing the smoothwall with casing treatment. Comparison of Fig. 26 and Fig. 10 shows that with casing treatment the surge lines with and without distortion are essentially identical indicating that sufficient aerodynamic tip loading capability has been added to the fan so that the tip is no longer controlling surge, even when subjected to severe inlet distortion. Casing treatment is being used in modern engines to reduce the compressor sensitivity to inlet tip radial distortions.

6. Design for Engine Transients

It is apparent that engine transients cause large excursions of compressor operating lines. The excursions must be accurately predicted to establish the required stability margin, and the operating line excursions must be controlled to minimize the required stability margin. Engine designers have now developed powerful dynamic engine simulation techniques (ref. 24, 25) which predict the compressor transient operating points over the entire flight envelope. Although we will not discuss details of these simulations we will use the results obtained from them to evaluate design approaches to handle engine transients.

6.1 Bleeds

In many instances the threats to stable engine operation occur rather infrequently. For example, thermal ingestion from missile firings, thrust reversing, or rapid decelerations occur over only a small portion of total mission time, but require large amounts of stability margin. In such situations it is desirable to provide temporary additional stability via bleeds and complex control systems. A mid-compressor bleed can be used to lower the loading of the stages in front of the bleed location and thus provide additional stall margin. This benefit is most pronounced at low engine speed where the front compressor stages are operating toward stall.

The bleed and its associated control system add weight and plumbing complexity to the engine. However, the improvement in compressor performance may offset these disadvantages. Fig. 27 illustrates an effective application of a bleed downstream of a low compressor in a two spool engine. The lower operating line would have given an adequate stability margin at low speeds but an excessive margin at high speeds and thereby would have penalized the pressure ratio capability and the operating line efficiency of the compressor at the higher speeds. The higher operating line would have given an adequate stability margin, utilized the pressure ratio capability and peak efficiency of the compressor at the high speeds but would have given an inadequate stability margin at the low speeds. Using the bleed which is open at low speeds and closed at high speeds we have optimized the compressor performance. The benefits more than offset the added mechanical complications.

6.3 Variable Geometry

In some applications it is advantageous to use variable stagger stators to provide flexibility for setting the desired stability margin at all compressor speeds. The front stage stators can be set at negative incidence at part speed so as to reduce the flow area and thereby reduce the front stage loadings, and then at full speed set at minimum or positive incidence to gain flow capacity and efficiency. The strong influence of using variable stator to modify the compressor map is shown in Fig. 28.

Variable stators are usually scheduled as a function of corrected speed or airflow; but in certain instances the stators control is overriden by a command signal to set the stators at pre-determined negative incidence to provide additional stall margin. The command signal can be triggered by an inlet thermocouple used to sense reverser produced thermal distortion or by the missile firing sequencer, to name a few of the many possible applications.

Variable stator vanes can also be used very effectively to reduce the compressor sensitivity to inlet distortion. In particular, when the front stage stator vanes are set at negative incidence the compressor distortion sensitivity is reduced markedly. This appears to be caused by a reduction in aerodynamic loading of the front stages which gives them more incidence range, and by the steepening of the front stage characteristic which improves the distortion attenuation. Data from ref. 26) illustrates the power of this technique.

6.4 Surge Warning Devices

One of the most promising means of achieving stable operation at minimum performance penalty is by coupling surge warning devices to a control system that is capable of rapidly providing additional stability margin. The basic idea is to match the compression system to peak efficiency and to rely on some signal preceeding surge to trigger the control system to provide the additional stability when needed. The approach appears feasible since most violent engine instabilities are usually preceeded for some period of time by localized rotating stalls at definite characteristic frequencies. In such cases complete compression system instability can be prevented in principle by adding additional stability margin to eliminate the local stall.

An active research program in this area is focusing on the development of sensors and control circuitry which is fast and reliable enough to sense rotating stall and take rapid preventative action. At Pratt & Whitney Aircraft we have sensed a stall signal and effected a 6° closure of the high compressor variable stators within 0.06 seconds. The results lead us to believe that development of practical surge warning devices is possible.

6.5 Control System

The complexity of bleeds, variable stator geometry and fuel schedules makes it mandatory that the engine designer have an adequate transient simulation in order to know where the compressor operating lines are at any time. It is also apparent that fuel flow can be varied to minimize transient operating line excursions and also maintain required acceleration and deceleration times. Thus the engine designer is forced to use computer simulations to design his control systems which become progressively more complex as they are required to

perform more functions. It is, therefore, not surprising that the trend in modern engines is towards electronic control systems which basically function as computers.

One can anticipate that in the future the application of control technology will practically eliminate transient excursions and make it possible to design compressors with lower stability margin and thereby increase the compressor efficiency and reduce the compressor weight and cost.

7. Conclusions

In this paper we have discussed many of the techniques that are used by the engine designer to provide adequate stability within tolerable performance limits. The techniques range from highly analytic unsteady flow calculations for prediction of distortion tolerance to "cut and try" approaches of wall casing treatment. Most of the approaches which have been outlined here involve trading stability for other performance parameters such as efficiency or weight or cost.

The need for accurate prediction of stability limits is providing an impetus for the development of two-dimensional and three-dimensional unsteady flow field calculations. The use of these sophisticated analytical techniques coupled with transient engine simulations should reduce stability margin requirements by 30-50% within the next decade. The progress will be translated directly into improvements in engine fuel consumption, cost and weight.

Acknowledgements

The authors wish to thank Pratt & Whitney Aircraft Division of United Aircraft Corporation for its permission to present this paper. The authors are also indebted to Mr. Mazzawy and Dr. Greitzer for their help in preparing the manuscript.

References

1. Hanely, W. T., "A Correlation of End Wall Losses in Plane Compressor Cascades" Journal of Engineering for Power, Trans. ASME, Ser. A, Vol. 90, No. 3, July 1968, pp. 251-257.

2. Mellor, G. L., and Wood, G. M., "An Axial Compressor End-Wall Boundary-Layer Theory", Journal of Basic Engineering, Trans. ASME, Ser. D, Vol. 93, 1971, pp. 300-316.

3. Smith, Jr., L. H., "The Effect of Tip Clearance on the Peak Pressure Rise of Axial-Flow Fans and Compressors", ASME SYMPOSIUM ON STALL, New York, Dec. 1958.

4. Reeder, J. A., "Tip Clearance Problems in Axial Compressors – Survey of Available Literature", Union Carbide Nuclear Corp., Jan. 1968.

5. Hurlimann, R., "On the Problem of the Gap Losses in the Straight Blade Lattice", 1965. (German Translation)

6. Osborn, M. W., Lewis, Jr., G. W., and Heidelberg, L. J., "Effect of Several Porous Casing Treatments on Stall Limit and an Overall Performance of an Axial Flow Compressor Rotor", NASA TN D 6537, Nov. 1971.

7. Yershov, V. N., "Unstable Conditions of Turbodynamics Rotating Stall", AD-731355, FTD-MT-24-04-71.

8. Greitzer, E. M., Nikkanen, J. P., Private Communication, June 1973.

9. Camarata, F. J., and Marteney, P. J., "A Wind Tunnel Study of the Influence of Slotted and Non-slotted Moving Endwalls on a Cascade at High Incidence", United Aircraft Research Labs Report UAR-M15, Jan. 1973.

10. Horlock, J. H., Lakwani, C. K., "Propagating Stall in Compressors with Porous Walls", CUED/A, Turb./TR 52, 1974.

11. Horlock, J. H., "Axial Flow Compressors", Butterworths, London, 1958.

12. Dunham, J., "Non-Axisymmetric Flows in Axial Compressors", Mechanical Engineering Science Monograph No. 3, Oct. 1965.

13. Ehrich, F., "Circumferential Inlet Distortions in Axial-Flow Compressors", Journal of the Aeronautical Sciences, June 1957.

14. Rannie, W. D., and Marble, F. E., "Unsteady Flows in Axial Turbomachines", Communication aux Journees Internationales de Science Aeronatiques, ONERA, Paris, France, May 1957.

15. Katz, R., "Performance of Axial Compressors with Asymmetric Inlet Flows", Ph.D. Thesis, California Institute of Technology, 1958.

16. Mokelke, H., "The Development of Inlet Flow Distortions in Multi-Stage Axial Compressors of High Hub-Tip Ratio", SRC Turbomachinery Laboratory, Cambridge University.

17. Moritz, R. R., "Axial Compressor Stall", Lecture to V.K.I., Feb. 1970.

18. Reid, C., "The Response of Axial Flow Compressors to Intake Flow Distortion", ASME Paper 69-GT-29, 1969 ASME Gas Turbine Conference.

19. Greitzer, E. M., Private Communication, Feb. 1974.

20. Roberts, F., Plourde, G. A., and Smakula, F., "Insights into Axial Compressor Response to Distortion", AIAA Paper No. 68-595, Fourth Propulsion Joint Specialist Conference, 1968.

21. Mazzawy, R. S., Private Communication, Nov. 1972.

22. Greitzer, E. M., and Griswold, H., "Inlet Static Pressure Distortions in Annular Diffusers", Unpublished Pratt & Whitney Aircraft Report, March 1974.

23. Howell, A. R., "Fluid Dynamics of Axial Compressors", ASME, Jan. 1957.

24. Ward, G. G., "First Semi-annual Report of Compressor Stability Assessment Program", PWA-4080, Dec. 1970.

25. Ward, G. G., "Second Semi-annual Report on Compressor Stability Assessment Program", PWA-4213, June 1971.

26. Bilwakesh, K. R., Koch, C. C., and Prince, D. C., "Evaluation of Range and Distortion Tolerance for High Mach Number Transonic Fan Stages", NASA CR-72880, June 1972.

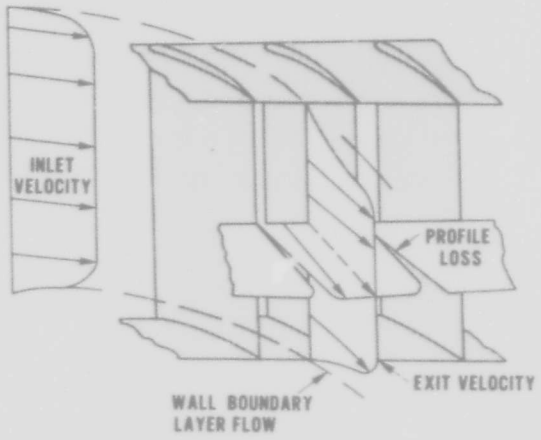

Figure 1 Spanwise and Circumferential Deterioration in Velocity Profile Through a Blade Row Causing Endwall and Profile Losses

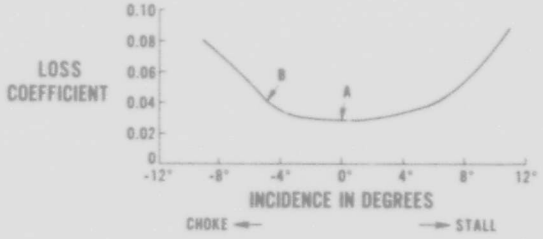

Figure 2 Variation of Cascade Profile Loss With Flow Incidence Angle

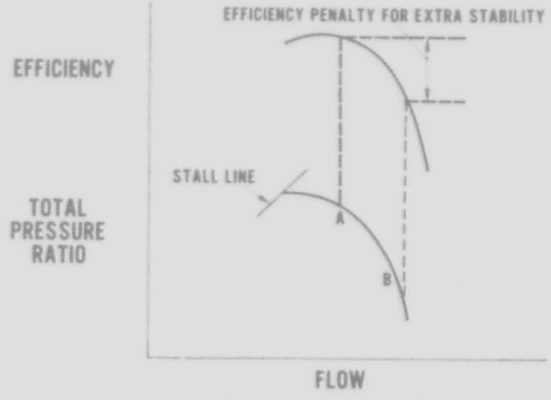

Figure 3 Operating Line Efficiency is Traded for Increased Stability by Setting Airfoil at Non-Minimum Incidence

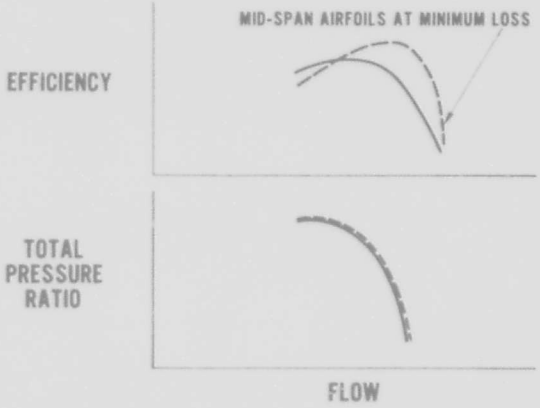

Figure 4 Matching Midspan Airfoils at Minimum Loss and Endwall Sections Towards Coke Provides Stability Without Efficiency Penalty

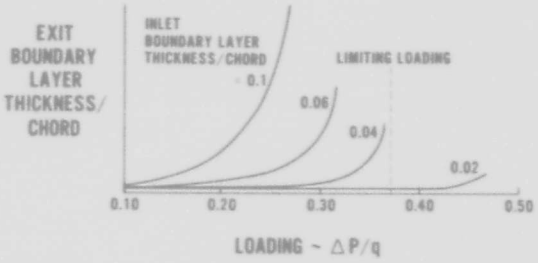

Figure 5 Correlation of Inlet and Exit Boundary Layer Displacement Thickness and Aerodynamic Loading in a Cascade. A Limiting Loading for a 0.04 Inlet Boundary Layer Displacement Thickness to Chord Ratio is Shown.

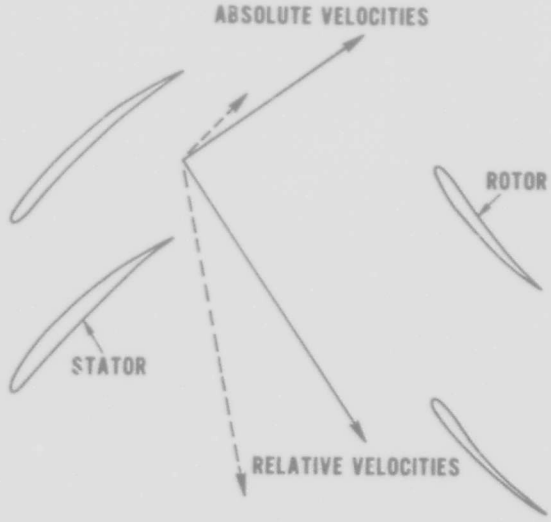

Figure 6 The Endwall Boundary Layer From a Stator is Effectively Re-Energized by the Additon of Rotor Wheel Speed

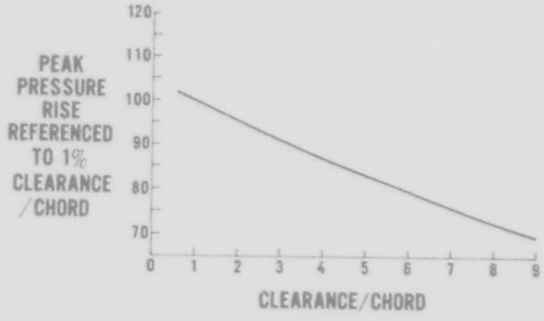

Figure 7 Rotor Tip Modification to Reduce Effective Tip Clearance

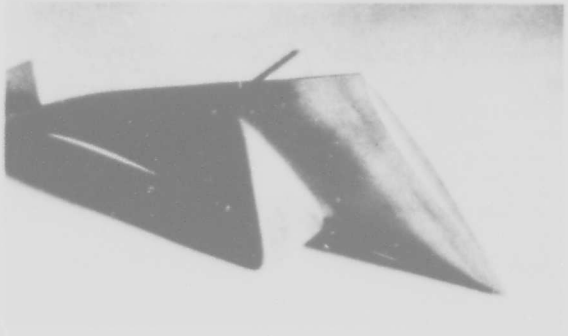

Figure 8 Rotor Tip Modification to Reduce Effective Tip Clearance

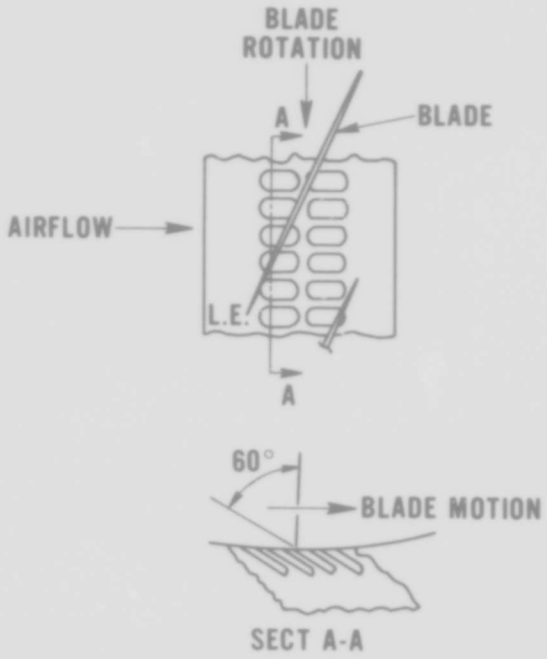

Figure 9 Rotor Tip Casing Treatment for Raising Fan Surge Line

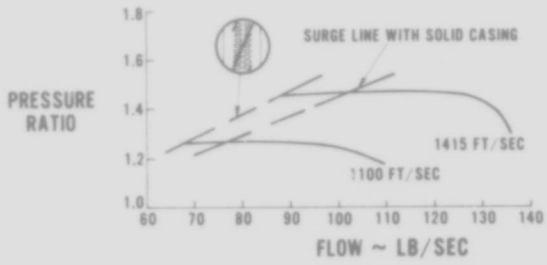

Figure 10 Tip Treatment Raises the Fan Surge Line and Increases Stability Margin

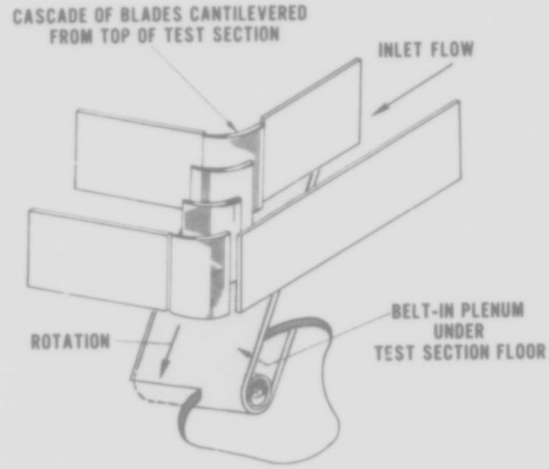

Figure 11 Tip Flow Simulation Using a Rotating Belt Under a Stationary Cascade

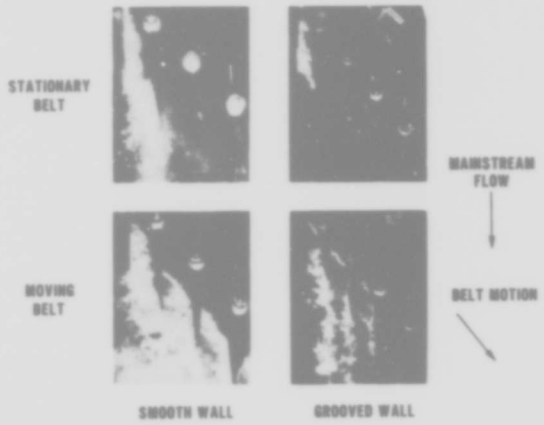

Figure 12 Visualization of Endwall Flow in the Presence of Casing Treatment and Endwall Motion

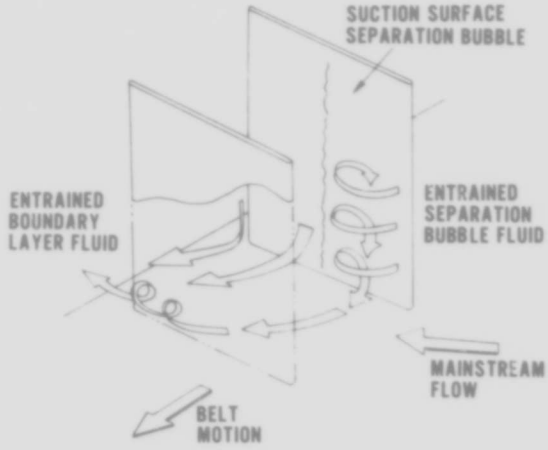

Figure 13 Schematic Model of Endwall Flow in the Presence of Moving Wall With Casing Treatment

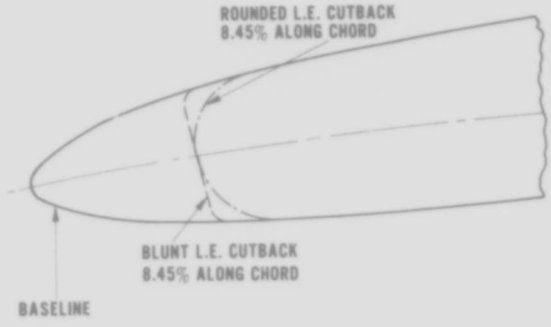

Figure 14 Modifications of Airfoil Leading Edge Contour to Simulate Impact Damaged Airfoil and Reoperated Airfoil

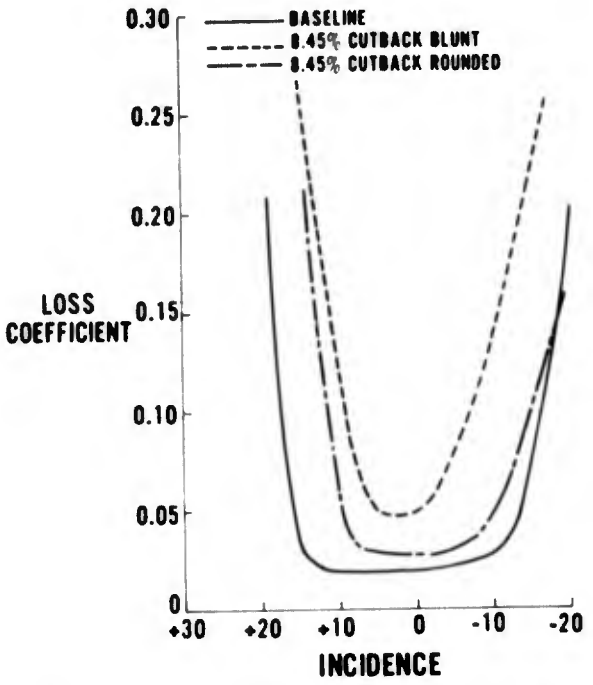

Figure 15 Effect of Leading Edge Shape Shown in Figure 14 on Loss Coefficient of Cascaded Airfoils

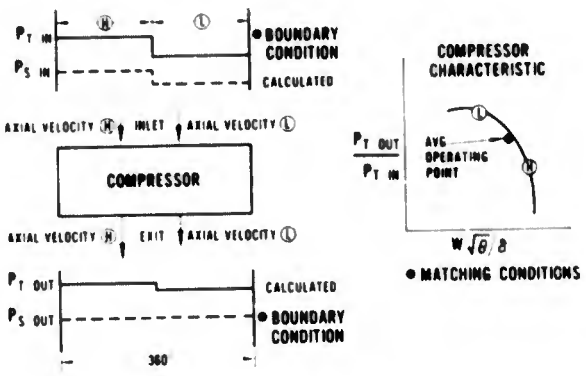

Figure 16 Parallel Compressor Model

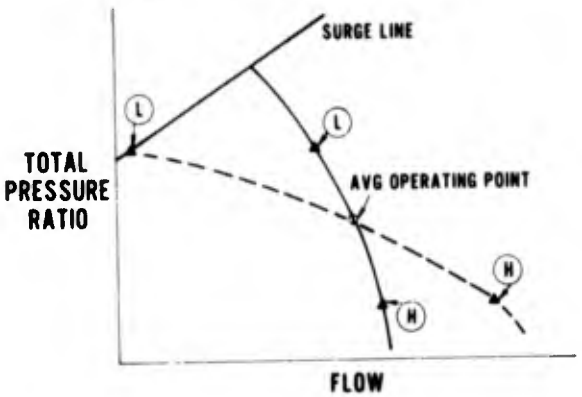

Figure 17 Compressor With Steep Characteristics Has Improved Tolerance to Circumferential Inlet Distortion

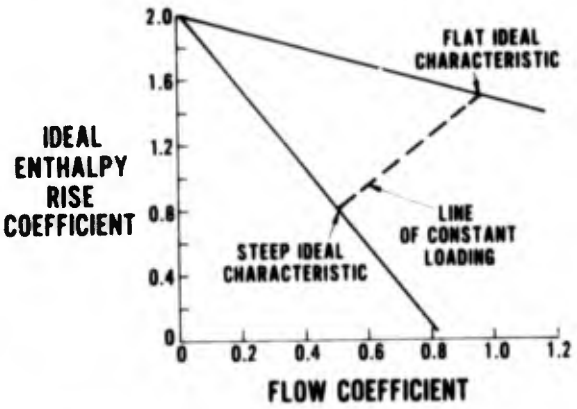

Figure 18 Steepness of Compressor Characteristics is a Design Variable for Improved Distortion Tolerance

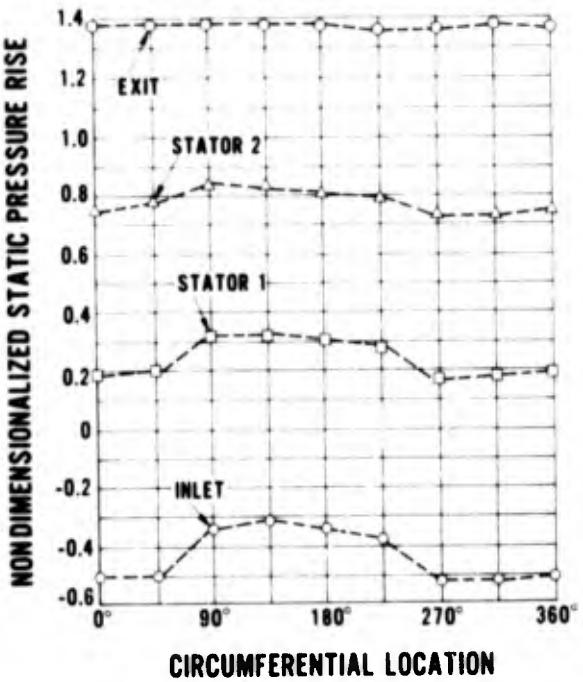

Figure 19 Circumferential Stator Exit Static Pressure Distribution Through a 3 Stage Compressor Subjected to 180° Circumferential Distortion

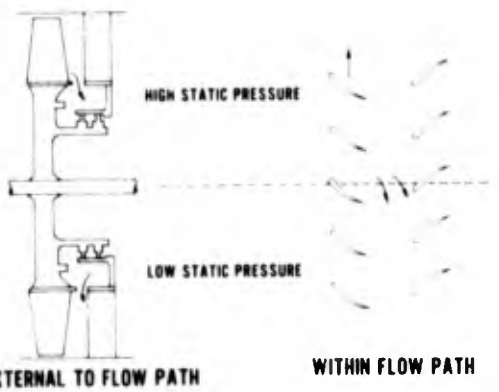

Figure 20 Circumferential Flow in a Compressor Subjected to a Circumferential Inlet Distortion

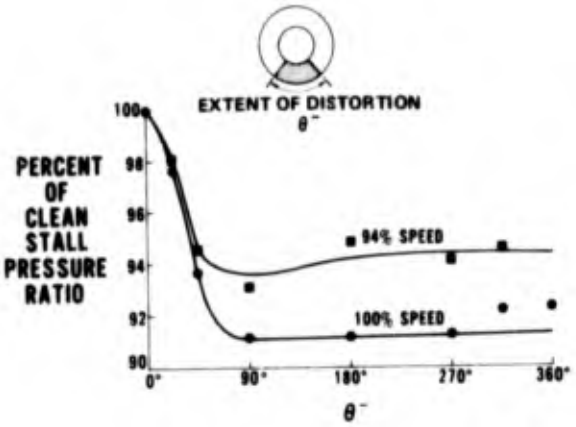

Figure 21 Effect of Circumferential Extent of Distortion on Surge Pressure Rise Capability

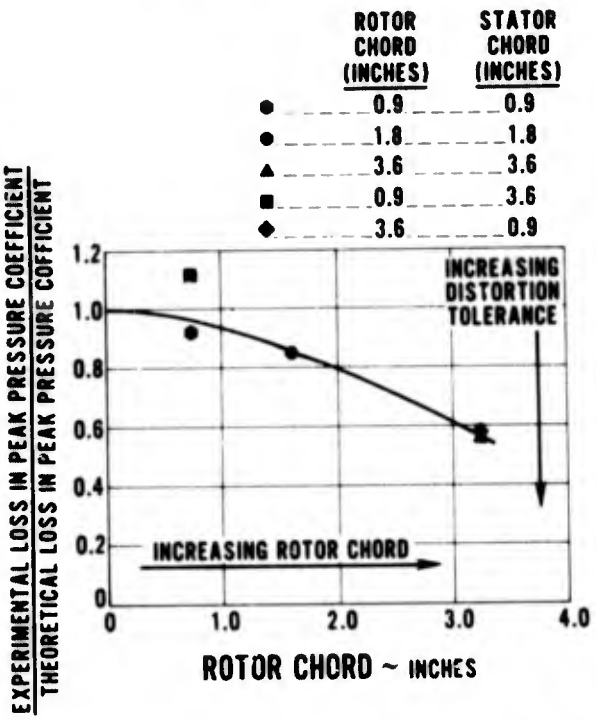

Figure 22 Effect of Rotor and Stator Chord Length on Distortion Tolerance

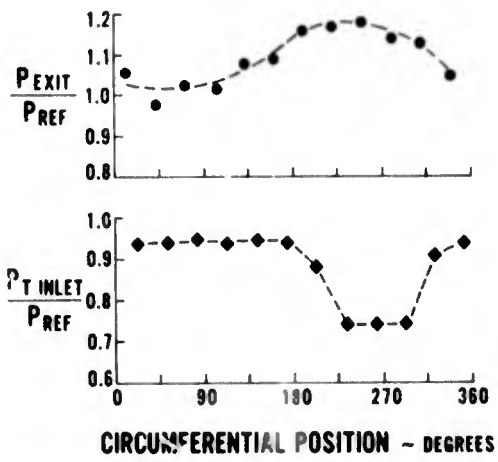

Figure 23 Circumferential Variation in Exit Statis Pressure for a Research Compressor Rig Followed by a Downstream Diffuser

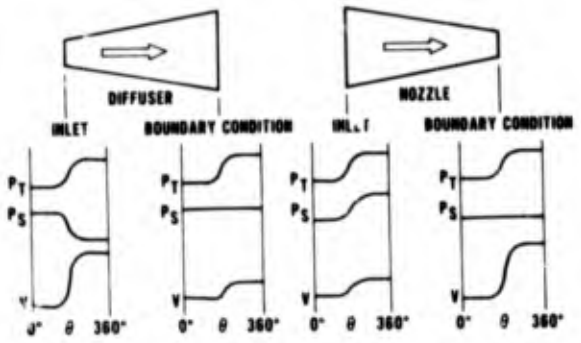

Figure 24 Influence of a Diffuser and Nozzle on the Compressor Exit Static Pressure

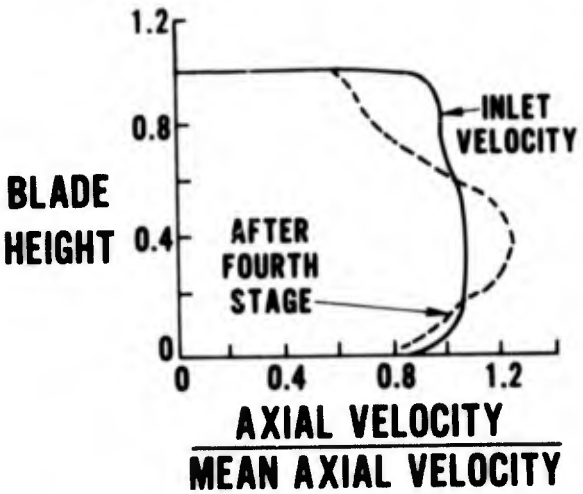

Figure 25 An Extreme Example of Radial Profile in a Milti-Stage Compressor

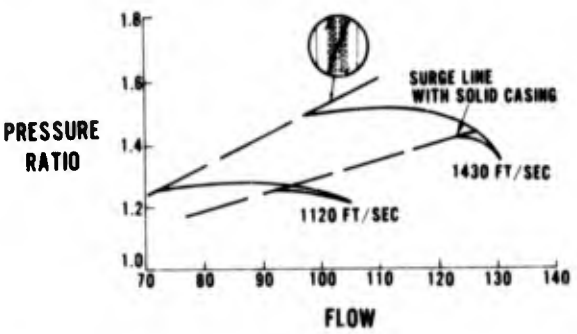

Figure 26 Effect of Casing Treatment on the Performance of a Fan Subjected to Tip Radial Distortion ($\Delta P/P = 0.2$ Over 40% of Span)

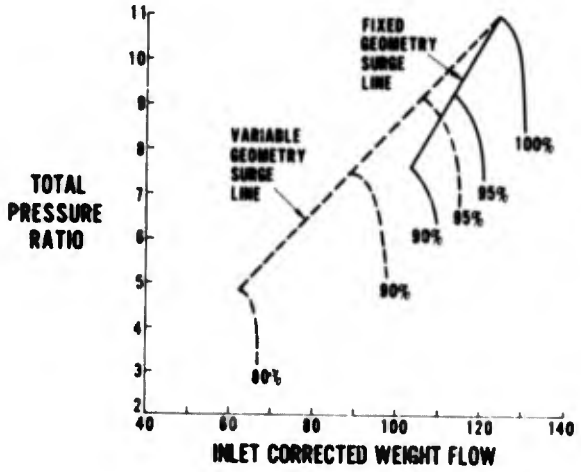

Figure 27 Use of Compressor Bleed to Provide Adequate Surge Margin at Low and High Speeds

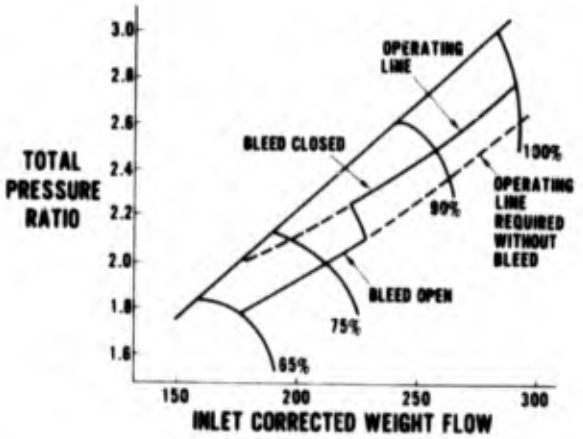

Figure 28 Use of Variable Stagger Stators Raises the Surge Line at Low Speeds